Loss of cytoskeletal and polarity regulation as key pathogenic principles in glomerular disease

Inaugural-Dissertation

zur

Erlangung des Doktorgrades

der Mathematisch-Naturwissenschaftlichen Fakultät

der Universität zu Köln

vorgelegt von

Johanna Odenthal

aus Troisdorf

Köln 2022

Diese Dissertation wurde angenommen von der Mathematisch-Naturwissenschaftlichen Fakultät der Universität zu Köln

Tag der Abgabe:	22. August 2022
Berichterstatter:	Prof. Dr. Thomas Benzing
Gutachter:	Prof. Dr. Siegfried Roth
Tag der Disputation:	24. Oktober 2022

Dedicated to my great Drosophila teachers and peers, past and present,

who inspired me with their joy of learning and teaching and the love for basic science,

and to my parents and friends.

Publications

Original articles

2023 **Odenthal J**, Dittrich S, Ludwig V, Merz T, Reitmeier K, Reusch B, Höhne M, Cosgun ZC, Hohenadel M, Putnik J, Göbel, H, Rinschen MM, Altmüller J, Koehler S, Schermer B, Benzing T, Beck BB, Brinkkötter PT, Habbig S, Bartram MP. *Modeling of ACTN4-based podocytopathy using Drosophila nephrocytes.* Kidney International Reports

doi: 10.1016/j.ekir.2022.10.024

2021 Koehler S*, **Odenthal J***, Ludwig V, Unnersjö Jess D, Höhne M, Jüngst C, Grawe F, Helmstädter M, Janku JL, Bergmann C, Hoyer PF, Hagmann HH, Walz G, Bloch W, Niessen C, Schermer B, Wodarz A, Denholm B, Benzing T, Iden S, Brinkkoetter PT. *Scaffold polarity proteins Par3A and Par3B share redundant functions while Par3B acts independent of atypical protein kinase C/Par6 in podocytes to maintain the kidney filtration barrier.* Kidney International

doi: 10.1016/j.kint.2021.11.030. *Authors contributed equally

2019 **Odenthal J** and Brinkkoetter PT. *Drosophila melanogaster and its nephrocytes: A versatile model for glomerular research.* Methods in Cell Biology Volume 154 – Methods in Kidney Cell Biology – Part B

doi: 10.1016/bs.mcb.2019.03.011

Conference contributions

Poster presentation

2022 **Odenthal J**, Reitmeier K, Kuehne L, Schermer B, Benzing T, Brinkkoetter PT. *Mitochondrial ROS sensitize podocytes to insulin resulting in mTOR activation.* Kidney Week of the American Society of Nephrology, Orlando, USA (3rd – 6th November 2022)

2022 **Odenthal J**, Beck BB, Schermer B, Benzing T, Brinkkoetter PT, Bartram MP. Using *Drosophila melanogaster to characterize potentially pathogenic patient mutations associated with nephrotic syndrome and FSGS.* Kidney Week of the American Society of Nephrology, Orlando, USA (3rd – 6th November 2022)

2021 **Odenthal J**, Beck BB, Schermer B, Benzing T, Brinkkoetter PT, Bartram MP. *Characterization of a novel FSGS-associated ACTN4 mutation in Drosophila melanogaster.* Kidney Week of the American Society of Nephrology, San Diego, USA (4th – 7th November 2021)

2021 **Odenthal J**, Dittrich S, Beck BB, Schermer B, Benzing T, Brinkkoetter PT, Bartram MP. *Using Drosophila melanogaster to study novel FSGS-associated ACTN4 mutations.* 13th International Podocyte Conference, Manchester, United Kingdom (27th – 31st July 2021)

2020 **Odenthal J**, Dittrich S, Beck BB, Schermer B, Benzing T, Brinkkoetter PT, Bartram MP. *Using Drosophila melanogaster to study novel FSGS-associated ACTN4 mutations.* 12th Annual Meeting of the German Society of Nephrology (1st – 4th October, 2020)

2019 Kuehne L, **Odenthal J**, Schermer B, Benzing T, Brinkkoetter PT. *Using Drosophila nephrocytes to study insulin signaling in genetic forms of SRNS.* Kidney Week of the American Society of Nephrology, Washington DC, USA (5th – 10th November 2019)

2019 Oezel C, Schoemig T, Matin M, **Odenthal J**, Schermer B, Coward R, Benzing T, Brinkkoetter PT. *Mitochondrial programming of metabolic signaling in glomerular podocytes.* Kidney Week of the American Society of Nephrology, Washington DC, USA (5th – 10th November 2019)

2019 **Odenthal J**, Dittrich S, Beck BB, Schermer B, Benzing T, Rinschen MM, Brinkkoetter PT, Bartram MP. *Functional analysis of a novel FSGS-associated ACTN4 mutation in podocytes and Drosophila melanogaster.* Kidney Week of the American Society of Nephrology, Washington DC, USA (5th – 10th November 2019)

2019 **Odenthal J**, Dittrich S, Beck BB, Rinschen MM, Schermer B, Benzing T, Koehler S, Brinkkoetter PT, Bartram MP. *Functional analysis of a novel FSGS-associated ACTN4 mutation in podocytes and Drosophila melanogaster*. 13th Annual Meeting of the German Society of Nephrology, Düsseldorf, Germany (10th – 13th October 2019)

2019 **Odenthal J**, Dittrich S, Ludwig V, Schermer B, Benzing T, Koehler S, Bartram MP, Brinkkoetter PT. *Drosophila Nephrocytes – a versatile model for glomerular research.* European *Drosophila* Research Conference, Lausanne, Switzerland (5th – 8th September 2019)

2018 Koehler S, **Odenthal J**, Niessen CM, Iden S, Bloch W, Schermer B, Benzing T, Denholm B, Brinkkoetter PT. *Par3A and Par3B orchestrate podocyte polarity.* 12th International Podocyte Conference, Montreal, Canada (31st May – 2nd June 2018)

Table of Contents

List of figures

Abbreviations

aa – Amino acids

ACTN4 – Alpha-actinin-4

AJ – Adherens junction

AP-1 – Activator protein 1

ANOVA – Analysis of variance

aPKC – Atypical protein kinase C

aPKCι – Atypical protein kinase C iota

aPKCζ – Atypical protein kinase C zeta

Arp – Actin-related protein

Arp2/3 – Actin-related proteins 2/3

AU – Arbitrary units

Baz - Bazooka

BDSC – Bloomington Drosophila Stock Center

BM – Basement membrane

Cas – CRISPR-associated endonuclease

Ccd42 – Cell-divison control protein 42 homolog

CD2AP – CD2-associated protein

CKD – Chronic kidney disease

CRB – Crumbs

CRB3 – Crumbs3

CRIB - Cdc42/Rac interaction binding

CRISPR - Clustered Regularly Interspaced Short Palindromic Repeats

CR1 – Conserved protein 1

Dcr2 – Dicer 2

Dlg – Discs large

DN – Dominant negative

ECM – Extracellular matrix

FA – Focal adhesion

F-actin – Filamentous actin

FE – Fenestrated epithelium

FITC – Fluorescein isothiocyanate

FP – Foot process

FPE – Foot process effacement

G-actin – globular actin

GBM – Glomerular basement membrane

GEF – Guanine nucleotide exchange factor

GFP – Green fluorescent protein

GTP – Guanosintriphosphate

HRP – Horse radish peroxidase

JAM – Junctional adhesion molecule

JAM-1 – Junctional adhesion molecule 1

JAM-2 – Junctional adhesion molecule 2

JAM-3 – Junctional adhesion molecule 3

kDa – Kilo Dalton

Lgl – Lethal giant larvae

Lgl1 – Lethal giant larvae 1

Lgl2 – Lethal giant larvae 2

µm – Mikro meter

NCK – Non-catalytic region of tyrosine kinase

ND – Nephrocyte diaphragm

Nm – Nano meter

N-WASP – Neuronal Wiskott-Aldrich syndrome protein

PALS1 – Protein associated with Lin-7 1

Par3 – Partitioning defective 3

Par3A – Partitioning defective 3 A

Par3B – Partitioning defective 3 B

Par6 – Partitioning defective 6

Par6α – Partitioning defective 6 alpha

Par6β – Partitioning defective 6 beta

PATJ – PALS1-associated tight junction protein

PB1 – Phox/Bem 1

PDZ – Post synaptic density protein, Drosophila disc large tumor suppressor, Zonula occludens-1 protein

Pyd – Polychaetoid

Rac1 – Ras-related C3 botulinum toxin substrate 1

RhoA – Ras homology A

RNA – Ribonucleic acid

RNAi – Ribonucleic acid interference

SD – Slit diaphragm

SNP – Single nucleotide polymorphism

Sns – Sticks and stones

SRNS – Steroid resistant nephrotic syndrome

STDV – Standard deviation

TIAM – T-cell lymphoma invasion and metastasis-inducing protein

TIAM1 – T-cell lymphoma invasion and metastasis-inducing protein 1

TJ – Tight junction

Tm2 – Tropomyosin 2

TRPC6 – Short transient receptor potential channel 6

UAS – Upstream activating sequence

VDRC – Vienna Drosophila Resource Centre

ZO-1 – Zonula occludens protein 1

Abstract

Injury to glomerular podocytes constitutes the predominant cause of glomerular diseases and therefore loss of kidney function. Podocytes are specialized epithelial cells within glomeruli indispensable for the filtration process. Their cell bodies extrude numerous large primary and smaller foot processes that completely enwrap glomerular capillaries. The only cell-cell contact established between adjacent foot processes of neighbouring cells is the slit diaphragm. In addition to contributing to the filtration barrier and preventing the loss of blood proteins into the urine, the slit diaphragm is a vital signaling platform that integrates external signals with the intracellular signaling machinery. The sophisticated architecture of podocytes and their foot processes requires a dynamic actin cytoskeleton and its tight regulation through pathways such as polarity signalling. Upon injury, podocytes start to retract their foot processes, leading to loss of the slit diaphragm and ultimately disruption of the filter apparatus. A common finding upon this so-called effacement are actin cytoskeleton rearrangements. Understanding pathways and key players of actin regulation in podocytes that could prevent the progression of foot process effacement is therefore desirable. This thesis investigated the loss of actin and polarity regulation as key principles of podocyte injury. A first focus was thereby put on utilizing the fruit fly *Drosophila melanogaster* and in particular nephrocytes as *in vivo* model for glomerular diseases and to establish solid and reproducible experimental read-outs. Expression of human transgenes in nephrocytes was then used to characterize a so far unknown patient mutation in alpha-Actinin 4, an actin-crosslinking protein. In addition to demonstrating that the mutation alters actin localization, the *Drosophila* model was utilized to assess the pathogenic potential of the mutant protein. In light of the fact that expression of the mutant variant resulted in severe morphological and functional phenotypes in nephrocytes, it was determined that the novel variant is indeed a pathogenic ACTN4 variant. By this, the power of *Drosophila* as *in vivo* tool to complement clinical and genetic diagnostics was emphasized. Lastly, a possible link between podocyte polarity signaling and actin regulation was further investigated by using both, murine and *Drosophila* models. Here, single and double knockout of *Par3A* and *Par3B* in murine podocytes revealed, that the proteins share redundant functions, as only double knockout of *Par3A* and *-B* led to a glomerular phenotype. Further analyses in *Drosophila* nephrocytes focussed on knockdown of the *Drosophila* Par3 homologue *bazooka*. Depletion of Bazooka in nephrocytes led to differential expression of various actin-binding and -regulating proteins, including increased activity of the small GTPase Rho1 (the *Drosophila* RhoA homologue). Interestingly, Rho1 activation could be reverted upon transgenic expression of murine Par3A but not Par3B, indicating that the two proteins also exhibit distinct but unknown functions. These findings strengthen the link between perturbed polarity signalling and dysregulated actin dynamics, making polarity proteins a strong target to possibly counteract the progression of podocyte disease.

1 Introduction

1.1 Podocytes – cells at the centre of the renal filtration barrier

Renal blood filtration into primary urine is essential for human life. The filtration process, by which blood is detoxified from a variety of metabolic waste products, takes place in two million filtration units called glomeruli, located in the kidney cortex (Pavenstädt et al., 2003). A glomerulus consists of a capillary loop enclosed by Bowman's capsule which terminates into the tubular system of the nephron (Fig. 1). The actual filtration barrier is three-layered, comprising fenestrated epithelial cells of the capillary, a glomerular basement membrane (GBM), and podocytes, specialized, post-mitotic epithelial cells of the glomerulus (Brenner et al., 1978a, 1978b; Rennke & Venkatachalam, 1979). Podocytes are characterized by a sophisticated three-dimensional architecture: Their cell body extrudes primary and secondary processes that ultimately terminate in a large number of smaller foot processes (FPs) (Haraldsson et al., 2008). The latter interdigitate with FPs of neighbouring podocytes forming a large sieve-like network of cellular extensions that completely enwrap the glomerular capillaries (Brinkkoetter et al., 2013; Huber & Benzing, 2005; Pavenstädt et al., 2003). The only cell-cell contact that is hereby established between adjoining FPs of the podocytes is the so-called slit diaphragm (SD). It is formed by interaction of the extracellular parts of transmembrane proteins nephrin* and NEPH1, leading to a membranous structure that bridges an approximately 40 nm wide filtration slit and defines the outermost part of the charge- and 60 kDa size-selective filtration barrier (Brenner et al., 1978b; Donoviel et al., 2001; Kestilä et al., 1998; Rennke & Venkatachalam, 1979; Rodewald & Karnovsky, 1974). Examining SD-associated proteins more closely reveals that the SD is a highly specialized cell-cell contact. During podocyte development, the apical cell-cell contacts of the initially columnar shaped epithelial cells translocate towards the more basolateral part of the cell where the SD is finally established at the cell's FPs (Schell et al., 2014; Schnabel et al., 1990). Thus, both tight junction proteins such as zonula occludens protein 1 (ZO-1), Junctional adhesion molecules (JAMs) and occludin (Fukasawa et al., 2009; Schnabel et al., 1990) as well as adherens junction typical proteins like catenins and cadherins (Reiser et al., 2000) are part of the SD multiprotein complex.

* Protein names and symbols were adapted according to the NCBI Protein database.

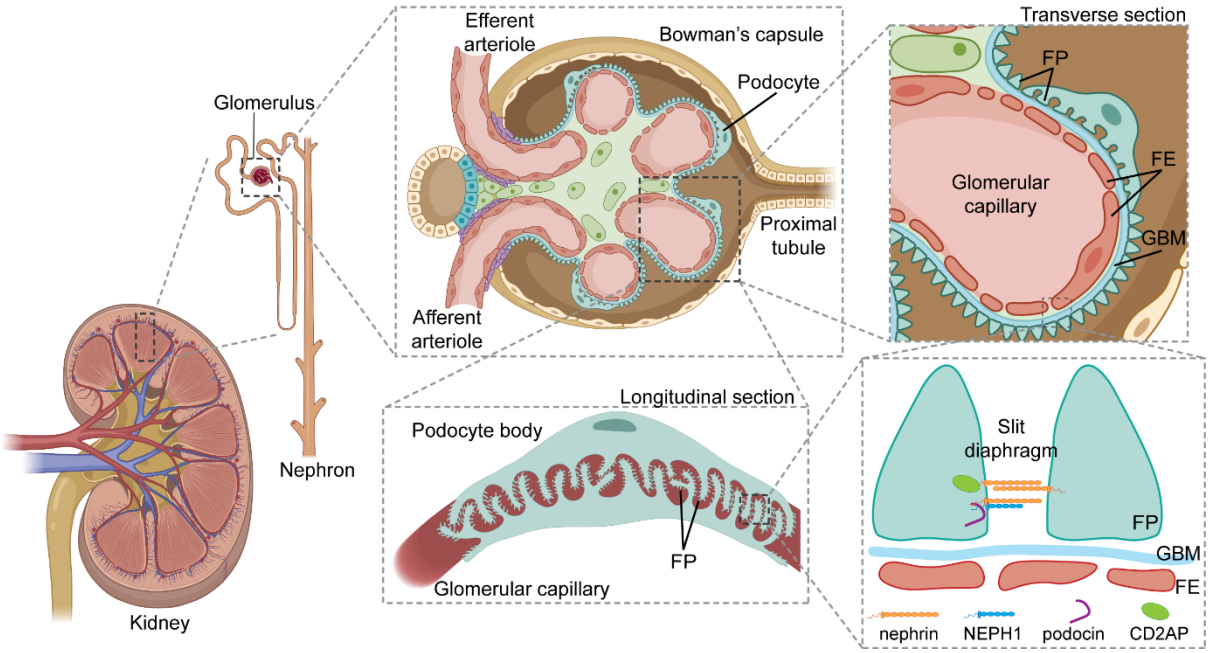

Figure 1: Morphology and structure of mammalian podocytes and the filtration barrier. Approximately one million nephrons comprise the functional units of each kidney in humans. Filtration of blood into primary urine takes place in the glomeruli. They consist of a capillary tuft covered by foot processes (FPs) of glomerular epithelial cells – podocytes – and surrounded by Bowman's capsule which terminates into the proximal tubule. FPs of neighbouring podocytes interdigitate establishing a sieve-like network that completely enwraps the glomerular capillaries. Blood is filtered through a three-layered filtration barrier comprising fenestrated epithelium (FE) of the capillary, the glomerular basement membrane (GBM) and finally the slit diaphragm (SD), a specialized cell-cell contact between FPs of podocytes. The SD is composed of transmembrane proteins nephrin and NEPH1. The SD constitutes a charge- and size selective barrier, withholding macromolecules larger than 60 kDa in the blood. The intracellular domains of nephrin and NEHP1 furthermore interact with other adaptor proteins including podocin and CD2-associated protein (CD2AP), whereby intracellular signalling cascades are initiated, highlighting the function of the SD as signalling hub. *Figures created with BioRender; ID: ST25CTV43N.*

Moreover, the SD complex acts as a signalling hub (Benzing, 2004; Huber & Benzing, 2005) as well as anchoring point for the actin-based cytoskeleton (Lehtonen et al., 2005; Shih et al., 1999; Welsch et al., 2001). Signalling events from the SD into the cell are generally initiated by phosphorylation of the cytoplasmic part of nephrin or NEPH1 by tyrosine-protein kinase Fyn, which leads to recruitment of various signalling proteins of different downstream pathways (Garg et al., 2007; Verma et al., 2003). These include podocyte specific proteins podocin and CD2-associated protein (CD2AP), which interact with the cytoplasmic tail of nephrin (Benzing, 2004; Huber & Benzing, 2005; Shih et al., 1999; Welsch et al., 2001) and are important for various further intracellular signalling events and actin cytoskeleton regulation

via proteins like alpha-actinin-4 (ACTN4) and synaptopodin (Kaplan et al., 2000; Lehtonen et al., 2005; Mundel et al., 1991). In summary, the SD not only represents the third component of the filtration barrier, facilitating the clearance of macromolecules smaller than 60 kDa. It also serves as attachment site for the FPs actin cytoskeleton and as signalling platform, and is therefore essential for maintenance of the podocyte's three-dimensional structure and intracellular signalling events, respectively.

1.2 Podocyte injury and clinical hallmarks of glomerular diseases

Podocytes are cells at risk: They reside at a highly exposed anatomical location where they must endure a variety of environmental conditions. Among these are exposure to immunological, infectious and toxic factors (Fujii et al., 2018; Glorieux et al., 2015; Pozdzik et al., 2018). Moreover, podocytes are subjected to mechanical forces such as circumferential wall stress and tangential shear stress transmitted by filtration pressure (Butt et al., 2020, 2021; Kriz, 2020). Thus, the podocyte's integrity might be comprised by different external insults. On the other hand, podocyte injury can also have a genetic cause. To date, more than 50 podocyte-associated genes have been identified in patients with monogenic podocyte disease (Kopp et al., 2020; Liu & Wang, 2017; Vivante & Hildebrandt, 2016). They encode for proteins that are essential for a variety of cellular compartments and pathways including SD-associated and extracellular matrix-interacting proteins as well as actin cytoskeleton-modulating proteins but also mitochondrial proteins and transcriptional regulators (Fig. 2).

Podocytopathies are the most common cause of glomerular disorders, which in turn account for the majority of chronic kidney diseases (CKDs) (Saran et al., 2018; Wanner et al., 2014). Hereby, the podocytes and thereupon the kidney as such, experience a gradual loss of function which ultimately leads to kidney failure. Glomerular disorders comprise idiopathic as well as genetic factors that lead to podocyte injury (Davin, 2016; Kopp et al., 2020; McCarthy et al., 2010; Vivante & Hildebrandt, 2016). Secondary forms of glomerular disease may also emerge as a consequence of other, systemic diseases such as hypertension, systemic lupus erythematosus or diabetes mellitus (Badal & Danesh, 2014; Greka & Mundel, 2012; Kriz, 2020; Levy, 2007; Rico-Fontalvo et al., 2022).

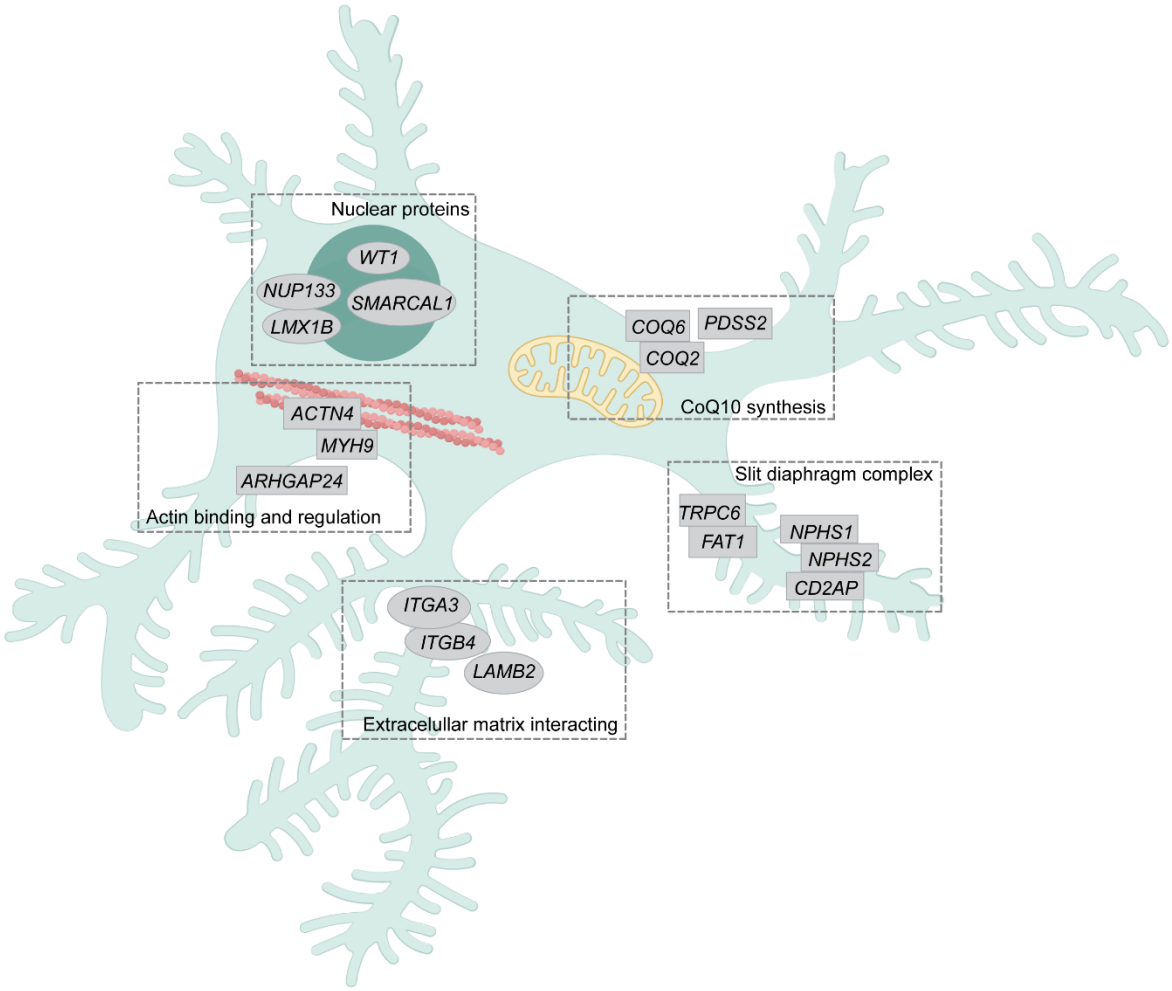

Figure 2: Genes involved in monogenic podocyte disease. To date, more than 50 podocyte expressed genes, a few of which are depicted here, have been identified in patients suffering from podocyte disease and nephrotic syndrome. They encode for proteins of different subcellular compartments and are implicated in various cellular functions. These include proteins of the slit diaphragm complex, those involved in actin binding and regulation as well as extracellular matrix interaction, but also mitochondrial and nuclear proteins. Gene products: *WT1* – WT1 transcription factor; *NUP133* – Nuclear pore complex protein Nup133; *LMX1B* - LIM homeobox transcription factor 1-beta; *SMARCAL1* – SWI/SNF-related, matrix-associated, actin dependent regulator of chromatin, subfamily a like 1; *ACTN4* – alpha-actinin-4; *MYH9* – myosin-9; *ARHGAP24* – Rho GTPase-activating protein 24; *COQ6* – coenzyme Q6, monooxygenase; *COQ2* – coenzyme Q2, polyprenyltransferase; *PDSS2* – decaprenyl diphosphate synthase subunit 2; *ITGA3* – integrin subunit alpha 3; *ITGB4* – integrin subunit beta 4; *LAMB2* – laminin subunit beta 2; *TRPC6* – short transient receptor potential channel 6; *FAT1* – protocadherin Fat 1; *NPHS1* – nephrin; *NPHS2* – podocin; *CD2AP* – CD2-associated protein. *Figures created with BioRender; ID: SA25CTUWV3.*

On cellular level, the earliest histopathological sign of podocyte injury, independent of its molecular origin, manifests as an ultrastructural finding commonly referred to as 'foot process effacement' (FPE): the re-structuring of the cells' morphology seen as flattening and retraction of the cells' FPs and loss of SDs up to detachment and complete loss of the podocyte ultimately leading to disruption of the filter apparatus (D'Agati, 2003; Deegens et al., 2008; Mundel & Shankland, 2002). Since podocytes are terminally differentiated, post-mitotic cells, they do not have the capacity of self-renewal after injury or loss resulting in an overall reduction in podocyte density within the glomerulus (Kriz, 2020; Pavenstädt et al., 2003) . This is accompanied by increased mechanical forces and exposition to harming factors on the remaining podocytes leading to hypertrophy and further podocyte detachment and loss (Greka & Mundel, 2012; Kriz et al., 2013; Matsusaka et al., 2011; Wiggins et al., 2005) – a vicious circle that nurtures the progressive decline in filter function. Due to the disrupted filtration barrier, patients suffering from glomerular disease present with loss of plasma proteins, especially albumin, into the primary urine (proteinuria and albuminuria, respectively), hyperlipidaemia, edema of peripheral tissues as well as scarring of the glomerular tissue (glomerulosclerosis), which are the clinical parameters of nephrotic syndrome (Liebeskind, 2014; Politano et al., 2020; C. shi Wang & Greenbaum, 2019). Since FPE is in general reversible during early stages (Chang et al., 2012; Kriz et al., 2013; Seiler et al., 1977), it is therefore of outermost importance to further study and understand underlying patho-mechanisms of FPE to potentially counteract the morphological changes of the podocyte. A substantial amount of research has been done and concepts of the process of FPE have been postulated over the past decades, whereby disruption of actin cytoskeleton integrity and actin dynamics seems to be a fundamental process (Kerjaschki, 2001; Shirato, 2002; Tryggvason & Wartiovaara, 2001; Ye et al., 2022), as will be addressed in the following section.

1.3 Dysregulated actin dynamics as key principle of foot process effacement

In contrast to the podocyte's primary processes in which microtubuli are the predominant cytoskeletal component, secondary and foot processes possess an actin-based cytoskeleton (Blaine & Dylewski, 2020). There are two distinct types of actin networks found in FPs that orchestrate the structural flexibility of podocytes. Loosely assembled actin filaments that bundle together in the centre of FPs along the longitudinal axis as well as a cortical network of filamentous actin (F-actin) (Ichimura et al., 2007) (Fig. 3). Rearrangement and modification of the actin cytoskeleton in FPs is part of the podocyte's response and adaptation to the diverse and changing physical filtration forces the cells must withstand (Kerjaschki, 2001; Sever & Schiffer, 2018). As changes in podocyte morphology and structure are the earliest signs of podocyte injury, a tight regulation of actin dynamics is fundamental to maintain podocyte function and to preserve the integrity of the filtration apparatus. FPE, as the underlying principle of podocyte injury, can hereby be divided into two stages (Blaine & Dylewski, 2020; Kriz et al., 2013): Within the first stage, the cells start to retract their numerous FPs into shorter cell projections of irregular shape. At the same time, due to shortening of the FPs, the SD covered area is reduced. During the second phase of FPE, processes have retracted in such a degree, that primary, flattened processes and ultimately the cell bodies themselves cover and adhere to the GBM. In this stage, the actin cytoskeleton undergoes a tremendous rearrangement and finally, a dense "mat" of F-actin is formed in close proximity to the GBM. This process is accompanied by increased expression of actin itself and actin-regulatory proteins synaptopodin and ACTN4 (Shirato et al., 1996). Over the past decades, numerous studies and various mouse models have highlighted the importance of actin-regulatory and actin-interacting proteins in podocytes. Moreover, many of these proteins have been shown to be mutated in patients suffering from monogenic forms of glomerular diseases (Kopp et al., 2020; Sadowski et al., 2015; Vivante & Hildebrandt, 2016). These include the SD proteins nephrin and podocin per se, adaptor proteins including CD2AP as well as numerous proteins involved in direct actin regulation and -binding such as ACTN4. Given the structural requirement of the actin cytoskeleton for podocyte morphology and function as well as the growing evidence of its role during FPE, a deep understanding of how exactly actin regulation is established in podocytes is therefore desirable. Regulation of actin

dynamics hereby occurs at two distinct signalling hubs: the SD multiprotein complex as well as focal adhesions (FAs), located at the base of the FP (Ye et al., 2022) (Fig. 3).

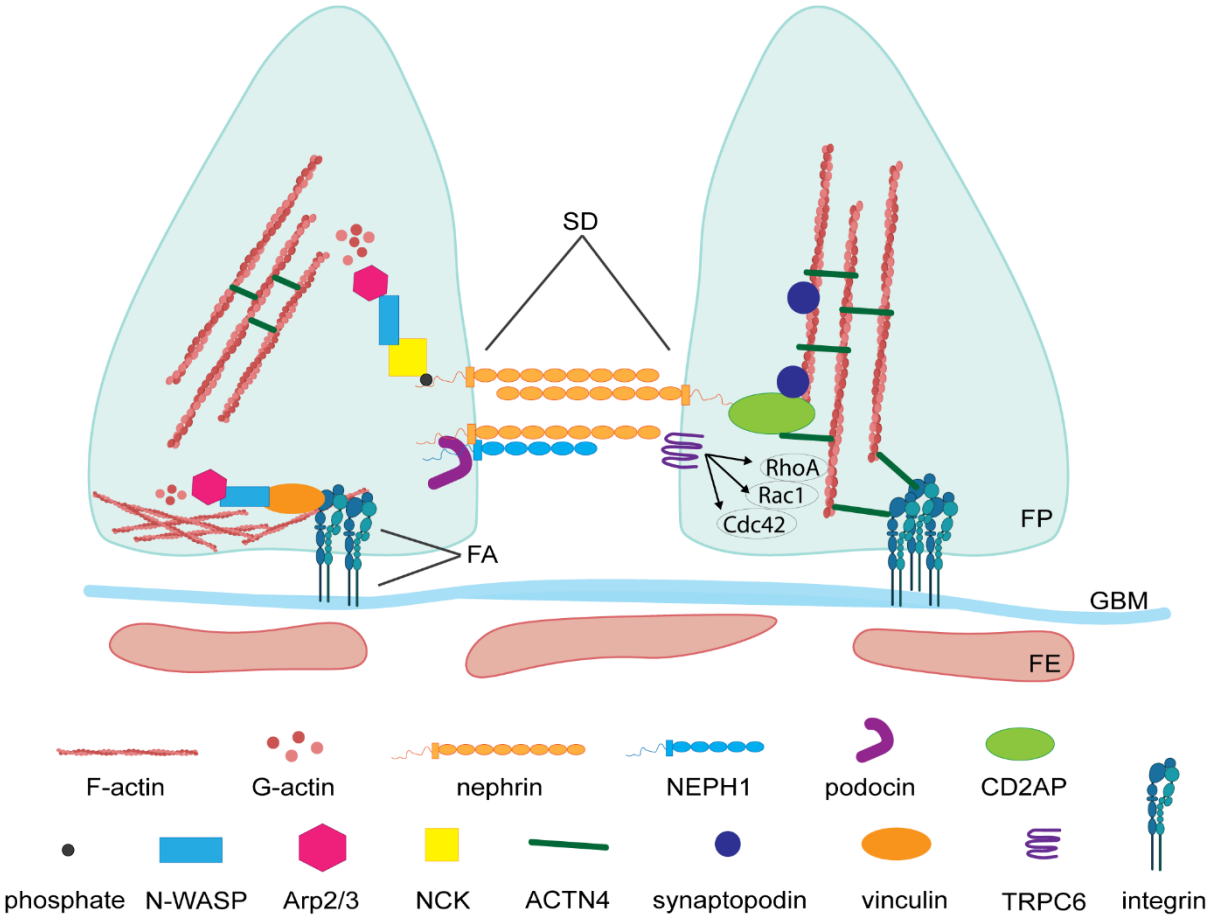

Figure 3: Structure and regulation of the actin cytoskeleton in podocyte foot processes. Schematic drawing of the actin cytoskeleton in foot processes (FPs) and the major actin-regulatory proteins. Actin filaments are either bundled along the longitudinal axis of the FP or arranged as a cortical network. Regulation of actin dynamics is achieved via two signalling hubs: the slit diaphragm (SD) as well as focal adhesions (FAs). An interplay of signal receptors (e.g. nephrin or integrin), adaptor proteins (e.g. CD2AP or vinculin) as well as downstream effectors and small GTPases ensures a tight regulation of the actin cytoskeleton and adaptation to external changes in health and disease. GBM, glomerular basement membrane; F-actin, filamentous actin; G-actin, globular actin; CD2AP, CD2-associated protein; N-WASP, Neuronal Wiskott-Aldrich syndrome protein; Arp2/3, actin-related proteins 2/3; NCK, non-catalytic region of tyrosine kinase; ACTN4, alpha-actinin-4; TRPC6, short transient receptor potential channel 6; RhoA, Ras homology A; Rac1, Ras-related C3 botulinum toxin substrate 1; Ccd42, Cell division control protein 42 homolog. *Figures partially created with BioRender; IDs: GM25CTVH0X and QO25CTVA4S.*

Signalling from the SD to the actin cytoskeleton is established by either an interplay of signal receptors and adaptor proteins that directly or indirectly link to actin or by signal integrators such as small GTPases that interact with actin-modulating proteins (Blaine & Dylewski, 2020). Focussing on nephrin as primary signaling receptor, the initial step in cell signalling may include phosphorylation of intracellular tyrosine residues due to external stimuli, followed by the recruitment of adaptor proteins (Garg et al., 2007; Verma et al., 2003). These include for example the adaptor NCK (non-catalytic region of tyrosine kinase) leading to activation of the N-WASP (Neuronal Wiskott-Aldrich syndrome protein) and Arp2/3 (actin-related proteins 2/3) complex pathway, which in its active state results in actin nucleation and branching of F-actin (Jones et al., 2006; Mullins, 2000; New et al., 2013; Verma et al., 2006). Thus, phosphorylation of nephrin is highly important for actin *de novo* polymerization and the formation of actin filaments. Besides regulation via phosphorylation, nephrin also binds the adaptor protein CD2AP (Tossidou et al., 2019). The latter is a scaffolding protein that constitutes a direct link to actin as well as F-actin interacting proteins synaptopodin and ACTN4 (Asanuma et al., 2005; Lehtonen et al., 2002). Among the signal integrators associated with the SD and broadly known to be essential for actin dynamics are small GTPases like RhoA (ras homology A), Rac1 (ras-related C3 botulinum toxin substrate 1) and Cdc42 (cell division control protein 42 homolog) (Blaine & Dylewski, 2020). Studies have shown that hyperactivation as well as inactivation of e.g. RhoA both lead to FPE and proteinuria in mice which indicates that activity of these GTPases needs to be tightly regulated (L. Wang et al., 2012; Zhu et al., 2011). Activity of small GTPases is hereby regulated by a variety of factors, including calcium influx mediated by SD protein TRPC6 (short transient receptor potential channel 6) (Jiang et al., 2011).

Focal adhesions, the second important site of actin regulation, generally are multiprotein complexes that link the actin cytoskeleton within the cell to the extracellular matrix (Perico et al., 2016; Sever & Schiffer, 2018), i.e. in podocytes, they comprise the site where F-actin is linked to the GBM. Thus, FAs are crucial for podocyte adhesion to the GBM. The structural component of FAs in podocytes is integrin α3β1, which due to its composition of alpha and beta subunits interacts with laminin of the GBM network (Sachs & Sonnenberg, 2013). Similar to downstream signalling from the SD, signalling at FAs arises from interaction of the cytoplasmic tail of active integrin with intracellular adaptor proteins such as talin, paxillin,

vinculin and ACTN4 (Sever & Schiffer, 2018; Ye et al., 2022). These adaptor proteins in turn can either bind directly to actin, as in the case of ACTN4, which bundles and cross-links F-actin (Djinović-Carugo et al., 1999; Tang et al., 2001), or indirectly via other anchor proteins such as N-WASP (Sever & Schiffer, 2018). Moreover, integrin adaptors can also signal to actin-regulatory small GTPases of the RhoA family as well as the non-canonical, multidomain GTPase dynamin. Active dynamin interacts with other actin-regulatory proteins such as NCK or cortactin, through which the protein is implicated in regulating actin polymerization via Arp2/3, to name one of its various functions (Ferguson & de Camilli, 2012; Gu et al., 2010).

In summary, there is growing evidence that actin-dysregulation is a common final pathway of FPE. It is therefore worthwhile to study actin dynamics as well as actin regulation by the SD and FAs in podocytes in more depth. As FPE generally is a reversible process, the SD and FAs not least comprise compelling druggable targets and understanding their role in FPE is desirable to ultimately develop therapeutics that counteract FPE in patients suffering from podocytopathies.

1.4 Cell polarity

1.4.1 General concepts of apico-basal polarity in epithelia

Regulation of cell polarity is essential to define structural and functional differences in a spatial manner from cells through to whole organisms (J. Chen & Zhang, 2013; Roignot et al., 2013). Apico-basal polarity hereby describes the bipolar structure of epithelial cells, which comprises two distinct domains. The apical part faces the external medium whereas the basolateral part of the cell is associated with the basement membrane of the respective tissue. Regarding their protein composition, these membrane domains are highly diverse (Assémat et al., 2008). Proteins targeted towards the apical domain predominantly include those necessary for specific functions such as uptake or secretion. The basolateral domain on the other hand primarily consists of adherens junction proteins or other proteins necessary to connect the cells with the underlying extracellular matrix, thereby mainly serving mechanical linkage within the group of cells. Apico-basal polarity is a tightly regulated process and established by three well-characterized polarity protein complexes (Fig. 4): The Scribble complex, the Crumbs complex and the Par complex (Nelson, 2003; Pieczynski & Margolis,

2011). The Scribble complex, consisting of lethal giant larvae (Lgl), discs large (Dlg) and scribble (SCRIB), is located at the basolateral domain, associated with adherens junctions, and involved in functions such as vesicle trafficking, signal transduction and cytoskeletal remodelling (Bilder et al., 2000; Humbert et al., 2006).

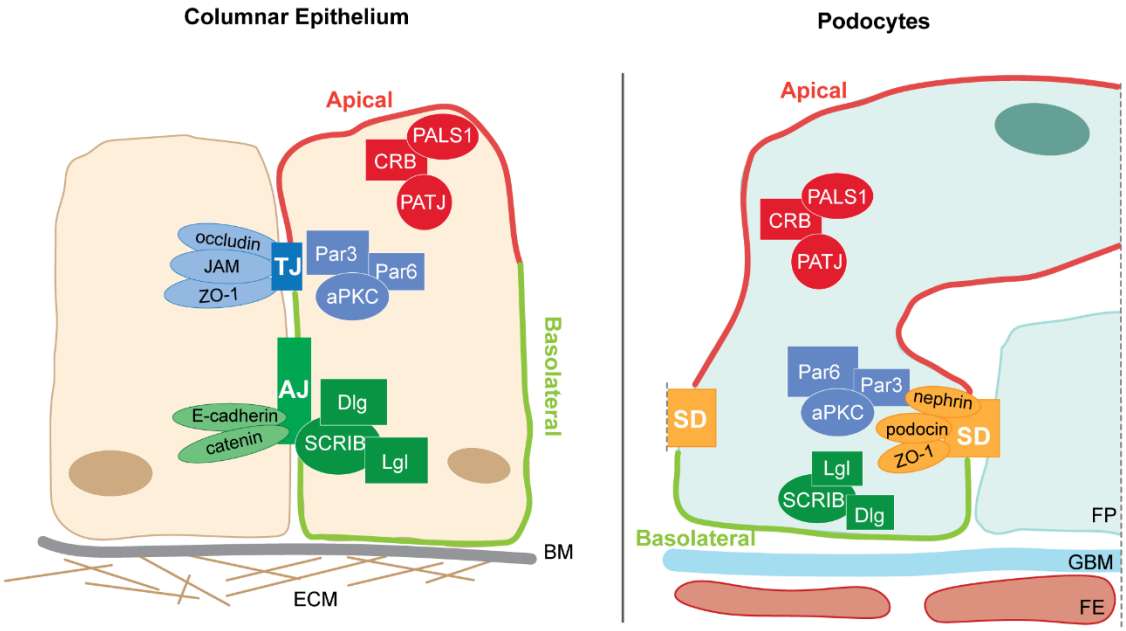

Figure 4: Polarity complexes in columnar epithelium vs. podocytes. Schematic drawing of conventional epithelial cells of the columnar type (left) and podocytes (right) showing the exemplified distribution of the three main polarity complexes. In columnar epithelia, the Crumbs complex (red) is localized at the apical domain. The Par complex (blue) is associated with proteins of tight junctions (TJs) such as occludin, junctional adherens molecules (JAMs) and zoluna occludens protein 1 (ZO-1) and defines the apico-basolateral border of the cell. Lastly, the Scribble complex (green) is located at adherens junctions (AJs) together with AJ-typical proteins E-cadherin and catenins at the basolateral cell domain. In podocytes, the Crumbs complex also localizes to the apical domain, while the Par complex is closely associated with the slit diaphragm (SD) located towards the lower part of the podocytes foot process (FP). The Scribble complex is associated with the basolateral part of the cell and located primarily at the 'sole' of the FP. ECM, extracellular matrix; BM, basement membrane; GBM, glomerular basement membrane; FE, fenestrated epithelium; PALS1, protein associated with Lin-7 1; CRB, crumbs; PATJ, PALS1-associated tight junction protein; PAR3, Partitioning defective 3 homolog; PAR6, Partitioning defective 6 homolog; aPKC, atypical protein kinase C; Dlg, discs large; SCRIB, scribble; Lgl, lethal giant larvae.

The Crumbs polarity proteins, which include Crumbs (CRB), protein associated with Lin-7 1 (PALS1) as well as PALS1-associated tight junction protein (PATJ), target the apical membrane where the complex stabilizes apical cell junctions (Roh et al., 2002). Lastly, the polarity complex Par is established by interaction of Partitioning defective 3 homolog (Par3), Partitioning defective 6 homolog (Par6) and atypical protein kinase C (aPKC) and determines the cell's apical-basolateral border (J. Chen & Zhang, 2013; Suzuki & Ohno, 2006). Crosstalk of these complexes is achieved by interaction and phosphorylation of different complex members via their specialized protein domains. In this way, the complexes activate and mutually exclude one another and thereby precisely define their temporal and spatial localization (Hurd et al., 2003; Margolis & Borg, 2005). Depending on tissue- and cell type, different homologues or isoforms of the complex members may be expressed, which adds another-regulatory level onto the process of polarization. To give an example, the alpha isoform of Par6 does not only interact with its complex members Par3 and aPKC, but also Lgl1 and CRB3 (Lemmers et al., 2004; Plant et al., 2003), whereas Par6β does not interact with CRB proteins but with Lgl1 and Lgl2 (Assémat et al., 2008). Therefore, the polarization process is highly dynamic and is still not completely understood for all tissues or cell types. This thesis includes the investigation of the functional role of the Par polarity complex for podocyte biology. Thus, a more detailed introduction of the complex is given in the following.

1.4.2 The Par polarity complex

As mentioned above, the Par complex is established by interaction of its three members: two scaffolding proteins Par3 and Par6 as well as the serine/threonine kinase aPKC (J. Chen & Zhang, 2013; Margolis & Borg, 2005; Suzuki & Ohno, 2006). The proteins can interact with each other but also with a wide range of other cell polarity regulating proteins via their highly conserved domains (Fig. 5). The interactome of proteins of the Par complex hereby varies depending on the proteins' isoforms. Par3A and Par3B for example, are two Par3 proteins that are encoded by two distinct genes, *PARD3A* and *PARD3B*, respectively (Gao et al., 2002). Par3A holds an N-terminal conserved protein 1 (CR1) domain, followed by three PDZ (post synaptic density protein, drosophila disc large tumor suppressor, zonula occludens protein 1)

domains (Joberty et al., 2000; Lin et al., 2000; Mizuno et al., 2003; Suzuki et al., 2001). The C-terminus contains several protein binding motifs including a binding site for aPKC as well as TIAM (T-cell lymphoma invasion and metastasis-inducing protein), a Rac1 guanine nucleotide exchange factor (GEF) (Mertens et al., 2006). In contrast to Par3A, the C-terminal region of Par3B and its interacting function is far less understood. It was however proven, that the protein does not interact with aPKC (Gao et al., 2002; Kohjima et al., 2002). The second scaffold protein Par6 contains an N-terminal Phox/Bem 1 (PB1) domain and a semi-Cdc42/Rac interaction binding (semi-CRIB) motif, which is ultimately followed by the C-terminal PDZ domain (Joberty et al., 2000; Lemmers et al., 2004; Lin et al., 2000). Lastly, aPKC harbours an N-terminal PB1 domain as well as its catalytic kinase domain within the C-terminus of the protein (Suzuki et al., 2001; Wodarz et al., 2000). Multiple proteins have been identified as aPKC targets to date. In addition to phosphorylating Par3A, aPKC has been shown to phosphorylate Lgl1- and -2, suggesting that aPKC/Par6 can form independent complexes with either Par3A or Lgl1/2 to regulate cell polarity in epithelial cells (Nagai-Tamai et al., 2002; Plant et al., 2003; Yamanaka et al., 2003).

A thorough understanding of the polarization process of conventional epithelia has been gained in the past. Herein, the Par polarity complex is essential for the establishment of an apico-basolateral border: Par3A initially self-associates and forms homodimers via its N-terminal CR1 domain (Mizuno et al., 2003). This homodimerization leads to interaction with junctional adhesion molecules (JAM-1, -2 and -3) via the first PDZ domain, which localizes Par3A to the apical side of newly forming cell-cell contacts (Ebnet et al., 2001; Itoh et al., 2001). Simultaneously, Par6 and aPKC start to interact via their PB1 domains. Par3A then acts as scaffold for the recruitment of Par6/aPKC which is facilitated by binding of the first PDZ domain of Par3 and the Par6 PDZ domain (Joberty et al., 2000). Close proximity of the now tripartite complex to cell-cell junctions results in binding of GTP-bound Cdc42 present in cell-cell contacts to the Par6 semi-CRIB motif (Lin et al., 2000). This interaction induces a conformational change in Par6 leading to activation of aPKC catalytic properties (Garrard et al., 2003). aPKC phosphorylates Par3A at Serine 827, which leads to Par3A dissociation from the complex and translocation to tight junctions, where phospho-Par3A colocalizes with ZO-1 and is involved in tight junction stabilization (Nagai-Tamai et al., 2002).

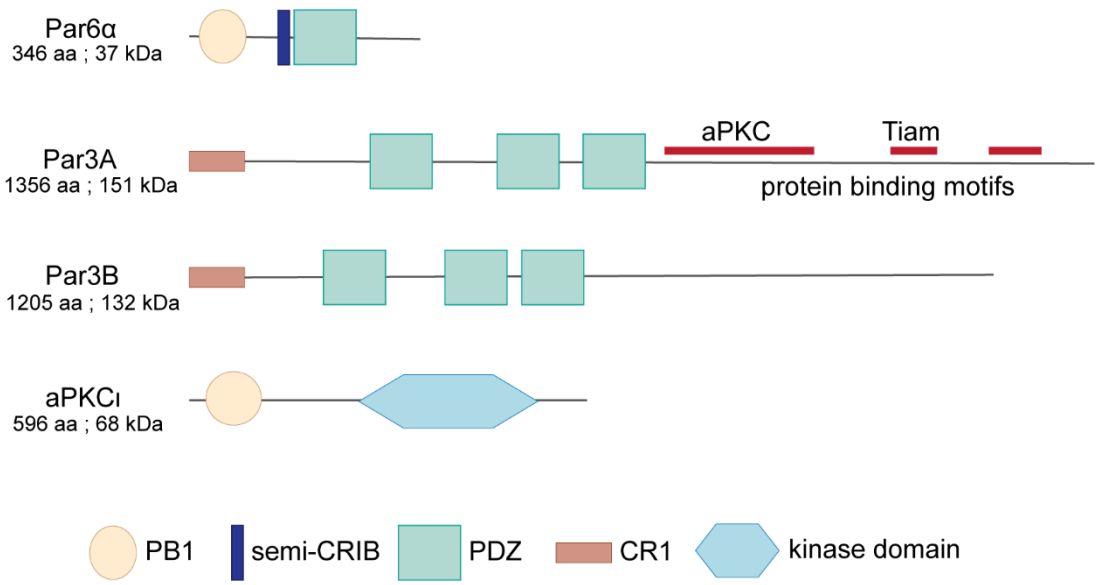

Figure 5: Par polarity complex members and their protein domains. Schematic drawing of the protein and domain structure of partitioning defective 6 (Par6), partitioning defective 3 (Par3) and atypical protein kinase C (aPKC) which together constitute the Par polarity complex. Shown here are isoforms Par6-alpha (Par6α), aPKCiota (aPKCι) as well as both Par3 isoforms, Par3A and Par3B. Via their conserved protein domains, the complex members can interact with one another but also with other regulatory and structural proteins. Different isoforms of the proteins can form distinct complex compositions and thereby protein interactions, which discriminates different cell types and tissues. Due to the absence of an aPKC binding motif, Pa3B does not interact with aPKC, unlike Par3A. aa, amino acids; PB1, Phox/Bem 1; semi-CRIB, semi-Cdc42/Rac interaction binding; PDZ, post synaptic density protein, drosophila disc large tumor suppressor, zonula occludens protein 1; CR1, conserved protein 1.

Similar to Par3A, aPKC now phosphorylates Lgl, which leads to Lgl dissociation from Par6/aPKC and inclusion of Lgl into the Scribble complex, located at the basolateral part of the cell (Plant et al., 2003). To summarize, aPKC can be considered a molecular switch, controlling apical and lateral membrane identities via selective phosphorylation of its targets Par3A and Lgl. Par6 on the other hand acts as scaffold as well as regulator of aPKC activity, by bringing aPKC and its substrates in close proximity.

1.4.3 Polarity in podocytes

The role of the Par complex in epithelial cells has been intensively studied in a variety of tissues including the kidney (Roignot et al., 2013), where tubular cells represent epithelial cells of the classical type. Regulation of apico-basal polarity in tubular cells is essential to guarantee the interplay of both absorption and secretion (Wilson, 1997). The cells need to be highly polarized to maintain a strict distribution of transporters, channels and other important proteins, of which mislocalization has been shown to underly kidney diseases, e.g. polycystic kidney disease (Wilson, 2011; Wilson et al., 1991). As opposed to tubular cells, glomerular podocytes represent non-classical renal epithelial cells. Polarity signalling in these cells is less understood, but seminal work of the past decade could further shape the overall concept of podocyte polarity signalling, revealing partial differences to conventional epithelia. Over the past years, a link between polarity proteins and actin cytoskeleton organization has been well established (Raman et al., 2018). Especially the Par complex is noteworthy here: Par6 is known to interact with Cdc42 and Rac1 via its semi-CRIB motif (Bose & Wrana, 2006; Nishimura et al., 2005) and Par3A is able to bind to TIAM1 with its C-terminus (Chen & Macara, 2005; Mertens et al., 2005, 2006; Nishimura et al., 2005). Since dysregulation of actin dynamics is a key feature of podocyte injury (see 1.3), studying polarity proteins in podocytes hence seemed a reasonable approach.

Initial research consisted of a functional examination of the Par complex in podocytes. Par3A as well as aPKC have been shown to be expressed during early stages of kidney development (Huber et al., 2009). At first, the proteins are localized to the apical membrane in close proximity to early cell-cell contacts. During podocyte differentiation, Par3A and aPKC translocate together with the cell-cell contacts to the basolateral part of the cell, where they are ultimately associated with the SD (Fig. 4) due to direct interaction with nephrin via the first PDZ domain of Par3A (Hartleben et al., 2008; Huber et al., 2009). The researchers then characterized the murine podocyte-specific knockout of either *aPKCiota* and *aPKCzeta*, two isoforms of aPKC that share a high degree of similarity and are both expressed in podocytes. While knockout of *aPKCiota* led to severe proteinuria, glomerulosclerosis and premature death of the mice (Hirose et al., 2009; Huber et al., 2009), loss of aPKCzeta did not cause any glomerular phenotype (Hartleben et al., 2013).

Other analyses focused on the Scribble complex and its function in podocytes. Like proteins of the Par complex, SCRIB is expressed during early podocyte development and ultimately localizes to the base of the FP associated with the basolateral membrane and partially with the SD (Fig.4) (Hartleben et al., 2012). Podocyte specific knockout of *SCRIB* in mice did not result in any basal phenotype nor a phenotype when mice were subjected to models of podocyte stress (Hartleben et al., 2012) – a surprising observation, since loss of SCRIB in other tissues promotes cell transformation and mammary tumorigenesis (Zhan et al., 2008), disturbed cell polarity and elevated proliferation in prostate cancer (Pearson et al., 2011) as well as impairment of neuronal tube development and neonatal death (Murdoch et al., 2003). Moreover, SCRIB was shown to be essential for the recruitment of Ccd42 and Rac1 and hence for actin cytoskeleton regulation (Dow et al., 2007). These data already hint towards polarity regulation being quite different from the canonical regulation in other epithelia.

Subsequent investigations then assessed the role of the small GTPases in podocytes. Knockout of *Cdc42* in podocytes leads to severe glomerular disease and premature death in mice (Blattner et al., 2013; Scott et al., 2012). In contrast, podocyte-specific knockout of Rho family members *Rac1* and *RhoA* did not result in glomerular dysfunction (Blattner et al., 2013; Scott et al., 2012). Interestingly, knockout of *Cdc42* in podocytes showed decreased expression of ZO-1, Par3A and aPKC at the SD (Scott et al., 2012). This is further evidence for an interplay of cell polarity and actin cytoskeleton dynamics and puts the Par polarity complex once more in strong focus as essential for podocyte integrity and function. First analyses in our group then focussed on the scaffold protein Par3A. Interestingly, knockout of *Par3A* in podocytes did not lead to an apparent phenotype in the mice (Koehler et al., 2016). Par3A loss was however accompanied by an upregulation of the second Par3 isoform, Par3B (Koehler et al., 2016), which led to the hypothesis of a possible redundancy of the two proteins. The fact, that Par3B, in contrast to Par3A, does not comprise an aPKC binding domain (Fig. 5) but seems to be able to stabilize and maintain podocyte integrity, challenges the general concept of epithelial cell polarity as known from conventional epithelia, in which the Par3A/aPKC interaction and phosphorylation is essential. It is therefore of high interest to study the consequences of aPKC loss and Par3 redundancy and to generally understand polarity signalling in podocytes in more detail. Since retraction of FPs and de-differentiation of podocytes are hallmarks of FPE, it is worth considering polarity signalling as possible target to stabilize podocyte integrity and counteract FPE upon podocyte disease.

1.5 *Drosophila melanogaster* as advanced *in vivo* tool in glomerular research

In order to study glomerular diseases and underlying molecular pathways, *in vivo* systems are indispensable. Taking into account previously published work in the podocyte field, it becomes obvious that to date the most frequently used model to assess podocyte biology and glomerular diseases *in vivo* is the mouse model, not least because of the high conservation between mice and humans (Batzoglou et al., 2000; Nadeau & Taylor, 1984; Waterston et al., 2002). The recent technical advances regarding genomic engineering and genetic manipulation such as the CRISPR/Cas system increased the attractiveness of mouse models even more (Y. Wang et al., 2022). Still, one has to consider possible disadvantages that come with utilizing mouse models: In addition to costly husbandry, possibly few offspring and long generation times, researchers are confronted with a lot of administrational paperwork, whereby the application process for a new mouse model might already take a long time. This strictly regulated process is of course highly appropriate regarding animal protection laws. The point that needs to be underlined here is: Are mice always the ultimate organism in which the particular research question can be modelled, or might there be other *in vivo* systems that are equally robust but more convenient in this case. Choosing the appropriate model organisms that suits the respective research question is therefore highly important.

A significant part of this thesis focusses on using the fruit fly *Drosophila melanogaster* and in particular the flies' nephrocytes as model to study podocyte biology. Being part of the excretory system in insects, nephrocytes filter and endocytose waste products from the haemolymph, the fly's blood equivalent, and therefore contribute to maintaining water, salt and pH homeostasis (Denholm & Skaer, 2009). Originally described as 'storage kidneys' (Kovalevsky, 1886, 1889), nephrocytes were re-discovered as being functional homologues of mammalian podocytes about a decade ago (Weavers et al., 2009; Zhuang et al., 2009). Since then, *Drosophila* has gained attraction as a model in glomerular research and its utilization in the field is increasing (Cagan, 2011; Helmstädter et al., 2017; Hermle et al., 2017). The advantages of the model over higher organisms concern several aspects including simple and cheap husbandry, a huge number of progeny and a short life cycle. What makes *Drosophila* however stand out are the numerous ways of techniques to genetically manipulate the organism as well as the diverse publicly available fly stock libraries (Brand & Perrimon, 1993;

Hales et al., 2015; Heigwer et al., 2018; Jennings, 2011; Venken et al., 2016). These make *Drosophila* especially convenient to perform large scale screens and to study genetic interactions in a short time frame. Hence, it is worthwhile considering *Drosophila* as a 'starting point' to gain first insights into 1) the role of a protein for podocyte biology, 2) possible genetic interactors and therefore potentially unknown molecular pathways or 3) the necessity of different domains of a protein when expressing truncated variants, to give a few examples.

A further introduction into the *Drosophila melanogaster* model organism including more detailed information on nephrocyte biology, methods for nephrocyte-specific genetic manipulation as well as protocols to assess potential nephrocyte phenotypes are given in chapter 2.1 of the results part.

1.6 Research objectives

Actin dynamics and their tight regulation are essential to maintain podocyte morphology and function in health and especially disease, as rearrangements of the actin cytoskeleton is an outstanding hallmark of FPE and podocyte injury (Kriz et al., 2013; Perico et al., 2016; Sever & Schiffer, 2018). Polarity proteins are known to play a role in the organization and stabilization of F-actin, and a preliminary link between actin-regulation and differential expression of Par polarity proteins has been established (Raman et al., 2018; Scott et al., 2012). Several studies over the past years have contributed to the hypothesis that polarity signalling in podocytes seems to be different to the widely accepted concept of apico-basal polarity we know from classical epithelial cells (Hartleben et al., 2012; Koehler et al., 2016). A detailed understanding of essential polarity proteins in podocytes and their contribution to podocyte injury and FPE is therefore desirable and will potentially contribute to the development of therapeutics in the future. The overarching goal of this thesis was to gain further insights into the link between polarity signalling and actin cytoskeleton organization and to what extent loss of cytoskeletal and polarity regulation contributes to glomerular disease. Three main aims have been addressed:

1. Exploiting the genetic power of the fruit fly *Drosophila melanogaster* as advanced *in vivo* tool to study podocyte biology. This included the development of solid read outs to assess nephrocyte phenotypes on morphological and functional level. Nephrocytes are podocyte-like cells in *Drosophila* and have been emerging as model for podocytopathies over the past decade. Chapter 1 within the results part will give an overview of nephrocyte biology and ways to genetically manipulate nephrocytes as well as general protocols used in our laboratory, which are fundamental to the research questions of chapters 2 and 3.

2. Establish *Drosophila* as rapid tool to investigate the pathogenicity of newly discovered patient mutations associated with nephrotic syndrome. Here, it was of interest to exploit the genetic toolbox of *Drosophila* and the high similarity between podocytes and nephrocytes to characterize a novel ACTN4 variant identified in a paediatric patient suffering from nephrotic syndrome. ACTN4 is an actin-binding and -crosslinking protein and essential for podocyte morphology and integrity (Dandapani et al., 2007; Kaplan et al., 2000; Kos et al., 2003). This is highlighted by increased expression of the protein during

FPE (Shirato et al., 1996). By transgenic expression of the new variant and comparison to wildtype and previously known pathogenic variants of ACTN4, the aim was to draw conclusion on the pathogenicity of the variant, which ultimately affects therapeutic strategies of the clinicians. These *in vivo* experiments hereby accompanied *in silico* and *in vitro* analyses, leading to a thorough workflow described in chapter 2 of the results part as part of an experimental pipeline for our national FOrMe (Völker et al., 2019) patient registry for glomerular disease.

3. Investigating the role of the Par polarity complex for podocyte morphology and function.
   Studies identified the Par complex as component of the SD complex and knockout of *aPKCiota* but not *Par3A* in podocytes leads to severe glomerular disease in mice (Huber et al., 2009; Koehler et al., 2016). Loss of Par3A results in up-regulation of Par3B, which led to the hypothesis of a possible redundancy of the two proteins. However, studies could show that Par3B does not interact with aPKC (Gao et al., 2002; Kohjima et al., 2002), raising the question how Par3B can compensate for the loss of Par3A. It was therefore of high interest to explore the polarity proteins aPKC, Par3A as well as Par3B in more detail to understand the underlying mechanism of Par3 redundancy. The data on Par3A dispensability in podocytes have now been extended by a wide range of experimental work in the thesis at hand. Mechanistic insight into the roles of Par3A and Par3B for podocyte maintenance and podocyte disease is given in chapter 3 of the results part. First data on the role of aPKC and its different domains have recently been collected and will be added to this thesis in the appendix and incorporated into the discussion.

2 Results

Each chapter within the results part will be introduced with a short description of the major aim of the particular manuscript in the context of the complete thesis, the authors and their individual contribution to the manuscript as well as the current status of the manuscript.

2.1 Chapter 1 – *Drosophila melanogaster* and its nephrocytes: A versatile model for glomerular research

Glomerular disorders constitute the predominant cause of nephrotic syndrome and end-stage renal disease (Saran et al., 2018). Substantial research has been done over the past decades to understand underlying patho-mechanisms, yet therapeutic options other than dialysis and renal replacement therapy are still rare. To identify pathways essential for podocyte maintenance in health and disease, well-established model organisms are required. Most frequently, mice as a mammalian system are used for this purpose. The high conservation and similarity between humans and mice however come at the expense of costly husbandry, long generation times and increased administrational work. Depending on the purpose, it is therefore worthwhile considering other model organisms.

The following chapter comprises a publication in the 154th edition of the 'Methods in Cell Biology' series – 'Methods in Kidney Cell Biology' – edited by Thomas Weimbs and published in 2019. Within this publication, we introduced *Drosophila melanogaster* as a convenient model organism to assess podocyte biology. We first introduced nephrocytes as podocyte-like cells in the fly and summarized methods of genetic manipulation in *Drosophila* and specifically in nephrocytes, followed by protocols on how to dissect and isolate nephrocytes for subsequent *ex vivo* studies. Finally, we provide protocols on how to assess podocyte morphology and function by immunofluorescent stainings and tracer uptake assays, respectively.

Authors: **Johanna Odenthal** and Paul T. Brinkkötter

Author contributions:

Johanna Odenthal	–	performed the experiments and analysed the data created figures and drafted the manuscript
Paul T. Brinkkötter	–	revised the manuscript

Status:

Published in „Methods in Cell Biology”

Volume 154: “Methods in Kidney Cell Biology – Part B”, Page 217-240, 01. September 2019

Published online: 30. April 2019

Citation:

Odenthal J, Brinkkoetter PT. Drosophila melanogaster and its nephrocytes: A versatile model for glomerular research. Methods Cell Biol. 2019; 154:217-240.

doi: 10.1016/bs.mcb.2019.03.011

PMID: 31493819

CHAPTER

12

Drosophila melanogaster and its nephrocytes: A versatile model for glomerular research

Johanna Odenthal[a,b], **Paul Thomas Brinkkoetter**[a,b,*]

[a]*Department II of Internal Medicine and Center for Molecular Medicine Cologne, University of Cologne, Faculty of Medicine and University Hospital Cologne, Cologne, Germany*

[b]*CECAD, University of Cologne, Faculty of Medicine and University Hospital Cologne, Cologne, Germany*

**Corresponding author: e-mail address: paul.brinkkoetter@uk-koeln.de*

Chapter outline

Methods in Cell Biology, Volume 154, ISSN 0091-679X, https://doi.org/10.1016/bs.mcb.2019.03.011

Abstract

Glomerular disorders are a predominant cause of chronic kidney diseases and end-stage renal failure. Especially podocytes, epithelial cells which represent the outermost part of the filtration barrier, are affected by disease and experience a gradual loss of function. Despite recent advances in identifying potential pathways underlying podocyte injury, treatment remains challenging. It is therefore desirable to employ suitable model organisms in order to study glomerular disease and elucidate affected pathways. Due to its diverse ways of genetic manipulation and high genomic conservation, *Drosophila melanogaster* is a powerful model organism for biomedical research. The fly was recently used to assess podocytopathies by exploiting the nephrocyte system. Nephrocytes are spherical cells within the body cavity of the fly responsible for detoxification and clearance of unwanted substances. More importantly, they share many characteristics with mammalian podocytes. Here, we summarize how to use *Drosophila* as a model organism for podocyte research. We discuss examples of techniques that can be used to genetically manipulate nephrocytes and provide protocols for nephrocyte isolation and for morphological as well as functional analysis.

1 Introduction

Chronic kidney diseases (CKDs) are often characterized by the gradual loss of kidney function. Disorders affecting the kidney's filtration units, glomeruli, account for the majority of CKD cases (Saran et al., 2018; Wanner et al., 2014). Initially, most individuals affected by CKD do not present with clinical symptoms or critical limitations and, as a consequence, the disease usually remains undiscovered and progresses silently. This not only puts patients at high risk for end-stage renal failure as such. More importantly, CKD patients have a significantly increased prevalence to develop cardiovascular diseases, making CKD an independent risk factor for cardiovascular mortality (Sarnak et al., 2003; Tonelli et al., 2012). Despite continuous progress in understanding the underlying causes and histological pattern of CKD, therapeutic interventions remain symptomatic and dialysis and renal replacement therapy continue to be the ultimate options. Specific therapies are scarce. Hence, it is important to further study the structure and function of the glomerular filtration barrier and to unveil the patho-mechanisms of CKD in more detail.

The filtration barrier comprises three well-defined anatomical layers: fenestrated capillary epithelial cells, the glomerular basement membrane and glomerular podocytes which form a narrow filtration slit (Fig. 1B) (Haraldsson, Nyström, & Deen, 2008). Podocytes are specialized, terminally differentiated epithelial cells

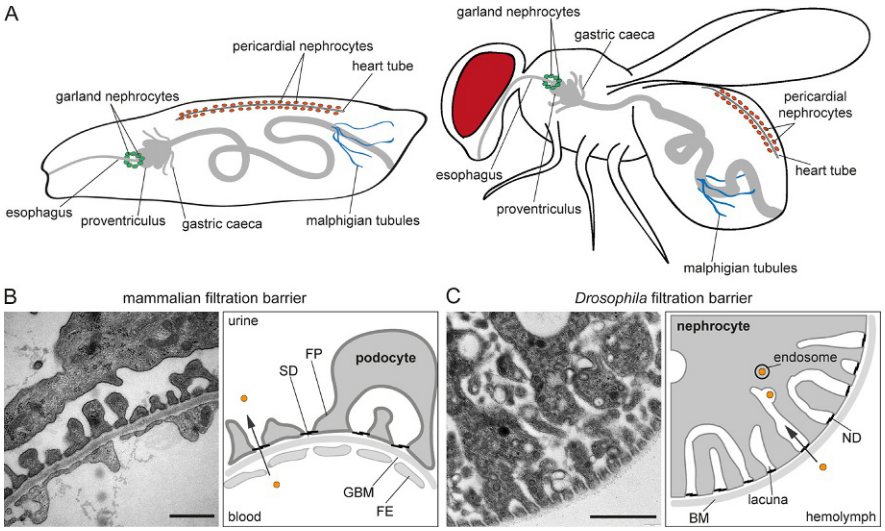

FIG. 1

Nephrocytes are podocyte-like cells in *Drosophila melanogaster*. (A) Schematic drawing of *Drosophila* in the larval stage (left) and the adult animal (right), respectively. The renal system consists of malphigian tubules and two distinct clusters of nephrocytes. Garland nephrocytes localize as a necklace around the junction of esophagus and proventriculus. Pericardial nephrocytes flank the heart tube. (B–C) Comparison of the filtration barrier of mammals and *Drosophila*. Transmission electron micrographs and its schematic representation are shown. (B) The mammalian filtration apparatus is three layered, comprising fenestrated epithelium (FE) of the capillary, the glomerular basement membrane (GBM) and the slit diaphragm (SD). The latter is established as unique cell-cell contact between foot processes (FPs) of neighboring podocytes. (C) Nephrocytes, which are considered podocyte-like cells, are responsible for clearing the hemolymph of toxic substances in *Drosophila*. They show numerous membrane invaginations which are flanked by foot processes. The filtration barrier consists of the basement membrane (BM) surrounding the spherical cell, as well as the nephrocyte diaphragm (ND). After entering the lacunae, substances are endocytosed by the nephrocyte. Scale bars in TEM pictures represent 1 μm.

characterized by their distinct three-dimensional architecture as they project numerous foot processes which completely enwrap the glomerular capillaries. Foot processes of neighboring podocytes interdigitate whereby the slit diaphragm (SD) is established as a unique cell-cell contact between adjacent podocytes (Fig. 1B) (Brinkkoetter, Ising, & Benzing, 2013; Huber & Benzing, 2005; Pavenstädt, Kriz, & Kretzler, 2003). This membranous structure is formed by interaction of transmembrane proteins Nephrin and Neph1 (Donoviel et al., 2001; Kestilä et al., 1998; Rodewald & Karnovsky, 1974). These bridge a slit of approximately 40 nm width and are the outermost barrier that holds back macromolecules larger than

65 kDa (Brenner, Hostetter, & Humes, 1978; Rennke & Venkatachalam, 1979). In most cases, patients suffering from glomerular diseases present with podocyte damage resulting in a common ultrastructural finding known as "foot process effacement" (D'Agati, 2003; Deegens et al., 2008). This is characterized by drastic alterations of the podocyte's cyto-architecture such as flattening of foot processes and, eventually, loss of podocytes, leading to severe filtration defects and, ultimately, increasing amounts of proteinuria.

In the past decades, the pathogenesis of progressive kidney disease became clearer. The first models to study podocyte biology in more detail were cell culture models (Ni, Saleem, & Mathieson, 2012; Shankland, Pippin, Reiser, & Mundel, 2007). "Podocytes in a dish" can be modified on gene and protein level or challenged externally by manipulating environmental conditions. Various podocyte cell lines obtained from human, mouse or rat renal tissue are available and widely used (Kambham et al., 2000; Kohli et al., 2014; Mele et al., 2011). As well established these cell culture systems have become over the years, they come with certain limitations. Podocytes are cultured in the absence of other glomerular cells such as mesangial or endothelial cells and are not exposed to mechanical forces usually mediated by urine flow and the filtration pressure (Endlich, Kliewe, & Endlich, 2017). Moreover, the unique architecture of podocytes is completely abolished in cell culture as cells do not form foot processes nor a slit diaphragm and expression of podocyte specific proteins such as Nephrin and Podocin is nearly undetectable (Garg, Verma, Nihalani, Johnstone, & Holzman, 2007; Huber et al., 2003; Rinschen et al., 2016; Schroeter et al., 2018). Thus, it is inevitable to make use of an *in vivo* system for more detailed analysis on how the filtration apparatus is constituted and functions. In this context, mammalian models such as rodents are widely used and often considered to be the model system of choice. However, researchers are restricted and less flexible due to costly maintenance, a long reproductive cycle and, lastly, strict regulations placed by the respective authorities. Therefore, additional *in vivo* models have to be considered that can accompany or complement mouse experiments.

The fruit fly *Drosophila melanogaster* has raised attention over the past years also with regards to modeling renal disease. Flies have an open circulatory system where excretory organs lay freely in the body cavity and are bathed in hemolymph, the fly's blood equivalent (Fig. 1A) (Kovalevsky, 1889; Schmidt-Rhaesa, 2007). The excretory system consists of physically distinct components: the Malpighian tubules, analogous to renal tubules, and nephrocytes, equivalents to the glomerular part of the mammalian kidney (Denholm & Skaer, 2009). Nephrocytes are specialized spherical cells whose primary function is to perform filtration and, subsequently, endocytosis of unwanted substances from the hemolymph regulating hemolymph composition. Hence, they are responsible for detoxification and maintenance of water, salt and pH homeostasis. Nephrocytes were first described in the 19th century as storage kidneys that take up multiple compounds (Kovalevsky, 1886) and over the past century, the ultrastructure of these cells was described in more detail: *Drosophila* comprises two clusters of nephrocytes – the garland nephrocytes associated with the esophagus as well as pericardial nephrocytes located along the heart tube

(Fig. 1A) (Denholm & Skaer, 2009). They form multiple in-foldings of the plasma membrane, so-called labyrinthine channels or lacunae, which are flanked by cellular protrusions often simplified as "foot processes" (Fig. 1C) (Aggarwal & King, 1967; Crossley, 1972; Mills & King, 1965). The ca. 30 nm wide entrance of these invaginations is bridged by a diaphragm structure and the whole cell is surrounded by a basement membrane (Fig. 1C). In 2009, Weavers et al. as well as Zhuang et al. independently contributed the molecular proof for nephrocytes to be podocyte-like cells (Weavers et al., 2009; Zhuang et al., 2009). The nephrocyte diaphragm (ND) is established by interaction of transmembrane proteins Sticks and stones (Sns) and Dumbfounded (Duf) (also known as Kirre), which are the homologs of mammalian SD components Nephrin and Neph1, respectively. Proteins that interact with mammalian SD proteins such as Zonula occludens-1 (ZO-1) and Podocin likewise have respective homologs in *Drosophila* which are located at the ND (Weavers et al., 2009), indicating that molecular pathways can be studied in these podocyte-equivalents. In the following chapter, we will introduce the *Drosophila* model to study glomerular function in more detail and describe principles of targeted genetic modification in nephrocytes. We further show how to dissect nephrocytes from the animals and provide protocols for immunofluorescence and tracer uptake assays used to study nephrocytes on a morphological and functional level.

2 Nephrocyte specific genetic modification in *Drosophila melanogaster*

2.1 Overview

Drosophila melanogaster has become a highly valued model organism in biomedical research. More than 75% of human disease associated genes are conserved and have an identified homolog in the fly genome (Reiter, Potocki, Chien, Gribskov, & Bier, 2001). *Drosophila* husbandry is cheap and simple and experimental permission can be arranged quite easily. The *Drosophila* life cycle is relatively short and temperature dependent: at 25 °C, embryogenesis and the larval stages one and two each take approx. 24 h whereas the third larval stage takes 2 days. After larval development, the holometabolous insects pupate and undergo metamorphosis for approx. 5 days. Adult flies (imagos) finally eclose from the puparium 9–10 days after egg laying (Ashburner, 1989). Due to this short generation time, data can be collected in a reasonable time frame as compared to higher organisms. Besides the beneficial factors of cost and time, it is the broad range of genetic tools which make *Drosophila* stand out. The fly's genome has a reduced size (180 Mb) and encodes for about 13,900 genes that are distributed over four chromosomes: the gonosomes X or Y, also referred to as first chromosome, and three autosomes, the second–fourth chromosome (Hales, Korey, Larracuente, & Roberts, 2015). This simplicity made it possible to perform chemical as well as transposable element-mediated mutagenesis on a large scale and a resulting mutant-library can be ordered from stock centers. Genomic

engineering approaches have evolved drastically in the past decades. As the fly's genome is fully sequenced and well annotated (Adams et al., 2000; Myers et al., 2000), genes of interest can be targeted by homologous recombination, CrispR/Cas9 or RNA interference approaches to name a few. In the following, we want to introduce the well-established *GAL4-UAS*-System for spatial and temporal modifications on gene and protein level and give an understanding of how protein expression can be altered specifically in nephrocytes. For further information on basic *Drosophila* husbandry, genetics and mating schemes we refer to the book "Fly Pushing: the theory and practice of *Drosophila* genetics" (Greenspan, 2004).

2.2 The *GAL4-UAS*-system for targeted genetic manipulation in nephrocytes

Being able to introduce transgenes into the fly using a range of genetic tools enables researchers to recapitulate human diseases in order to study their underlying pathomechanisms. Since its first description in 1993, the conventional *GAL4-Upstream Activator Sequence (UAS)*-System has proven to be the most applied and powerful genetic tool for transgenic expression in this context (Brand & Perrimon, 1993). Based on the *Saccharomyces cerevisiae* transcription factor GAL4, it can be used for spatial and temporal expression of transgenic constructs. The approach is bipartite, meaning that two parental fly lines are required (Fig. 2A). One line, the driver line, harbors the GAL4 transcription factor under the control of an endogenous promotor or enhancer. As a result of this, GAL4 expression can be targeted to a specific tissue or cell type. The second line, known as the effector line, comprises a target gene under control of a UAS, the GAL4 binding motif. Both parental lines are phenotypically unaffected and considered wild-typic, as the two constructs, GAL4 and its binding motif, are held separately. After crossing driver and effector line, both constructs are combined, and transgenes will be expressed in the GAL4 specific tissue or cell type (Fig. 2A). GAL4 is temperature sensitive and a shift from 25 °C to 29 °C, for example, will lead to increased GAL4 activity. Thus, transgene expression can be controlled by the temperature at which crosses are raised and maintained.

GAL4-driver lines are publicly available or passed down in the fly community. For nephrocyte "specific" transgene expression, a number of different driver lines have been described in the past. The most frequently used ones (see Table 1) are *Dorothy-GAL4* (*dot-GAL4*, Kimbrell et al., 2002; Zhang, Zhao, & Han, 2013), *Sticks and Stones-GAL4* (*Sns-GAL4*, Kocherlakota et al., 2008; Zhuang et al., 2009), and *Hand-GAL4* (Hermle, Braun, Helmstädter, Huber, & Hildebrandt, 2017; Sellin et al., 2006). They are characterized by GAL4 expression in both, the garland and pericardial nephrocyte population. In contrast, *prospero-GAL4* (*pros-GAL4*, Ohshiro et al., 2000; Weavers et al., 2009) has rather been utilized for garland nephrocytes. Each of these driver lines was employed for studies in larval stages, whereas *dot-GAL4*, *Sns-GAL4* as well as *Hand-GAL4* have also been used for analyses in adult flies. In addition and not utilized as frequently, the *G447.2-GAL4*

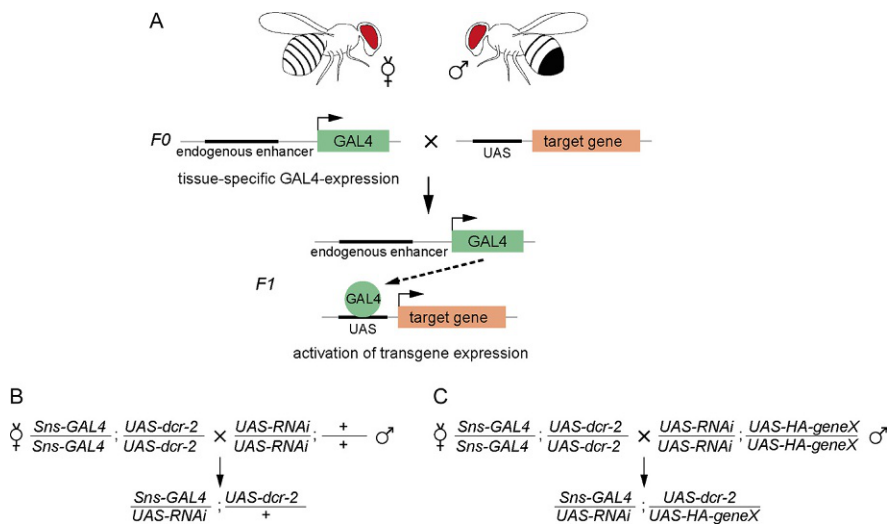

FIG. 2

The *GAL4-UAS*-System is used for nephrocyte specific genetic manipulation. (A) Schematic of the bipartite *GAL4-Upstream Activating Sequence (UAS)*-System for targeted genetic interventions. Necessary are two parental fly lines (F0): the driver line comprises the yeast transcription factor GAL4 under the control of an endogenous enhancer. The effector line harbors a target gene of interest downstream of a UAS-binding motif. Upon crossing driver and effector line, GAL4 will bind the UAS and thereby initiate transcription of the target gene. Transgenes can thereby be restrictively expressed in only those cells or tissues in which the enhancer of the utilized *GAL4*-driver line is active. (B–C) Mating scheme for nephrocyte specific knockdown (B) and rescue (C) experiments using homozygous viable fly lines. For simplification, only chromosomes two and three are depicted (chromosomes are separated by semicolon; + = wildtype chromosome). (B) To achieve a nephrocyte specific knockdown, virgin females of the *Sns-GAL4*-driver line are crossed to males of a *UAS-RNAi* line. The F1 generation all comprise a single copy of the respective constructs. In addition, the *Sns-GAL4*-driver line harbors a *UAS-dcr-2*-construct, leading to expression of the Dicer-2 protein and thereby increased knockdown efficiency. (C) For rescue experiments, virgins of the homozygous *Sns-Gal4; UAS-dcr-2* line are crossed to males of a line harboring both, a *UAS-RNAi*- as well as an overexpression construct (*UAS-HA-geneX*) in homozygosity. All progeny will have the same genotype and nephrocytes specifically will express an HA-tagged Protein-X in the knockdown background.

driver was reported to target embryonic garland nephrocytes (Weavers et al., 2009). All of the above described driver lines do not exclusively exhibit GAL4 expression in nephrocytes and a detailed study on the expression profiles of these driver lines is currently missing. Expression data of the respective genes whose enhancer regulate GAL4 transcription is summarized in Table 1 and can also be found on

Table 1 Most common nephrocyte *GAL4*-driver lines and their expression profile.

Name	Reference	Associated gene	Expression data of associated gene
Sns-GAL4	Kocherlakota, Wu, McDermott, and Abmayr (2008)	*sticks and stones* (CG33141)	– Embryonic, larval and adult garland and pericardial cell (Weavers et al., 2009) – Interommatidial cell (Hoehne, Gert de Couet, Stuermer, & Fischbach, 2005) – Differentiated myoblasts (Gildor, Schejter, & Shilo, 2012)
Dot-GAL4	Kimbrell, Hice, Bolduc, Kleinhesselink, and Beckingham, (2002)	*Ugt36A1* (CG2788) (encoding the Dorothy protein)	– Embryonic and larval lymph gland (Honti et al., 2010) – Embryonic and larval garland and pericardial cell (Lim, Wang, Chen, Ocorr, & Bodmer, 2014; Pendse et al., 2013) – Adult pericardial cell (Hartley, Motamedchaboki, Bodmer, & Ocorr, 2016; Lim et al., 2014)
Hand-GAL4	Sellin, Albrecht, Kölsch, and Paululat (2006)	*Hand* (CG18144)	– Heart, muscle fiber, dorsal vessel, cardial cell, pericardial and garland cell from embryonic through to adult stages (Das, Ashoka, Aradhya, & Inamdar, 2008; Sellin et al., 2006)
pros-GAL4	Ohshiro, Yagami, Zhang, and Matsuzaki (2000)	*prospero* (CG17288)	– Embroyonic and larval garland cell (Tutor, Prieto-Sánchez, & Ruiz-Gómez, 2014; Vaessin et al., 1991; Weavers et al., 2009) – Embryonic, larval and adult central nervous system and neuroblasts (Doe, Chu-LaGraff, Wright, & Scott, 1991; Micchelli & Perrimon, 2006; Vaessin et al., 1991)

Information on expression data summarized from FlyBase (FB2018_06).

FlyBase (https://www.flybase.org, Thurmond et al., 2019). In most cases, the extra-nephrocyte expression of GAL4 and the concomitant expression of transgenes in other tissues or cells does not prevent from morphological and functional analyses of the nephrocyte itself. It should however be considered when recording systemic phenotypes such as larval development.

Taken together, the *GAL4-UAS*-System allows for cell specific targeting of nephrocytes. Depending on the choice of transgene, it can be used for depletion or overexpression of proteins, as described in the following.

2.3 Achieving gene silencing in nephrocytes via RNA interference

A simple way to mimic protein loss-of-function is by silencing the gene of interest post-transcriptionally. A well-established approach utilizes the RNA interference (RNAi) pathway: Overexpression of long double stranded RNA (dsRNA) or short hairpin RNAs (shRNAs) in *Drosophila* leads to degradation of the targeted, partly complementary mRNA resulting in decreased protein levels and eventually in a knockdown (Heigwer, Port, & Boutros, 2018; Tomari & Zamore, 2005).

In the past decade, several consortia have contributed to the development of an off-the-shelf *Drosophila* RNAi library. Ready to use fly strains in which expression of the interfering RNA is under UAS control, are publicly available and can be ordered from the *National Institute of Genetics* (NIG; https://shigen.nig.ac.jp/fly/nigfly/), the *Vienna Drosophila Resource Center* (VDRC; Dietzl et al., 2007; https://stockcenter.vdrc.at) as well as the *Bloomington Drosophila Stock Center* (BDSC; https://bdsc.indiana.edu/). The NIG was the first institute to make RNAi strains and offer them for distribution in the fly community. The approach uses long dsRNAs under UAS control which are integrated randomly into the genome by P-element-mediated insertion (Hummel & Klämbt, 2008). Currently, the NIG collection comprises approx. 11,000 RNAi lines. The VDRC offers RNAi lines of three independent collections (the GD-, KK- and shRNA-collection), thereby covering around 12,000 protein-coding genes. The main difference of the libraries concerns the integration mechanism of the inducible *UAS-RNAi*-constructs. The GD-collection was established using a P-element-mediated approach whereby construct insertion occurs randomly (Dietzl et al., 2007). The *UAS-RNAi*-constructs are mapped to a chromosome (X, 2 or 3), but the actual insertion site remains unknown, resulting in varying expression levels of the RNAi transgenes, depending on its integration site. In contrast, integration of *UAS-RNAi*-constructs of the KK-collection as well as the shRNA-collection is based on phiC31-recombinase-activity where specific docking sites are targeted (Bischof, Maeda, Hediger, Karch, & Basler, 2007). This approach comes with the advantage of avoiding integration-dependent differences on the level of transgene expression and the viability of the *UAS-RNAi* line itself. A similar approach was followed by the Transgenic RNAi Project (TRiP) at Harvard Medical School (http://www.flyrnai.org; Perkins et al., 2015). Also here, *UAS-hairpin RNA*-constructs are inserted by a phiC31-approach at two distinct integrations sites, on the second and third chromosome, respectively. Since 2008, the TRiP generated over 12,000 RNAi lines and are continuing to expand the collection, which is distributed to the community through the BDSC.

As the interfering RNAs are under control of a UAS, lines can be crossed to any *GAL4*-driver line to silence the respective gene in a spatially and/or temporally controlled manner. A mating scheme for RNAi mediated knockdown is exemplified in Fig. 2B. The parental generation is homozygous for either the *GAL4*-driver or the *UAS-RNAi*-construct. Therefore, all progeny harbors one copy of the respective constructs. Heterozygous *GAL4*-driver or *UAS-RNAi* lines can also be employed. In this case, identification of the correct genotype among the progeny is mediated by using

balancer chromosomes (Greenspan, 2004). In our example, the *Sns-GAL4*-driver line was furthermore combined with a *UAS-dcr-2*-construct which leads to overexpression of the Dicer-2 (Dcr-2) protein (Fig. 2B). Dcr-2 is part of the RNAi machinery, where it functions as a double-stranded RNA specific endonuclease responsible for processing long dsRNA into short siRNA (Lee et al., 2004). A simultaneous expression of Dcr-2 enhances RNAi efficiency (Dietzl et al., 2007). There are several *UAS-dcr-2* lines available on the X, second and third chromosome, respectively, fitting into all mating schemes. They are offered at the RNAi-line distributer's websites.

A draw-back of RNAi technology are possible false-positive results due to off-target effects (Ma, Creanga, Lum, & Beachy, 2006). These can appear upon unintentional targeting of other, partially homologous mRNA sequences. Therefore, it is recommended to perform experiments with at least two independent *UAS-RNAi*-constructs that target different parts of the respective mRNA. A different approach to achieve nephrocyte specific loss-of-function was recently introduced by Hermle et al. (2017). The authors performed a CrispR/Cas9-mediated knockout specifically in nephrocytes. Hereby, the expression of Cas9, which is under the control of a UAS (lines available at the BDSC), was restricted to nephrocytes and initiated by using the *Hand-GAL4*-driver. The guide RNA, targeting the gene of interest, on the other side was expressed ubiquitously under control of the dU6:1 promotor. The plasmid for gRNA integration into the fly was established by Port, Chen, Lee, and Bullock (2014) and can be obtained from addgene (pCDF4, #49411; https://www.addgene.org/).

2.4 Transgenic expression of proteins in nephrocytes

Early-onset CKDs (disease onset before the age of 25) such as steroid resistant nephrotic syndrome are often characterized by mutations in a single gene. To date, numerous of such disease associated genes and their specific base alterations have been identified by sequencing patient samples (Vivante & Hildebrandt, 2016). Recent studies exploited the nephrocyte system to study the function of mammalian renal proteins and their specific mutant alleles. Here, we will describe how these genes can be introduced into the fly genome and be expressed in nephrocytes transgenically. In combination with the previously described RNAi approach (see Section 2.3), it is possible to replace the fly protein with the human homolog and therefore study function and, if applicable, mutation-related phenotypes of the disease associated protein in more detail.

As knockdown of the endogenous fly protein is achieved in a *GAL4-UAS*-mediated fashion, it is necessary to subclone the cDNA of the respective human disease gene into a plasmid providing a UAS-motif. Integration of the generated plasmid is done by injecting *Drosophila* embryos. This transgenic service is offered by companies such as BestGene (https://www.thebestgene.com/) or GenetiVision (http://www.genetivison.com). A range of vectors that harbor a UAS-motif can be obtained from the *Drosophila Genomics Resource Center* (DGRC; https://dgrc.bio.indiana.edu). The original pUASt vector described in 1993 (Brand &

Perrimon, 1993, DGRC#1000), for example, can be used for P-element-mediated random integration into the genome. This vector has to date be modified in much extend so that a palette of fusion proteins with different tags can be generated and integrated into the fly. Other vectors are based on homologous recombination and follow the gateway system (Hartley, Temple, & Brasch, 2000). The plasmids comprise a gateway cassette for phiC31-integrase-mediated integration into specific docking sites. Transgenic companies provide different founder lines for this purpose. One can commission integration into different attP landing sites, covering all chromosomes, and therefore define a distinct integration locus. In Fig. 2C, we give an example of a mating scheme for simultaneous expression of a *UAS-RNAi*-construct and an HA-tagged protein (*HA-gene-X*) from our own laboratory. For this purpose, the pTHW vector (DGRC #1099), providing the HA-tag, was used for site-specific integration of *gene-X* into the P2(3L)68A4 docking site (transgenesis by GenetiVision). The HA-tag hereby allows for detection of the transgenic protein so that it's proper expression can be validated.

3 Dissection of nephrocytes in larvae and adult flies

3.1 Overview

As described above, *Drosophila* has two subsets of nephrocytes: garland nephrocytes as well as pericardial nephrocytes (Fig. 1A). Garland nephrocytes (GNs) are located in proximity of the foregut. Here, they build a chain (a garland) of cells that surround the junction of esophagus and proventriculus/cardia. Toward the end of embryogenesis, GNs undergo a fusion process leading to binucleated cells which makes them easily identifiable (Zhuang et al., 2009). Pericardial nephrocytes on the other hand can be found in two rows of approximately 20 cells flanking both sides of the heart tube (Denholm & Skaer, 2009; Sellin et al., 2006). Both nephrocyte populations originate from mesodermal precursor cells and require *Drosophila* Krüppel-like factor 15 (dKLF15) for differentiation, the functional homolog of the mammalian podocyte differentiation factor KLF15 (Ivy et al., 2015; Mallipattu et al., 2012). For further reading on biology and development of nephrocytes as well as utilization of the nephrocyte system, we refer to excellent previous reviews (Cagan, 2011; Denholm & Skaer, 2009; Helmstädter, Huber, & Hermle, 2017; Helmstädter & Simons, 2017; Simons & Huber, 2009). GNs and PNs are both frequently utilized for morphological and functional analyses. We will here demonstrate how nephrocytes can be dissected from third instar larvae as well as adult flies. Depending on the application for which they are isolated, they can be dissected in phosphate buffered saline (PBS) (for immunofluorescence or immunohistochemistry) or, as recommended for *ex vivo* assays prior to fixation, in hemolymph like medium (HL3, Stewart, Atwood, Renger, Wang, & Wu, 1994) or Schneider's S2 medium to ensure best possible physiological conditions.

3.2 Dissection of garland nephrocytes in third instar larvae

3.2.1 Materials and reagents (*Fig. 3A*)

- Dissection medium (HL3; 70 mM NaCl, 5 mM KCl, 1.5 mM $CaCl_2 \cdot 2H_2O$, 20 mM $MgCl_2 \cdot 6H_2O$, 10 mM $NaHCO_3$, 5 mM Trehalose, 115 mM Sucrose, 5 mM HEPES; Stewart et al., 1994)
- Staining block, glass (VWR, #631-9301)
- Dissection dish (5 cm plastic dish filled with Sylgard™ 184 Silicone Elastomer)
- Dumont #5 and #55 forceps (World Precision Instruments, #14098 and # 14099)
- Vannas scissors (World Precision Instruments, #500086)
- Stereo dissecting microscope

3.2.2 Method

Prior to dissection, larvae should be rinsed with water or 1 × PBS in a staining block to wash off remaining food traces. They are then transferred to a dissection dish filled with cold dissection medium.

1. Fix the larva with the help of forceps in the head region (Fig. 3B). Remove the anterior head part at the level of the anterior spiracles (Fig. 3B, dashed line) with

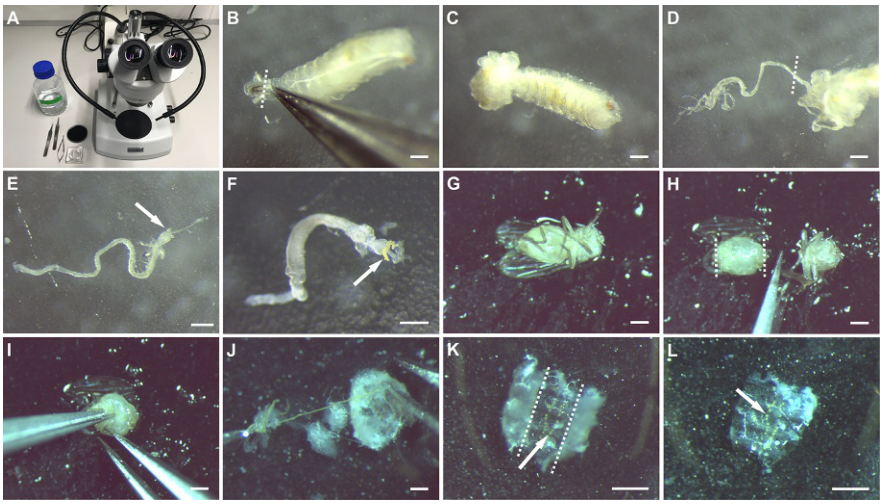

FIG. 3

Dissections of nephrocytes in *Drosophila* larvae and adults. (A–L) Pictures depicting the individual steps conducted for nephrocyte dissection. For visualization, fly food was supplemented with silver nitrate as described in Weavers et al. (2009). (A) Material for nephrocyte dissection. (B–F) Dissection of garland nephrocytes in third instar wandering larvae. (G–H) Pericardial nephrocyte dissection in adults. All scale bars represent 500 μm. Dashed lines in B, D, H, and K show cutting lines. Arrows in E, F, K and L point to nephrocytes. For description of the individual steps see Sections 3.2.2 and 3.3.2.

forceps or vannas scissors (the latter will help to precisely separate the foregut from the mouth hooks). The inner organs emerge and the esophagus will eventually be exposed (Fig. 3C).
2. Grab any part of the gut or the exposed esophagus and pull out the intestine as much as possible (Fig. 3D).
3. Detach the midgut as much as you prefer (Fig. 3D, dashed line). For further handling in Eppendorf tubes, we recommend to leave a fair amount of tissue attached to the proventriculus, so that the tissue is still detectable by eyesight and sinks by its weight.
4. Remove the gastric caeca from the midgut (Fig. 3E). This will prevent them to rest on the nephrocytes when mounted.
5. Transfer the tissue with forceps into Eppendorf tubes or PCR tubes containing fixative for the respective application (formaldehyde or paraformaldehyde for immunofluorescence; glutaraldehyde for electron microscopic analyses).

3.3 Dissection of pericardial nephrocytes in adult flies

3.3.1 Materials and reagents

- Dissection medium (HL3; 70 mM NaCl, 5 mM KCl, 1.5 mM $CaCl_2 \cdot 2H_2O$, 20 mM $MgCl_2 \cdot 6H_2O$, 10 mM $NaHCO_3$, 5 mM Trehalose, 115 mM Sucrose, 5 mM HEPES; Stewart et al., 1994)
- Dissection dish (5 cm plastic dish filled with Sylgard™ 184 Silicone Elastomer)
- Dumont #5 and #55 forceps (World Precision Instruments, #14098 and #14099)
- Vannas scissors (World Precision Instruments, #500086)
- Stereo dissection microscope

3.3.2 Method

Prior to dissection, the flies are anesthetized with CO_2 and the head is cut off from the thorax and abdomen with forceps or vannas scissors. Then, the bodies are transferred to a dissection dish filled with dissection medium.

1. Position the fly with the ventral side facing upwards and fix the thorax region with forceps (Fig. 3G). Now, with the help of vannas scissors, perform two sections orthogonally to the anterior-posterior axis at the anterior part of the abdomen as well as the posterior end of the fly, respectively (Fig. 3H, dashed lines).
2. The abdomen is now detached and is open at both ends. With vannas scissors, perform a straight cut from the posterior opening toward the anterior opening following the abdomen's centerline (Fig. 3I).
3. The abdomen can now be unfolded. Clear out the remaining inner organs (Fig. 3J) and cut off the lateral parts of the cuticle (Fig. 3K, dashed lines). The heart and nephrocytes (Fig. 3L, arrow) are still attached to the cuticle and can now be fixed or processed otherwise (Fig. 3L).

4 Immunofluorescent staining in garland nephrocytes

4.1 Overview

Although considered as complementary to electron microscopy, which gives a much better depiction of the nephrocyte's architecture and distinct structure, immunofluorescence (IF) gives a first insight into possible phenotypes arising from genetic interventions. For example, staining with antibodies for ND proteins Sns or Duf can reveal if the proteins are correctly localized to the outer aspect of the cell and whether NDs are present. Moreover, IF is surely mandatory to assess proper expression of transgenic proteins or to validate knockdown efficiency when overexpressing *UAS-RNAi*-constructs. Here, we provide a protocol for IF in garland nephrocytes and, as an example, depict staining for Duf in a control line (*Sns-GAL4>GFP-RNAi*) as well as a line depleted for Duf (*Sns-GAL4>duf-RNAi*) (Fig. 4). For this, we crossed *Sns-GAL4;UAS-dcr-2* (Dietzl et al., 2007; Kocherlakota et al., 2008) with *UAS-GFP-RNAi* (BDSC #41553) and *UAS-duf-RNAi* (VDRC #109585), respectively, and flies were maintained at 25 °C. We co-stained the nephrocytes with anti-HRP, which is known to detect an epitope on nephrocytes as well as neurons in *Drosophila* (Jan & Jan, 1982; Weavers et al., 2009).

4.2 Materials and reagents

- Dissection medium (HL3; 70 mM NaCl, 5 mM KCl, 1.5 mM $CaCl_2 \cdot 2H_2O$, 20 mM $MgCl_2 \cdot 6H_2O$, 10 mM $NaHCO_3$, 5 mM Trehalose, 115 mM Sucrose, 5 mM HEPES; Stewart et al., 1994)
- Formaldehyde solution 37% (FA, Roth #4979)
- Methanol (optional)
- Wash buffer (0.3% Triton-X and 0.5% bovine serum albumin in 1 × PBS)
- Normal donkey serum (NDS, Jackson ImmunoResearch, #017-000-121)
- Primary antibodies (goat-anti-HRP, 1:200, Jackson ImmunoResearch #123-005-021; rabbit-anti-Duf, 1:100, kind gift from Barry Denholm)
- Secondary antibodies (Jackson ImmunoResearch; donkey-anti-goat-Cy3 #705-165-033; donkey-anti-rabbit-Alexa488 #711-545-152)
- Vectashield mounting medium with DAPI (Linaris, H-1200)

4.3 Method

All steps are performed at room temperature if not specified otherwise. We recommend conducting all steps in 200 µL final volume.

1. Dissect nephrocytes in cold dissection medium (as described in Section 3.2) and collect the tissue of 10 larvae in 3.7% FA in 1 × PBS in a 1.5 mL Eppendorf or PCR tube on ice until all samples are prepared.
2. Fix for 20 min at room temperature. Depending on the antibody an additional fixation in methanol for a minimum of 1 h might be beneficial.

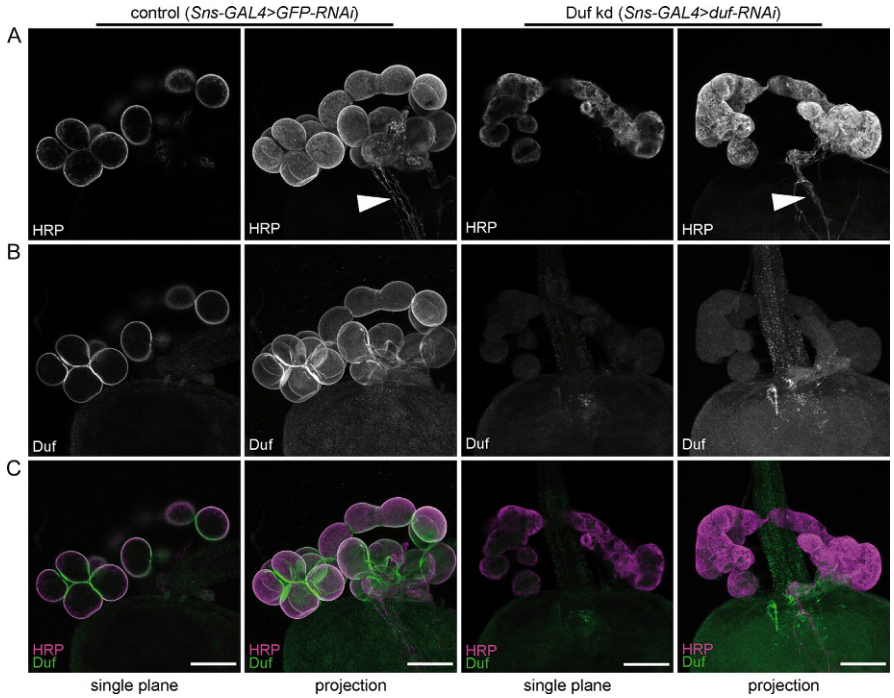

FIG. 4

Immunofluorescene for knockdown validation and morphological analysis. Garland nephrocytes of third instar control larvae (*Sns-GAL4>GFP-RNAi*) and Duf knockdown larvae (Duf kd; *Sns-GAL4> duf-RNAi*) were stained with anti-HRP and anti-Duf antibodies. (A) HRP single channel shown in gray. The HRP antibody can be used to identify nephrocytes, as it is described to detect glycoproteins on membranes of nephrocytes as well as neurons (arrowhead) in *Drosophila* (Jan & Jan, 1982; Weavers et al., 2009). In control animals, HRP staining appears as a ring-like structure and a chain of individual cells can be observed. Upon knockdown of Duf, a fusion of nephrocytes can be noticed as it has previously been described in Duf mutants and Duf knockdown animals (Helmstädter et al., 2012; Hermle et al., 2017). (B) Duf single channel shown in gray. As a component of the nephrocyte diaphragm, Duf is localized to the outermost border of the cell, leading to a ring-like structure in control animals. When depleting Duf levels, no specific signal can be detected in the Duf channel which validates knockdown efficiency. (C) HRP (magenta) and Duf (green) channels presented as composite image. Scale bars represent 50 μm in all micrographs. Projection show maximum intensity projection from a z-stack of approx. 70 slices.

3. Carefully pipette off the fixative. The tissue can still be covered with a bit of liquid. Rinse 1 × and wash the samples 3 × 15 min in wash buffer.
4. Incubate with primary antibodies diluted in wash buffer over night at 4 °C.
5. The next day, rinse 1 × and wash 3 × 15 min in wash buffer. Afterward, block with 5% NDS in wash buffer for 30 min.

6. Incubate with secondary antibodies diluted in wash buffer for 2 h in the dark.
7. Rinse 1 × and wash 3 × 15 min in wash buffer before mounting the tissue. For this, put a drop of mounting medium on a microscope slide and carefully pipette the tissue into the medium without transferring too much liquid. Unscramble the individual samples and seal with a cover slip.

5 Tracer uptake assays as functional readouts

5.1 Overview

Nephrocytes are part of the fly's waste disposal system and detoxify the hemolymph to ensure a homeostatic state. The process of detoxification involves an interplay of filtration and endocytosis: molecules smaller than approximately 70 kDa are filtered by the nephrocyte diaphragm and enter the labyrinthine channels, where they are eventually taken up by the cell *via* receptor mediated endocytosis and degraded or stored intracellularly (Fig. 1C) (Hermle et al., 2017; Zhang, Zhao, Chao, Muir, & Han, 2013). Due to the presence of a filtration apparatus but also the high endocytic activity, nephrocytes share characteristics of both, podocytes and tubular cells (Zhang, Zhao, Chao, et al., 2013; Zhang, Zhao, & Han, 2013). The nephrocyte's capacity of taking up molecules is actively connected to a proper constitution of the ND. A defective ND, mediated by loss of the ND protein Sticks and stones, leads to decreased labyrinthine channel area and abolished endocytic activity (Hermle et al., 2017). Hence, the ability to take up molecules from the hemolymph can be exploited as a functional assay to analyze possible defects within the nephrocyte. The first tracer uptake assays were performed by Kovalevsky, when he initially described nephrocytes: upon feeding silver nitrate to larvae of the Muscidae family, he observed accumulation of the substance solely in nephrocytes (Kovalevsky, 1886). Until today silver nitrate is used to study the nephrocyte's functionality. However, even wildtype larvae show a severe developmental delay when fed with the toxic silver nitrate (own observations and personal communication with Barry Denholm) and it should be considered to use non-toxic substances instead that are harmless for the animal. Over the past decade, several alternative substances have been described to assess nephrocyte function. Among others, the most frequently used tracers are fluorescent proteins as well as fluorescently labeled proteins and polysaccharides like albumin and dextrans, respectively. Hereby, two main approaches to perform tracer uptake assays can be distinguished: nephrocytes can either be isolated from the animal and exposed to the tracer *ex vivo* in a pulsed approach. Alternatively, an endogenous tracer can be used to address nephrocyte function *in vivo*. The Han laboratory introduced the tool to perform such *in vivo* experiments in 2013. A transgenic construct within the established fly line leads to GFP expression under the endogenous sequences of the Hand promotor, so that nephrocytes can be identified. Additionally, the construct initiates expression of an atrial natriuretic factor (ANF)—red fluorescent protein (RFP) fusion protein under control of the myosin

heavy chain (MHC) promotor. These flies will express ANF-RFP in muscles, from which the fusion protein is secreted into the hemolymph and taken up by nephrocytes. Finally, the strain contains the *pros-GAL4*-driver on another chromosome to enable protein knockdown when crossed to *UAS-RNAi* lines. It can therefore be used to analyze possible filtration defects upon protein knockdown *in vivo*. For further reading on this see (Fu et al., 2017; Zhang, Zhao, Chao, et al., 2013; Zhang, Zhao, & Han, 2013).

Here, we are providing a protocol for *ex vivo* tracer uptake of fluorescently labeled albumin in garland nephrocytes. We use FITC-albumin at a concentration of 0.2 mg/mL as described in Hermle et al., 2017. As filtration defects and reduced tracer uptake is a known phenotype upon nephrocyte specific depletion of Duf (Helmstädter et al., 2012; Hermle et al., 2017), we made use of nephrocyte specific knockdown of Duf (*Sns-GAL4 > duf-RNAi*) to demonstrate the functionality of the assay (Fig. 5A and C). Moreover, we compare filtration capacity of wildtype larvae (OregonR; BDSC #5) to that of larvae expressing GFP-RNAi in nephrocytes (*Sns-GAL4 > GFP-RNAi*) to demonstrate suitability of *Sns-GAL4 > GFP-RNAi* as a control (Fig. 5A and C). Crosses were set up as described in Section 4.1.

5.2 Materials and reagents

- Dissection medium (HL3; 70 mM NaCl, 5 mM KCl, 1.5 mM $CaCl_2 \cdot 2H_2O$, 20 mM $MgCl_2 \cdot 6H_2O$, 10 mM $NaHCO_3$, 5 mM Trehalose, 115 mM Sucrose, 5 mM HEPES; Stewart et al., 1994)
- FITC-albumin (Sigma #A9771, 10 mg/mL stock solution diluted in 10 mM TRIS pH8, working solution further diluted in HL3)
- Formaldehyde solution 37% (FA; Roth #4979)
- Staining block, glass (VWR #631-9301)
- Vectashield Mounting Medium with DAPI (Linaris, H-1200)

5.3 Method

1. Dissect nephrocytes of 10 third instar larvae as described in Section 3.2 in HL3 medium and collect tissue in staining block in HL3. The medium should be at room temperature or preheated to 25 °C, so that endocytosis won't be prevented.
2. Exchange the HL3 medium with 0.2 mg/mL FITC-albumin solution and incubate for 30 s in the dark (the incubation time is variable, however we observe overexposure when incubating too long, even at a laser intensity as low as 0.1%; Leica TSC SP8 confocal microscope).
3. Remove the albumin solution and rinse the tissue 3 × with HL3 medium before fixing it for 15 min in 3.7% FA in 1× PBS in the dark.
4. Rinse the tissue 3 × in HL3 or 1× PBS.

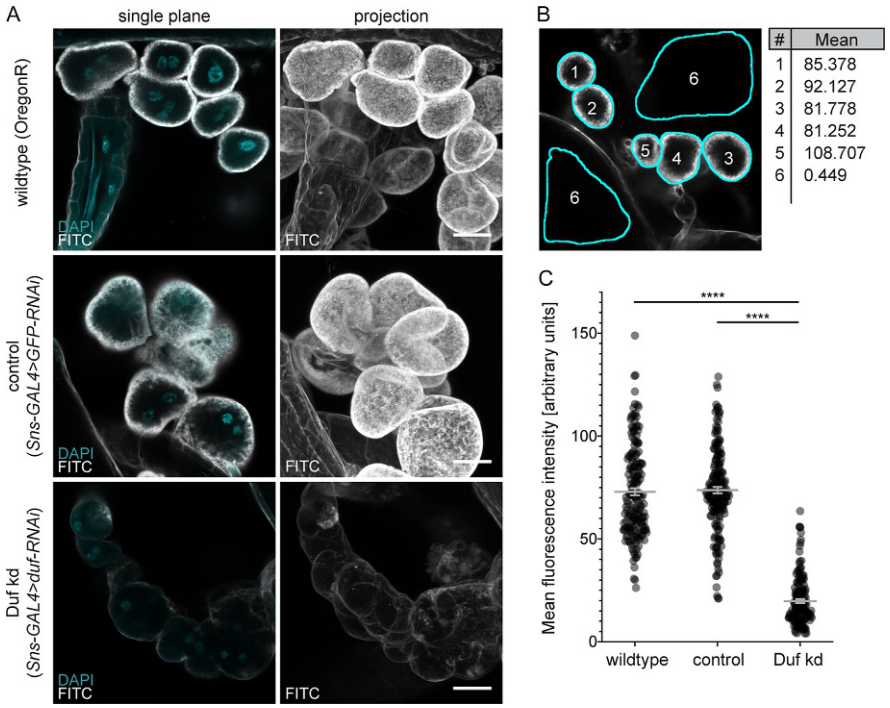

FIG. 5

Tracer uptake assays can be used to study nephrocytes on a functional level. Garland nephrocytes of wildtype (OregonR), control (*Sns-GAL4>GFP-RNAi*) and Duf knockdown (*Sns-GAL4>duf-RNAi*) larvae were isolated and incubated in 0.2 mg/mL FITC-albumin solution for 30 s. Images were taken with a Leica TSC SP8 confocal laser scanning microscope. (A) Micrographs of third instar garland nephrocytes after *ex vivo* exposure to FITC-albumin (FITC, gray) and mounting in Vectashield containing DAPI (cyan). The uptake capacity of control larvae is comparable to that of wildtype animals, underlining the suitability of GFP knockdown animals as controls. When knocking down Duf expression levels in nephrocytes, uptake of FITC-albumin is abolished, indicating that endocytosis is prevented and that nephrocytes have a severe functional phenotype. All scale bars represent 20 μm. (B) Analysis of the micrograph with FIJI software (Schindelin et al., 2012). Nephrocytes (gray) are defined as regions of interest (ROI 1–5, cyan) individually and added to the ROI manager. The mean fluorescence intensity can then be determined and subtracted by the mean intensity of the background (ROI 6, cyan). (C) Quantification of experiments from (A) represented as individual data points. Gray line and error bars indicate mean ± SEM. $n = 150$–180 nephrocytes of 30–35 animals from at least three different crossings. Statistical significance was calculated by applying One-way ANOVA and Tukey's post hoc analysis; ****$P < 0.0001$.

5. Transfer the samples individually to a microscope slide with a drop of mounting medium and seal with a cover slip. The samples can then be imaged with a fluorescent microscope (Fig. 5A, in our experiment a Leica TSC SP8 confocal laser scanning microscope was used). The slides should be scanned for the brightest sample (usually the control samples) and the laser set accordingly.

6. Analysis: Import files into any image analysis software (e.g., FIJI; Schindelin et al., 2012) to measure the mean fluorescence intensity of the individual nephrocytes (e.g., by defining them as regions of interest (Fig. 5B). Additionally, measure the mean fluorescence intensity of areas, where no tissue was mounted (Fig. 5B). Once this background intensity is subtracted the mean fluorescence intensity can be depicted as arbitrary units (Fig. 5C).

6 Conclusion

The *Drosophila* toolbox enables researchers to study gene and protein function with straightforward and easy assessable technologies. A vast number of disease associated genes are conserved in the fly, which makes it possible to interfere with signaling pathways involved in the disease process. In the past decade, *Drosophila* gained attractiveness as a model organism for renal diseases and, especially, podocytopathies, as shown for nephrocytes which can be considered as podocyte-like cells. Here, we summarize how podocyte injury can be studied in the fruit fly and provide protocols that enable a first evaluation of possible phenotypes such as morphological changes or impaired functionality arising from genetic manipulation. These methods can also be used to screen for other undiscovered genes that might be involved in podocyte disease.

Acknowledgments

This work is supported by the German Research Foundation (BR 2955/4-1 and BR 2955/8-1 (clinical research unit; KFO 329) to P.T.B. and the Koeln Fortune Programm of the University of Cologne to P.T.B. The authors thank Sybille Köhler for providing electron micrographs and Barry Denholm for supplying the Duf antibody. The authors thank Martin Hoehne and Pilar Carrera for fruitful discussion and insightful comments.

Declaration of interest

The authors declare no competing interests.

References

Adams, M. D., Celniker, S. E., Holt, R. A., Evans, C. A., Gocayne, J. D., Amanatides, P. G., et al. (2000). The genome sequence of Drosophila melanogaster. *Science (New York, N.Y.)*, *287*(5461), 2185–2195.

Aggarwal, S. K., & King, R. C. (1967). The ultrastructure of the wreath cells of Drosophila melanogaster larvae. *Protoplasma*, *63*(4), 343–352.

Ashburner, M. (1989). *Drosophila. A laboratory handbook*. New York: Cold Spring harbor Laboratory Press.

Bischof, J., Maeda, R. K., Hediger, M., Karch, F., & Basler, K. (2007). An optimized transgenesis system for Drosophila using germ-line-specific phiC31 integrases. *Proceedings of the National Academy of Sciences of the United States of America*, *104*(9), 3312–3317.

Brand, A. H., & Perrimon, N. (1993). Targeted gene expression as a means of altering cell fates and generating dominant phenotypes. *Development (Cambridge, England)*, *118*(2), 401–415.

Brenner, B. M., Hostetter, T. H., & Humes, H. D. (1978). Glomerular permselectivity: Barrier function based on discrimination of molecular size and charge. *American Journal of Physiology-Renal Physiology*, *234*(6), F455–F460.

Brinkkoetter, P. T., Ising, C., & Benzing, T. (2013). The role of the podocyte in albumin filtration. *Nature Reviews. Nephrology*, *9*(6), 328–336.

Cagan, R. L. (2011). The Drosophila nephrocyte. *Current Opinion in Nephrology and Hypertension*, *20*(4), 409–415.

Crossley, A. C. (1972). The ultrastructure and function of pericardial cells and other nephrocytes in an insect: Calliphora erythrocephala. *Tissue & Cell*, *4*(3), 529–560.

D'Agati, V. (2003). Pathologic classification of focal segmental glomerulosclerosis. *Seminars in Nephrology*, *23*(2), 117–134.

Das, D., Ashoka, D., Aradhya, R., & Inamdar, M. (2008). Gene expression analysis in postembryonic pericardial cells of Drosophila. *Gene Expression Patterns: GEP*, *8*(3), 199–205.

Deegens, J. K. J., Dijkman, H. B. P. M., Borm, G. F., Steenbergen, E. J., van den Berg, J. G., Weening, J. J., et al. (2008). Podocyte foot process effacement as a diagnostic tool in focal segmental glomerulosclerosis. *Kidney International*, *74*(12), 1568–1576.

Denholm, B., & Skaer, H. (2009). Bringing together components of the fly renal system. *Current Opinion in Genetics & Development*, *19*(5), 526–532.

Dietzl, G., Chen, D., Schnorrer, F., Su, K.-C., Barinova, Y., Fellner, M., et al. (2007). A genome-wide transgenic RNAi library for conditional gene inactivation in Drosophila. *Nature*, *448*(7150), 151–156.

Doe, C. Q., Chu-LaGraff, Q., Wright, D. M., & Scott, M. P. (1991). The prospero gene specifies cell fates in the Drosophila central nervous system. *Cell*, *65*(3), 451–464.

Donoviel, D. B., Freed, D. D., Vogel, H., Potter, D. G., Hawkins, E., Barrish, J. P., et al. (2001). Proteinuria and perinatal lethality in mice lacking NEPH1, a novel protein with homology to NEPHRIN. *Molecular and Cellular Biology*, *21*(14), 4829–4836.

Endlich, K., Kliewe, F., & Endlich, N. (2017). Stressed podocytes—Mechanical forces, sensors, signaling and response. *Pflügers Archiv—European Journal of Physiology*, *469*(7–8), 937–949.

Fu, Y., Zhu, J.-Y., Richman, A., Zhao, Z., Zhang, F., Ray, P. E., et al. (2017). A Drosophila model system to assess the function of human monogenic podocyte mutations that cause nephrotic syndrome. *Human Molecular Genetics*, *26*(4), 768–780.

Garg, P., Verma, R., Nihalani, D., Johnstone, D. B., & Holzman, L. B. (2007). Neph1 cooperates with nephrin to transduce a signal that induces actin polymerization. *Molecular and Cellular Biology*, *27*(24), 8698–8712.

Gildor, B., Schejter, E. D., & Shilo, B.-Z. (2012). Bidirectional notch activation represses fusion competence in swarming adult Drosophila myoblasts. *Development (Cambridge, England)*, *139*(21), 4040–4050.

Greenspan, R. J. (2004). *Fly pushing: The theory and practice of Drosophila genetics. 2004*. Cold Spring Harbor Laboratory Press.

Hales, K. G., Korey, C. A., Larracuente, A. M., & Roberts, D. M. (2015). Genetics on the Fly: A primer on the Drosophila model system. *Genetics*, *201*(3), 815–842.

Haraldsson, B., Nyström, J., & Deen, W. M. (2008). Properties of the glomerular barrier and mechanisms of proteinuria. *Physiological Reviews*, *88*(2), 451–487.

Hartley, P. S., Motamedchaboki, K., Bodmer, R., & Ocorr, K. (2016). SPARC-dependent cardiomyopathy in Drosophila. *Circulation. Cardiovascular Genetics*, *9*(2), 119–129.

Hartley, J. L., Temple, G. F., & Brasch, M. A. (2000). DNA cloning using in vitro site-specific recombination. *Genome Research*, *10*(11), 1788–1795.

Heigwer, F., Port, F., & Boutros, M. (2018). RNA interference (RNAi) screening in Drosophila. *Genetics*, *208*(3), 853–874.

Helmstädter, M., Huber, T. B., & Hermle, T. (2017). Using the Drosophila nephrocyte to model podocyte function and disease. *Frontiers in Pediatrics*, *5*(December), 262.

Helmstädter, M., Lüthy, K., Gödel, M., Simons, M., Ashish, Nihalani, D., et al. (2012). Functional study of mammalian Neph proteins in Drosophila melanogaster. *PLoS One*, *7*(7), e40300.

Helmstädter, M., & Simons, M. (2017). Using Drosophila nephrocytes in genetic kidney disease. *Cell and Tissue Research*, *369*(1), 119–126.

Hermle, T., Braun, D. A., Helmstädter, M., Huber, T. B., & Hildebrandt, F. (2017). Modeling monogenic human nephrotic syndrome in the Drosophila garland cell nephrocyte. *Journal of the American Society of Nephrology: JASN*, *28*(5), 1521–1533.

Hoehne, M., Gert de Couet, H., Stuermer, C. A. O., & Fischbach, K.-F. (2005). Loss- and gain-of-function analysis of the lipid raft proteins reggie/flotillin in Drosophila: They are post-translationally regulated, and misexpression interferes with wing and eye development. *Molecular and Cellular Neuroscience*, *30*(3), 326–338.

Honti, V., Csordás, G., Márkus, R., Kurucz, E., Jankovics, F., & Andó, I. (2010). Cell lineage tracing reveals the plasticity of the hemocyte lineages and of the hematopoietic compartments in Drosophila melanogaster. *Molecular Immunology*, *47*(11 – 12), 1997–2004.

Huber, T. B., & Benzing, T. (2005). The slit diaphragm: A signaling platform to regulate podocyte function. *Current Opinion in Nephrology and Hypertension*, *14*(3), 211–216.

Huber, T. B., Simons, M., Hartleben, B., Sernetz, L., Schmidts, M., Gundlach, E., et al. (2003). Molecular basis of the functional podocin-nephrin complex: Mutations in the NPHS2 gene disrupt nephrin targeting to lipid raft microdomains. *Human Molecular Genetics*, *12*(24), 3397–3405.

Hummel, T., & Klämbt, C. (2008). Element mutagenesis. In C. Dahmann (Ed.), *Drosophila. Methods in molecular biology* (420th ed., pp. 97–117). Humana Press.

Ivy, J. R., Drechsler, M., Catterson, J. H., Bodmer, R., Ocorr, K., Paululat, A., et al. (2015). Klf15 is critical for the development and differentiation of Drosophila nephrocytes. *PLoS One*, *10*(8), e0134620.

Jan, L. Y., & Jan, Y. N. (1982). Antibodies to horseradish peroxidase as specific neuronal markers in Drosophila and in grasshopper embryos. *Proceedings of the National Academy of Sciences of the United States of America*, *79*(8), 2700–2704.

Kambham, N., Tanji, N., Seigle, R. L., Markowitz, G. S., Pulkkinen, L., Uitto, J., et al. (2000). Congenital focal segmental glomerulosclerosis associated with beta4 integrin mutation and epidermolysis bullosa. *American Journal of Kidney Diseases: The Official Journal of the National Kidney Foundation*, *36*(1), 190–196.

Kestilä, M., Lenkkeri, U., Männikkö, M., Lamerdin, J., McCready, P., Putaala, H., et al. (1998). Positionally cloned gene for a novel glomerular protein—Nephrin—Is mutated in congenital nephrotic syndrome. *Molecular Cell*, *1*(4), 575–582.

Kimbrell, D. A., Hice, C., Bolduc, C., Kleinhesselink, K., & Beckingham, K. (2002). The Dorothy enhancer has Tinman binding sites and drives hopscotch-induced tumor formation. *Genesis*, *34*(1–2), 23–28.

Kocherlakota, K. S., Wu, J.-M., McDermott, J., & Abmayr, S. M. (2008). Analysis of the cell adhesion molecule sticks-and-stones reveals multiple redundant functional domains, protein-interaction motifs and phosphorylated tyrosines that direct myoblast fusion in Drosophila melanogaster. *Genetics*, *178*(3), 1371–1383.

Kohli, P., Bartram, M. P., Habbig, S., Pahmeyer, C., Lamkemeyer, T., Benzing, T., et al. (2014). Label-free quantitative proteomic analysis of the YAP/TAZ interactome. *American Journal of Physiology. Cell Physiology*, *306*(9), C805–C818.

Kovalevsky, A. (1886). Zur Verhalten des Rückengefässes und des guirlandenförmigen Zellenstrangs der Musciden während der Metamorphose. *Biologisches Zentralblatt*, *6*, 74–79.

Kovalevsky, A. (1889). Ein Beitrag zur Kenntnis der Exkretionsorgane. *Biologisches Zentralblatt*, *9*, 74–79.

Lee, Y. S., Nakahara, K., Pham, J. W., Kim, K., He, Z., Sontheimer, E. J., et al. (2004). Distinct roles for Drosophila Dicer-1 and Dicer-2 in the siRNA/miRNA silencing pathways. *Cell*, *117*(1), 69–81.

Lim, H.-Y., Wang, W., Chen, J., Ocorr, K., & Bodmer, R. (2014). ROS regulate cardiac function via a distinct paracrine mechanism. *Cell Reports*, *7*(1), 35–44.

Ma, Y., Creanga, A., Lum, L., & Beachy, P. A. (2006). Prevalence of off-target effects in Drosophila RNA interference screens. *Nature*, *443*(7109), 359–363.

Mallipattu, S. K., Liu, R., Zheng, F., Narla, G., Ma'ayan, A., Dikman, S., et al. (2012). Kruppel-like factor 15 (KLF15) is a key regulator of podocyte differentiation. *The Journal of Biological Chemistry*, *287*(23), 19122–19135.

Mele, C., Iatropoulos, P., Donadelli, R., Calabria, A., Maranta, R., Cassis, P., et al. (2011). MYO1E mutations and childhood familial focal segmental glomerulosclerosis. *The New England Journal of Medicine*, *365*(4), 295–306.

Micchelli, C. A., & Perrimon, N. (2006). Evidence that stem cells reside in the adult Drosophila midgut epithelium. *Nature*, *439*(7075), 475–479.

Mills, R. P., & King, R. C. (1965). The pericardial cells of Drosophila melanogaster. *The Quarterly Journal of Microscopical Science*, *106*(3), 261–268.

Myers, E. W., Sutton, G. G., Delcher, A. L., Dew, I. M., Fasulo, D. P., Flanigan, M. J., et al. (2000). A whole-genome assembly of Drosophila. *Science*, *287*(5461), 2196–2204.

Ni, L., Saleem, M., & Mathieson, P. W. (2012). Podocyte culture: Tricks of the trade. *Nephrology (Carlton, Vic.)*, *17*(6), 525–531.

Ohshiro, T., Yagami, T., Zhang, C., & Matsuzaki, F. (2000). Role of cortical tumour-suppressor proteins in asymmetric division of Drosophila neuroblast. *Nature*, *408*(6812), 593–596.

Pavenstädt, H., Kriz, W., & Kretzler, M. (2003). Cell biology of the glomerular podocyte. *Physiological Reviews*, *83*(1), 253–307.

Pendse, J., Ramachandran, P. V., Na, J., Narisu, N., Fink, J. L., Cagan, R. L., et al. (2013). A Drosophila functional evaluation of candidates from human genome-wide association studies of type 2 diabetes and related metabolic traits identifies tissue-specific roles for dHHEX. *BMC Genomics*, *14*(1), 136.

Perkins, L. A., Holderbaum, L., Tao, R., Hu, Y., Sopko, R., McCall, K., et al. (2015). The transgenic RNAi project at Harvard Medical School: Resources and validation. *Genetics*, *201*(3), 843–852.

Port, F., Chen, H.-M., Lee, T., & Bullock, S. L. (2014). Optimized CRISPR/Cas tools for efficient germline and somatic genome engineering in Drosophila. *Proceedings of the National Academy of Sciences of the United States of America*, *111*(29), E2967–E2976.

Reiter, L. T., Potocki, L., Chien, S., Gribskov, M., & Bier, E. (2001). A systematic analysis of human disease-associated gene sequences in Drosophila melanogaster. *Genome Research*, *11*(6), 1114–1125.

Rennke, H. G., & Venkatachalam, M. A. (1979). Glomerular permeability of macromolecules. Effect of molecular configuration on the fractional clearance of uncharged dextran and neutral horseradish peroxidase in the rat. *Journal of Clinical Investigation*, *63*(4), 713–717.

Rinschen, M. M., Schroeter, C. B., Koehler, S., Ising, C., Schermer, B., Kann, M., et al. (2016). Quantitative deep mapping of the cultured podocyte proteome uncovers shifts in proteostatic mechanisms during differentiation. *American Journal of Physiology. Cell Physiology*, *311*(3), C404–C417.

Rodewald, R., & Karnovsky, M. J. (1974). Porous substructure of the glomerular slit diaphragm in the rat and mouse. *The Journal of Cell Biology*, *60*(2), 423–433.

Saran, R., Robinson, B., Abbott, K. C., Agodoa, L. Y. C., Bhave, N., Bragg-Gresham, J., et al. (2018). US renal data system 2017 annual data report: Epidemiology of kidney disease in the United States. *American Journal of Kidney Diseases: The Official Journal of the National Kidney Foundation*, *71*(3S1), A7.

Sarnak, M. J., Levey, A. S., Schoolwerth, A. C., Coresh, J., Culleton, B., Hamm, L. L., et al. (2003). Kidney Disease as a risk factor for development of cardiovascular disease. American heart association councils on kidney in cardiovascular disease, high blood pressure research, clinical cardiology, and epidemiology and prevention. *Circulation*, *108*(17), 2154–2169.

Schindelin, J., Arganda-Carreras, I., Frise, E., Kaynig, V., Longair, M., Pietzsch, T., et al. (2012). Fiji: An open-source platform for biological-image analysis. *Nature Methods*, *9*(7), 676–682.

Schmidt-Rhaesa, A. (2007). Excretory systems. In *2007. The evolution of organ systems* (pp. 169–190). Oxford University Press.

Schroeter, C. B., Koehler, S., Kann, M., Schermer, B., Benzing, T., Brinkkoetter, P. T., et al. (2018). Protein half-life determines expression of proteostatic networks in podocyte differentiation. *The FASEB Journal*, *32*(9), 4696–4713.

Sellin, J., Albrecht, S., Kölsch, V., & Paululat, A. (2006). Dynamics of heart differentiation, visualized utilizing heart enhancer elements of the Drosophila melanogaster bHLH transcription factor hand. *Gene Expression Patterns: GEP*, *6*(4), 360–375.

Shankland, S. J., Pippin, J. W., Reiser, J., & Mundel, P. (2007). Podocytes in culture: Past, present, and future. *Kidney International*, *72*(1), 26–36.

Simons, M., & Huber, T. B. (2009). Flying podocytes. *Kidney International*, *75*(5), 455–457.

Stewart, B. A., Atwood, H. L., Renger, J. J., Wang, J., & Wu, C. F. (1994). Improved stability of Drosophila larval neuromuscular preparations in haemolymph-like physiological solutions. *Journal of Comparative Physiology. A, Sensory, Neural, and Behavioral Physiology*, *175*(2), 179–191.

Thurmond, J., Goodman, J. L., Strelets, V. B., Attrill, H., Gramates, L. S., Marygold, S. J., et al. (2019). FlyBase 2.0: The next generation. *Nucleic Acids Research*, *47*(D1), D759–D765.

Tomari, Y., & Zamore, P. D. (2005). Perspective: Machines for RNAi. *Genes & Development*, *19*(5), 517–529.

Tonelli, M., Muntner, P., Lloyd, A., Manns, B. J., Klarenbach, S., Pannu, N., et al. (2012). Risk of coronary events in people with chronic kidney disease compared with those with diabetes: A population-level cohort study. *The Lancet*, *380*(9844), 807–814.

Tutor, A. S., Prieto-Sánchez, S., & Ruiz-Gómez, M. (2014). Src64B phosphorylates dumbfounded and regulates slit diaphragm dynamics: Drosophila as a model to study nephropathies. *Development (Cambridge, England)*, *141*(2), 367–376.

Vaessin, H., Grell, E., Wolff, E., Bier, E., Jan, L. Y., & Jan, Y. N. (1991). Prospero is expressed in neuronal precursors and encodes a nuclear protein that is involved in the control of axonal outgrowth in Drosophila. *Cell*, *67*(5), 941–953.

Vivante, A., & Hildebrandt, F. (2016). Exploring the genetic basis of early-onset chronic kidney disease. *Nature Reviews. Nephrology*, *12*(3), 133–146.

Wanner, N., Hartleben, B., Herbach, N., Goedel, M., Stickel, N., Zeiser, R., et al. (2014). Unraveling the role of podocyte turnover in glomerular aging and injury. *Journal of the American Society of Nephrology*, *25*(4), 707–716.

Weavers, H., Prieto-Sánchez, S., Grawe, F., Garcia-López, A., Artero, R., Wilsch-Bräuninger, M., et al. (2009). The insect nephrocyte is a podocyte-like cell with a filtration slit diaphragm. *Nature*, *457*(7227), 322–326.

Zhang, F., Zhao, Y., Chao, Y., Muir, K., & Han, Z. (2013). Cubilin and amnionless mediate protein reabsorption in Drosophila nephrocytes. *Journal of the American Society of Nephrology: JASN*, *24*(2), 209–216.

Zhang, F., Zhao, Y., & Han, Z. (2013). An in vivo functional analysis system for renal gene discovery in Drosophila pericardial nephrocytes. *Journal of the American Society of Nephrology*, *24*(2), 191–197.

Zhuang, S., Shao, H., Guo, F., Trimble, R., Pearce, E., & Abmayr, S. M. (2009). Sns and Kirre, the Drosophila orthologs of Nephrin and Neph1, direct adhesion, fusion and formation of a slit diaphragm-like structure in insect nephrocytes. *Development*, *136*(14), 2335–2344.

2.2 Chapter 2 – Modelling of ACTN4-based podocytopathy using *Drosophila* nephrocytes

In paediatric patients, the most cases of steroid resistant nephrotic syndrome (SRNS), i.e. non-responders to corticoid treatment, are due to inherited, monogenic forms of glomerular disorders (Vivante & Hildebrandt, 2016). Besides clinical and histological analyses, a genetic diagnosis in these patients is essential to ultimately pave the way for the individual therapeutic strategy. Occasionally, next generation sequencing hereby leads to the identification of previously uncharacterized genetic variants or single nucleotide polymorphisms (SNPs), which are likely to constitute the origin of disease, but whose pathogenic potential still needs to be evaluated properly.

In the following article, we characterized a so far unknown genetic variant in the *ACTN4* gene, found in a paediatric patient suffering from SRNS. Our aim for this manuscript was to demonstrate the thorough characterization of a newly discovered SNP that causes nephrotic syndrome using *Drosophila melanogaster* and its nephrocytes in addition to more established methods such as cell culture work and computational analyses. The genetic toolbox of *Drosophila* hereby allowed us to transgenically express the novel ACTN4 variant in nephrocytes and analyse its impact on nephrocyte morphology and function in comparison to the wildtype variant as well as other, previously described pathogenic variants of the protein. The interplay of *in silico*, *in vitro* and *in vivo* analyses offers a time efficient experimental workflow, we hereby aim at introducing as pipeline that could accompany the diagnostic workup of monogenic forms of the disease in the future.

Authors: **Johanna Odenthal**, Sebastian Dittrich, Vivian Ludwig, Tim Merz, Katrin Reitmeier, Björn Reusch, Martin Höhne, Zülfü C. Cosgun, Maximilian Hohenadel, Jovanna Putnik, Heike Göbel, Markus M. Rinschen, Janine Altmüller, Bernhard Schermer, Thomas Benzing, Bodo B. Beck, Paul T. Brinkkoetter, Sandra Habbig and Malte P. Bartram

Author contributions:

Johanna Odenthal	–	designed and performed *Drosophila* experiments
		analysed the data
		created the figures and drafted the manuscript
Sebastian Dittrich	–	performed *in silico* and cell culture experiments
		analysed the data and revised the manuscript
Vivian Ludwig	–	performed experiments
Tim Merz	–	performed experiments
Katrin Reitmeier	–	performed experiments
Björn Reusch	–	performed genetic analyses
Martin Höhne	–	analysed the data and revised the manuscript
Zülfü C. Cosgun	–	cared for the patient and contributed clinical data
Maximilian Hohenadel	–	cared for the patient and contributed clinical data
Jovanna Putnik	–	performed genetic analyses
Heike Göbel	–	performed the nephropathological work up
Markus M. Rinschen	–	performed experiments and analysed the data
		revised the manuscript
Janine Altmüller	–	performed genetic analyses
Bernhard Schermer	–	revised the manuscript
Thomas Benzing	–	revised the manuscript
Bodo B. Beck	–	performed genetic analyses and analysed the data
		revised the manuscript
Paul T. Brinkkötter	–	supervised the study and revised the manuscript

Sandra Habbig	–	cared for the patient and contributed clinical data
		supervised the study and revised the manuscript
Malte P. Bartram	–	analysed the data
		supervised the study and revised the manuscript

Status:

Published in „Kidney International Reports"

Volume 8, Issue 2, Pages 317-329. February 2023

Published online: 31. October 2022

Citation:

Odenthal J, Dittrich S, Ludwig V, Merz T, Reitmeier K, Reusch B, Höhne M, Cosgun ZC, Hohenadel M, Putnik J, Göbel H, Rinschen MM, Altmüller J, Koehler S, Schermer B, Benzing T, Beck BB, Brinkkötter PT, Habbig S, Bartram MP. Modeling of ACTN4-Based Podocytopathy Using Drosophila Nephrocytes. Kidney Int Rep. 2022 Oct 31;8(2):317-329.

doi: 10.1016/j.ekir.2022.10.024

PMID: 36815115

KI REPORTS
KIReports.org
CLINICAL RESEARCH

Modeling of *ACTN4*-Based Podocytopathy Using *Drosophila* Nephrocytes

Johanna Odenthal[1], Sebastian Dittrich[1], Vivian Ludwig[1], Tim Merz[1], Katrin Reitmeier[1], Björn Reusch[3,4], Martin Höhne[1], Zülfü C. Cosgun[5], Maximilian Hohenadel[6], Jovana Putnik[7], Heike Göbel[8], Markus M. Rinschen[9,10,11], Janine Altmüller[12,13], Sybille Koehler[1], Bernhard Schermer[1,2], Thomas Benzing[1,2], Bodo B. Beck[3,4], Paul T. Brinkkötter[1], Sandra Habbig[5,14] and Malte P. Bartram[1,14]

[1]Department II of Internal Medicine and Center for Molecular Medicine Cologne, Faculty of Medicine, University of Cologne, University Hospital Cologne, Cologne, Germany; [2]Cologne Excellence Cluster on Cellular Stress Responses in Aging-Associated Diseases, Faculty of Medicine, University of Cologne, University Hospital Cologne, Cologne, Germany; [3]Center for Molecular Medicine Cologne, Faculty of Medicine, University of Cologne, University Hospital Cologne, Cologne, Germany; [4]Institute of Human Genetics, Faculty of Medicine, University of Cologne, University Hospital Cologne, Cologne, Germany; [5]Department of Pediatrics, Faculty of Medicine, University of Cologne, University Hospital Cologne, Cologne, Germany; [6]Department of Pediatrics, Division of Pediatric Nephrology, University of Bonn, Bonn, Germany; [7]Mother and Child Health Care Institute of Serbia "Dr Vukan Čupić," Department of Nephrology, Faculty of Medicine, University of Belgrade, Belgrade, Serbia; [8]Institute of Pathology, University Hospital of Cologne, Cologne, Germany; [9]Department of Biomedicine, Aarhus University, Aarhus, Denmark; [10]Aarhus Institute of Advanced Studies, Aarhus University, Aarhus, Denmark; [11]III Medical Clinic, University Hospital Hamburg Eppendorf, Hamburg, Germany; [12]Berlin Institute of Health at Charité-Universitätsmedizin Berlin, Max Delbrück Center for Molecular Medicine, Berlin, Germany; and [13]Cologne Center for Genomics, University of Cologne, Cologne, Germany

Introduction: Genetic disorders are among the most prevalent causes leading to progressive glomerular disease and, ultimately, end-stage renal disease (ESRD) in children and adolescents. Identification of underlying genetic causes is indispensable for targeted treatment strategies and counseling of affected patients and their families.

Methods: Here, we report on a boy who presented at 4 years of age with proteinuria and biopsy-proven focal segmental glomerulosclerosis (FSGS) that was temporarily responsive to treatment with ciclosporin A. Molecular genetic testing identified a novel mutation in alpha-actinin-4 (p.M240T). We describe a feasible and efficient experimental approach to test its pathogenicity by combining *in silico*, *in vitro*, and *in vivo* analyses.

Results: The *de novo* p.M240T mutation led to decreased alpha-actinin-4 stability as well as protein mislocalization and actin cytoskeleton rearrangements. Transgenic expression of wild-type human alpha-actinin-4 in *Drosophila melanogaster* nephrocytes was able to ameliorate phenotypes associated with the knockdown of endogenous actinin. In contrast, p.M240T, as well as other established disease variants p.W59R and p.K255E, failed to rescue these phenotypes, underlining the pathogenicity of the novel alpha-actinin-4 variant.

Conclusion: Our data highlight that the newly identified alpha-actinin-4 mutation indeed encodes for a disease-causing variant of the protein and promote the *Drosophila* model as a simple and convenient tool to study monogenic kidney disease *in vivo*.

Kidney Int Rep (2023) **8,** 317–329; https://doi.org/10.1016/j.ekir.2022.10.024
KEYWORDS: *ACTN4*; *Drosophila*; FSGS; nephrocyte; nephrotic syndrome; podocyte

FSGS represents a histopathological pattern of injury and is classified as primary or secondary depending on whether an underlying cause can be identified. These entities are further subdivided on the basis of their response to immunosuppressive therapy, relapse frequency, and histologic subvariants and whether genetic variants can be identified. Clinically, FSGS can present with proteinuria in the nephrotic or subnephrotic range,

Correspondence: Paul T. Brinkkoetter, Department II of Internal Medicine, Faculty of Medicine, University of Cologne, University Hospital Cologne, Kerpener Street 62, Cologne 50935, Germany. E-mail: paul.brinkkoetter@uk-koeln.de

[14]SH and MPB share senior authorship.

Received 7 September 2022; revised 17 October 2022; accepted 24 October 2022; published online 31 October 2022

and signs of nephrotic syndrome may be present.[1] The prevalence of FSGS is rising, and FSGS is a major contributor to ESRD requiring dialysis or kidney transplantation.[2,3] The driving factors leading to FSGS are diverse and differ between pediatric and adult populations. Although immunologic causes and genetic mutations predominate in children, obesity or reduced nephron mass leading to glomerular hyperfiltration, viral infections, or autoimmune diseases as well as medications are further factors in adult populations. Therefore, a very careful examination of each patient is required to (i) determine the underlying cause, (ii) optimize the patient's treatment and counseling, and (iii) predict the risk of recurrence after kidney transplantation.

A monogenetic form of glomerular and podocyte disorders can be detected in up to one-third of patients.[4] Genotype information is important for personalized treatment approaches because it predicts response to treatment options and risk of FSGS recurrence after transplantation, helps to avoid unnecessary drug toxicity and side effects, and aids in the selection of an appropriate kidney donor in the case of a living transplant strategy as well as the assessment of other family members at risk. To date, more than 50 FSGS-associated genes have been discovered, most of which encode proteins that play central roles in regulating the podocyte's architecture and function.[5] Among these, especially proteins associated with the slit diaphragm such as nephrin or podocin and components of the cytoskeleton and cytoskeleton-associated proteins such as *ACTN4* and *INF2* were identified as causative for inherited forms of FSGS.[6] Although most mutations in children are inherited in an autosomal recessive mode, there are autosomal-dominant forms with rather slowly progressive courses that present mainly in adults.

These patients often do not respond well to standard immunosuppressive therapy. However, recently, several case reports have been published reporting on partial or complete remission in particular types of genetic FSGS.[7] Large cohort studies combining comprehensive analyses of both genotypes and phenotypes with a long-term follow-up over several years will be essential to stratify patients to a specific management course. Recently, we established a clinical research unit (CRU329–www.podocyte.org) and a clinical registry (FOrMe registry, ClinicalTrials.gov identifier: NCT03949972[8]) in Germany. Within this registry, we provide comprehensive genetic analysis, monitor the clinical outcome, and provide *in vitro* and *in vivo* analysis of novel mutations to predict the outcome.

Here, we report on 3 patients with *de novo ACTN4* mutations that were identified within the clinical research unit and that developed kidney disease with a rapid deterioration of kidney function at a rather younger age than most published patients with mutations in *ACTN4*.[9] The mutation of 1 patient was previously analyzed *in vitro*[10]. Applying *in silico*, *in vitro*, and *in vivo* analyses using the *Drosophila melanogaster* nephrocyte model, we now characterized the biological consequences of a further *ACTN4* mutation resulting in amino acid change p.M240T and demonstrate its pathogenicity. We established a thorough workflow to elucidate and evaluate the pathogenic potential of unknown variants that might be disease-causing in nephrotic syndrome, eventually guiding and facilitating further treatment options for the individual patient and hereby emphasize the genetic power of the *Drosophila* model in translational kidney research.

METHODS

Probands

All investigations were conducted in accordance with the principles of the Declaration of Helsinki and after obtaining written informed consent from the patient and his parents. Clinical and biochemical data were collected from medical charts. Standard methods were used to analyze electrolytes, creatinine, and other laboratory parameters. This study was carried out with the approval of the ethics committee of the University Hospital Cologne (number 15-215).

Genetic Analysis

DNA of patients 1 and 2 was analyzed by next-generation sequencing as described previously.[10] We performed Sanger sequencing of DNA from patient 3 for 8 genes commonly found in mainly nonsyndromic steroid-resistant nephrotic syndrome (SRNS)/FSGS (*NPHS1*, *NPHS2*, *WT1*, *TRPC6*, *INF2*, *ACTN4*, *PLCE1*, and *PAX2*). Segregation of all parents DNA confirmed that all pathogenic *ACTN4* variants occurred *de novo* in the patients (see Supplementary Table S1).

Analysis of Thermodynamic Stability *In Silico*

Computational analyses were carried out as described before[10]: The respective protein data bank files were obtained from the PubMed structure (protein data bank: 2EYN [*ACTN1*], 1WKU [*ACTN3*], 2R0O [*ACTN4*]). Because there is no crystal structure for wild-type (WT) *ACTN4* available, we used the structure of *ACTN4* K255E, which shows no significant structural change in comparison with the WT protein.[11] The files were uploaded to the respective web servers, and calculation of free energy (delta-delta-G) was performed using the default settings. The effect of an amino acid substitution (M to P for the respective residues) was calculated.[12-16]

Actin Fractionation Assay

Differential centrifugation was performed to investigate the subcellular localization of *ACTN4* and its clustering with components of the actin cytoskeleton. For this, Flag-tagged hACTN4-WT or hACTN4-M240T was transfected into human embryonic kidney 293 T cells, which were harvested in ice-cold phosphate-buffered saline the next day. Cells were lysed in lysis buffer (20-mM Tris-HCl, pH 7.5, 50-mM NaCl, 50-mM NaF, 15-mM $Na_4P_2O_7$, 2-mM Na_3VO_4, 1% Triton X-100, and protease inhibitor mix complete protease inhibitor mix [Roche]). After low-speed centrifugation of the whole-cell lysate at 14,000 × *g* for 15 minutes, large cytoskeletal structures such as actin bundles were pelleted into the Triton insoluble fraction. The supernatant (Triton soluble fraction) was further centrifugated at 100,000 × *g* for 30 minutes, after which fractions were separated into F-actin (pellet) and G-actin (supernatant). The fractions were then analyzed by western blot.

Fly Lines and Husbandry

Flies were kept on standard medium and maintained at 25 °C. As a nephrocyte-specific driver, we used Sticks and Stones–GAL4 (sns-GAL4)[17] combined with upstream activating sequence (UAS)-dcr2,[18] to achieve higher knockdown efficiency. UAS-GFP-RNA interference (RNAi) (BDSC #41553) served as control, and UAS-*actn*-RNAi-1 (VDRC #7762) and UAS-*actn*-RNAi-2 (VDRC #110719) were used to silence the actinin gene. Strains transgenically expressing the human hemagglutinin (HA)-tagged alpha-actinin-4 variants were generated via phi31-mediated recombination into the attP1:(2R) 55C4 locus (GenetiVision) and recombined with VDRC #110719 to generate stable lines expressing both UAS-*actn*-RNAi2 and HA-*hACTN4*-variants.

Immunofluorescence Stainings in Nephrocytes

Immunofluorescence stainings in nephrocytes were performed as described before.[19] In brief, nephrocytes were dissected in phosphate-buffered saline followed by fixation in 4% formaldehyde for 20 minutes and methanol for 1 hour at room temperature. After 3 washing steps in wash buffer (phosphate-buffered saline, 0.3% Triton, 0.5% bovine serum albumin), primary antibodies were incubated in wash buffer overnight at 4 °C. Primary antibodies were as follows: mouse antipolychaetoid 2 (Developmental Studies Hybridoma Bank, 1:25), goat anti–horseradish peroxidase (Jackson ImmunoResearch #123-005-021, 1:200), and rabbit anti–HA (Sigma #H6908, 1:100). After 3 washing steps and 30 minutes blocking in 5% normal donkey serum, the tissue was incubated with secondary antibodies (donkey anti-rabbitCy3, Jackson ImmunoResearch #711-165-152, 1:250; donkey anti-goatAlexa488, Jackson ImmunoResearch #705-545-003, 1:250; goat anti-mouseAtto647N, Sigma #50185, 1:1000) for 1 hour at room temperature. Following 3 washing steps, the tissue was mounted in Vectashield mounting medium (Linaris, H-1200).

Tracer Uptake Assay in Nephrocytes

Tracer uptake assays were performed using fluorescein isothiocyanate (FITC)–labeled bovine albumin (Sigma#A9771) as described earlier.[19] Nephrocytes were dissected in HL3 medium (70-mM NaCl, 5-mM KCl, 5-mM $CaCl_2{*}2H_2O$, 20-mM $MgCl_2{*}6H_2O$, 10-mM $NaHCO_3$, 5-mM trehalose, 115-mM sucrose, 5-mM HEPES) and incubated in 0.2 mg/ml FITC-albumin for 30 seconds at room temperature. After rinsing the tissue with HL3 medium several times, nephrocytes were fixed for 20 minutes in 4% formaldehyde and mounted in Vectashield mounting medium (Linaris, H-1200).

Microscopy and Image Analysis

Cultured cells were imaged using an Axiovert 200 microscope (C-Apochromat 63x/1.22 W objective, Carl Zeiss MicroImaging, Jena, Germany) using Axiovision 4.8 (Carl Zeiss MicroImaging) for acquisition and subsequent image processing. *Drosophila* nephrocytes were imaged with a Leica TCS SP8 confocal microscope using a 20× air objective with a numerical aperture of 0.75 (PL APO 20x/0.75 DRY, Leica Microsystems). Images were analyzed using Fiji[20], and the fluorescence intensity of the nephrocytes was quantified as described previously.[19] For high-resolution stimulated emission depletion (STED) images, a Leica TCS SP8 gSTED 3× microscope (Leica Microsystems) equipped with a white light laser for excitation and hybrid detectors (HyDs) for time-gated detection was used. After acquisition with a 100× oil immersion objective with a numerical aperture of 1.4 (PL APO 100×/1.4 Oil STED, Leica Microsystems), the images were further processed using the Huygens Essential software (Scientific Volume Imaging) for deconvolution. Quantification of the nephrocyte diaphragm (ND) length was done using a previously published Fiji macro.[21]

Further Methods are provided in Supplementary Methods.

RESULTS

Clinical Course and Genetic Findings

All patients presented as sporadic cases of childhood onset of nephrotic syndrome (Supplementary Table S1). Patient 1 presented with SRNS at the age of 17 years. Renal biopsy confirmed FSGS, and genetic analysis by whole-exome sequencing identified the previously reported recurrent *ACTN4* p.F153L mutation. Proteinuria could be reduced by ciclosporin A treatment and supportive medication.

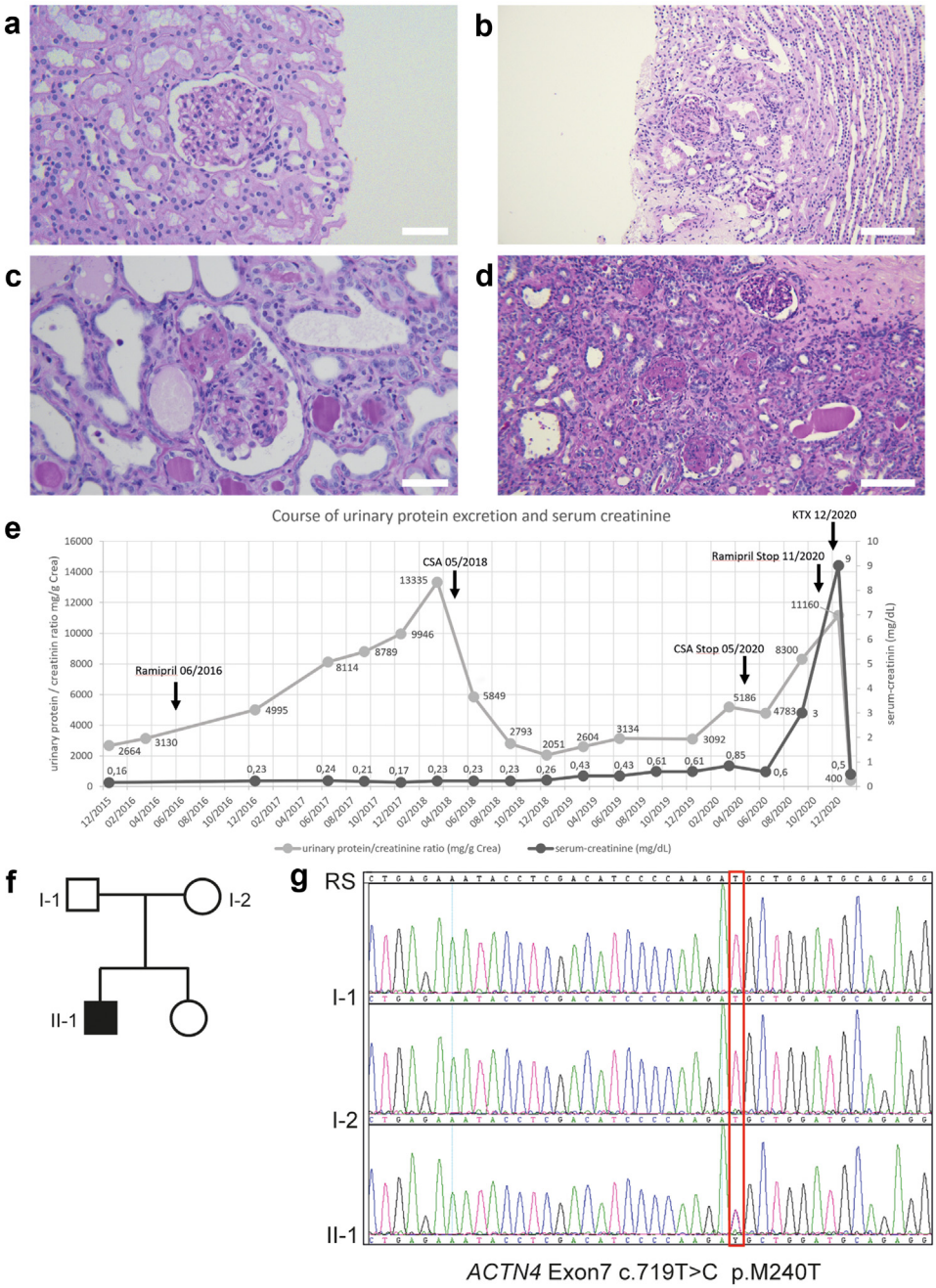

Figure 1. Identification of a novel *ACTN4* mutation in a patient presenting with steroid-resistant nephrotic syndrome. (a–d) Periodic acid–Schiff stainings of kidney biopsies of the index patient. (a) Initial kidney biopsy in 2015 showing glomeruli with normal appearing capillary tuft. Electron microscopy revealed foot process effacement of the podocytes leading to the diagnosis of minimal change glomerulopathy. (b) Kidney biopsy in 2017 with 1 glomerulum showing a perihilar focal and segmental glomerulosclerosis. (c,d) Nephrectomy specimen of (c) right and (d) left native kidney with increased globally sclerosed glomeruli and increased interstitial fibrosis and tubular atrophy. (e) Overview of the clinical course of the patient. Gray: urinary protein/creatinine ratio in mg/g. Black: serum-creatinine level in mg/dl. The patient first presented with proteinuria in December 2015. After a first biopsy (2015) showing minimal change glomerulopathy and, in the absence of clinical nephrotic syndrome, rampiril was initiated in June 2016. A second biopsy in June 2017 confirmed focal segmental glomerulosclerosis. Therapy with CSA resulted in a prompt but transient decrease of proteinuria and was stopped in May 2020 when renal function declined and proteinuria increased despite treatment. The patient was then prepared for kidney transplantation and received a living-donor graft in December 2020. (f,g) Pedigree of the index patient and targeted Sanger sequencing of *ACTN4* exon 7. Electropherograms depict the relevant sequence section around c.719T>C (p.M240T) in the index patient (II-1) and both parents (I-1 and I-2). Scale bars: 50 μm in (a) and (c), 100 μm in (b) and (d). CSA, ciclosporin A; KTx, kidney transplantation; RS, reference sequence.

Patient 2 presented with ESRD at the age of 13 years. The identified *de novo* mutation in *ACTN4* (p.G195D) was analyzed *in vitro* and published before.[10] Initiation of dialysis was necessary. After living-related kidney transplantation, no recurrence of FSGS occurred in the follow-up.

Patient 3 presented with asymptomatic proteinuria at the age of 4 years. A first kidney biopsy at the age of 5 years showed minimal change glomerulopathy (Figure 1a). Comprehensive workup excluded immunologic or infectious causes. Because proteinuria persisted though treatment with angiotensin-converting enzyme inhibition (Figure 1e), a second kidney biopsy was performed at the age of 6 years that revealed FSGS (Figure 1b).

At the same time, a gene panel analysis of 8 genes commonly found in mainly nonsyndromic SRNS/FSGS (*NPHS1*, *NPHS2*, *WT1*, *TRPC6*, *INF2*, *ACTN4*, *PLCE1*, and *PAX2*) was performed and yielded unremarkable results except for a heterozygous variant c.719T>C (p.M240T) in *ACTN4*. Segregation of the parents' DNA confirmed that p.M240T occurred *de novo* in the patient (Figure 1f and g). The identified ACTN4 variant p.M240T could not be found in either large genome databases (gnomAD[22] and HGMD mutational databases [HGMD professional 2022.2]) or our local rare kidney disease database.

Therapy with ciclosporin A was initiated (targeted blood level trough 80–120 ng/ml) and resulted in a significant decrease of proteinuria (Figure 1e). In 2020, at the age of 9 years, however, the patient developed increasing proteinuria, edema, and deterioration of kidney function (Figure 1e). Ciclosporin A therapy was discontinued at that time, and the patient progressed to end-stage kidney failure within 6 months. He received a preemptive living-donor kidney transplant from his father and has had a stable transplant function since then. A nephrectomy of both native kidneys was performed (Figure 1c and d) due to persisting proteinuria, and since removal, the boy has not shown any signs of proteinuria.

ACTN4-M240T Leads to Decreased Stability *In Silico* and *In Vitro*

The *ACTN4* mutation c.719T>C leads to amino acid change p.M240T in the N-terminal actin-binding calponin-homology domain. This is similar to other, previously described disease-associated mutations such as p.W59R, p.G195D, and p.K255E, which were reported to result in altered protein stability.[10,23,24]

To evaluate the impact of p.M240T exchange within the molecule, we used molecular dynamics analyses based on the solved crystal structure. All algorithms and platforms[12-16] predicted a strong decrease in stability caused by introduction of the amino acid exchange M240T (Figure 2a). Similar results were obtained for the highly conserved structures of *ACTN1* and *ACTN3*.[25,26] In line with these observations, p.M240T showed a reduced expression in human embryonic kidney 293T cells compared with ACTN4-WT (Figure 2b and c).

ACTN4-M240T Expression Results in Protein Mislocalization and Aggregate Formation

To analyze functional consequences of the M240T mutation, we created human podocyte cell lines that either overexpress hACTN4-WT or hACTN4-M240T. In cells expressing hACTN4-WT, the protein could be detected at the cell cortex where it colocalized with F-

a

Algorithm	ACTN4 (PDB: 2R0O)		ACTN1 (PDB: 2EYN)		ACTN3 (PDB: 1WKU)	
	ΔΔG (kcal/mol)	Effect	ΔΔG (kcal/mol)	Effect	ΔΔG (kcal/mol)	Effect
DUET	-1.797	Destabilizing	-1.767	Destabilizing	-1.893	Destabilizing
PoPMuSiC v 3.1	1.43	Destabilizing	1.3	Destabilizing	1.27	Destabilizing
CUPSAT	-1.04	Destabilizing	-4.95	Destabilizing	-3.18	Destabilizing
IMutant v2.0	-1.96	Destabilizing	-1.9	Destabilizing	-2.21	Destabilizing

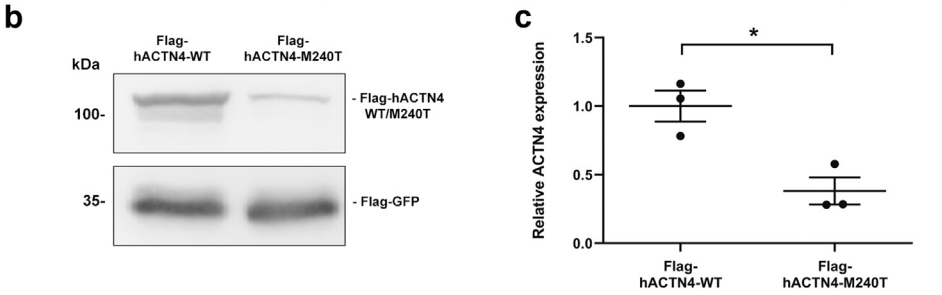

Figure 2. *In silico* and *in vitro* characterization of hACTN4-M240T stability. (a) *In silico* prediction of M240T mutation on alpha-actinin protein stability (delta-delta-G) using 4 different computational algorithms. M>T amino acid exchange in the conserved domain has a destabilizing effect in *ACTN4* as well as *ACTN1* and *ACTN3*. (b) Representative western blot analysis of whole-cell lysates cotransfected with Flag-hACTN4-WT or Flag-hACTN4-M240T and Flag-GFP serving as expression control. (c) Densitometric quantification of 3 independent experiments as shown in (b). Compared with the WT variant, hACTN4-M240T is significantly lower expressed ($n = 3$, error bars indicate SD, $^*P < 0.05$, two-tailed *t* test). GFP, green fluorescent protein; WT, wild-type.

actin (Figure 3a). In contrast, hACTN4-M240T expression led to severely perturbed localization of the protein. hACTN4-M240T was observed to be located toward the center of the cell forming large aggregates that partially overlapped with F-actin (Figure 3a). Similar observations were made by performing an actin fractionation assay in human embryonic kidney 293T cells. Cell lysates of cells either expressing hACTN4-WT or hACTN4-M240T were subjected to differential centrifugation. The Triton insoluble fraction contains large actin bundles, whereas the Triton soluble fraction, further divided into a pellet and supernatant fraction, contains unbundled filamentous actin and globular actin, respectively. Upon western blot analysis, it was observed that the mutated protein was more abundant in the Triton insoluble fraction (Figure 3b and c), that is, associated with bundled actin.

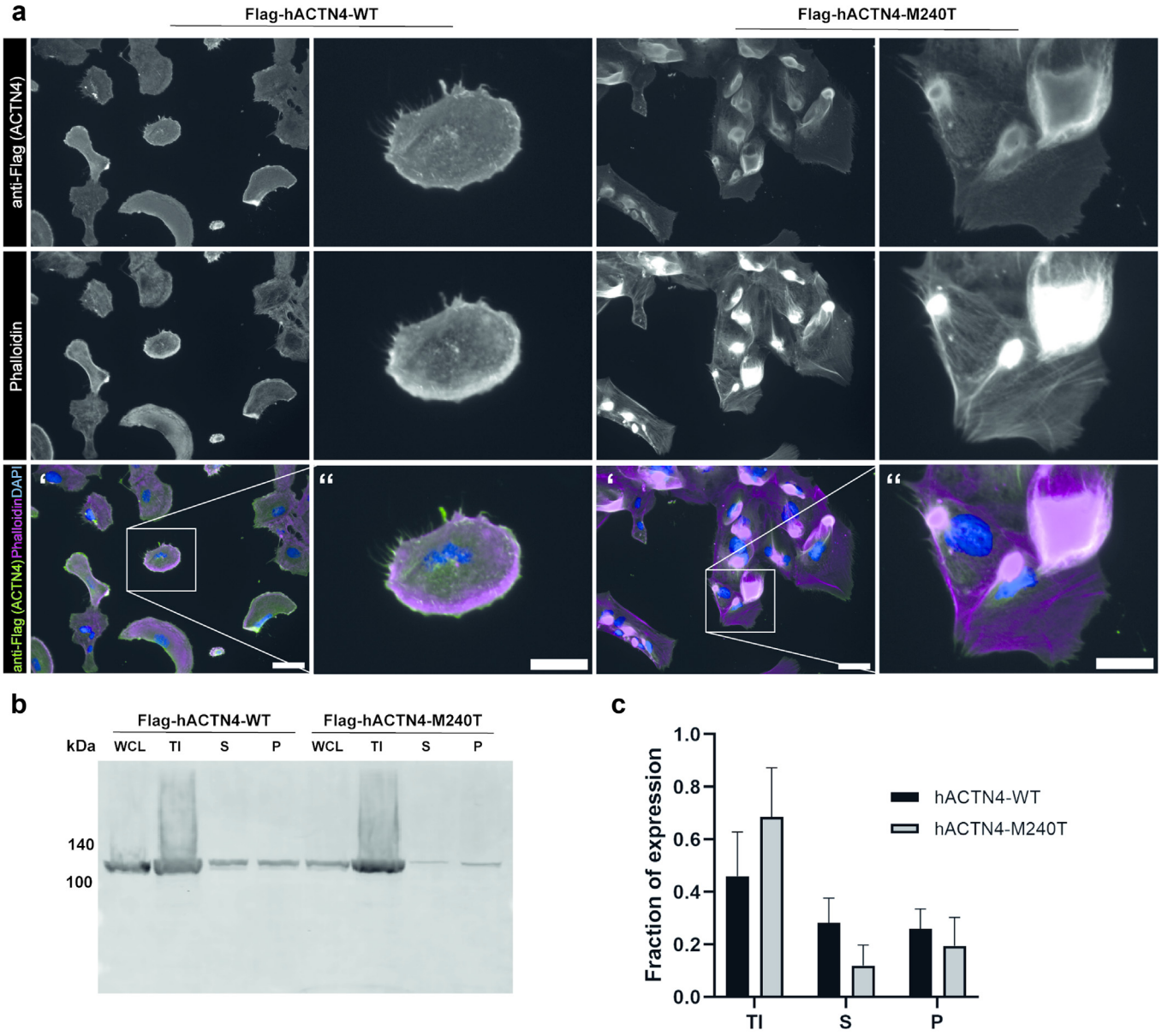

Figure 3. ACTN4-M240T mutation leads to perturbed cellular localization and aggregate formation. (a) Immunofluorescence analysis of podocyte cell lines stably expressing Flag-tagged hACTN4-WT or hACTN4-M240T. Cells were stained with anti-FLAG antibody as well as Phalloidin and 4′,6-diamidino-2-phenylindole to visualize filamentous actin and the nucleus, respectively. In contrast to cells expressing the WT variant, where the protein is located in the cortical region together with F-actin, localization of ACTN4-M240T can be detected more toward the center of the cells, partially associated with large F-actin positive aggregates. Single channels are shown in gray, and scale bar indicates 50 μm in ′ and 25 μm in ″. (b) Representative western blot analysis of fractionation assays performed in cells transiently expressing either hACTN4-WT or hACTN4-M240T. Whole-cell lysates were subjected to differential centrifugation and the Triton X-100 insoluble as well as the supernatant and pellet derived from the Triton X-100 soluble fraction were analyzed by western blot stained with anti-FLAG antibodies. (c) Densitometric analysis of ACTN4 distribution in TI, S, and P fractions for ACTN4-WT and ACTN4-M240T ($n = 4$). P, pellet; S, supernatant; TI, Triton X-100 insoluble; WCL, whole-cell lysates; WT, wild-type.

Knockdown of Actinin in *Drosophila* Nephrocytes Leads to Reduced ND Length and Filtration Deficits

Next, we made use of the model organism *Drosophila melanogaster* and analyzed the impact of hACTN4-M240T on nephrocyte morphology and function *in vivo*. Nephrocytes are podocyte-like cells in the fly that built an ND (Figure 4a) via nephrin and NEPH1 homologous proteins Sticks and Stones and Dumbfounded, respectively, and they are responsible for clearing the hemolymph, the fly's blood equivalent, by an interplay of filtration and endocytosis.[27,28] To express human variants of *ACTN4* in a knockdown background, we first aimed to characterize the nephrocyte-specific RNAi-mediated knockdown of endogenous actinin (*ACTN*), the sole homolog of alpha-actinin 1 to 4 proteins in the fly, using the GAL4-UAS-System.[29] The Actin protein shows an amino acid identity of about 68% with human *ACTN4*, whereby the actin-

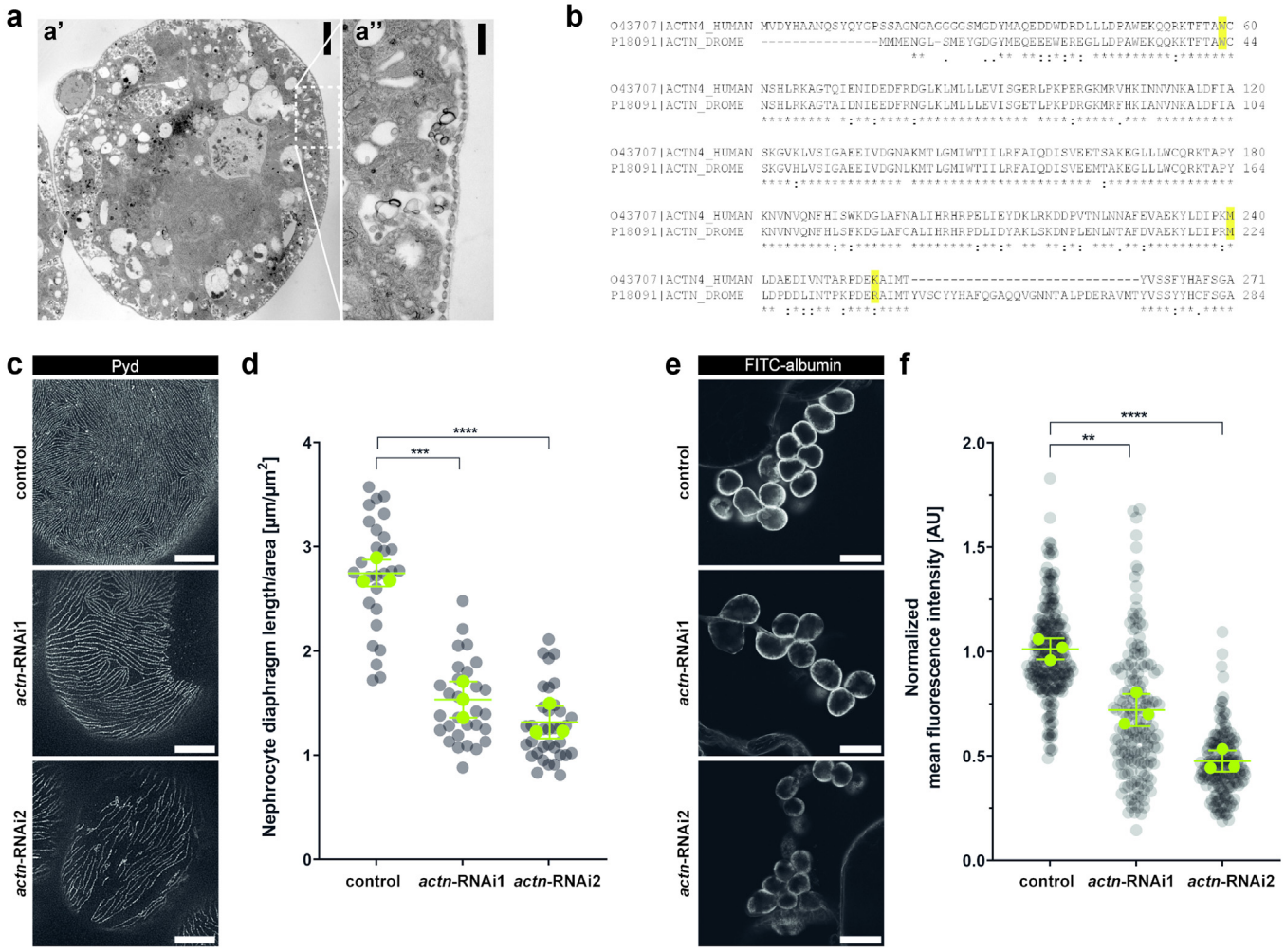

Figure 4. Knockdown of *Drosophila* actinin in nephrocytes results in decreased ND length and reduced filtration function. (a) Electron micrograph depicting a wild-type nephrocyte. Scale bars indicate 5 µm in A' and 500 nm in A'' (b) Protein alignment of the N-terminal actin-binding domain of human *ACTN4* and *Drosophila* actinin. Highlighted are amino acids known to be causative of monogenic nephrotic syndrome. Actinin shares 68.83% overall identity with *ACTN4*, the actin-binding domain of the 2 proteins shares 78.8% identity. (c,d) Representative micrographs of nephrocytes stained with (c) anti-Pyd and (d) quantification of the ND length. Nephrocytes derived from either control larvae, or larvae with nephrocyte-specific knockdown of actinin (ACTN), by using 2 different UAS-RNAi-lines (*actn*-RNAi1 and *actn*-RNAi2). Compared with control nephrocytes, the ND length of actn-depleted nephrocytes is significantly reduced (gray dots show all nephrocytes measured, green dots represent means of $n = 3$ independent experiments performed in 3 experimental crossings, error bars indicate SD, $^{**}P < 0.01$, $^{***}P < 0.001$, one-way ANOVA with Tukey's *post hoc* test). (e,f) Representative micrographs of nephrocytes subjected to (e) FITC-albumin tracer and (f) quantification of fluorescence intensity as a measure of uptake capacity. Control and *ACTN* knockdown nephrocytes were incubated in 0.2 mg/ml FITC-albumin solution for 30 seconds, and fluorescence intensity was quantified using Fiji. The data are presented as normalized to control levels. Both, *actn*-RNAi1 and *actn*-RNAi2 nephrocytes show a significantly reduced capacity of FITC-albumin uptake with respect to control nephrocytes, indicating severe filtration defects (gray dots show all nephrocytes measured, green dots indicate means of $n = 3$ independent experiments performed in 3 experimental crossings, error bars indicate SD, $^{**}P < 0.01$, $^{****}P < 0.0001$, one-way ANOVA with Tukey's *post hoc* test). Scale bars indicate 5 µm in (c) and 25 µm in (f). FITC, fluorescein isothiocyanate; ND, nephrocyte diaphragm; Pyd, polychaetoid; RNAi, RNA interference.

binding domain in general as well as also single critical amino acids known to be affected in patients with glomerular disease, are especially conserved (Figure 4b). For nephrocyte-specific expression of target genes, the Sticks and Stones-GAL4 driver line[17] was used. To exclude off-target effects, 2 different *actn*-RNAi lines (*actn*-RNAi1 and *actn*-RNAi2, respectively) were used to achieve nephrocyte-specific depletion of *actn* levels. Overexpression of a short hairpin directed against green fluorescent protein served as control.

To study morphologic consequences of actn depletion in nephrocytes, we first performed immunofluorescent stainings with an antibody directed against polychaetoid, the homolog of ZO-1, which localizes to the ND. Visualizing the cells' surface by super-resolution microscopy, a fingerprint-like pattern of NDs can be detected, which can be quantified as a representation of the ND length (Figure 4b and c) using a previously published ImageJ/Fiji macro.[21] Knockdown of *actn* resulted in a loosened ND pattern with both RNAi-lines. Quantification showed that the reduction in ND length is comparable in both lines (Figure 4c and d). To analyze nephrocyte function, we performed a tracer uptake assay[19] and assessed the nephrocytes' capacity of taking up FITC-labeled albumin. As described before,[30,31] knockdown of *actn* led to a severe functional phenotype, as uptake capacity was significantly decreased in both knockdown lines with respect to control nephrocytes (Figure 4e and f).

hACTN4-M240T Is Not Able to Rescue the *actn* Knockdown Phenotype in *Drosophila*

To elucidate whether hACTN4-M240T is a disease-causing variant of *ACTN4*, we studied its potential to rescue the above-described *actn* knockdown–associated phenotypes in comparison to hACTN4-WT. We also included hACTN4-W59R and hACTN4-K255E in our studies, 2 well-characterized pathogenic *ACTN4* variants. We expressed the individual HA-tagged hACTN4-variants in the background of *actn*-RNAi2, owing to its more pronounced and robust phenotype regarding both morphology and filtration. The newly generated fly lines, which were holding both constructs, UAS-*actn*-RNAi2 and UAS-HA-hACTN4-variant, were validated on the level of protein expression by detection of the protein's HA-tag in immunofluorescence stainings (Supplementary Figure S1).

When expressing hACTN4-WT in the knockdown background, we could observe a significant rescue capacity of ND length (Figure 5a and b) and of filtration capacity (Figure 5c and d). hACTN4-M240T, however, was not able to ameliorate either the morphologic or the functional phenotype, which was also observed when expressing hACTN-W59R and hACTN-K255E (Figure 5).

DISCUSSION

In childhood and adolescence, genetic causes are among the most common origins of chronic kidney disease. Even in adults, a significant number of patients carry a known genetic defect that contributes to the development of ESRD.[32] INF2, TRPC6, and *ACTN4* are the prime examples of autosomal-dominant forms of SRNS, whereas most of the mutations leading to ESRD are inherited in an autosomal recessive manner and often occur as compound heterozygous alleles.[9,24,33] To date, 20 different mutations have been reported for *ACTN4*-associated glomerular disease, most of them (nonsynonymous) missense mutations (HGMD professional 2022.2).

Within the CRU329, we identified disease-causing mutations in *ACTN4* in 3 patients (Supplementary Table S1). One of these mutations was already reported in 3 other patients (p.F153L). A second identified mutation (p.G195D) was analyzed *in vitro* and reported in 2016.[10] Here, we report on the analysis of the mutation identified in the third patient who developed proteinuria at the age of 4 years and responded temporarily to ciclosporin A. Genetic workup revealed a *de novo* ACTN4 p.M240T single-nucleotide polymorphism. To test the pathogenicity of ACTN4 p.M240T, we established a time-efficient experimental pipeline using *in silico*, *in vitro*, and *in vivo* experiments. ACTN4 p.M240T was found to be less stable and mislocalized, resulting in aggregates disturbing the actin-based cytoskeleton. *In vivo* experiments using the *Drosophila* nephrocyte model confirmed the pathogenicity of hACTN4-M240T and thereby establish the diagnosis for the described patient.

Mutations in *ACTN4* are inherited in an autosomal-dominant fashion and mostly lead to FSGS and ESRD in adult patients,[9] although several reports including this manuscript describe patients that develop severe kidney disease at a rather young age.[10,24] The responsible mutations are located in 1 of the 2 calponin-homology-domains constituting the N-terminal actin-binding domain. Among other scaffolding proteins, *ACTN4* has been shown to colocalize with nephrin at the podocytes' slit diaphragm.[34,35] As part of this group of slit diaphragm complex proteins, it is involved in anchoring the actin cytoskeleton to junctional proteins and the glomerular basement membrane.[35] Ultimately, *ACTN4* is implicated in several cellular functions and, in particular, to establish and maintain the podocyte's sophisticated 3D structure, adhesion to the glomerular basement membrane, and signal transduction processes.[36-38] The biological consequences of *ACTN4* mutations and the mechanism by which they lead to disease are not fully understood. It is postulated that a

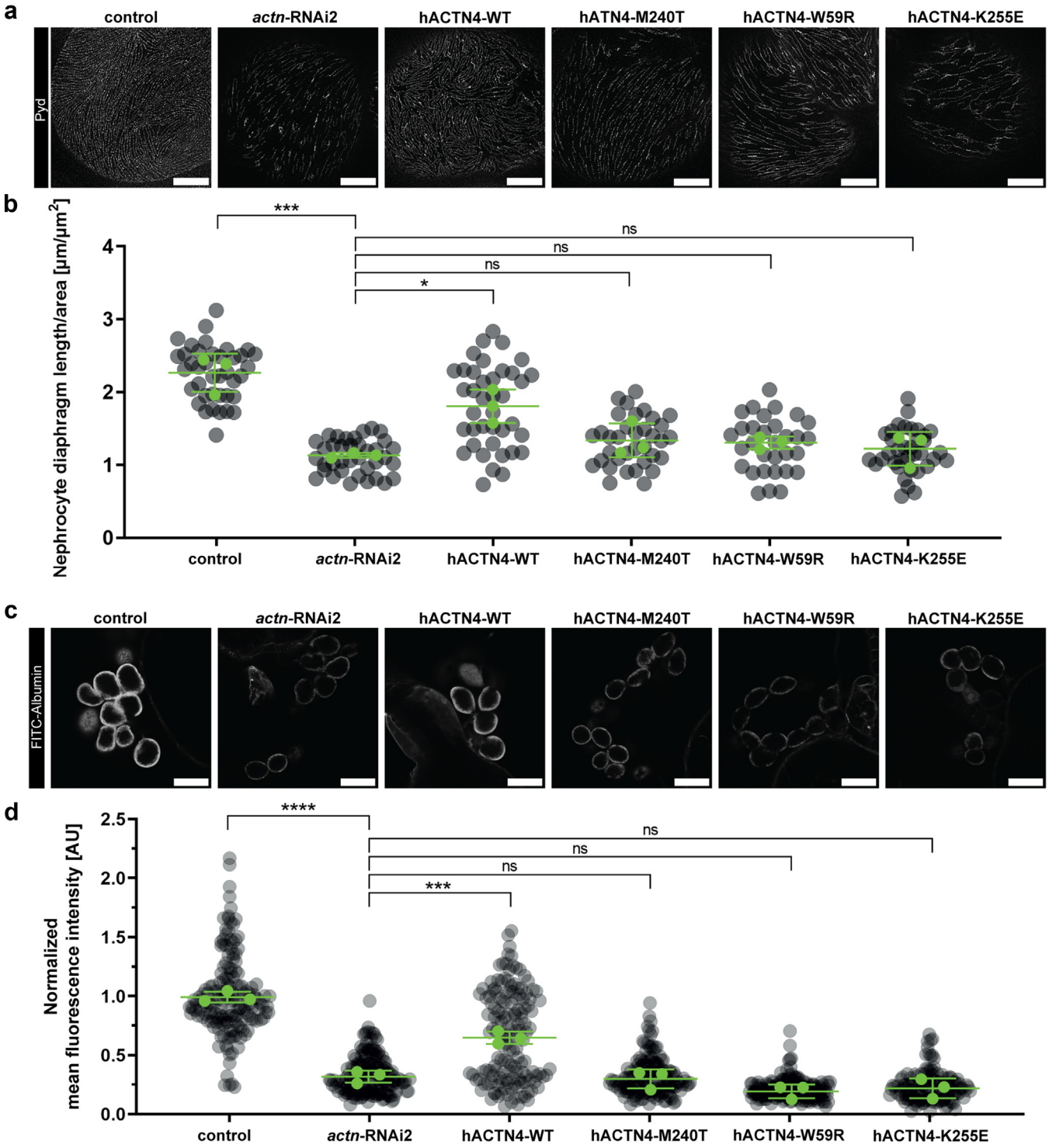

Figure 5. hACTN4-M240T reexpression does not ameliorate actinin knockdown–associated phenotypes. (a,b) Representative micrographs of nephrocytes stained with (a) anti-Pyd and (b) quantification of the ND length. Nephrocytes derived from either control larvae, larvae with nephrocyte-specific knockdown of *actinin* (*actn*-RNAi2) as well as larvae reexpressing the indicated hACTN4-variant in the knockdown background. hACTN4-WT is able to partially rescue the actinin knockdown–associated reduction in ND length, whereas reexpression of hACTN-M240T does not lead to increased ND length. This is also true for FSGS-associated mutations FSGS-W59R and FSGS-K255E (gray dots indicate all nephrocytes measured, green dots show means of $n = 3$ independent experiments performed in 3 experimental crossings, error bars indicate SD, $^{***}P < 0.001$, $^{*}P < 0.05$, one-way analysis of variance with Tukey's *post hoc* test). (c,d) Representative micrographs of nephrocytes subjected to (c) FITC-albumin tracer and (d) quantification of fluorescence intensity as a measure of uptake capacity. Nephrocytes were incubated in 0.2 mg/ml FITC-albumin solution for 30 seconds, and fluorescence intensity was quantified using Fiji. The data are presented as normalized to control levels. Reexpression of hACTN4-WT also leads to a significant increase in tracer uptake capacity, compared with hACTN4-M240T, hACTN4-W59R, and hACTN4-K255E, where a rescue of actinin knockdown–associated reduction of tracer uptake cannot be observed (gray dots indicate all nephrocytes measured, green dots show means of $n = 3$ independent experiments performed in 3 (continued)

conformational change occurs when *ACTN4*-mutants bind to F-actin, which results in an altered binding affinity for mutant proteins as compared with WT *ACTN4*.[39] The dissociation rate of *ACTN4*-K255E from F-actin is much slower as compared with the WT protein[40] and also promotes the formation of F-actin aggregates,[39] a finding that is also observed with further *ACTN4* mutations including this study.[10] One might speculate whether the disease is driven by the loss of *ACTN4* function itself or owing to its mislocalization or both. Several other *ACTN4* mutants have been described to be less stable *in vitro* and to be more rapidly degraded whereby protein synthesis remains stable[41] or to possess a higher affinity for F-actin.[10,23,24,41] Moreover, *ACTN4* knockout mice develop profound proteinuria and FSGS at the age of 10 weeks and show a decreased number of glomerular podocytes.[36,42] Lower expression levels of *ACTN4* were also reported in patients with glomerulopathies including FSGS.[43]

We used the genetic toolbox of *Drosophila melanogaster* to study the impact of *ACTN4*-M240T on nephrocyte morphology and function. The *Drosophila* system has several advantages over higher organisms such as mouse models. In addition to simple and cheap husbandry, the fruit fly stands out with its diverse methods of genetic manipulation.[44,45] Numerous commercially available fly lines, including mutant and RNAi libraries and custom-made stocks for the expression of, for example, human transgenes make it possible to study a gene of interest and its genetic interactors in a shorter time frame. It is noteworthy, that although it is an invertebrate system, *Drosophila* shares a high genomic, molecular, and structural conservation with mammals, which is why its use in biomedical research has been and still is increasing.[46–52] The rediscovery of nephrocytes and their structural and functional similarity to mammalian podocytes[27,28] broadened that scope to glomerular kidney diseases, emphasizing the feasibility of the *Drosophila* nephrocyte system not only to address basic podocyte research but also to accompany diagnostics of glomerular diseases in the future.

The presented case underlines several important aspects regarding diagnostics and treatment in patients with FSGS. First, the trigger leading to the FSGS has to be identified. An in-depth workup is necessary and genetic testing is a central piece in diagnostics, especially when no other overt cause is found. Second, apart from the growing number of known genes and mutations contributing to SRNS and FSGS, sequencing approaches facilitate the establishment of a potential genetic diagnosis.[53] In this context, it is necessary to keep in mind that there is a substantial rate of polymorphisms or rare benign variants that are not disease-causing.[54,55] Therefore, further workup is necessary to provide evidence of whether a novel discovered variant is indeed pathogenic. Besides *in silico* predictions and *in vitro* cell culture experiments, the *Drosophila* nephrocyte is an attractive and feasible system to add *in vivo* data to these critical analyses. This is not just necessary to ensure the diagnosis in the individual patient, but it also helps to guide therapy decisions (e.g., avoiding medications with potentially adverse side effects that are unlikely to be effective in certain conditions) and to counsel the patient and the family regarding future treatment options, such as whether a living-donor kidney transplantation is suggested and possible. Third, the presented case confirms and adds to the growing body of literature that indicates that in cases of FSGS attributed to a genetic cause, immunosuppressive treatment strategies such as ciclosporin A might result at least in a partial response and can delay the time until a kidney replacement therapy or transplantation is necessary.[7,56] This positive effect might be attributed to direct effects of certain drugs on podocyte structures such as the cytoskeleton.[57] Furthermore, proteinuria itself triggers an immune response that accelerates the glomerular injury. This can be controlled—at least to some extent—by immunosuppressive drugs.[58]

The growing complexity in genetics, clinical presentation, molecular characterization of the affected proteins, and individual treatment options of these patients also emphasizes the need for inclusion of patients in registries and databases.[8,59,60] The characterization of unclear variants is key to optimizing patient care and guidance, especially when the clinical presentation and course differ from the published literature. Bioinformatic prediction tools such as the ClinPred score[61] are helpful to estimate the potential pathogenic impact of novel sequence variants, but formal proof of deleterious effects and altered function should be aimed for in cases where far-reaching clinical decisions such as preemptive living-donor kidney transplantation depend on the genotype data. Of note, the presented cases underline that *ACTN4* mutations should also be considered in young (sporadic) patients with FSGS.

Figure 5. (continued) experimental crossings, error bars indicate SD, ***$P < 0.001$, ****$P < 0.0001$, one-way analysis of variance with Tukey's *post hoc* test). Scale bars indicate 5 μm in (a) and 25 μm in (c). FITC, fluorescein isothiocyanate; ND, nephrocyte diaphragm; Pyd, polychaetoid; WT, wild-type.

In conclusion, we present a feasible combined way to evaluate the pathogenic potential of novel mutations in podocyte genes. This might be a blueprint for a pipeline analyzing unclear genetic variants in patients with podocyte diseases such as FSGS.

DISCLOSURE

All the authors declared no competing interests.

ACKNOWLEDGMENTS

We thank the patient and his parents for participating in our study. We thank all members of our laboratories for the helpful discussion. We thank Martyna Brütting and Steffi Keller for their excellent technical assistance.

Funding

MPB was supported in part by an intramural grant from the University of Cologne (Gerok program). PTB was supported by a DFG fellowship BR2955/6-1) and the clinical research unit (KFO 329, BR 2955/8-1). JA, BBB, and SH were supported by the clinical research unit (KFO 329, AL901/2-1 and AL901/3-1 to JA, BE6072/2-1 and BE6072/3-1 to BBB, HA 8479/1-2 to SH). Additional support was provided from the consortium STOP-FSGS by the German Ministry for Science and Education (BMBF 01GM1901E to PTB and TB) and the Else-Kröner-Fresenius Foundation (2017_A135 to SK).

AUTHOR CONTRIBUTIONS

JO, PTB, SH, and MPB conceived the study; JO, SD, VL, TM, KR, and MMR performed experiments; JO, SD, MMR, BBB, MH, SH, and MPB analyzed the data. BR, JP, JA, and BBB performed the genetic analyses; HG performed the nephropathological workup; ZCG, MH, and SH cared for the patient in the clinic and contributed clinical data and data analyses, JO created the figures and drafted the paper; JO, SD, MH, MMR, SK, BS, TB, BBB, PTB, SH, and MPB revised the paper; all authors approved the final version of the manuscript.

SUPPLEMENTARY MATERIAL

Supplementary File (PDF)

Supplementary Methods.

Supplementary References.

Figure S1. Validation of protein expression of hACTN4-variants in *Drosophila* nephrocytes.

Table S1. ACNT4 *de novo* variants identified in pediatric SRNS/FSGS cases.

REFERENCES

1. Rosenberg AZ, Kopp JB. Focal segmental glomerulosclerosis. *Clin J Am Soc Nephrol*. 2017;12:502–517. https://doi.org/10.2215/CJN.05960616
2. McGrogan A, Franssen CF, de Vries CS. The incidence of primary glomerulonephritis worldwide: a systematic review of the literature. *Nephrol Dial Transplant*. 2011;26:414–430. https://doi.org/10.1093/ndt/gfq665
3. Shabaka A, Ribera AT, Fernández-Juárez G. Focal segmental glomerulosclerosis: state-of-the-art and clinical perspective. *Nephron*. 2020;144:413–427. https://doi.org/10.1159/000508099
4. Sadowski CE, Lovric S, Ashraf S, et al. A single-gene cause in 29.5% of cases of steroid-resistant nephrotic syndrome. *J Am Soc Nephrol*. 2015;26:1279–1289. https://doi.org/10.1681/ASN.2014050489
5. Liu J, Wang W. Genetic basis of adult-onset nephrotic syndrome and focal segmental glomerulosclerosis. *Front Med*. 2017;11:333–339. https://doi.org/10.1007/s11684-017-0564-1
6. Feng D, DuMontier C, Pollak MR. Mechanical challenges and cytoskeletal impairments in focal segmental glomerulosclerosis. *Am J Physiol Ren Physiol*. 2018;314:F921–F925. https://doi.org/10.1152/ajprenal.00641.2017
7. Tullus K, Webb H, Bagga A. Management of steroid-resistant nephrotic syndrome in children and adolescents. *Lancet Child Adolesc Health*. 2018;2:880–890. https://doi.org/10.1016/S2352-4642(18)30283-9
8. Völker LA, Ehren R, Grundmann F, Benzing T, Weber LT, Brinkkötter PT. A newly established clinical registry of minimal change disease and focal and segmental glomerulosclerosis in Germany. *Nephrol Dial Transplant*. 2019;34:1983–1986. https://doi.org/10.1093/ndt/gfz046
9. Feng D, DuMontier C, Pollak MR. The role of alpha-actinin-4 in human kidney disease. *Cell Biosci*. 2015;5:44. https://doi.org/10.1186/s13578-015-0036-8
10. Bartram MP, Habbig S, Pahmeyer C, et al. Three-layered proteomic characterization of a novel ACTN4 mutation unravels its pathogenic potential in FSGS. *Hum Mol Genet*. 2016;25:1152–1164. https://doi.org/10.1093/hmg/ddv638
11. Lee SH, Weins A, Hayes DB, Pollak MR, Dominguez R. Crystal structure of the actin-binding domain of alpha-actinin-4 Lys255Glu mutant implicated in focal segmental glomerulosclerosis. *J Mol Biol*. 2008;376:317–324. https://doi.org/10.1016/j.jmb.2007.11.084
12. Parthiban V, Gromiha MM, Schomburg D. CUPSAT: prediction of protein stability upon point mutations. *Nucleic Acids Res*. 2006;34:W239–W242. https://doi.org/10.1093/nar/gkl190
13. Capriotti E, Fariselli P, Casadio R. I-Mutant2.0: predicting stability changes upon mutation from the protein sequence or structure. *Nucleic Acids Res*. 2005;33:W306–W310. https://doi.org/10.1093/nar/gki375
14. Dehouck Y, Kwasigroch JM, Gilis D, Rooman M. PoPMuSiC 2.1: a web server for the estimation of protein stability changes upon mutation and sequence optimality. *BMC Bioinformatics*. 2011;12:151. https://doi.org/10.1186/1471-2105-12-151
15. Dehouck Y, Grosfils A, Folch B, Gilis D, Bogaerts P, Rooman M. Fast and accurate predictions of protein stability changes upon mutations using statistical potentials and neural networks: PoPMuSiC-2.0. *Bioinformatics*. 2009;25:2537–2543. https://doi.org/10.1093/bioinformatics/btp445
16. Pires DE, Ascher DB, Blundell TL. DUET: a server for predicting effects of mutations on protein stability using an integrated computational approach. *Nucleic Acids Res*. 2014;42:W314–W319. https://doi.org/10.1093/nar/gku411

17. Kocherlakota KS, Wu JM, McDermott J, Abmayr SM. Analysis of the cell adhesion molecule sticks-and-stones reveals multiple redundant functional domains, protein-interaction motifs and phosphorylated tyrosines that direct myoblast fusion in Drosophila melanogaster. *Genetics*. 2008;178:1371–1383. https://doi.org/10.1534/genetics.107.083808

18. Dietzl G, Chen D, Schnorrer F, et al. A genome-wide transgenic RNAi library for conditional gene inactivation in Drosophila. *Nature*. 2007;448:151–156. https://doi.org/10.1038/nature05954

19. Odenthal J, Brinkkoetter PT. Drosophila melanogaster and its nephrocytes: a versatile model for glomerular research. *Methods Cell Biol*. 2019;154:217–240. https://doi.org/10.1016/bs.mcb.2019.03.011

20. Schindelin J, Arganda-Carreras I, Friese E, et al. Fiji: an open-source platform for biological-image analysis. *Nature Methods*. 2012;9:676–682. https://doi.org/10.1038/nmeth.2019

21. Butt L, Unnersjö-Jess D, Höhne M, et al. A molecular mechanism explaining albuminuria in kidney disease. *Nat Metab*. 2020;2:461–474. https://doi.org/10.1038/s42255-020-0204-y

22. Karczewski KJ, Francioli LC, Tiao G, et al. The mutational constraint spectrum quantified from variation in 141,456 humans. *Nature*. 2020;581;2022 7809:434–443. https://doi.org/10.1038/s41586-020-2308-7

23. Michaud JLR, Chaisson KM, Parks RJ, Kennedy CRJ. FSGS-associated α-actinin-4 (K256E) impairs cytoskeletal dynamics in podocytes. *Kidney Int*. 2006;70:1054–1061. https://doi.org/10.1038/sj.ki.5001665

24. Weins A, Kenlan P, Herbert S, et al. Mutational and Biological Analysis of alpha-actinin-4 in focal segmental glomerulosclerosis. *J Am Soc Nephrol*. 2005;16:3694–3701. https://doi.org/10.1681/ASN.2005070706

25. Borrego-Diaz E, Kerff F, Lee SH, Ferron F, Li Y, Dominguez R. Crystal structure of the actin-binding domain of alpha-actinin 1: evaluating two competing actin-binding models. *J Struct Biol*. 2006;155:230–238. https://doi.org/10.1016/j.jsb.2006.01.013

26. Franzot G, Sjöblom B, Gautel M, Carugo KD. The crystal structure of the actin binding domain from alpha-actinin in its closed conformation: structural insight into phospholipid regulation of alpha-actinin. *J Mol Biol*. 2005;348:151–165. https://doi.org/10.1016/j.jmb.2005.01.002

27. Weavers H, Prieto-Sánchez S, Grawe F, et al. The insect nephrocyte is a podocyte-like cell with a filtration slit diaphragm. *Nature*. 2009;457:322–326. https://doi.org/10.1038/nature07526

28. Zhuang S, Shao H, Guo F, Trimble R, Pearce E, Abmayr SM. Sns and Kirre, the Drosophila orthologs of nephrin and Neph1, direct adhesion, fusion and formation of a slit diaphragm-like structure in insect nephrocytes. *Development*. 2009;136:2335–2344. https://doi.org/10.1242/dev.031609

29. Brand AH, Perrimon N. Targeted gene expression as a means of altering cell fates and generating dominant phenotypes. *Development*. 1993;118:401–415. https://doi.org/10.1242/dev.118.2.401

30. Hermle T, Braun DA, Helmstädter M, Huber TB, Hildebrandt F. Modeling monogenic human nephrotic syndrome in the drosophila garland cell nephrocyte. *J Am Soc Nephrol*. 2017;28:1521–1533. https://doi.org/10.1681/ASN.2016050517

31. Zhang F, Zhao Y, Han Z. An in vivo functional analysis system for renal gene discovery in drosophila pericardial nephrocytes. *J Am Soc Nephrol*. 2013;24:191–197. https://doi.org/10.1681/ASN.2012080769

32. Lepori N, Zand L, Sethi S, Fernandez-Juarez G, Fervenza FC. Clinical and pathological phenotype of genetic causes of focal segmental glomerulosclerosis in adults. *Clin Kidney J*. 2018;11:179–190. https://doi.org/10.1093/ckj/sfx143

33. Kaplan JM, Kim SH, North KN, et al. Mutations in ACTN4, encoding alpha-actinin-4, cause familial focal segmental glomerulosclerosis. *Nat Genet*. 2000;24:251–256. https://doi.org/10.1038/73456

34. Drenckhahn D, Franke RP. Ultrastructural organization of contractile and cytoskeletal proteins in glomerular podocytes of chicken, rat, and man. *Lab Invest*. 1988;59:673–682.

35. Lehtonen S, Ryan JJ, Kudlicka K, Iino N, Zhou H, Farquhar MG. Cell junction-associated proteins IQGAP1, MAGI-2, CASK, spectrins, and alpha-actinin are components of the nephrin multiprotein complex. *Proc Natl Acad Sci U S A*. 2005;102:9814–9819. https://doi.org/10.1073/pnas.0504166102

36. Dandapani SV, Sugimoto H, Matthews BD, et al. Alpha-actinin-4 is required for normal podocyte adhesion. *J Biol Chem*. 2007;282:467–477. https://doi.org/10.1074/jbc.M605024200

37. Zhao X, Hsu KS, Lim JH, Bruggeman LA, Kao HY. α-actinin 4 potentiates nuclear factor κ-light-chain-enhancer of activated B-cell (NF-κB) activity in podocytes independent of its cytoplasmic actin binding function. *J Biol Chem*. 2015;290:338–349. https://doi.org/10.1074/jbc.M114.597260

38. Nakatsuji H, Nishimura N, Yamamura R, Kanayama HO, Sasaki T. Involvement of actinin-4 in the recruitment of JRAB/MICAL-L2 to cell-cell junctions and the formation of functional tight junctions. *Mol Cell Biol*. 2008;28:3324–3335. https://doi.org/10.1128/MCB.00144-08

39. Weins A, Schlondorff JS, Nakamura F, et al. Disease-associated mutant α-actinin-4 reveals a mechanism for regulating its F-actin-binding affinity. *Proc Natl Acad Sci U S A*. 2007;104:16080–16085. https://doi.org/10.1073/pnas.0702451104

40. Ward SM, Weins A, Pollak MR, Weitz DA. Dynamic viscoelasticity of actin cross-linked with wild-type and disease-causing mutant alpha-actinin-4. *Biophys J*. 2008;95:4915–4923. https://doi.org/10.1529/biophysj.108.131722

41. Yao J, Le TC, Kos CH, et al. Alpha-actinin-4-mediated FSGS: an inherited kidney disease caused by an aggregated and rapidly degraded cytoskeletal protein. *PLoS Biol*. 2004;2:e167. https://doi.org/10.1371/journal.pbio.0020167

42. Kos CH, Le TC, Sinha S, et al. Mice deficient in alpha-actinin-4 have severe glomerular disease. *J Clin Invest*. 2003;111:1683–1690. https://doi.org/10.1172/JCI17988

43. Liu Z, Blattner SM, Tu Y, et al. Alpha-actinin-4 and CLP36 protein deficiencies contribute to podocyte defects in multiple human glomerulopathies. *J Biol Chem*. 2011;286:30795–30805. https://doi.org/10.1074/jbc.M111.255984

44. Venken KJT, Bellen HJ. Emerging technologies for gene manipulation in Drosophila melanogaster. *Nat Rev Genet*. 2005;6:167–178. https://doi.org/10.1038/nrg1553

45. Venken KJ, Sarrion-Perdigones A, Vandeventer PJ, Abel NS, Christiansen AE, Hoffman KL. Genome

engineering: Drosophila melanogaster and beyond. *Wiley Interdiscip Rev Dev Biol*. 2016;5:233–267. https://doi.org/10.1002/wdev.214

46. Jennings BH. Drosophila–a versatile model in biology & medicine. *Mater Today*. 2011;14:190–195. https://doi.org/10.1016/S1369-7021(11)70113-4
47. Stephenson R, Metcalfe NH. Drosophila melanogaster: a fly through its history and current use. *J R Coll Phys Edinb*. 2013;43:70–75. https://doi.org/10.4997/JRCPE.2013.116
48. Kornberg TB, Krasnow MA. The Drosophila genome sequence: implications for biology and medicine. *Science*. 2000;287:2218–2220. https://doi.org/10.1126/science.287.5461.2218
49. Adams MD, Celniker SE, Holt RA, et al. The genome sequence of Drosophila melanogaster. *Science*. 2000;287:2185–2195. https://doi.org/10.1126/science.287.5461.2185
50. Wangler MF, Yamamoto S, Bellen HJ. Fruit flies in biomedical research. *Genetics*. 2015;199:639–653. https://doi.org/10.1534/genetics.114.171785
51. Cauchi RJ, van den Heuvel M. The fly as a model for neurodegenerative diseases: is it worth the jump? *Neurodegener Dis*. 2006;3:338–356. https://doi.org/10.1159/000097303
52. Reiter LT, Potocki L, Chien S, Gribskov M, Bier E. A systematic analysis of human disease-associated gene sequences in Drosophila melanogaster. *Genome Res*. 2001;11:1114–1125. https://doi.org/10.1101/gr.169101
53. Ng SB, Buckingham KJ, Lee C, et al. Exome sequencing identifies the cause of a mendelian disorder. *Nat Genet*. 2010;42:30–35. https://doi.org/10.1038/ng.499
54. Cassa CA, Tong MY, Jordan DM. Large numbers of genetic variants considered to be pathogenic are common in asymptomatic individuals. *Hum Mutat*. 2013;34:1216–1220. https://doi.org/10.1002/humu.22375
55. Heller R, Bolz HJ. The challenge of defining pathogenicity: the example of AHI1. *Genet Med*. 2015;17:508. https://doi.org/10.1038/gim.2015.46
56. Malakasioti G, Iancu D, Tullus K. Calcineurin inhibitors in nephrotic syndrome secondary to podocyte gene mutations: a systematic review. *Pediatr Nephrol*. 2021;36:1353–1364. https://doi.org/10.1007/s00467-020-04695-0
57. Mallipattu SK, He JC. The podocyte as a direct target for treatment of glomerular disease? *Am J Physiol Ren Physiol*. 2016;311:F46–F51. https://doi.org/10.1152/ajprenal.00184.2016
58. Abbate M, Zoja C, Remuzzi G. How does proteinuria cause progressive renal damage? *J Am Soc Nephrol*. 2006;17:2974–2984. https://doi.org/10.1681/ASN.2006040377
59. Gadegbeku CA, Gipson DS, Holzman LB, et al. Design of the Nephrotic Syndrome Study Network (Neptune) to evaluate primary glomerular nephropathy by a multidisciplinary approach. *Kidney Int*. 2013;83:749–756. https://doi.org/10.1038/ki.2012.428
60. UK renal registry. UK Kidney Association. Accessed August 20, 2022. https://ukkidney.org/about-us/who-we-are/uk-renal-registry
61. Alirezaie N, Kernohan KD, Hartley T, Majewski J, Hocking TD. ClinPred: prediction tool to identify disease-relevant nonsynonymous single-nucleotide variants. *Am J Hum Genet*. 2018;103:474–483. https://doi.org/10.1016/j.ajhg.2018.08.005

Supplementary Material

Supplementary Methods:

Molecular cloning

Human ACTN4 wildtype plasmids were already available from [1]. Site-directed mutagenesis to clone hACTN4-W59R, -M240T, and -K255E was performed according to standard protocols using hACTN4-WT in a modified pENT1A vector (Invitrogen). For transient transfection of HEK293T cells, the constructs were subcloned into a modified pcDNA6 vector (Invitrogen) containing an N-terminal Flag-tag. Generation of human podocyte cell lines, which stably express Flag-tagged hACTN4-WT or ACTN4-M40T, or transgenic *Drosophila* fly lines expressing HA-tagged hACTN4 variants under UAS control was achieved by recombining the constructs into pLenti6.3 (Invitrogen) or pTHW (Drosophila Genomics Resource Centre), respectively, using standard GATEWAY technology protocols. All plasmids were verified by sequencing.

Cell culture

HEK293T cells were kept in Dulbecco's modified Eagle's medium supplemented with 10 % fetal bovine serum (FBS). Transient transfection of the cells was achieved using standard calcium-phosphate transfection protocols, adding pcDNA6-GFP as a transfection control. HEK293T cells were also utilized for the production of lentivirus using the pLenti6.3 system. Change to regular podocyte growth medium with 20 mM HEPES was done after 8 hours. Virus containing medium was finally collected after 72 hours, filtered, and stored at 4 °C. For stable expression of human ACTN4 variants in podocyte cell culture, a previously described immortalized human podocyte cell line [2] was used. Cells were cultivated in RPMI 1640 medium supplemented with 10 % FBS as well as insulin-transferrin supplement. They were transduced with lentivirus for 24 hours adding polybrene under growth conditions, before performing medium changes every 24 hours. For selection purposes, blasticidin (1 µg/ml) was added to the medium 48 hours after transduction. Cells were used for further experiments after 96 hours.

Western Blot analysis

For western blot analysis, equal amounts of protein were separated by SDS-PAGE and blotted onto a PVDF membrane using semi-dry transfer methods. After blocking in 5 % BSA for 30 minutes and three washing steps in 1x PBS, the membranes were incubated in primary

antibodies in PBS-T (0.1 % Tween in 1x PBS) overnight at 4 °C. The following primary antibodies were used: Mouse anti-Flag (Sigma F1804, 1:10000) and rabbit anti-pan-actin (Cell Signaling #8456). After three washing steps, membranes were incubated in secondary antibodies coupled to horseradish peroxidase (goat anti-mouse, Jackson #115-035-003, goat anti-rabbit, Jackson #111-035-003, 1:15000) or fluorescent secondary antibodies (IRDye 800CW Goat anti-Mouse, LI-COR #926-32210), followed by three further washing steps. Visualization was performed using the FUSION or LI-COR detection systems, respectively.

Immunofluorescence of cultured cells

After splitting the human podocyte cell line onto coverslips and growth to a confluency of about 60 % (24 hours), cells were washed in PBS and fixed in 4 % PFA for 15 minutes at room temperature. After several washing steps and blocking in 5 % normal donkey serum in PBS containing 0.1 % Triton-X for 1 hour, the samples were incubated in primary antibody (mouse anti-Flag, Sigma F1804, 1:1000) overnight at 4 °C. Incubation with secondary antibody (goat anti-mouse 488, Jackson #115-545-003, 1:500) and Phalloidin-Alexa647 (Dyomics, 647P1-33, 1:250) was performed at room temperature for 1 hour. The coverslips were finally mounted in ProLong Diamond + DAPI (Thermofisher, P36971).

Supplementary Figure S1:

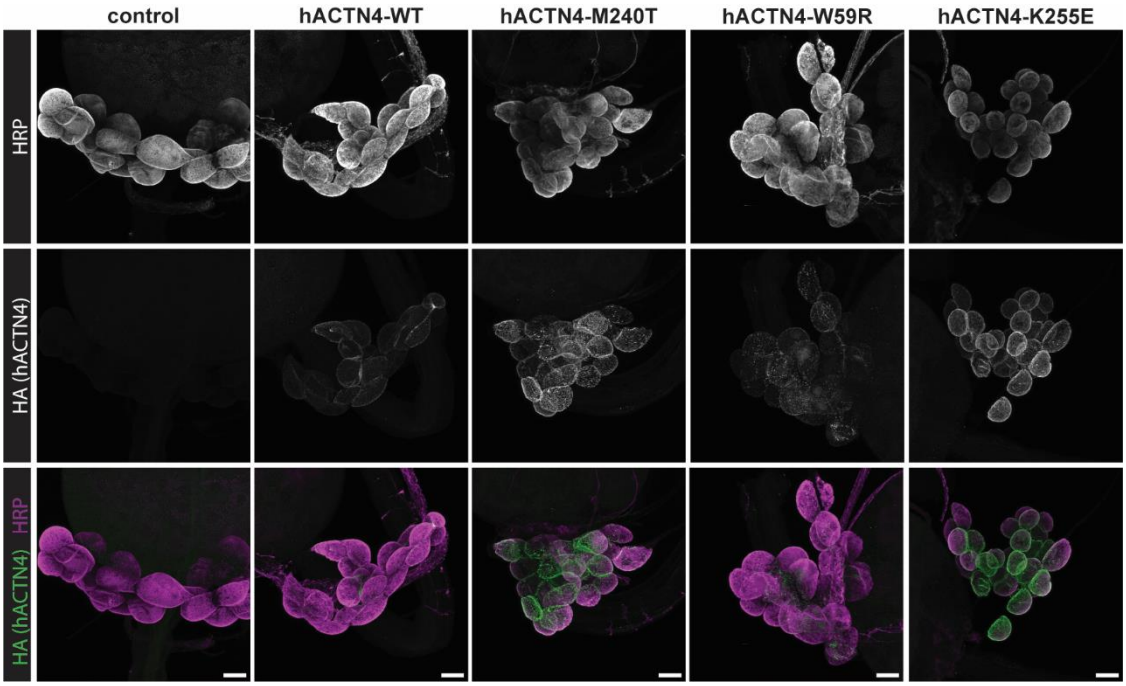

Supplementary Figure S1: Validation of protein expression of hACTN4-variants in *Drosophila* nephrocytes. Immunofluorescence analysis of nephrocytes expressing HA-tagged hACTN4-variants under UAS-control. Nephrocytes were stained with anti-HRP (nephrocyte membrane) and anti-HA (detecting HA-tag of hACTN4-variants). Scale bar indicates 25 µm.

Supplementary Table S1:

Patient Number	1	2	3
HGVS cDNA	c.457T>C	c.584G>A	c.719T>C
HGVS protein	p.F153L	p.G195D	p.M240T
Mutation type	missense	missense	missense
ACMG class	5	4	4
Status	reported thrice	reported once	novel this study
Reference **ClinVar** **ClinPred** **prediction**	PMID: 23014460 [3] NA 0.997	PMID: 26740551 [1] 1 submission 0.999	this study 2 submissions 0.998
AF gnomAD	not found	not found	not found
Patient course	Clinical presentation at age 17 with SRNS, KB: FSGS. PR with cyclosporine A (reduction of proteinuria from 15g/d to 6-8g/d), moderate decline in kidney function	Clinical presentation with NS and ESRD at age 13, initiation of PD, L-KTX one year later	Clinical presentation at age 4 with proteinuria, first KB: MCD; persisting proteinuria, second KB: FSGS, PR with cyclosporine A; progression to ESRD and preemptive L-KTX at 9 years of age

Supplemental Table S1: *ACNT4 de novo* variants identified in pediatric SRNS /FSGS cases.

Abbreviations: NS, nephrotic syndrome, PD, peritoneal dialysis; L-KTX, living donor kidney transplantation; PR, partial remission; KB, kidney biopsy; MCD, minimal change disease; FSGS, focal segmental glomerulosclerosis

Supplementary References

1. Bartram MP, Habbig S, Pahmeyer C, et al. Three-layered proteomic characterization of a novel ACTN4 mutation unravels its pathogenic potential in FSGS. *Hum Mol Genet*. 2016;25(6):1152-1164.
2. Saleem MA, O'Hare MJ, Reiser J, et al. A conditionally immortalized human podocyte cell line demonstrating nephrin and podocin expression. *J Am Soc Nephrol*. 2002;13(3):630-638.
3. Barua M, Brown EJ, Charoonratana VT, Genovese G, Sun H, Pollak MR. Mutations in the INF2 gene account for a significant proportion of familial but not sporadic focal and segmental glomerulosclerosis. *Kidney Int*. 2013;83(2):316-322.

2.3 Chapter 3 – Scaffold proteins Par3A and Par3B share redundant functions while Par3B acts independent of atypical protein kinase C/Par6 in podocytes to maintain the kidney filtration barrier

Apico-basal polarity is essential for the integrity of any epithelium and has been studied intensively (Assémat et al., 2008; Roignot et al., 2013; Wilson, 1997). Polarity in podocytes, being highly specialized and morphologically distinct epithelial cells, is hereby far less understood. The necessity of Par polarity complex for podocyte integrity has been shown by several groups over the past years. Loss of aPKCiota in podocytes leads to early proteinuria and glomerulosclerosis as well as premature death of the mice (Huber et al., 2009). Moreover, podocyte specific knockout of *Cdc42*, a small GTPase and important actin-regulating protein, was accompanied by decreased levels of aPKCiota and Par3A and a severe glomerular phenotype in mice (Scott et al., 2012). Since dysregulation of actin dynamics and de-differentiation of podocytes are key principles of FPE (Kriz et al., 2013; Perico et al., 2016; Shankland, 2006), maintaining the podocytes polarity might be a way to counteract podocyte injury. Previous work in our group focussed on the Par complex protein Par3A. Surprisingly, loss of Par3A in podocytes did not lead to a glomerular phenotype (Koehler et al., 2016). Subsequent analyses then revealed Par3B to be the predominant isoform of Par3 in podocytes. Moreover, loss of Par3A results in increased expression levels of Par3B, from which it was hypothesized, that the two proteins share redundant functions (Koehler et al., 2016). Interestingly, Par3B does not contain an aPKC binding domain (Gao et al., 2002; Kohjima et al., 2002) but still has compensatory properties, which tackles the overall concept of apico-basal polarity regulation we know from classical epithelial cells.

The following chapter comprises a publication in *Kidney International*, published online in December 2021 and printed in Volume 101, Issue 4 in April 2022. Within this article, we functionally analysed the Par polarity complex and especially the Par3 protein in murine podocytes and *Drosophila* nephrocytes. We found that Par3A and Par3B share redundant functions and are upstream of important actin-regulating and -binding proteins such as small GTPases and synaptopodin, linking podocyte polarity signalling to actin cytoskeleton regulation. We furthermore identified Par3B as new SD-associated protein and showed that it acts independent of the usual Par complex members aPKC and Par6, indicating functional

specificity of the protein that paves the way for further studies on Par3B function in podocytes.

Authors: Sybille Koehler*, **Johanna Odenthal***, Vivian Ludwig, David Unnersjö-Jess, Martin Höhne, Christian Jüngst, Ferdi Grawe, Martin Helmstädter, Johanna L. Janku, Carsten Bergmann, Peter F. Hoyer, H. Henning Hagmann, Gerd Walz, Wilhelm Bloch, Carien Niessen, Bernhard Schermer, Andreas Wodarz, Barry Denholm, Thomas Benzing, Sandra Iden and Paul T. Brinkkoetter

* contributed equally

Author contributions:

Sybille Koehler	–	conceived the study and performed experiments
		created figures and drafted the manuscript
Johanna Odenthal	–	performed experiments and analysed the data
		created figures and revised the manuscript
Vivian Ludwig	–	performed experiments
David Unnersjö-Jess	–	performed experiments and analysed the data
Martin Höhne	–	performed experiments and analysed the data
Christian Jüngst	–	performed experiments
Ferdi Grawe	–	performed experiments
Martin Helmstädter	–	performed experiments
Johanna L. Janku	–	performed experiments
Casrten Bergmann	–	performed experiments
Peter F. Hoyer	–	contributed human patient material
H. Henning Hagmann	–	revised the manuscript

Gerd Walz	–	revised the manuscript
Wilhelm Bloch	–	analysed the data
Carien Niessen	–	revised the manuscript
Bernhard Schmermer	–	revised the manuscript
Andreas Wodarz	–	revised the manuscript
Barry Denholm	–	revised the manuscript
Thomas Benzing	–	revised the manuscript
Sandra Iden	–	revised the manuscript
Paul T. Brinkkötter	–	supervised the study and revised the manuscript

Status:

Published in „Kidney International"

Volume 101, Issue 4, Page 733-751, 01. April 2022

Published online: 17.12.2021

Citation:

Koehler S, Odenthal J, Ludwig V, Unnersjö Jess D, Höhne M, Jüngst C, Grawe F, Helmstädter M, Janku JL, Bergmann C, Hoyer PF, Hagmann HH, Walz G, Bloch W, Niessen C, Schermer B, Wodarz A, Denholm B, Benzing T, Iden S, Brinkkoetter PT. Scaffold polarity proteins Par3A and Par3B share redundant functions while Par3B acts independent of atypical protein kinase C/Par6 in podocytes to maintain the kidney filtration barrier. Kidney Int. 2022 Apr;101(4):733-751.

doi: 10.1016/j.kint.2021.11.030

PMID: 34929254.

Scaffold polarity proteins Par3A and Par3B share redundant functions while Par3B acts independent of atypical protein kinase C/Par6 in podocytes to maintain the kidney filtration barrier

Sybille Koehler[1,2,3,13,14], Johanna Odenthal[1,2,13], Vivian Ludwig[1,2], David Unnersjö Jess[1,2], Martin Höhne[1,2,4], Christian Jüngst[4], Ferdi Grawe[2,4,5], Martin Helmstädter[6], Johanna L. Janku[1,2], Carsten Bergmann[7,8], Peter F. Hoyer[9], H. Henning Hagmann[1,2], Gerd Walz[6], Wilhelm Bloch[10], Carien Niessen[2,4,11], Bernhard Schermer[1,2,4], Andreas Wodarz[2,4,5], Barry Denholm[3], Thomas Benzing[1,2,4], Sandra Iden[2,4,12] and Paul T. Brinkkoetter[1,2]

[1]*Department II of Internal Medicine, University of Cologne, Faculty of Medicine, and University Hospital Cologne, Cologne, Germany;* [2]*Center for Molecular Medicine Cologne, University of Cologne, Faculty of Medicine, and University Hospital Cologne, Cologne, Germany;* [3]*Biomedical Sciences, University of Edinburgh, Edinburgh, Scotland, UK;* [4]*Cologne Excellence Cluster on Cellular Stress Responses in Aging-Associated Diseases, University of Cologne, Cologne, Germany;* [5]*Molecular Cell Biology, Institute I for Anatomy, University of Cologne, Faculty of Medicine, and University Hospital Cologne, Cologne, Germany;* [6]*Renal Division, Department of Medicine, Faculty of Medicine and Medical Center, University of Freiburg, Freiburg, Germany;* [7]*Medizinische Genetik Mainz, Limbach Genetics, Mainz, Germany;* [8]*Department of Medicine, Nephrology, University Hospital Freiburg, Freiburg, Germany;* [9]*Klinik für Kinderheilkunde 2, Zentrum für Kinder- und Jugendmedizin, Universitätsklinikum Essen, Essen, Germany;* [10]*Department of Molecular and Cellular Sport Medicine, Institute of Cardiovascular Research and Sport Medicine, German Sport University Cologne, Cologne, Germany;* [11]*Department of Dermatology, University Hospital of Cologne, Cologne, Germany; and* [12]*Institute for Cell and Developmental Biology, Saarland University, Homburg/Saar, Germany*

Glomerular diseases are a major cause for chronic kidney disorders. In most cases podocyte injury is causative for disease development. Cytoskeletal rearrangements and morphological changes are hallmark features of podocyte injury and result in dedifferentiation and loss of podocytes. Here, we establish a link between the Par3 polarity complex and actin regulators necessary to establish and maintain podocyte architecture by utilizing mouse and *Drosophila* models to characterize the functional role of Par3A and Par3B and its fly homologue Bazooka *in vivo*. Only simultaneous inactivation of both Par3 proteins caused a severe disease phenotype. Rescue experiments in *Drosophila* nephrocytes revealed atypical protein kinase C (aPKC)-Par6 dependent and independent effects. While Par3A primarily acts via aPKC-Par6, Par3B function was independent of Par6. Actin-associated synaptopodin protein levels were found to be significantly upregulated upon loss of Par3A/B in mouse podocytes. Tropomyosin2, which shares functional similarities with synaptopodin, was also elevated in Bazooka depleted nephrocytes. The simultaneous depletion of Bazooka and Tropomyosin2 resulted in a partial rescue of the Bazooka knockdown phenotype and prevented increased Rho1-GTP, a member of a GTPase protein family regulating the cytoskeleton. The latter contribute to the nephrocyte phenotype observed upon loss of Bazooka. Thus, we demonstrate that Par3 proteins share a high functional redundancy but also have specific functions. Par3A acts in an aPKC-Par6 dependent way and regulates RhoA-GTP levels, while Par3B exploits Par6 independent functions influencing synaptopodin localization. Hence, Par3A and Par3B link elements of polarity signaling and actin regulators to maintain podocyte architecture.

Translational Statement

Glomerular disorders are a leading cause of chronic kidney diseases. An early hallmark of almost all glomerular injuries comprises morphologic changes in the filtration barrier, in particular, in podocytes. Herein, we show that the polarity proteins Par3A and Par3B are essential for podocyte function. They share redundant and exclusive functions, and only loss of both proteins leads to a breakdown of the filtration barrier. Utilizing the genetic power of the *Drosophila* model, we delineated the downstream effects linking polarity proteins to actin cytoskeleton regulation. These findings have the potential to form the basis for new diagnostics and therapeutics in the future.

Correspondence: *Sybille Koehler or Paul Brinkkoetter, Department II of Internal Medicine, Center for Molecular Medicine Cologne, University Hospital Cologne, Kerpener Str. 62, 50937 Cologne, Germany. E-mail: sy.koehler@uke.de or paul.brinkkoetter@uk-koeln.de*

[13]SK and JO contributed equally.

[14]Current address: Biomedical Sciences, University of Edinburgh, Hugh Robson Building, George Square, EH8 9XD, Edinburgh, Scotland.

Received 19 April 2021; revised 8 November 2021; accepted 22 November 2021; published online 17 December 2021

Kidney International (2022) **101,** 733–751; https://doi.org/10.1016/j.kint.2021.11.030

KEYWORDS: cell polarity signaling; *Drosophila* melanogaster; glomerular disease; nephrocyte; Par3 polarity complex; podocyte

Most kidney diseases originate from glomeruli, small vascular units responsible for the filtration of plasma into protein-free urine. The glomerular filtration barrier is composed of a fenestrated endothelium, the glomerular basement membrane, and podocytes. The latter exhibit primary and secondary foot processes and enwrap the glomerular capillaries completely. Foot processes from adjacent podocytes are joined by a specialized cell-cell contact known as the slit diaphragm (SD).[1–3] During glomerular disease, podocytes dedifferentiate into a columnar epithelial cell phenotype, and plasma proteins leak into the urine. Ultimately, podocytes detach from the glomerular basement membrane and are lost into the urine, leaving denuded capillaries, resulting in glomerulosclerosis and progressive kidney failure.[4]

Most of the 50+ known gene defects leading to inherited forms of podocyte diseases are mainly genes encoding for cytoskeleton- or SD-associated proteins, thereby emphasizing the importance of the podocytes' architecture.[5–7] However, there is still limited knowledge about how podocyte morphology is established during development. In single-layered, columnar epithelial cells, there are 3 major polarity complexes: the Par complex, the Scribble complex, and the Crumbs complex.[8] Surprisingly, neither loss of Par3A (*Pard3*) nor Scribble did result in a glomerular phenotype.[9,10] In contrast, loss of the atypical protein kinase C ι/λ (aPKCι/λ), which is part of the Par complex, caused a severe glomerular disease phenotype.[11,12]

Recently, we identified a second *Pard3* variant known as *Pard3B/Pard3L*[13,14] to be expressed in podocytes. Par3B protein function and particularly whether the 2 Par3 proteins might share compensatory functions remain elusive. Par3B shows high sequence similarity to Par3A with respect to its 3 PDZ (post-synaptic density protein [PSD95], *Drosophila* disc large tumor suppressor [Dlg1], and zonula occludens-1 protein [zo-1]) domains and localizes to podocyte foot processes similar to Par3A.[9] In contrast to Par3A, Par3B does not contain a classic aPKC binding domain and, as a consequence, does not directly interact with aPKC.[13,14]

Herein, we utilized the *Drosophila* nephrocyte model to investigate the functional role of the Par-complex components. Nephrocytes share evolutionary conserved functional similarities with mammalian podocytes as they filter fly hemolymph and present with a highly comparable morphology, including foot processes connected by the nephrocyte diaphragm.[15,16] This highly specialized cell contact is built out of homologous proteins to the mammalian SD proteins Nephrin (*Drosophila* sticks and stones [Sns]) and Neph1 (*Drosophila* Dumbfounded [Duf]).[15,17] We show a critical role for Par3 proteins in controlling podocyte architecture. Par3A and Par3B have redundant functions despite their ability to interact with other components of the Par complex, as only loss of both orthologues resulted in a severe glomerular disease phenotype. We demonstrate, that the role of the Par complex is highly conserved, as loss of Bazooka (Baz), the only Par3 homologue in *Drosophila melanogaster*, results in loss of shape and function in nephrocytes. Rho-guanosine triphosphate (GTP) serves as downstream effector of the Par complex, involving the actin-associated protein synaptopodin. Taken together, we identified how Par3A and Par3B link elements of polarity signaling and actin regulators to maintain podocyte architecture.

METHODS

Cell culture experiments

For cell culture experiments, murine inner medullary collecting duct cells were used, as these cells are highly polarized. They were cultivated with Dulbecco's modified Eagle's medium (Sigma-Aldrich) with 5% fetal bovine serum and 1% Glutamax. Cells were kept at 37 °C with 5% CO_2.

For transfection purposes, cells were grown to a 60% density. Transfection was performed with GeneJuice (MerckMillipore), according to manufacturer's description, using the plasmids listed in the plasmid section (Table 1). After 48 hours, cells were lysed in immunoprecipitation buffer (20 mM Tris, 1% [v/v] Triton X-100, 50 mM NaCl, 15 mM $Na_4P_2O_7$, and 50 mM NaF, pH 7.5) with protease inhibitor mix without ethylenediamine tetraacetic acid (Roche). Lysates were incubated with anti-flag M2 beads (Sigma-Aldrich) for 1 hour at 4 °C. After washing with immunoprecipitation buffer, the beads were incubated with 80 µl 5% sodium dodecylsulfate at 95 °C for 5 minutes. The supernatant was reduced using 5 mM dithiothreitol for 30 minutes and alkylated using 10 mM iodoacetamide for 45 minutes at dark. Proteins were prepared and digested using trypsin and lysin C using the SP3 ultrasensitive proteomics technique, as previously described.[18]

Fly husbandry

Flies (for stocks, see Table 2[19–21]) were kept at 25 °C for all experiments. To achieve a nephrocyte-specific knockdown, flies were mated with an Sns regulatory protein Gal4 (GAL4)-driver line.

Transgenic mouse models

The $Par3A^{fl/fl}$ mouse model was previously published[9] and kept in a pure CD-1 background. The $Par3B^{fl/fl}$ mouse model was generated using embryonic stem cells from the European Conditional Mouse Mutagenesis Program (EUCOMM) and crossed onto a pure CD-1 background. Double-knockout animals were generated by mating and kept in a pure CD-1 background. Mating with a podocyte-specific Cre mouse model[22] resulted in podocyte-specific knockouts of Par3A, Par3B, and both together. For podocyte isolation,

Table 1 | List of plasmids

Name	Origin
Flag.Par3A pcDNA6.3	Self-made
Flag.Par3B pcDNA6.3	Self-made
Flag.pcDNA6.3	Self-made

Table 2 | List of fly stocks

Fly strain	Origin	Purpose	Localization
Baz-GFP-trap *baz*^{CC01941}	Buszczak *et al.*[19]; BDSC (51572)	Rescue	X Chr
Sns-GAL4;UAS-Dicer2		Nephrocyte-specific driver	2. + 3. Chr
UAS-*baz*-RNAi	VDRC (2915)	Knockdown	2. Chr
UAS-GFP-RNAi	BDSC (41551)	Knockdown	3. Chr
UAS-Par3A 180 kDa	Self-made/injections done by GenetiVision	Rescue	3. Chr
UAS-Par3A 150 kDa	Self-made/injections done by GenetiVision	Rescue	3. Chr
UAS-Par3A 100 kDa	Self-made/injections done by GenetiVision	Rescue	3. Chr
UAS-Par3A delta E18	Self-made/injections done by GenetiVision	Rescue	3. Chr
UAS-Par3B	Self-made/injections done by GenetiVision	Rescue	3. Chr
UAS-Par3B	Self-made/injections done by GenetiVision	Rescue	X Chr
UAS-*aPKC*-CAAX-wt	Sotillos *et al.*[20]	Rescue	3. Chr
UAS-*aPKC*-CAAX-DN	Sotillos *et al.*[20]	Rescue	3. Chr
UAS-*baz*-wt	Krahn *et al.*[21]	Rescue	3. Chr
UAS-*baz*-delta 968-996	Self-made/injections done by GenetiVision	Rescue	3. Chr
UAS-*tropomyosin2*-RNAi	BDSC (41695)	Knockdown	3. Chr
UAS-*Par6*-RNAi	VDRC (19731)	Knockdown	3. Chr
UAS-*Vinculin*-RNAi	VDRC (34586)	Knockdown	3. Chr
UAS-*Titin*-RNAi	VDRC (47300)	Knockdown	3. Chr
UAS-*Tiggrin*-RNAi	VDRC (28257)	Knockdown	3. Chr
UAS-*CG1674*-RNAi	VDRC (42276)	Knockdown	3. Chr
UAS-*Coracle*-RNAi	VDRC (9788)	Knockdown	3. Chr
UAS-*RhoGDI*-RNAi	VDRC (46154)	Knockdown	3. Chr
UAS-mouseSYNPO	BDSC (41770)	Overexpression	2. Chr
UAS-Rok-RBD-GFP	BDSC (52290)	Rho1 sensor	3. Chr
UAS-Pak-RBD-GFP	BDSC (56548)	Rac/Cdc42 sensor	3. Chr
UAS-Rho1-N19	BDSC (7328)	Dominant negative	3. Chr
UAS-Rho1-V14	BDSC (8144)	Constitutively active	3. Chr
W^{1118}		Wild type	X Chr

2. Chr, second chromosome; 3. Chr, third chromosome; BDSC, Bloomington *Drosophila* Stock Centre; Chr, chromosome; VDRC, Vienna *Droosphila* Resource Centre.

floxed animals were mated with R26mTmG mice,[23] which were mated with hNphs2.PodCre mice to achieve green fluorescent protein (GFP) expression exclusively in podocytes.[22,23] For all animal experiments shown, we used both sexes. The mouse husbandry was done in the University of Cologne animal facility, according to standardized specific pathogen-free conditions. The experimental protocol was approved by the Landesamt für Natur, Umwelt und Verbraucherschutz Nordrhein-Westfalen (State Agency for Nature, Environment and Consumer Protection North Rhine-Westphalia; AZ 84-02.04.2013.A375).

Isolation of primary podocytes

Primary podocytes were isolated after sacrificing mice and glomerular preparation, as previously described.[24] Glomeruli were either digested to get a single-cell suspension, which was further used for FACs sorting, or were used for DNA isolation using the Blood and Tissue kit from Qiagen, according to manufacturer's instructions.

Immunofluorescence stainings and high-resolution imaging of *Drosophila* nephrocytes

Isolated nephrocytes were fixed with 4% formaldehyde for 20 minutes, followed by fixation in methanol for 2 hours at room temperature. Afterwards, they were washed 3 times in washing buffer (phosphate-buffered saline [PBS] with 0.5% bovine serum albumin and 0.3% Triton-X). Antibodies were used, as described in Table 3,[24] and incubated overnight at 4 °C. On the second day, nephrocytes were washed 3 times, blocked with 5% normal donkey serum for 30 minutes, and incubated with secondary antibody (see Table 3, either for normal confocal or superresolution microscopy) for 1 hour at room temperature and in the dark. Afterwards, nephrocytes were washed 3 times and mounted using Vectashield (Vectorlabs). Confocal images were obtained using a Zeiss confocal microscope LSM710/Axiobserver Z1 or a Leica SP8 confocal microscope and further processed using ImageJ/Fiji 1.50f8 and Adobe Photoshop Version 11.0. Superresolution images were acquired using a STED microscope (TCS SP8 gSTED 3x; Leica Microsystems) equipped with a white light laser for excitation and sensitive hybrid detectors for time-gated detection. A 100× oil immersion objective with a numerical aperture of 1.4 (PL Apo 100×/1.4 Oil STED; Leica Microsystems) was used, and the acquired images were processed using the deconvolution software Huygens Essential (Scientific Volume Imaging). Quantification was done using a previously published macro for FIJI to quantify SD length in mouse glomeruli.[26] We adapted the macro for *Drosophila* nephrocytes and used it for all STED images.

Electron microscopy of *Drosophila* nephrocytes

For structural analysis, garland cells were prepared from L3 larvae and fixed in 2.5% glutaraldehyde in HL3 buffer (70 mM NaCl, 4 mM $MgCl_2 \times 6\ H_2O$, 115 mM sucrose, 5 mM KCl, 10 mM $NaKO_3$, and 5 mM HEPES, pH 7.1). After washing in 100 mM phosphate buffer (NaH_2PO_4 and NaH_2PO_4, pH 7.2), the cells were post fixed in 2% osmium tetroxide in phosphate buffer for 1 hour on ice. After several washings in phosphate buffer and distilled H_2O, the specimens were dehydrated in increasing ethanol and embedded in Araldit using acetone as an intermediate solvent. Thin sections were stained with 2% uranyl acetate and lead citrate. The 50-to 100-nm sections were observed under an EM 109 (Zeiss) transmission electron microscope at 80 KV. Further processing was done by using ImageJ/Fiji 1.50f8 and Adobe Photoshop Version 11.0

Histologic analysis on mouse tissue

For histology, mice were sacrificed via perfusion with PBS via the heart. Kidneys were either fixed in 4% paraformaldehyde overnight,

Table 3 | List of antibodies

Name	Company/provider	Catalog no./ reference	Host species	Dilution IF
Anti-Baz	A. Wodarz	Wodarz *et al.*[25]	Rabbit	1:500
Anti-Duf	M. Ruiz-Gomez (via B. Denholm)	Weavers *et al.*[15]	Rabbit	1:100
Anti-HRP	Jackson ImmunoResearch	123-005-021	Goat	1:200
Anti-Nephrin	R&D Systems	AF4269	Sheep	1:50
Anti-Nephrin	Fitzgerald	20R-NP002	Guinea pig	1:100
Anti-Pyd	Developmental Studies Hybridoma Bank	PYD2	Mouse	1:25
Anti-Par3A	Millipore	07-330	Rabbit	1:100
Anti-Par3B	Santa Cruz	sc-168899	Goat	1:100
Anti-Podocin	Sigma	P0372	Rabbit	1:100
Anti-Rab7	Developmental Studies Hybridoma Bank	Rab7	Mouse	1:25
Anti-synaptopodin	Sigma	S9442	Rabbit	1:50
Anti- synaptopodin (human samples)	Sigma	HPA034631	Rabbit	1:200
Abberior STAR 635P anti-rabbit	Abberior	ST653P	Goat	1:1000
Abberior STAR 580 anti-mouse	Abberior	ST580	Goat	1:1000
Abberior STAR 580 anti-rabbit	Abberior	ST580	Goat	1:1000
Abberior STAR 635P anti-mouse	Abberior	ST653P	Goat	1:1000
Anti-rabbit-Cy3	Jackson ImmunoResearch	711-165-152	Donkey	1:250
Anti-mouse-Cy5	Jackson ImmunoResearch	715-175-150	Donkey	1:250
Anti-mouse-488	Jackson ImmunoResearch	715-545-150	Donkey	1:250
Anti-goat-Cy3	Jackson ImmunoResearch	705-165-147	Donkey	1:250
Anti-goat-549	Thermo Fisher	A-11058	Donkey	1:250

Baz, Bazooka; Duf, Dumbfounded; HRP, horseradish peroxidase; IF, immunofluorescence; Pyd, Polychaetoid.

followed by embedding in paraffin, or fixed in 4% paraformaldehyde for 2 hours and further kept in PBS at 4 °C (for high-resolution imaging). Periodic acid staining and trichrome (acidic fuchsine orange G) staining were performed on 2-µm-thick sections, according to standard methods. All images were taken with a Leica SCN400 slide scanner and further processed using Aperio ImageScope v12.0.1.5030.

For immunofluorescence staining, kidneys were embedded in Tissue-TEK O.C.T. compound, and 5-µm-thick sections were used for imaging. Tissue was fixed with 4% paraformaldehyde for 8 minutes, followed by washing for 3 times with PBS + 1% Triton-X. Afterwards, tissue was blocked with 5% normal donkey serum for 30 minutes, and subsequent primary antibody incubation was performed overnight at 4 °C (for antibodies, see Table 2). After 3 washing steps, the secondary antibody was incubated for 1 hour at room temperature, followed by washing and mounting with Prolong 4′,6-diamidino-2-phenylindole (New England Biolabs). Images were obtained using a Zeiss confocal microscope LSM710/Axiobserver Z1. Images were further processed using ImageJ/Fiji 1.50f8 and Adobe Photoshop Version 11.0. Exposure time was identical for comparative analyses.

For high-resolution microscopy, fixed pieces of kidney were incubated at 4 °C in hydrogel solution (4% v/v acrylamide, 0.25% w/v VA-044 initiator, and PBS 1×) overnight. The gel was polymerized at 37 °C for 3 hours, and the presence of oxygen was minimized by filling tubes all the way to the top with hydrogel solution. After that, kidney pieces were cut into 0.3-mm-thick slices using a Vibratome. Slices were then incubated at 50 °C in clearing solution (200 mM boric acid and 4% sodium dodecylsulfate, pH 8.5) for 24 hours. Before immunolabeling, samples were washed in 0.1% Triton-X in 1× PBS for 10 minutes.

For all steps, PBS 1× with 0.1% v/v Triton-X was used as dilutant. Samples were incubated in primary antibody for 24 hours at 37 °C and were then washed in 0.1% Triton-X in 1× PBS for 10 minutes at 37 °C, followed by secondary antibody incubation for 24 hours at 37 °C, and washed for 10 minutes at 37 °C before mounting. To stain for nephrin, a sheep anti-nephrin primary antibody and a donkey anti-goat Alexa-594 conjugated or a donkey anti-sheep Abberior STAR-635P conjugated secondary antibody was used. To stain for synaptopodin, a rabbit anti-synaptopodin primary antibody and a donkey anti-rabbit Atto-594 conjugated secondary antibody was used. Samples were immersed in 80% (w/w) fructose with 0.5% (v/v) 1-thioglycerol at 37 °C for 1 hour before imaging. Samples were then mounted in a glass bottom dish (MatTek P35G-1.5-14-C) and imaged using a Leica SP8 3X STED system. SD length per area was determined using ImageJ/Fiji. In brief, the fluorescent signal was enhanced using background subtraction, mean filtering, and contrast enhancement. The SD signal was detected with the help of the ridge detection plugin, similarly to previously published data by Siegerist *et al.* and Butt *et al.*[26,27] For quantification of synaptopodin intensity, a line profile was manually assigned to cross-sectional images. The thickness of the line profile was adjusted to include the whole filtration barrier. After this, the mean fluorescence intensity within the line profile was measured. The measurement was repeated at least 20 times in 3 different animals per group.

Electron microscopy of mouse tissue

Primary fixation was done with 2% glutaraldehyde and 4% formaldehyde in 0.1 M phosphate buffer for 48 hours. For transmission electron microscopy, the tissue was then postfixed in 0,5% osmium tetroxide in double-distilled H_2O for 60 minutes on ice and then washed 6 times in double-distilled H_2O. The tissue was incubated in 1% aqueous uranyl acetate solution for 2 hours in dark and washed 2 times in double-distilled H_2O.

Dehydration was performed by 15-minute incubation steps in 30%, 50%, 70%, 90%, and 2× 100% ethyl alcohol and 2× 100% acetone. After embedding in Durcupan resin, ultrathin sections were performed using a UC7 Ultramicrotome (Leica), collected on Formvar-coated copper grids. Post staining was done for 1 minute with 3% lead citrate, followed by imaging using a Zeiss Leo 912 transmission electron microscope.

For scanning electron microscopy, the fixated kidneys were dehydrated in 70%, 80%, 90% and 100% ethanol (each step for 1 hour at room temperature) and incubated in a 1:1 solution of ethyl

alcohol and hexamethyldisilazane for 30 minutes. After incubation in 100% hexamethyldisilazane, the solvent was allowed to evaporate. The dehydrated tissue was mounted onto sample holders and sputtered with gold using a Polaron Cool Sputter Coater E 5100. The resulting samples were imaged using a scanning electron microscope (Leo 1450 VP scanning).

Urinary analysis

Urinary albumin levels were measured with a mouse albumin enzyme-linked immunosorbent assay kit (ICL/Dunn Labortechnik GmbH), whereas urinary creatinine levels were measured with a urinary creatinine kit (Biomol). Urinary albumin levels were then normalized on the urinary creatinine.

Deletion polymerase chain reaction with glomerular lysates

Glomerular DNA was used for polymerase chain reaction using the RedTaq Ready MasterMix (Sigma-Aldrich), according to manufacturer's instructions. Used primers are listed in the primers section (Table 4). Cycling conditions were as follows: 95 °C for 3 minutes, 95 °C for 30 seconds, 60 °C for 30 seconds, 72 °C for 30 seconds, go to step 2, repeat 35 times, and 72 °C for 3 minutes. DNA was separated using agarose gel electrophoresis and UV light.

RNA isolation and quantitative polymerase chain reaction of murine podocytes

Podocytes were lysed with 500 µl Trizol (Sigma-Aldrich), and RNA was isolated using the Direct-Zoll RNA MiniPrep Kit from Zymo, according to manufacturer's instructions. Isolated RNA was used for cDNA synthesis by using the High Capacity cDNA RT-Kit (Applied Biosystems), according to manufacturer's instruction. Quantitative polymerase chain reaction was performed using the SYBR Green Mastermix (Thermo Fisher) and primers specific for mPar3B and murine actin B (mACTB; listed in the primers section). Par3B mRNA level were normalized to mACTB.

Fluorescein isothiocyanate–albumin uptake assay

To analyze the uptake and filtration capacity of nephrocytes, L3 larvae were dissected and garland nephrocytes were isolated. They were incubated in fluorescein isothiocyanate–albumin (0.2 mg/ml; Sigma-Aldrich) for 1 minute.[28] Afterwards, they were washed in HL3 buffer for 1 minute and then fixed in 4% formaldehyde for 20 minutes. Nephrocytes were mounted in Vectashield (Vectorlabs). Images were obtained with a Zeiss confocal microscope LSM710/Axiobserver Z1 or a Leica SP8 confocal microscope and further processed using ImageJ/Fiji 1.50f8 and Adobe Photoshop Version 11.0. Exposure time was identical for comparative analyses. The mean intensity of single nephrocytes was measured, and the values of the control cells (Sns-GAL4) were used for normalization.

Table 4 | List of primers

Name	Sequence
Par3B deletion PCR	
Par3B del for	TACCATTACCAGTTGGTCTGG
Pard3b-5′arm	GAAATGCCATATCCCTTTGTGACTGG
Pard3b-3′arm	CACAGCAACAGAACATGATTAATGGC
Quantitative PCR	
mPar3B sense	CGGTGCCATGCTGAGATTTG
mPar3B anti-sense	TTCTGCTCAGCCTTTCCGAC
mACTB sense	AAGAGCTATGAGCTGCCTGA
mACTB anti-sense	TACGGATGTCAACGTCACAC

mACTB, murine actin B; PCR, polymerase chain reaction.

Proteomic analysis of *Drosophila* nephrocytes

Garland nephrocytes from single larvae were isolated and directly transferred into 40 µl 8% sodium dodecylsulfate buffer. Samples were further reduced with 5 mM dithiothreitol and alkylated with 10 mM iodoacetamide in the dark. Afterwards, proteins were further prepared and digested with trypsin and lysin C, applying the SP3 method for ultrasensitive proteomics. Proteomics acquisition was performed on a quadrupole Orbitrap hybrid mass spectrometer (QExactive Plus; Thermo) coupled to a easynLC, as previously described, using 1-hour gradients for nephrocytes.[29]

Proteomic raw data deposition

The mass spectrometry proteomics data have been deposited to the ProteomeXchange Consortium via the Proteomics Identification Database - EMBL-EBI (PRIDE)[30] partner repository with the data set identifiers: project name: Par3A and Par3B interactome inner medullary collecting duct cells; project accession: PXD018637; reviewer account details: username: reviewer86334@ebi.ac.uk; password: F7M8n2xo; project name: *Drosophila* nephrocytes Par3A and B rescue; project accession: PXD018636; reviewer account details: username: reviewer34880@ebi.ac.uk; password: efI2ztnt; project name: *Drosophila* nephrocytes Bazooka knockdown vs control; project accession: PXD018635; reviewer account details: username: reviewer40147@ebi.ac.uk; password: tkxbDsCF.

Study approval and human patients

All investigations involving human subjects were conducted in accordance with the principles of the Declaration of Helsinki. All investigations were conducted after obtaining informed consent from the patients or their parents. All procedures were approved by local ethics committees in Cologne, Rare Kidney Disease 15-215, and FOrMe 21-1013.

The patient material used for immunohistochemistry was obtained from renal biopsy specimens after routine diagnostics were performed. The use of routine archival tissue sections for retrospective epidemiologic research, as described, is permitted by state law in Cologne (Berufsordnung der Nordrheinischen Ärztinnen und Ärzte, §15 Abs. 1).

Statistical analysis

Statistical significance was evaluated using GraphPad Prism version 6 for Windows (GraphPad Software). All results are expressed as means ± SEM. One data point represents one nephrocyte cell. We repeated experiments from 3 independent matings. For comparison of 2 groups, the Student *t* test was used. A $P < 0.05$ was considered to be significant. For 1 independent variable, 1-way analysis of variance combined with the Tukey multiple comparison test was performed. A $P < 0.05$ was considered to be significant. For 2 independent variables, 2-way analysis of variance combined with the Sidak multiple comparison test was applied, and a $P < 0.05$ was considered significant.

RESULTS

Par3A and Par3B maintain podocyte morphology and function

Previously, we were able to show that loss of Par3A does not result in a glomerular disease phenotype, but causes an upregulation of Par3B in podocytes.[9] In contrast to Par3A,

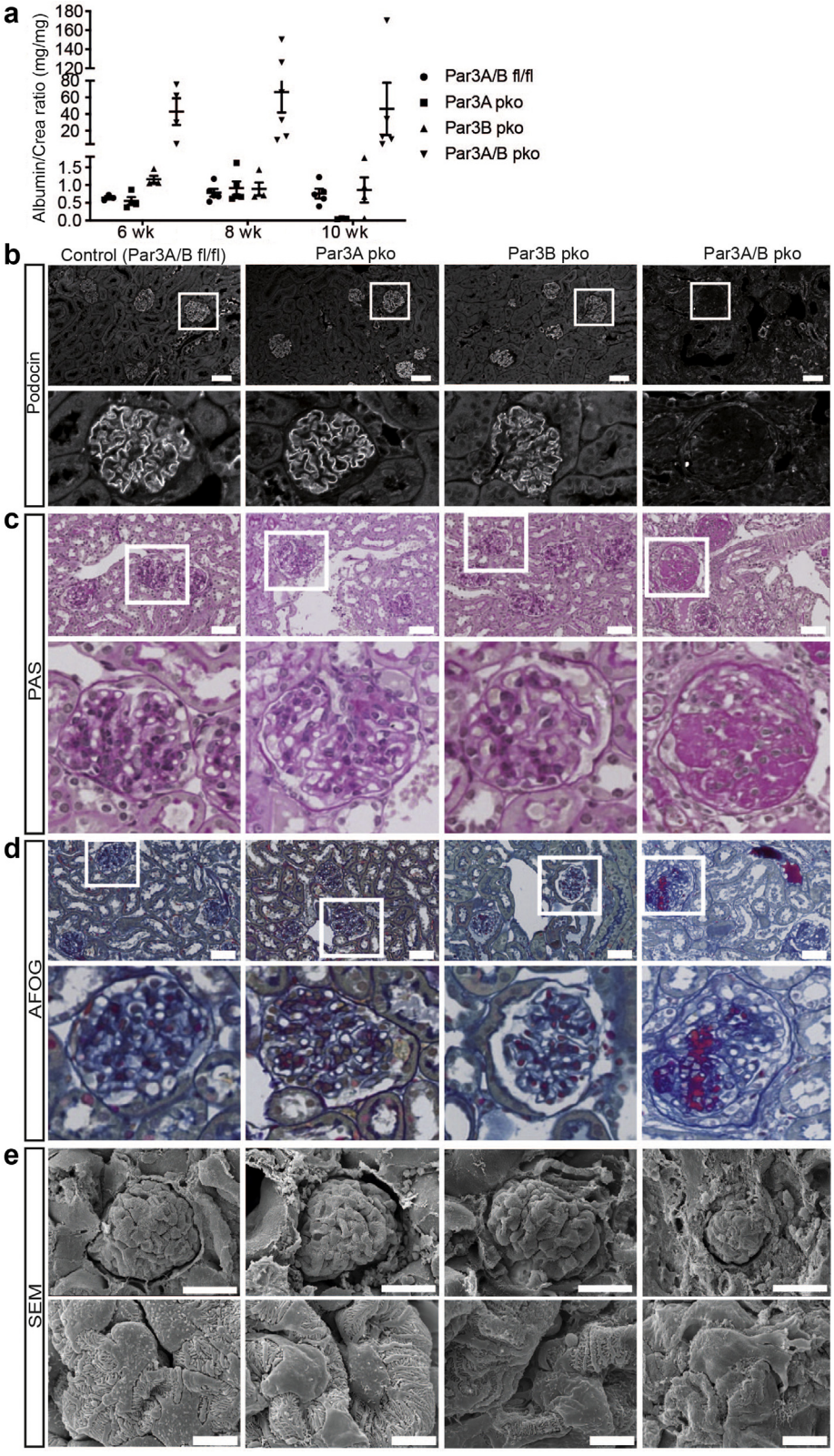

Figure 1 | Simultaneous depletion of Par3A and Par3B causes a severe glomerular disease phenotype. (**a**) Urinary albumin levels show an increase after 6 weeks only in Par3A/B double-knockout mice. Loss of Par3A or Par3B alone did not result in increased albumin levels. (**b**) Immunofluorescence stainings visualizing podocin revealed complete disruption of the slit diaphragm on loss of both Par3A and Par3B. Bar = 50 μm. (**c**) Histologic analysis by performing periodic acid–Schiff (PAS) staining showed severe glomerulosclerosis and protein casts in the tubular system in Par3A/B double-knockout mice. Bar = 50 μm. (**d**) Histologic analysis by performing acidic fuchsine orange G (AFOG) staining revealed a large amount of protein deposits and thickening of the glomerular basement membrane on loss of Par3A and Par3B. (Continued)

which is expressed ubiquitously throughout the whole glomerulus, Par3B is expressed specifically in podocytes (Supplementary Figure S1), where the protein localizes to foot processes,[9] suggesting a putative role for Par3B in the podocyte. Furthermore, coexpression of Par3A and Par3B in podocytes raises the possibility of functional redundancy, which may explain the lack of phenotype observed for loss of *Pard3a* alone.[9] To investigate Par3A/B function in more detail, we employed conditional *in vivo* targeting strategies specifically in podocytes to delete *Pard3b* alone or both *Pard3a* and *Pard3b*. Podocyte-specific gene deletion of *Pard3b* did not result in an overt glomerular disease phenotype, neither in mice held on a pure C57Bl/6 nor in a more susceptible CD-1 background (Figure 1 and Supplementary Figures S2 and S3). This is in line with the lack of any disease phenotype in podocyte-specific *Pard3a* knockout mice.[9] Although Par3A and Par3B single-knockout mice did not present with proteinuria or severe foot process effacement, high-resolution STED microscopy revealed mildly but statistically significant effaced foot processes compared with control mice, as quantified by measuring the SD length per capillary area (Supplementary Figure S4D). To study a functional redundancy between the 2 Par3 proteins, we generated podocyte-specific *Pard3a/b* double-knockout mice held in pure CD-1 background (Figure 1 and Supplementary Figure S4A and B). Loss of both *Pard3* genes resulted in a severe glomerular disease phenotype with significantly increased urinary albumin levels already evident after 6 weeks (Figure 1a). Histologic analyses revealed loss of the podocytes' ultrastructure, including foot process effacement (Figure 1b and e and Supplementary Figure S4C and D), glomerulosclerosis, and protein casts in the tubular apparatus (Figure 1c and d). Additional analysis, including body weight and histology, revealed a progressive disease phenotype, as Par3A/B double-knockout mice did not show any differences in body weight in the first weeks of life. At 5 weeks of age, we observed the first signs of glomerular disease in histology (Supplementary Figure S5). These data show Par3 activity is required in podocytes to maintain their morphology and function and that Par3A and Par3B have redundant functions in podocytes. However, as Par3B is able to compensate for the loss of Par3A despite its inability to interact with aPKC, we hypothesized that Par3 function in podocytes is at least partially independent of aPKC.

Loss of Baz causes severe morphologic and functional disturbances in *Drosophila* nephrocytes

To characterize the cellular and molecular function of the Par complex in the podocyte in greater detail, we utilized the *Drosophila* nephrocyte model, where *bazooka* is considered to be the only Par3 homologue for both Par3A and Par3B. Baz is expressed in nephrocytes from the late embryonic stage onwards, where it colocalizes with the Neph homologue Duf and the nephrin homologue Sns (garland cells, third instar larvae) (Supplementary Figure S6A and B). Baz localization is not restricted to the nephrocyte diaphragm, but also expands into the cell body along the lacunae membranes (Supplementary Figure S6A and B). To determine the function of Baz, we generated a nephrocyte-specific knockdown of *baz* using RNA interference and assessed the morphologic phenotype by observing the localization of the diaphragm proteins Duf and Polychaetoid (the *Drosophila* Zonula occludens-1 [ZO-1] orthologue) with high-resolution STED microscopy. In control nephrocytes (*sns-GAL4/+*), the nephrocyte diaphragm was visualized as a fingerprint-like pattern (similar to the SD pattern in podocytes; Supplementary Figure S4D) (Figure 2a). On loss of Baz, this fingerprint-like pattern was almost completely lost and the integrity of the nephrocyte diaphragm was significantly disrupted (Figure 2a). Disruption to the nephrocyte diaphragm was confirmed by the severe mislocalization of Duf, which no longer localized to the diaphragm at the periphery of the cell and was instead found within the cell (Figure 2b). The nephrocyte foot processes in Baz-depleted nephrocytes were also markedly reduced, resembling podocyte foot process effacement in Par3A/B double-knockout mice (Figure 2c). In line with the morphologic changes, loss of Baz also caused a severe filtration/uptake phenotype (Figure 2d). To differentiate between defective filtration and endocytosis, we used Rab7 staining to quantify endocytotic processes (Figure 2e). Rab7 regulates late endocytic trafficking and is important for nephrocyte biology.[31] Quantification of Rab7 vesicles did not reveal any differences between control and Baz-depleted nephrocytes. Hence, the severe phenotype observed upon decreased Baz levels in nephrocytes seems to be mainly caused by filtration disturbances. Loss of Baz resulted in a pronounced nephrocyte phenotype, including morphologic and functional disturbances. This phenotype is highly similar to that caused by loss of Par3A/B in mammalian podocytes.

Par3A and Par3B are both required to compensate for loss of Baz

To investigate redundant functions of Par3A and Par3B in greater detail, we tested the ability of different mammalian Par3 variants to rescue the *baz* knockdown phenotype (Supplementary Figure S7). We examined 4 different mammalian Par3A isoforms comprising the 180-, 150-, and 100-kDa variant as well as a fourth variant lacking parts of the aPKC binding domain (delta exon 18), which were previously identified in podocytes by mRNA sequencing.[32] In addition, we also studied the Par3B full-length variant, which is the predominant Par3 variant in mouse podocytes (Figure 3a and b).

Figure 1 | (Continued) Bar = 50 μm. (**e**) Scanning electron microscopy (SEM) revealed severe morphologic changes, including foot process effacement, after loss of Par3A and Par3B, whereas the single knockouts did not present with any morphologic abnormalities. Upper panel: bar = 30 μm; lower panel: bar = 5 μm. All data shown herein are obtained from 10-week-old mice in a CD-1 background. Crea, creatinine. To optimize viewing of this image, please see the online version of this article at www.kidney-international.org.

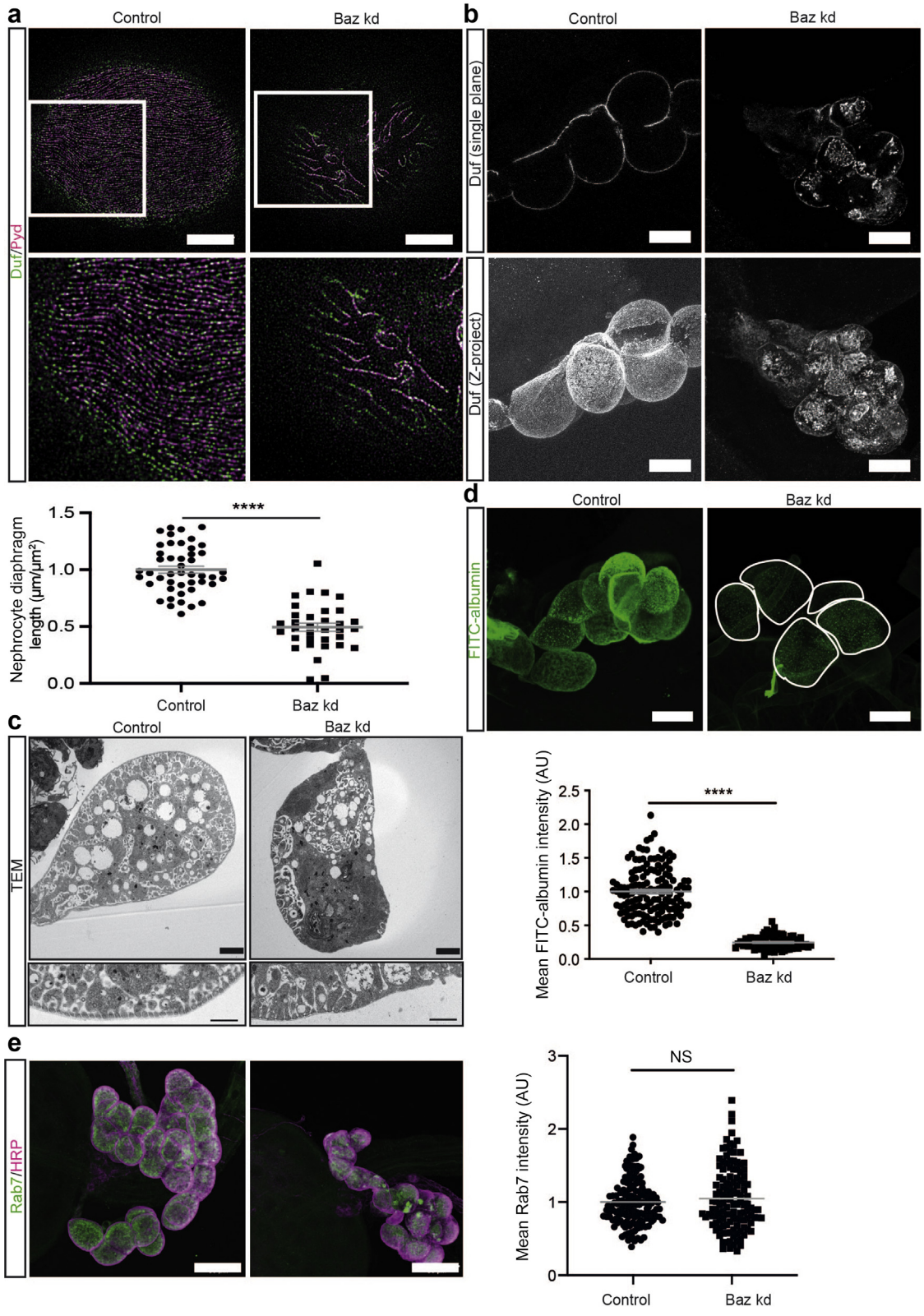

Figure 2| Loss of Bazooka (Baz) causes severe morphologic and functional disturbances in nephrocytes. (**a**) High-resolution microscopy revealed a fingerprint-like pattern in control cells (*sns-GAL4/+*). Dumbfounded (Duf) and Polychaetoid (Pyd) (dZO-1) show an interdigitating pattern. Upon loss of Baz, the fingerprint-like pattern is lost almost completely and the integrity of the nephrocyte diaphragm is severely disrupted. Bar = 5 µm. Control: w;Sns-GAL4;UAS-Dicer; Baz kd: w; *sns*-GAL4/UAS-*baz*-RNAi; UAS-*dicer2*/+. Quantification of the nephrocyte diaphragm length in control and *baz* knockdown nephrocytes revealed a significant reduction in diaphragm length on loss of Baz. Student *t* test: ****$P < 0.0001$. One data point represents one nephrocyte from at least 9 different animals obtained from 3 (continued)

Morphologic assessment using high-resolution STED and electron microscopy, together with a functional analysis, revealed different degrees of rescue potential with respect to nephrocyte morphology and function (Figure 3c–e). Expression of Par3A 180 kDa, Par3A delta exon 18, or the combination of Par3A 180 kDa and Par3B resulted in a significant rescue of the nephrocyte diaphragm integrity based on the localization of Duf and Pyd by high-resolution STED microscopy and quantification of the nephrocyte diaphragm integrity by measuring its length.[26] However, expressing Par3B alone did not cause a significant rescue of the morphologic phenotype induced by Baz depletion (Figure 3c).[32] Electron microscopy revealed a reduction of foot processes in Baz-depleted nephrocytes, which was rescued by the expression of the different mammalian Par3 variants (Figure 3d). In addition, we performed functional analyses and investigated the filtration/uptake capacity of the different rescue strains (Figure 3e). Expressing both Par3A and Par3B resulted in the best rescue (Figure 3e), superior to the full-length single rescue strains of Par3A and Par3B (Figure 3e). Expression of the Par3A 100-kDa variant lacking the aPKC binding domain alone also led to a partial rescue, although the increase of the fluorescein isothiocyanate–albumin intensity was not significant (mean intensity values: Baz knockdown, 0.25; Par3A 100 kDa, 0.36). Taken together, our data suggest that Par3A and Par3B have both redundant and independent functions. The expression of Par3A 180 kDa resulted in a substantially better morphologic rescue when compared with Par3B. However, the significantly better fluorescein isothiocyanate–albumin uptake in the Par3A/B double rescue strain indicates additional, complementary downstream pathways of Par3A and Par3B.

Par3 function is mediated via aPKC-dependent and aPKC-independent signaling pathways

As neither the Par3A 100-kDa variant nor Par3B possesses an aPKC binding domain but rescue the *baz* knockdown phenotype at least partially, Par3 may exert some of its function independently from aPKC. aPKC is normally localized to the appropriate region at the membrane by binding the aPKC binding domain in Baz.[33–35] Therefore, we analyzed an aPKC variant (aPKC-CAAX) that localizes to the cell membrane independently of Baz to uncouple aPKC-dependent and aPKC-independent functions of Baz. In addition, we also investigated the impact of the kinase domain on nephrocyte function by using a dominant negative aPKC^{K293W}-CAAX construct.[20] With regard to morphology, expression of the aPKC-CAAX variant was able to restore Duf and Pyd localization comparable to the Par3A/B double rescue (Figure 4a). Quantification of the nephrocyte diaphragm length revealed a significant rescue by expressing aPKC-CAAX as well as aPKC^{K293W}-CAAX-DN. Both result in a better rescue of the Baz knockdown phenotype as the Par3A/B double rescue. Transmission electron microscopy confirmed the rescue potential as seen in high-resolution microscopy (Figure 4b). However, functional analysis of the aPKC-CAAX rescue only revealed a partial rescue, which was significantly less efficient compared with the Par3A/B double rescue (Figure 4c). The aPKC-CAAX-DN variant showed the least rescue potential when compared with the Par3A/B double and aPKC-CAAX rescue (Figure 4c).

Next, we also studied the functional role of Par6 as a potential linker between aPKC and Par3B. Both morphology and filtration were significantly disrupted on loss of Par6 (Figure 5c and d). Although we did not identify Par6 as a significant interactor of Par3B in an interactome approach, Par6-specific peptides were identified (Supplementary Figure S9D and E). To unravel whether Par3B forms a complex with Par6 and aPKC and thereby exhibits aPKC-dependent functions, we simultaneously depleted Baz and Par6 in nephrocytes. This resulted in a morphologic and functional phenotype that was comparable to the single knockdown effects (Figure 5a and b). We also expressed the 2 mammalian Par3 proteins in Baz and Par6 double knockdown nephrocytes. The expression of Par3A did not result in a rescue of morphology or function (Figure 5a and b). Expressing Par3B, however, revealed a significant rescue of both morphology and filtration, even in the absence of Par6 (Figure 5a and b). In line with this, flies expressing a mutant form of Baz lacking the aPKC-binding domain (Baz delta 968–996) also showed a partial rescue of morphology and function (Supplementary Figure S8A–C).

Taken together, these results further emphasize aPKC-dependent and aPKC-independent functions of Par3A, Par3B, and Baz.

Actin cytoskeleton, matrix-associated, and junction proteins are upregulated on loss of Baz

On the basis of the findings that Baz exhibits aPKC-Par6 independent functions, we aimed to delineate potential downstream pathways and targets. To this end, we performed whole proteome analysis of isolated control and Baz-depleted garland nephrocytes and identified a significant upregulation of actin cytoskeleton–associated proteins (actin and tropomyosin), focal adhesion proteins (Vinculin), as well as matrix-associated proteins (Tiggrin), junction proteins

Figure 2 | (continued) independent matings. (**b**) Confocal microscopy shows an internalization of Duf on loss of Baz (upper panel: single plane; lower panel: Z-projection). Bar = 25 μm. (**c**) Electron microscopy of control and Baz-depleted nephrocytes shows a severe morphologic defect in the Baz knockdown cells, including loss of foot processes and nephrocyte diaphragm structures. Bar = 2500 nm. (**d**) Fluorescein isothiocyanate (FITC)–albumin filtration assays revealed a severe nephrocyte filtration defect after depletion of Baz. Student *t* test: ****$P <$ 0.0001. Bar = 25 μm. (**e**) Visualization of Rab7-positive vesicles revealed no difference between control and Baz-depleted nephrocytes. Student *t* test was used. AU, arbitrary unit; HRP, horseradish peroxidase; NS, not significant; TEM, transmission electron microscopy. To optimize viewing of this image, please see the online version of this article at www.kidney-international.org.

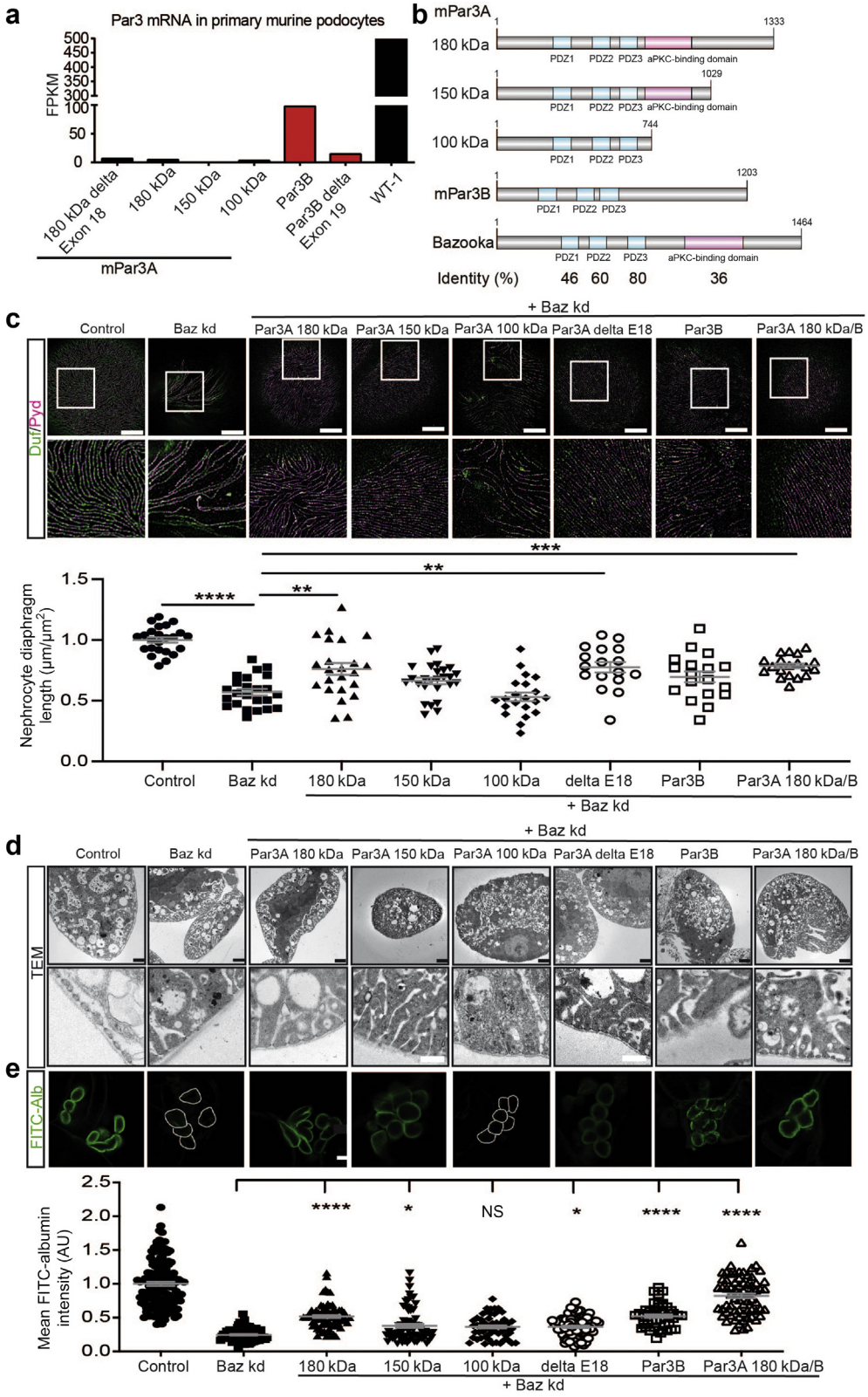

Figure 3 | Both Par3A and Par3B are required for proper nephrocyte function. (**a**) mRNA sequencing data from primary mouse podocytes revealed expression of 3 different Par3A variants (180 kDa, 100 kDa, and 180-kDa delta exon 18), whereas full-length Par3B was the most abundant Par3 protein.[32] (**b**) Par3A, Par3B, and Bazooka (Baz) share high sequence similarity in the 3 PDZ domains. The Par3A 100-kDa variant and Par3B do not have an atypical protein kinase C (aPKC) binding domain. (**c**) High-resolution microscopy of all rescue fly strains shows the best rescue potential in the Par3A 180-kDa/B double rescue fly strain. Nephrocyte diaphragm integrity was assessed (continued)

(Coracle), and GTPase inhibitors (RhoGDI) (Figure 6a). This upregulation was prevented by simultaneous expression of either Par3A or Par3B in the Baz knockdown background, suggesting a Baz-related effect (Figure 6b–d). To further investigate whether these changes are specific to Baz depletion rather than more general changes associated with nephrocyte dysfunction, we compared the Baz data set with whole proteome data sets from nephrocytes depleted for either Sns (nephrin homologue) or Mec2 (podocin homologue; Supplementary Figure S9A–C). This comparison revealed a specific upregulation of most of the candidates only upon loss of Baz and was not observed in injured nephrocytes lacking other functionally important proteins, like Mec2 or Sns. We then generated a list of candidates and investigated their functional role comprising Tiggrin, Titin, Vinculin, Coracle, and RhoGDI. Loss of Titin and Coracle resulted in a severe morphologic phenotype with a significant loss of nephrocyte diaphragm structures (Figure 6e). Depletion of Vinculin and Coracle as well as Tiggrin and RhoGDI revealed a significant decrease of filtration/uptake activities, with Tiggrin and RhoGDI mutants showing the most tremendous effect (Figure 6f).

Loss of Baz results in increased tropomyosin2 levels, exhibiting a detrimental effect on nephrocyte biology

Tropomyosin2 (Tm2), one of the candidates identified in our proteomics screen to be significantly upregulated upon loss of Baz, was further investigated, as Tm2 shares functional similarities with synaptopodin in *Drosophila*.[36] In addition, CG1674 was described to encode for and share some functional properties with a synaptopodin2-like related protein.[37] On the basis of these findings, we investigated the functional role of Tm2 and CG1674 for nephrocyte biology and whether overexpression of murine synaptopodin has an effect on nephrocyte morphology and function. Interestingly, morphology was not altered after depleting Tm2 or CG1674 or expressing murine synaptopodin. However, all genotypes resulted in a significant filtration defect (Figure 7a and b and Supplementary Figure S10A). To verify whether synaptopodin is also increased in our mammalian models, we performed high-resolution STED microscopy of control, Par3A and Par3B single, as well as Par3A/B double knockout animals, which revealed a significant upregulation of synaptopodin in the Par3A/B double knockout mice (Figure 7c–e). Strikingly, synaptopodin formed clusters along the SD in Par3B knockout mice (arrowheads; Figure 7c). We did observe similar staining patterns in mice treated with doxorubicin. Also, treatment with doxorubicin led to an increased synaptopodin expression (Figure 7d and e). Intrigued by the increased synaptopodin expression on injury and cluster formation in areas of foot process effacement, we also examined synaptopodin in human tissue derived from patients experiencing focal segmental glomerular sclerosis, minimal change disease, or diabetic nephropathy (DN) (Supplementary Figure S11). In line with our mouse data, we identified an accumulation of synaptopodin in areas of foot process effacement, characterized by loss of nephrin staining, in all 3 diseases (Supplementary Figure S11).

Next, we studied potential rescue effects and included vinculin and RhoGDI in our experiments. We could demonstrate a rescue of the morphologic *baz* knockdown phenotype only when depleting Tm2 in parallel (Figure 7f). To a minor extent, depletion of vinculin and RhoGDI resulted in a partial rescue of the functional phenotype (Figure 7g). Taken together, our data show that Tm2 and synaptopodin levels are increased on loss of Baz or Par3A/B, respectively, and that loss of Tm2 resulted in a filtration defect. Of note, loss of CG1674, which shares a small region of similarity within the PDZ domain protein synaptopodin2-like related protein, also resulted in a decreased filtration capacity. However, only the reduction of Tm2 levels, which shares functional similarities with synaptopodin, can rescue the morphologic *baz* knockdown phenotype. Together with the synaptopodin overexpression data, this suggests that synaptopodin levels need to be precisely regulated to achieve a protective function and no detrimental effects.

To provide further experimental evidence for the potential connection between Par3 and synaptopodin, we generated interactome data sets of Par3A and Par3B and identified unique and common interactors of the 2 Par3 proteins in inner medullary collecting duct cells (Supplementary Figures S9D and E and S10B and C). Among the common interactors, we identified CD2AP, which was previously shown to interact with synaptopodin in podocytes.[38,39] We

Figure 3 | (continued) by visualizing Dumbfounded (Duf) and Polychaetoid (Pyd). Expression of the 2 full-length variants resulted in an efficient and comparable rescue. Bar = 5 μm. Control (*sns*-GAL4/+), Par3A 180 kDa (w; *sns*-GAL4/UAS-*baz*-RNAi;UAS-*Par3A180kDa*/UAS-*dicer2*), Par3A 150 kDa (w; *sns*-GAL4/UAS-*baz*-RNAi;UAS-*Par3A150kDa*/UAS-*dicer2*), Par3A 100 kDa (w; *sns*-GAL4/UAS-*baz*-RNAi;UAS-*Par3A100kDa*/UAS-*dicer2*), Par3A delta E18 (w; *sns*-GAL4/UAS *baz*-RNAi;UAS-*Par3A delta Exon 18*/UAS-*dicer2*), Par3B (w; *sns*-GAL4/UAS-*baz*-RNAi;UAS-*Par3B*/UAS-*dicer2*), Par3A 180 kDa/B (UAS-*Par3B*; *sns*-GAL4/UAS-*baz*-RNAi;UAS-*Par3A180kDa*/UAS-*dicer2*). Quantification of the nephrocyte diaphragm length revealed a significant rescue of the *baz* knockdown phenotype, after expressing Par3A 180 kDa, Par3A delta exon 18, or Par3A 180 kDa and Par3B simultaneously. One-way analysis of variance (ANOVA) plus Tukey multiple comparison test: $^{**}P < 0.01$, $^{***}P < 0.001$, and $^{****}P < 0.0001$. (**d**) Performing electron microscopy confirmed the results obtained from the high-resolution microscopy. The expression of both Par3A and Par3B resulted in the best rescue potential, when compared with Baz-depleted nephrocytes. Bar = 2500 nm. (**e**) To assess filtration function, fluorescein isothiocyanate (FITC)–albumin assays were performed and again showed that the simultaneous expression of Par3A and Par3B resulted in the best rescue potential. Bar = 25 μm. One-way ANOVA plus Tukey multiple comparison test: $^{*}P < 0.05$, $^{****}P < 0.0001$. FPKM, fragments per kilo base per million mapped reads; TEM, transmission electron microscopy; WT-1, Wilms tumor protein. To optimize viewing of this image, please see the online version of this article at www.kidney-international.org.

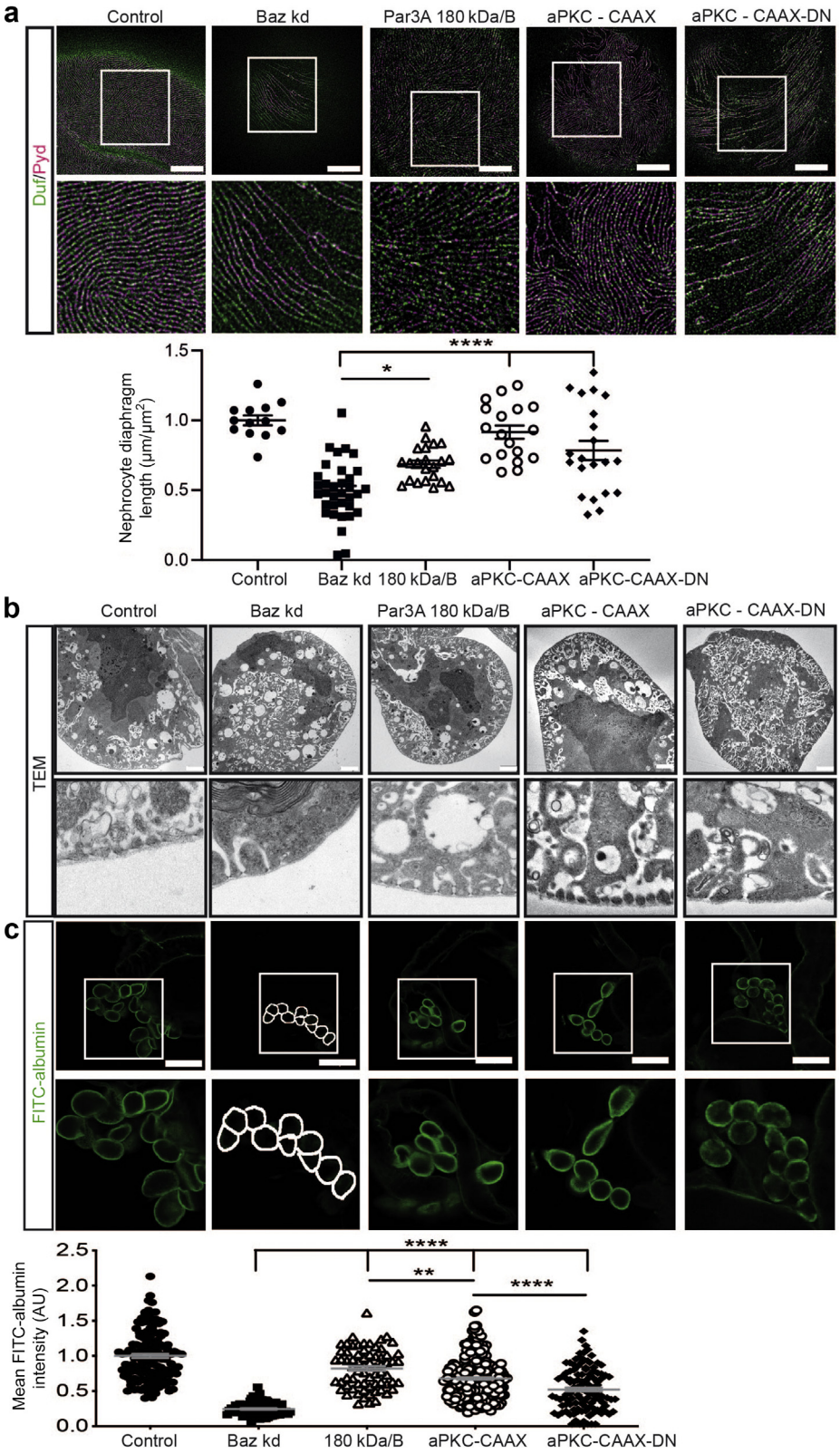

Figure 4 | Rescue of the *baz* knockdown phenotype with atypical protein kinase C (aPKC) reveals a predominant role of aPKC in maintaining nephrocyte morphology rather than function. (**a**) High-resolution microscopy of nephrocytes expressing either aPKC-CAAX or aPKC-CAAX-DN in a Bazooka (Baz) knockdown background shows a good rescue capacity in aPKC-CAAX nephrocytes, whereas expression of aPKC-CAAX-DN only resulted in a partial rescue. The rescue capacity of aPKC-CAAX was comparable to the rescue of the Par3A/B double rescue fly strain. Bar = 5 µm. Control (w;*sns*-GAL4/+;+), Baz knockdown (kd) (w;*sns*-GAL4/UAS-*baz*-RNAi; UAS-*dicer2*/+), Par3A 180 kDa/B (UAS-*Par3B*;*sns*-GAL4/UAS-*baz*-RNAi;UAS-*Par3A180kDa*/UAS-*dicer2*), aPKC-CAAX (w;*sns*-GAL4/UAS-*baz*-RNAi;UAS-*aPKC-CAAX*/UAS-*dicer2*), (continued)

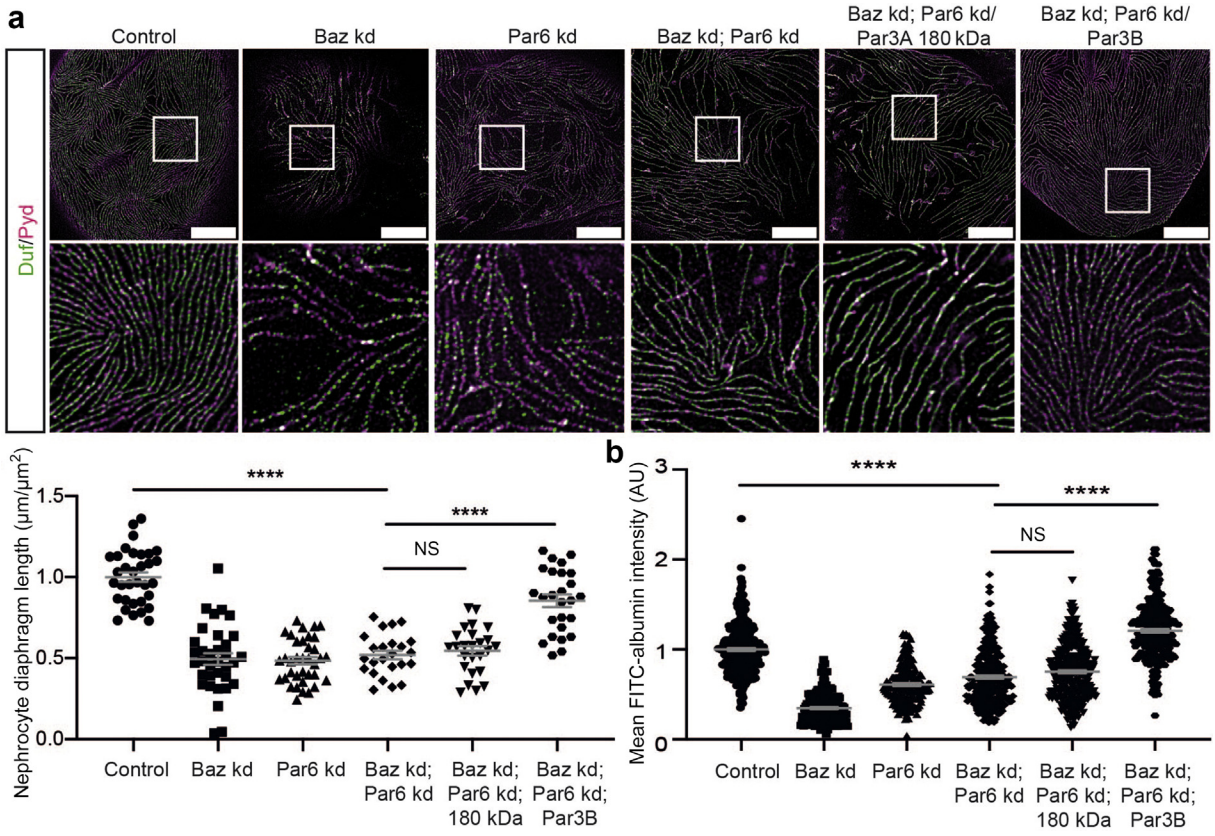

Figure 5 | Par3B exhibits Par6/ aPKC C–independent functions. (**a**) High-resolution microscopy revealed a severe morphologic phenotype when depleting Bazooka (Baz), Par6, or Baz and Par6 simultaneously. This morphologic phenotype could not be rescued by expressing Par3A 180 kDa but resulted in a significant rescue by expressing Par3B. One-way analysis of variance (ANOVA) plus Tukey multiple comparison test: ****$P < 0.0001$. (**b**) Fluorescein isothiocyanate (FITC)–albumin assay revealed a significant decrease of FITC intensity after depletion of Baz, Par6, and Baz and Par6 in parallel. This filtration phenotype could only be rescued by expressing Par3B, whereas Par3A 180 kDa failed to do so. One-way ANOVA plus Tukey multiple comparison test: ****$P < 0.0001$. AU, arbitrary unit; Duf, Dumbfounded; Pyd, Polychaetoid; NS, not significant. To optimize viewing of this image, please see the online version of this article at www.kidney-international.org.

also identified the Calpain-2 catalytic subunit as a unique interactor of Par3B. Calpain is involved in the cleavage of calcineurin and the dephosphorylation of synaptopodin.[40]

Loss of Baz resulted in increased active Rho1 levels, which could be reversed by either depleting Tm2 or expressing Par3A

As both synaptopodin and Tm2 regulate RhoA signaling (in *Drosophila* Rho1),[36,41] we employed Rho1 sensor flies (Rok-RBD-GFP) to analyze active Rho1 levels (Supplementary Figure S12A). Doing so, we identified a significant increase of active Rho1 levels in Baz depleted cells (Figure 8a). This upregulation could be reversed by depleting Tm2, which shares functional similarities with synaptopodin (Figure 8a). Interestingly, only the expression of Par3A 180 kDa reversed the elevated Rho1-GTP levels, whereas Par3B expression did not result in decreased Rho1-GTP levels (Figure 8a).

To further assess the functional role of small GTPases in nephrocyte biology, we investigated the effects after expressing different GTPase variants in wild-type flies. Expression of a dominant-negative Rho1 variant did not result in a nephrocyte phenotype, whereas expression of a constitutively

Figure 4 | (continued) aPKC-CAAX-DN (w;*sns*-GAL4/UAS-*baz*-RNAi;UAS-*aPKC-CAAX-DN*/UAS-*dicer2*). Nephrocyte diaphragm length quantification revealed a significant rescue of the *baz* knockdown phenotype, when expressing either aPKC-CAAX or aPKC-CAAX-DN. One-way analysis of variance (ANOVA) plus Tukey multiple comparison test: ****$P < 0.0001$. (**b**) Electron microscopy confirmed the good rescue potential of aPKC-CAAX, whereas the expression of aPKC-CAAX-DN only caused a partial rescue. Bar = 2500 nm. (**c**) Fluorescein isothiocyanate (FITC)–albumin filtration assays revealed a significant rescue in both aPKC-CAAX and aPKC-CAAX-DN fly strains, but also showed that the double rescue with Par3A/B resulted in a significantly better rescue, when compared with the reintroduction of aPKC. Bar = 25 µm. One-way ANOVA plus Tukey multiple comparison test: **$P < 0.01$, ****$P < 0.0001$. Duf, Dumbfounded; Pyd, Polychaetoid; TEM, transmission electron microscopy. To optimize viewing of this image, please see the online version of this article at www.kidney-international.org.

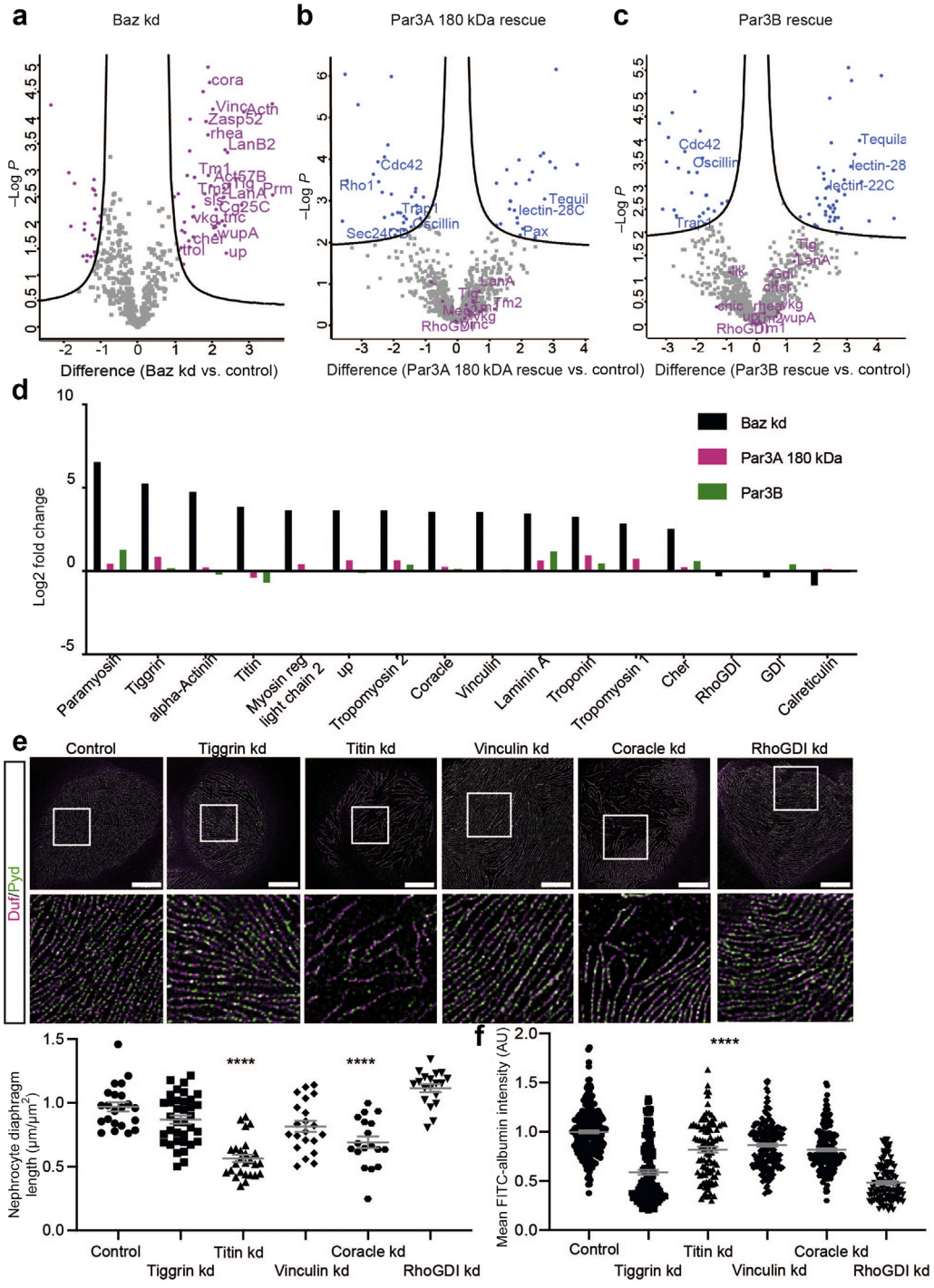

Figure 6| Actin cytoskeleton, matrix-associated, and junction proteins are upregulated on loss of Bazooka (Baz). (**a**) Volcano plot depicting differentially regulated proteins in Baz-depleted nephrocytes compared with control cells. Isolated garland nephrocytes from single L3 larvae were used for proteome analysis. Significantly upregulated or downregulated proteins are depicted in purple. False discovery rate (FDR) = 0.05, s0 = 0.1. (**b,c**) Volcano plot representing differentially regulated proteins in (**b**) Par3A 180-kDa rescue nephrocytes and (**c**) Par3B rescue nephrocytes compared with control cells (*sns*-GAL4/+). Blue: all proteins that are significantly upregulated or downregulated. Purple: proteins that are not significantly regulated but were identified as significantly regulated on loss of Baz. FDR = 0.05, s0 = 0.1. (**d**) Comparison of interesting candidates of the *baz* knockdown and the Par3A 180 kDa and Par3B rescue proteome. Depicted is the log2 fold change. (**e**) Interesting candidates (Tiggrin, Titin, Vinculin, Coracle, and RhoGDI) were depleted in nephrocytes by using specific RNA interference strains and used for high-resolution microscopy and nephrocyte diaphragm length quantification. Loss of Titin and Coracle resulted in a significant reduction of diaphragm length, whereas the others showed either a mild phenotype or no morphologic changes at all. One-way analysis of variance (ANOVA) plus Tukey multiple comparison test: ***$P < 0.001$, ****$P < 0.0001$. (**f**) Fluorescein isothiocyanate (FITC)–albumin uptake assays revealed a filtration phenotype in all genotypes, with Tiggrin and RhoGDI depletion resulting in the most severe effect. One-way ANOVA plus Tukey multiple comparison test: ****$P < 0.0001$. AU, arbitrary unit; Duf, Dumbfounded; Pyd, Polychaetoid. To optimize viewing of this image, please see the online version of this article at www.kidney-international.org.

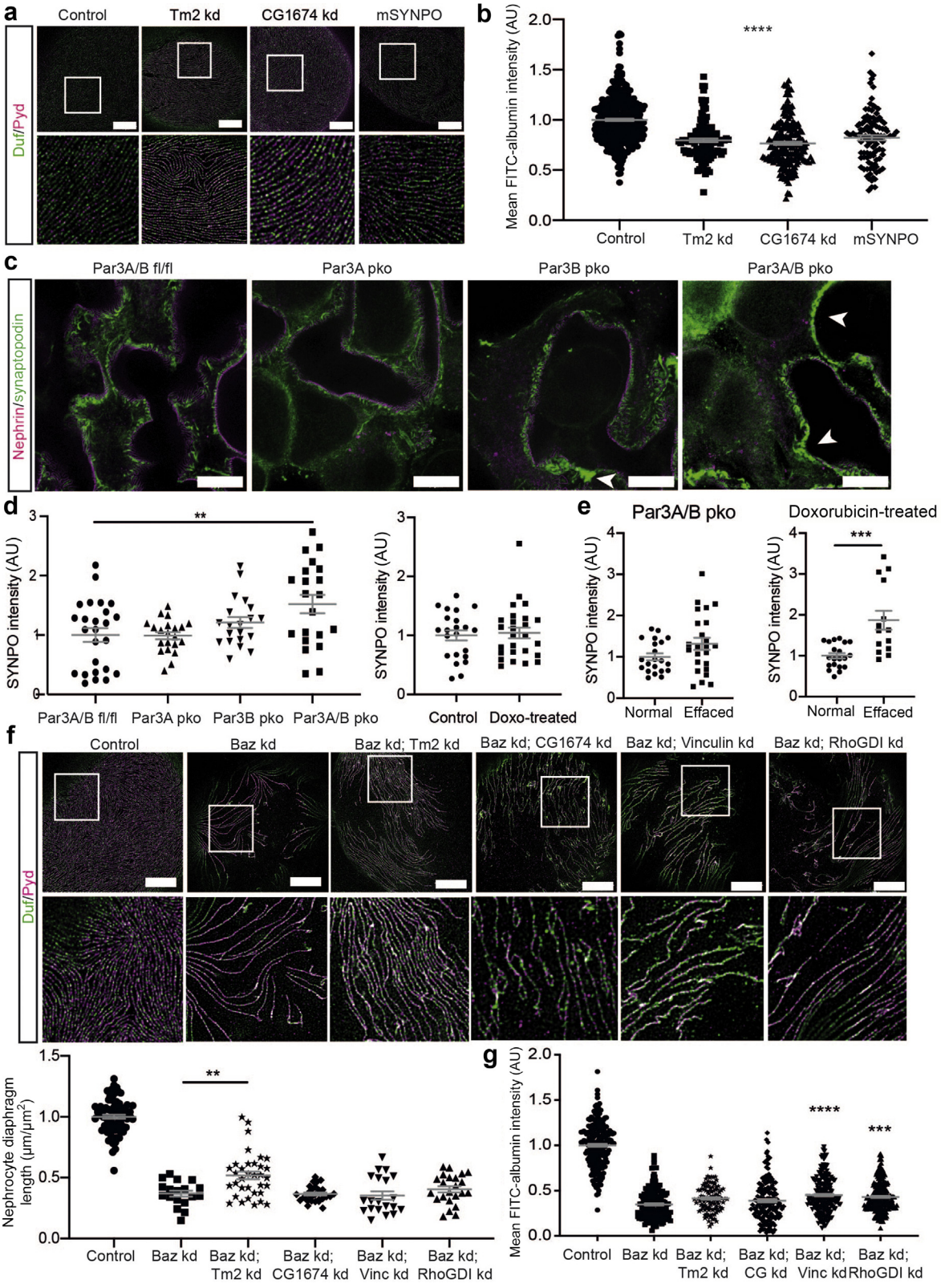

Figure 7 | Increased tropomyosin2 (Tm2) and synaptopodin levels appear to be detrimental for nephrocyte and podocyte biology. (**a**) Depletion of Tm2 and CG1674 as well as expression of murine synaptopodin (mSYNPO) in nephrocytes did not result in a morphologic phenotype, as depicted with high-resolution STED microscopy. Bar = 5 µm. (**b**) Fluorescein isothiocyanate (FITC)–albumin assays revealed a filtration defect in nephrocytes either depleted of Tm2 and CG1674 or expressing mSYNPO. One-way analysis of variance (ANOVA) plus Tukey multiple comparison test: ****$P < 0.0001$. (**c**) Synaptopodin visualization in control, Par3A ko, Par3B ko, and Par3A/B (continued)

active Rho1 caused a severe morphologic phenotype and filtration disturbances (Figure 8b and c). As proof of concept and to further strengthen the hypothesis of a functional interaction between Baz, Tm2, and Rho-GTP levels, we generated flies expressing dominant negative Rho1 and *baz*-RNA interference simultaneously. Expression of a dominant negative Rho1 variant was able to restore morphologic features and filtration function of the *baz* knockdown phenotype at least partially (Figure 8d and e). Active Rac1/Cdc42 levels were unchanged on loss of Baz compared with control cells (Supplementary Figure S12B). Taken together, we observed an elevation of Rho1-GTP levels after depleting Baz, which could be reversed by depleting Tm2 as well as by expressing Par3A. Diminishing Rho1-GTP levels in *baz* knockdown nephrocytes also resulted in a partial rescue of the phenotype.

DISCUSSION

In this study, we link elements of polarity signaling to actin regulators to support the cellular architecture of glomerular podocytes to maintain the kidney filtration barrier. We describe novel and redundant functions of Par3A and Par3B. Although Par3B is expressed at much higher levels in podocytes, only simultaneous loss of both Par3 proteins results in a severe glomerular disease phenotype. This was recapitulated in the *Drosophila* nephrocyte model by depleting the Par3 homologue Baz. Baz-depleted nephrocytes presented with severely affected cellular morphology and nephrocyte dysfunction. Loss of Par3 and its homologue Baz caused a significant increase of synaptopodin and Tm2 levels, respectively, and an activation of Rho1. This activation could be reversed by depleting Tm2, which shares functional similarities with synaptopodin.[36] Interestingly, expressing Par3A also reversed the increased Rho1-GTP levels, whereas Par3B failed to do so. Renal specimens from patients with focal segmental glomerular sclerosis, minimal change disease, and DN revealed a cluster formation of synaptopodin in effaced areas, characterized by loss of nephrin. In addition, available proteomics data also confirm an increase of synaptopodin protein levels in 2 patients with pathogenic Nephrin (NPHS1) mutations.[18]

The stringent control of GTPase signaling in podocytes in mice and humans is of central importance for podocyte function.[42–46] Expression of both dominant negative or constitutively active RhoA results in proteinuria and foot process effacement, whereas the expression of constitutively active Rac1 results in a spectrum of disease, including phenotypes resembling focal segmental glomerular sclerosis or minimal change disease.[42,45] The inhibition of Rho-associated protein kinase (ROCK), which is downstream of RhoA, protects kidney function, whereas patients harboring mutations in Rho GDP-Dissociation Inhibitor Alpha (ARHGDIA) experience steroid-resistant nephrotic syndrome.[43,44] This effect was also observed in our study, as depletion of RhoGDI, a Rho GDP-dissociation inhibitor, also resulted in a severe nephrocyte phenotype. On the basis of these findings, the activation of Rho1 on loss of Baz contributes to the nephrocyte phenotype. Epidermal deletion of Par3A resulted in an inactivation of RhoA in keratinocytes.[47] This opposite effect might be explained by the postmitotic nature of podocytes, as the upstream regulation of RhoA via Par3A in keratinocytes seems to be important to maintain mitotic accuracy.[47] Given that podocytes are different in shape to keratinocytes, one may also envision that cycling of RhoA between active/inactive states might be important in regulating the cytoskeleton to help maintain podocyte architecture.

Intrigued by the upregulation of Tm2 and synaptopodin on loss of Baz and Par3A/B and the previously described protective role of synaptopodin during acute podocyte injury,[48] we unraveled the effect of elevated synaptopodin levels in nephrocytes. This approach revealed a detrimental effect of increased synaptopodin levels on nephrocyte filtration, suggesting a tight control of synaptopodin levels is needed to exhibit protective functions.

In a recent study, the gene CG1674 was described to encode for and share some functional similarities with a synaptopodin2-like related protein.[37] CG1674 localizes to the Z-disc and is required for normal flight muscle development and function. Because of the similarities with the synaptopodin2-like protein, we investigated its function in nephrocytes as well, although CG1674 was not identified in our proteomic screen. Although loss of CG1674 also resulted in a filtration defect, its depletion failed to rescue the Baz phenotype.

Because of the podocytes' unique morphology, several studies have been performed to investigate the functional role of different polarity proteins belonging to the 3 major polarity

Figure 7 | (continued) double-knockout mice revealed an increased signal in areas of effacement, as visualized by loss of nephrin signal. Arrowheads show synaptopodin clusters. Bar = 5 μm. (**d**) Quantification of the synaptopodin (SYNPO) intensity at the slit diaphragm resulted in a significant increase of SYNPO levels in Par3A/B double-knockout mice. For comparison, doxorubicin (Doxo)-treated mice were also used for SYNPO level investigation and did not show a significant increase. One-way ANOVA: $^{**}P < 0.01$. (**e**) Comparison of normal and effaced areas in glomeruli from Par3A/B double-knockout and Doxo-treated mice showed an increase of SYNPO in effaced areas in both groups, whereas only the Doxo-treated group showed a significant effect. Student *t* test: $^{***}P < 0.001$. (**f**) High-resolution microscopy revealed a significant rescue of the nephrocyte diaphragm length, when depleting Bazooka (Baz) and Tm2 simultaneously. The combination of the *baz* knockdown with a *CG1674* knockdown, a *vinc* knockdown, or a *RhoGDI* knockdown did not result in a morphologic rescue. Bar = 5 μm. Control (w;*sns*-GAL4/+; UAS-*dicer2*/+), Baz knockdown (kd) (w;*sns*-GAL4/UAS-*baz*-RNAi; UAS-*dicer2*/+), Baz kd; Tm2 kd (w;*sns*-GAL4/UAS-*baz*-RNAi; UAS-*dicer2*/UAS-*tm2*-RNAi), Baz kd; CG1674 kd (w;*sns*-GAL4/UAS-*baz*-RNAi; UAS-*dicer2*/UAS-*CG1674*-RNAi), Baz kd; Vinculin kd (w;*sns*-GAL4/UAS-*baz*-RNAi; UAS-*dicer2*/UAS-*vinc*-RNAi), Baz kd; RhoGDI kd (w;*sns*-GAL4/UAS-*baz*-RNAi; UAS-*dicer2*/UAS-*RhoGDI*-RNAi). (**g**) FITC-albumin assays show only a slight rescue of all genotypes tested, when compared with the *baz* knockdown phenotype. One-way ANOVA: $^{***}P < 0.001$, $^{****}P < 0.0001$. AU, arbitrary unit; Duf, Dumbfounded; Pyd, Polychaetoid. To optimize viewing of this image, please see the online version of this article at www.kidney-international.org.

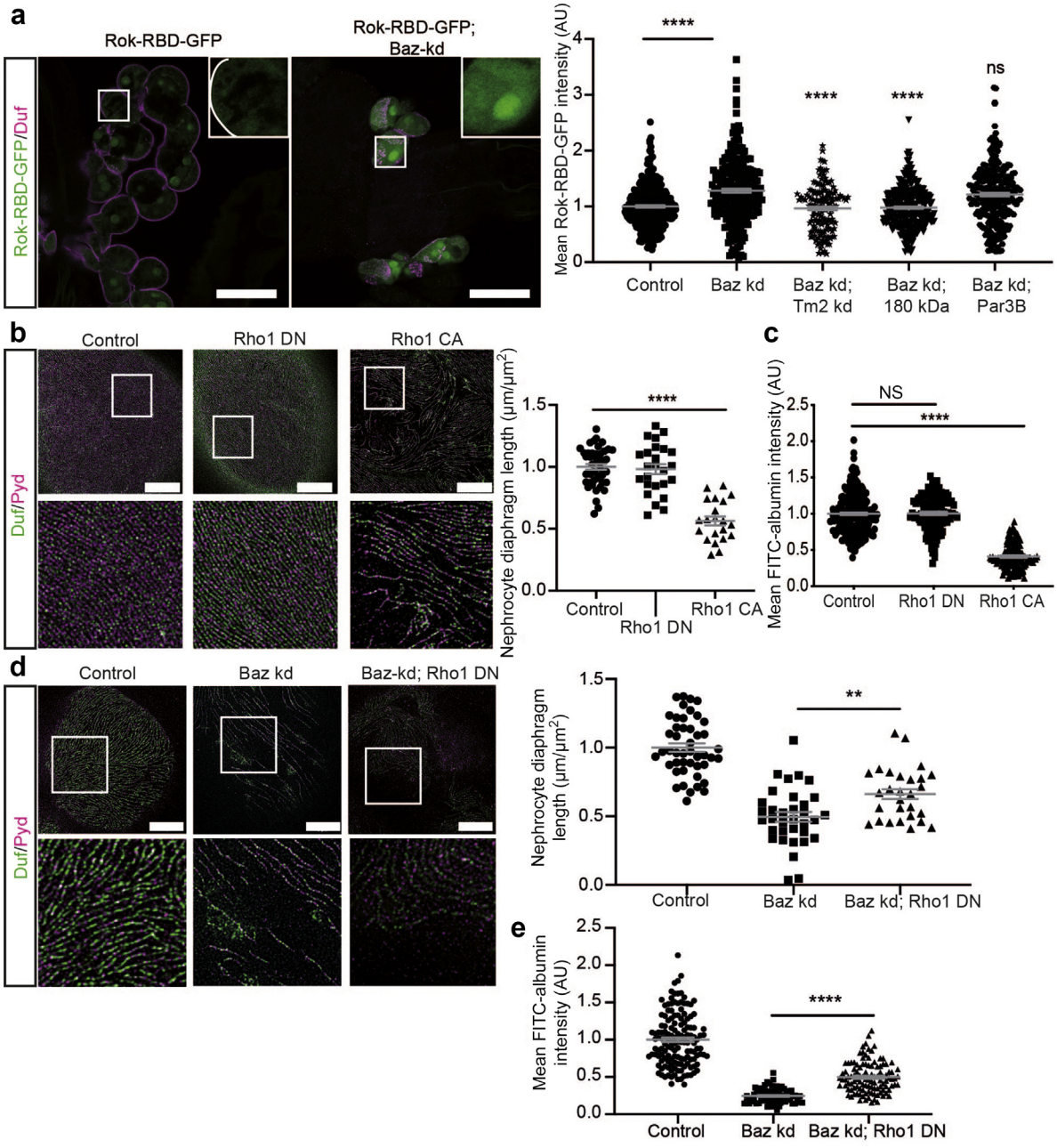

Figure 8 | Bazooka (Baz) depletion results in elevated Rho1-guanosine triphosphate (GTP) levels. (**a**) Confocal microscopy of Rho1 sensor flies showed a significant increase of Rok-RBD-GFP intensity in Baz-depleted nephrocytes, representing elevated Rho1-GTP levels on loss of Baz. Bar = 50 µm. Quantification of the mean Rok-RBD-GFP intensity revealed a rescue of the elevated Rho1-GTP levels almost back to baseline by either depleting tropomyosin2 or expressing Par3A 180 kDa. Expression of Par3B did not result in a reduction of Rho1-GTP levels. One-way analysis of variance (ANOVA): ***$P < 0.001$, ****$P < 0.0001$. (**b**) Expression of dominant negative Rho1 did not result in a morphologic phenotype, whereas expression of constitutively active Rho1 caused severe morphologic abnormalities, as depicted by high-resolution microscopy and quantification of the nephrocyte diaphragm length. Bar = 5 µm. Control: w;*sns*-GAL4/+;UAS-*dicer2*/+, Rho1 DN: w;*sns*-GAL4/+;UAS-*dicer2*/UAS-*rho1-DN*, Rho1 CA: w;*sns*-GAL4/+;UAS-*dicer2*/UAS-*rho1-CA*. One-way ANOVA: ****$P < 0.0001$. (**c**) Fluorescein isothiocyanate (FITC)–albumin filtration assays showed a severe filtration defect on expression of constitutively active Rho1. Expression of dominant negative Rho1 did not result in any changes in comparison to the control nephrocytes. One-way ANOVA: ****$P < 0.0001$. (**d**) High-resolution microscopy and nephrocyte diaphragm length quantification revealed a partial rescue by expression of dominant negative Rho1 in a *baz* knockdown background. Bar = 5 µm. Control: w;*sns*-GAL4/+;UAS-*dicer2*/+, Baz kd;Rho1 DN: w;*sns*-GAL4/UAS-*baz*-RNAi;UAS-*dicer2*/UAS-*rho1-DN*. One-way ANOVA: **$P < 0.01$. (**e**) FITC-albumin filtration assays revealed a significant and partial rescue of the filtration function on expression of dominant negative Rho1 in a Baz knockdown background. One-way ANOVA: ****$P < 0.0001$. AU, arbitrary unit; Duf, Dumbfounded; Pyd, Polychaetoid. To optimize viewing of this image, please see the online version of this article at www.kidney-international.org.

complexes (Par, Crumbs, and Scribble). Although loss of aPKCι and Crumbs resulted in a disease phenotype in mice, zebrafish, and *Drosophila*,[12,49,50] depletion of Scribble and Par3A remained without any overt phenotype.[9,10] As podocytes only exhibit a single type of cell-to-cell contact, combining properties of tight and adherens junctions, one can easily envision that polarity complexes localize and function differently in comparison to classic epithelial cells. Further studies need to be done to unravel these potential redundant interactions of the different polarity proteins.

Our data emphasize the importance of aPKC domains, such as the PB1 domain for nephrocyte function, as the expression of a kinase-dead membrane-associated aPKC variant (aPKC-CAAX-DN) also resulted in a partial rescue of the *baz* knockdown phenotype. Kinase activity independent functions of aPKC have been described before in other *Drosophila* tissues, including the follicular epithelium.[51] As aPKC has several protein-protein interaction domains, it may function as a scaffold to bring together proteins important for SD formation.

The functional role of Par3B is only poorly understood so far. Studies in mammary gland stem cells revealed a unique interaction of Par3B with the tumor suppressor Serine/threonine-protein kinase STK11/liver kinase B1 (LKB1), which results in the inhibition of its kinase activity.[52,53] In contrast, Par3A does not seem to have a function in mammary gland stem cells.[52] Our data show that Par3A and Par3B seem to have common functions, such as the interaction with CD2AP, which might influence the synaptopodin levels, but also distinct functions such as regulation of Rho1-GTP levels. Although Baz exhibits both functions, these were apparently divided into Par3A and Par3B during evolution. A similar effect was observed in a study rescuing depletion of Duf (dNeph) in nephrocytes by expressing the different Neph variants, Neph1, Neph2, and Neph3.[54] Only Neph1 was able to rescue the phenotype, suggesting a duplication of the genes during evolution and a division of functions. Our fly data also illustrate different localization patterns of Par3A and Par3B in nephrocytes, with Par3A 180 kDa localizing homogenously at the cell cortex, whereas Par3B forms cluster at the cell edges.

To date, no pathogenic mutations have been identified in Pard3A or Pard3B, suggesting that both Pard3 genes are required for the establishment and maintenance of cellular polarity during epithelial development and differentiation.

In conclusion, Par3A and Par3B are critical regulators of the podocyte architecture with high levels of redundancy, but also distinct functional roles, interactors, and localization patterns. Mechanistically, Par3 proteins regulate Rho-GTP and synaptopodin levels, thereby linking elements of polarity signaling to actin regulators to maintain the podocytes' architecture.

DISCLOSURE

All the authors declared no competing interests.

ACKNOWLEDGMENTS

The authors thank A. Koeser, G. Rappl, and the Cologne Excellence Cluster on Cellular Stress Responses in Aging-Associated Diseases (CECAD) imaging, proteomics, and *in vivo* facilities for their support. The anti-Polychaetoid monoclonal antibody, developed by A.S. Fanning,[55] and the anti-Rab7 monoclonal antibody, developed by S. Munro,[56] were obtained from the Developmental Studies Hybridoma Bank, created by the Eunice Kennedy Shriver National Institute of Child Health and Human Development of the National Institutes of Health, and maintained at The University of Iowa, Department of Biology, Iowa City, IA. SK received funding from the German Research Foundation (KO 6045/1-1), the Else-Kröner-Fresenius Foundation (2017_A135), the Köln Fortune Program of the University of Cologne, Germany, as well as the German Society of Nephrology (Fritz-Scheler-Stipend). This study was supported by the German Research Foundation: clinical research unit (KFO 329, BR 2955/8-1 to PTB, SCHE 1562/7-1 to BS, and BE 2212/23-1 + 2212/24-1 to TB). PTB was supported by a DFG fellowship (BR2955/6-1). Additional support was provided from the consortium STOP-FSGS by the German Ministry for Science and Education (BMBF 01GM1901E to PTB and TB).

AUTHOR CONTRIBUTIONS

SK and PTB conceived the study; SK, JO, VL, DUJ, CJ, FG, JLJ, CB, and MH performed experiments; SK, DUJ, MH, WB, and PTB analyzed the data; SI and CN contributed animal models; PFH contributed human patient material; SK made the figures and drafted the paper; SK, JO, HHH, SI, CN, GW, AW, BS, TB, BD, and PTB revised the paper; all authors approved the final version of the manuscript.

SUPPLEMENTARY MATERIAL

Supplementary File (PDF)

Figure S1. Single-cell sequencing data from murine glomeruli.
Figure S2. Generation of a novel podocyte-specific Par3B knockout mouse model.
Figure S3. Loss of Par3B does not result in a glomerular disease phenotype.
Figure S4. Generation of Par3A and Par3B double-knockout mice.
Figure S5. Par3A/B double-knockout mice present with a progressive disease phenotype.
Figure S6. Bazooka expression in nephrocytes.
Figure S7. Generation of Par3 rescue fly strains.
Figure S8. Baz exhibits Par6/atypical protein kinase C (aPKC)–independent functions.
Figure S9. Whole proteome analysis of sticks and stones (Sns) and Mec2 depleted nephrocytes and Par3 interactome studies.
Figure S10. Quantification of nephrocyte diaphragm integrity after manipulating synaptopodin levels and interactome analysis of Par3A and Par3B in inner medullary collecting duct cells (IMCDs).
Figure S11. Synaptopodin levels in human patient material.
Figure S12. Validation of GTPase sensor flies in nephrocytes.

REFERENCES

1. Pavenstädt H, Kriz W, Kretzler M. Cell biology of the glomerular podocyte. *Physiol Rev*. 2003;83:253–307.
2. Fissell WH, Miner JH. What is the glomerular ultrafiltration barrier? *J Am Soc Nephrol*. 2018;29:2262–2264.
3. Benzing T. Signaling at the slit diaphragm. *J Am Soc Nephrol*. 2004;15:1382–1391.
4. Brinkkoetter PT, Ising C, Benzing T. The role of the podocyte in albumin filtration. *Nat Rev Nephrol*. 2013;9:328–336.
5. Yu SM-W, Nissaisorakarn P, Husain I, Jim B. Proteinuric kidney diseases: a podocyte's slit diaphragm and cytoskeleton approach. *Front Med*. 2018;5:221.

6. Hildebrandt F. Genetic kidney diseases. *Lancet Lond Engl*. 2010;375:1287–1295.
7. Vivante A, Hildebrandt F. Exploring the genetic basis of early-onset chronic kidney disease. *Nat Rev Nephrol*. 2016;12:133–146.
8. Assémat E, Bazellières E, Pallesi-Pocachard E, et al. Polarity complex proteins. *Biochim Biophys Acta*. 2008;1778:614–630.
9. Koehler S, Tellkamp F, Niessen CM, et al. Par3A is dispensable for the function of the glomerular filtration barrier of the kidney. *Am J Physiol Renal Physiol*. 2016;311:F112–F119.
10. Hartleben B, Widmeier E, Wanner N, et al. Role of the polarity protein Scribble for podocyte differentiation and maintenance. *PLoS One*. 2012;7:e36705.
11. Hartleben B, Widmeier E, Suhm M, et al. aPKCλ/ι and aPKCζ contribute to podocyte differentiation and glomerular maturation. *J Am Soc Nephrol*. 2013;24:253–267.
12. Huber TB, Hartleben B, Winkelmann K, et al. Loss of podocyte aPKClambda/iota causes polarity defects and nephrotic syndrome. *J Am Soc Nephrol*. 2009;20:798–806.
13. Gao L, Macara IG, Joberty G. Multiple splice variants of Par3 and of a novel related gene, Par3L, produce proteins with different binding properties. *Gene*. 2002;294:99–107.
14. Kohjima M, Noda Y, Takeya R, et al. PAR3beta, a novel homologue of the cell polarity protein PAR3, localizes to tight junctions. *Biochem Biophys Res Commun*. 2002;299:641–646.
15. Weavers H, Prieto-Sánchez S, Grawe F, et al. The insect nephrocyte is a podocyte-like cell with a filtration slit diaphragm. *Nature*. 2009;457:322–326.
16. Cagan RL. The Drosophila nephrocyte. *Curr Opin Nephrol Hypertens*. 2011;20:409–415.
17. Zhuang S, Shao H, Guo F, et al. Sns and Kirre, the Drosophila orthologs of Nephrin and Neph1, direct adhesion, fusion and formation of a slit diaphragm-like structure in insect nephrocytes. *Dev Camb Engl*. 2009;136:2335–2344.
18. Höhne M, Frese CK, Grahammer F, et al. Single-nephron proteomes connect morphology and function in proteinuric kidney disease. *Kidney Int*. 2018;93:1308–1319.
19. Buszczak M, Paterno S, Lighthouse D, et al. The carnegie protein trap library: a versatile tool for Drosophila developmental studies. *Genetics*. 2007;175:1505–1531.
20. Sotillos S, Díaz-Meco MT, Caminero E, et al. DaPKC-dependent phosphorylation of Crumbs is required for epithelial cell polarity in Drosophila. *J Cell Biol*. 2004;166:549–557.
21. Krahn MP, Klopfenstein DR, Fischer N, Wodarz A. Membrane targeting of Bazooka/PAR-3 is mediated by direct binding to phosphoinositide lipids. *Curr Biol*. 2010;20:636–642.
22. Moeller MJ, Sanden SK, Soofi A, et al. Podocyte-specific expression of cre recombinase in transgenic mice. *Genes N Y N 2000*. 2003;35:39–42.
23. Muzumdar MD, Tasic B, Miyamichi K, et al. A global double-fluorescent Cre reporter mouse. *Genes N Y N 2000*. 2007;45:593–605.
24. Boerries M, Grahammer F, Eiselein S, et al. Molecular fingerprinting of the podocyte reveals novel gene and protein regulatory networks. *Kidney Int*. 2013;83:1052–1064.
25. Wodarz A, Ramrath A, Kuchinke U, Knust E. Bazooka provides an apical cue for inscuteable localization in Drosophila neuroblasts. *Nature*. 1999;402:544–547.
26. Butt L, Unnersjö-Jess D, Höhne M, et al. A molecular mechanism explaining albuminuria in kidney disease. *Nat Metab*. 2020;2:461–474.
27. Siegerist F, Ribback S, Dombrowski F, et al. Structured illumination microscopy and automatized image processing as a rapid diagnostic tool for podocyte effacement. *Sci Rep*. 2017;7:11473.
28. Hermle T, Braun DA, Helmstädter M, et al. Modeling monogenic human nephrotic syndrome in the Drosophila garland cell nephrocyte. *J Am Soc Nephrol*. 2017;28:1521–1533.
29. Rinschen MM, Bharill P, Wu X, et al. The ubiquitin ligase Ubr4 controls stability of podocin/MEC-2 supercomplexes. *Hum Mol Genet*. 2016;25:1328–1344.
30. Perez-Riverol Y, Csordas A, Bai J, et al. The PRIDE database and related tools and resources in 2019: improving support for quantification data. *Nucleic Acids Res*. 2019;47:D442–D450.
31. Fu Y, Zhu J, Zhang F, et al. Comprehensive functional analysis of Rab GTPases in Drosophila nephrocytes. *Cell Tissue Res*. 2017;368:615–627.
32. Kann M, Ettou S, Jung YL, et al. Genome-wide analysis of Wilms' tumor 1-controlled gene expression in podocytes reveals key regulatory mechanisms. *J Am Soc Nephrol*. 2015;26:2097–2104.
33. McCaffrey LM, Macara IG. The Par3/aPKC interaction is essential for end bud remodeling and progenitor differentiation during mammary gland morphogenesis. *Genes Dev*. 2009;23:1450–1460.
34. McCaffrey LM, Montalbano J, Mihai C, Macara IG. Loss of the Par3 polarity protein promotes breast tumorigenesis and metastasis. *Cancer Cell*. 2012;22:601–614.
35. Rodriguez-Boulan E, Macara IG. Organization and execution of the epithelial polarity programme. *Nat Rev Mol Cell Biol*. 2014;15:225–242.
36. Wong JS, Iorns E, Rheault MN, et al. Rescue of tropomyosin deficiency in Drosophila and human cancer cells by synaptopodin reveals a role of tropomyosin α in RhoA stabilization. *EMBO J*. 2012;31:1028–1040.
37. Czajkowski ER, Cisneros M, Garcia BS, et al. The Drosophila CG1674 gene encodes a synaptopodin 2-like related protein that localizes to the Z-disc and is required for normal flight muscle development and function. *Dev Dyn Off Publ Am Assoc Anat*. 2021;250:99–110.
38. Huber TB, Kwoh C, Wu H, et al. Bigenic mouse models of focal segmental glomerulosclerosis involving pairwise interaction of CD2AP, Fyn, and synaptopodin. *J Clin Invest*. 2006;116:1337–1345.
39. Yanagida-Asanuma E, Asanuma K, Kim K, et al. Synaptopodin protects against proteinuria by disrupting Cdc42:IRSp53:Mena signaling complexes in kidney podocytes. *Am J Pathol*. 2007;171:415–427.
40. Faul C, Donnelly M, Merscher-Gomez S, et al. The actin cytoskeleton of kidney podocytes is a direct target of the antiproteinuric effect of cyclosporine A. *Nat Med*. 2008;14:931–938.
41. Asanuma K, Yanagida-Asanuma E, Faul C, et al. Synaptopodin orchestrates actin organization and cell motility via regulation of RhoA signalling. *Nat Cell Biol*. 2006;8:485–491.
42. Wang L, Ellis MJ, Gomez JA, et al. Mechanisms of the proteinuria induced by Rho GTPases. *Kidney Int*. 2012;81:1075–1085.
43. Babelova A, Jansen F, Sander K, et al. Activation of Rac-1 and RhoA contributes to podocyte injury in chronic kidney disease. *PLoS One*. 2013;8:e80328.
44. Gee HY, Saisawat P, Ashraf S, et al. *ARHGDIA* mutations cause nephrotic syndrome via defective RHO GTPase signaling. *J Clin Invest*. 2013;123:3243–3253.
45. Robins R, Baldwin C, Aoudjit L, et al. Rac1 activation in podocytes induces the spectrum of nephrotic syndrome. *Kidney Int*. 2017;92:349–364.
46. Asao R, Seki T, Takagi M, et al. Rac1 in podocytes promotes glomerular repair and limits the formation of sclerosis. *Sci Rep*. 2018;8:1–11.
47. Dias Gomes M, Letzian S, Saynisch M, Iden S. Polarity signaling ensures epidermal homeostasis by coupling cellular mechanics and genomic integrity. *Nat Commun*. 2019;10:3362.
48. Ning L, Suleiman HY, Miner JH. Synaptopodin is dispensable for normal podocyte homeostasis but is protective in the context of acute podocyte injury. *J Am Soc Nephrol*. 2020;31:2815–2832.
49. Hochapfel F, Denk L, Mendl G, et al. Distinct functions of Crumbs regulating slit diaphragms and endocytosis in Drosophila nephrocytes. *Cell Mol Life Sci*. 2017;74:4573–4586.
50. Ebarasi L, He L, Hultenby K, et al. A reverse genetic screen in the zebrafish identifies crb2b as a regulator of the glomerular filtration barrier. *Dev Biol*. 2009;334:1–9.
51. Kim S, Gailite I, Moussian B, et al. Kinase-activity-independent functions of atypical protein kinase C in Drosophila. *J Cell Sci*. 2009;122(pt 20):3759–3771.
52. Huo Y, Macara IG. The Par3-like polarity protein Par3L is essential for mammary stem cell maintenance. *Nat Cell Biol*. 2014;16:529–537.
53. Li T, Liu D, Lei X, Jiang Q. Par3L enhances colorectal cancer cell survival by inhibiting Lkb1/AMPK signaling pathway. *Biochem Biophys Res Commun*. 2017;482:1037–1041.
54. Helmstädter M, Lüthy K, Gödel M, et al. Functional study of mammalian Neph proteins in Drosophila melanogaster. *PLoS One*. 2012;7:e40300.
55. Choi W, Jung K-C, Nelson KS, et al. The single Drosophila ZO-1 protein Polychaetoid regulates embryonic morphogenesis in coordination with Canoe/afadin and Enabled. *Mol Biol Cell*. 2011;22:2010–2030.
56. Riedel F, Gillingham AK, Rosa-Ferreira C, et al. An antibody toolkit for the study of membrane traffic in Drosophila melanogaster. *Biol Open*. 2016;5:987–992.

Supplemental Table of Contents

Supplementary Figure 1: Single cell sequencing data from murine glomeruli.

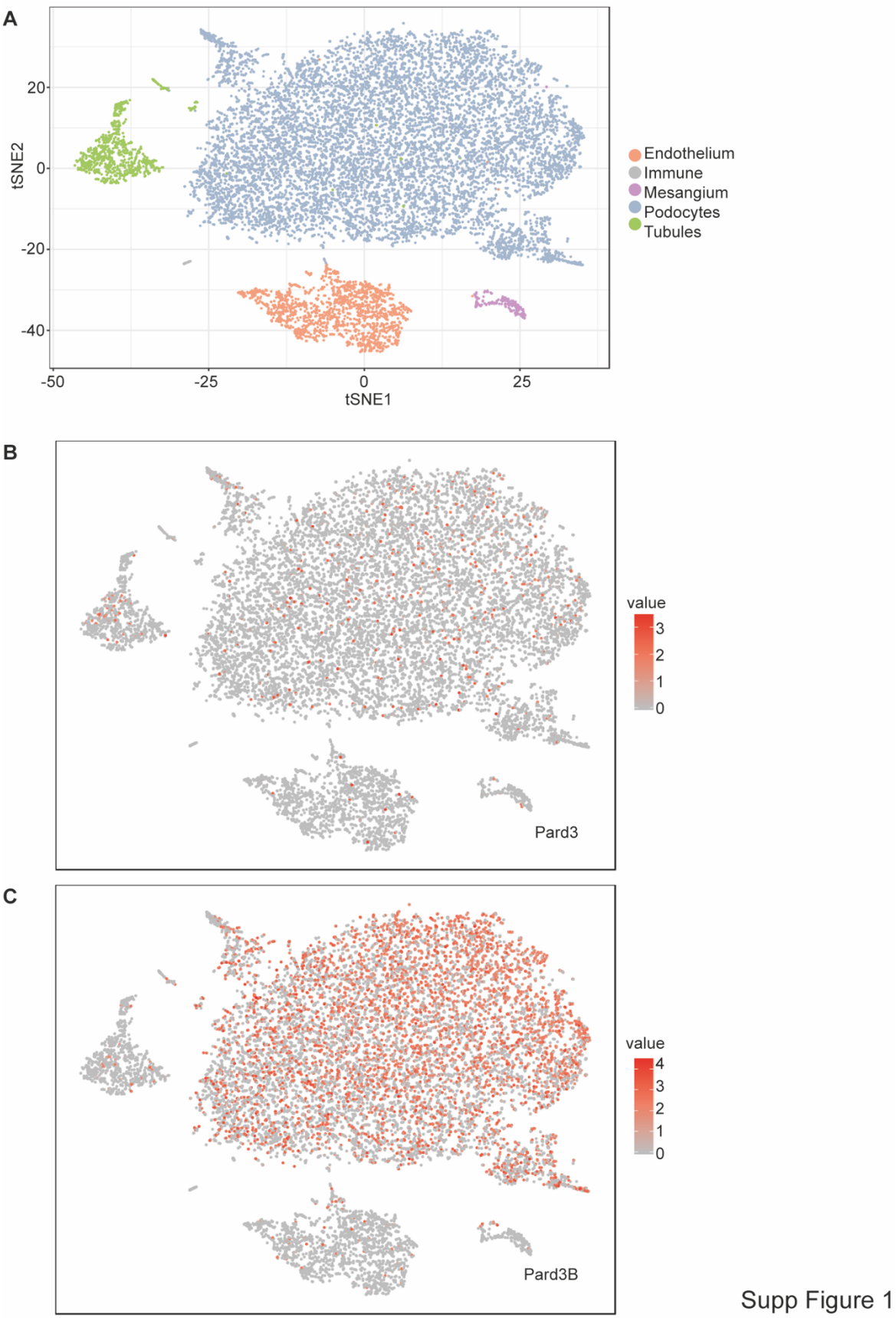

Supp Figure 1

Supplementary Figure 2: Generation of a novel podocyte-specific Par3B knockout mouse model.

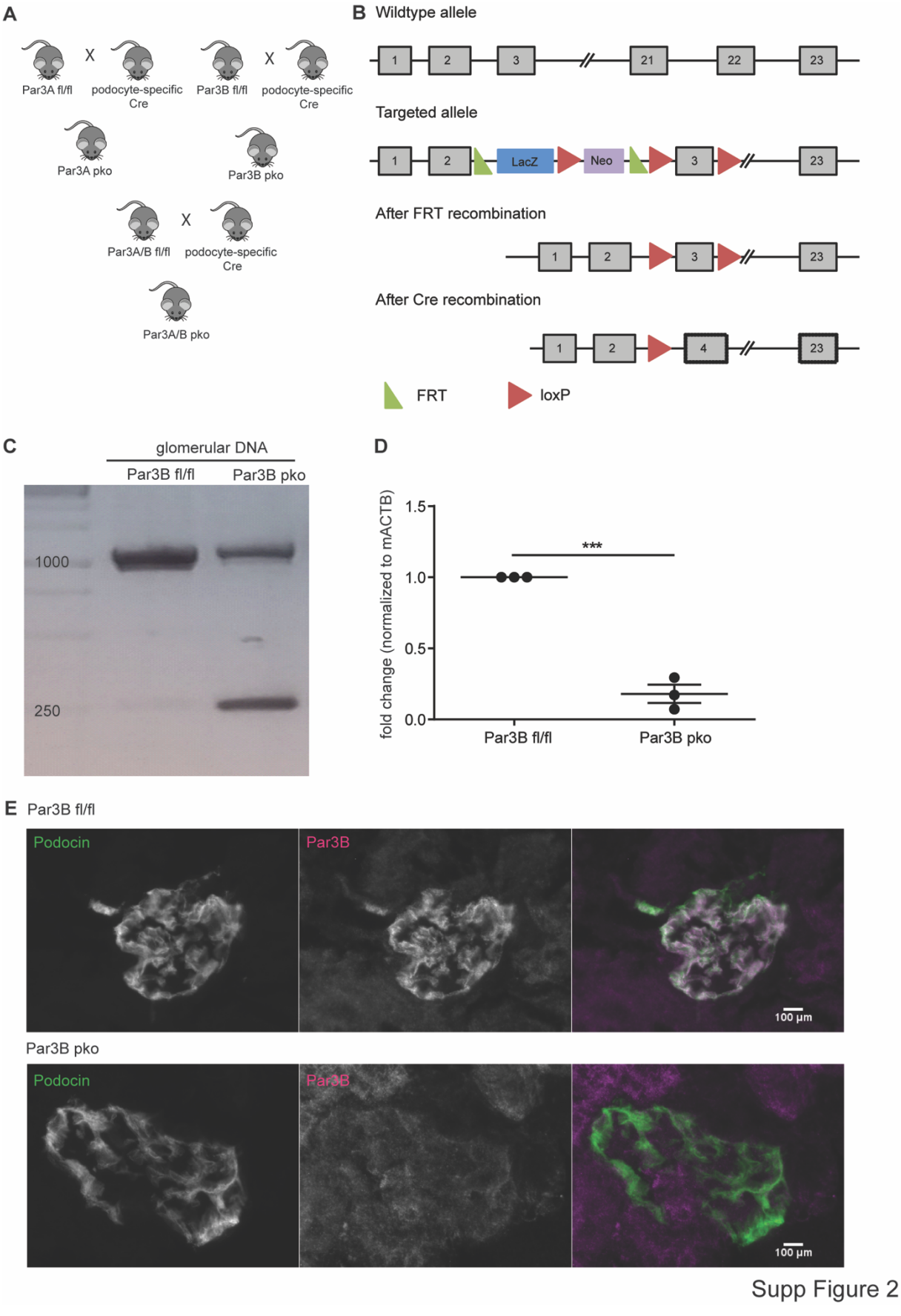

Supp Figure 2

Supplementary Figure 3: Loss of Par3B does not result in a glomerular disease phenotype.

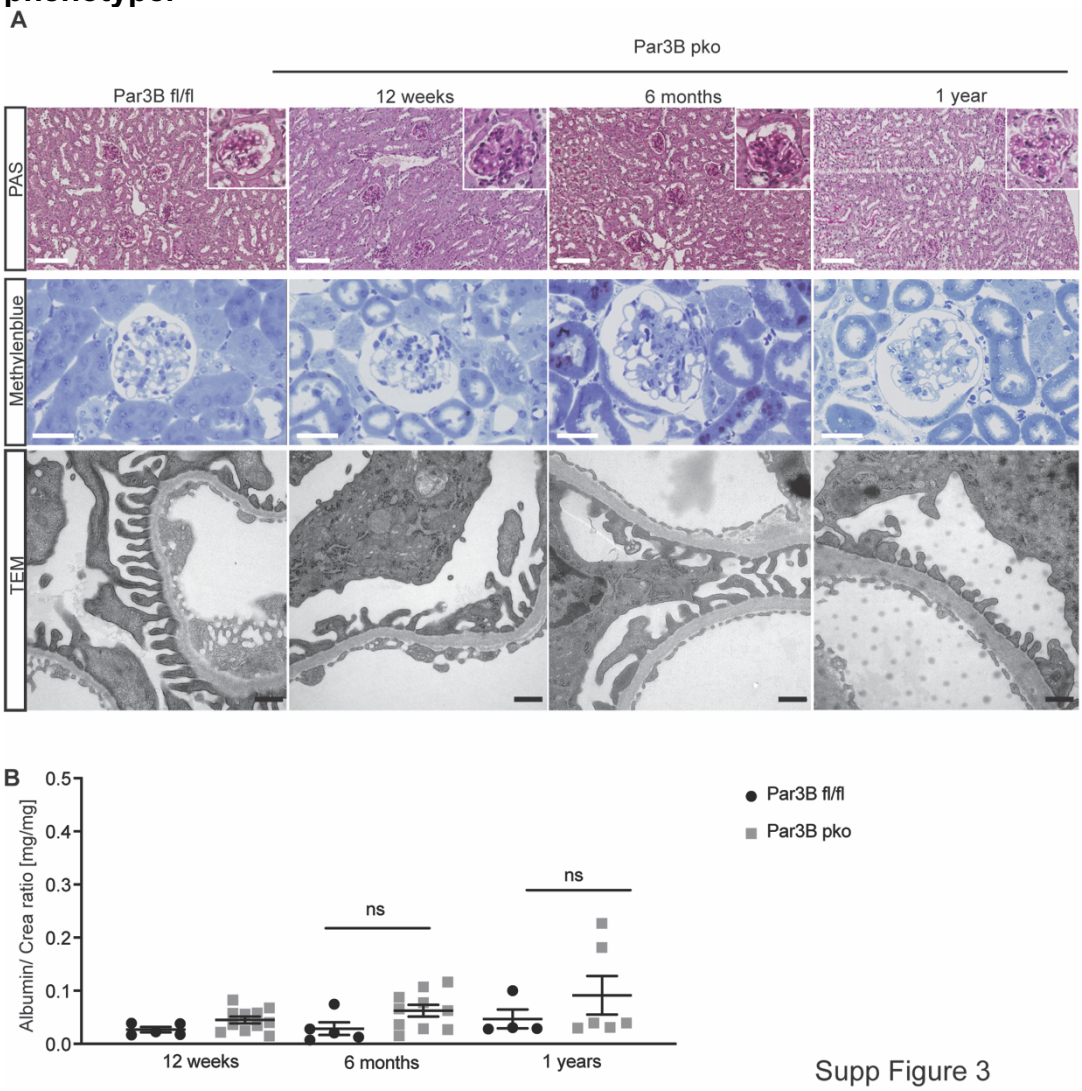

Supp Figure 3

Supplementary Figure 4: Generation of Par3A and Par3B double knockout mice.

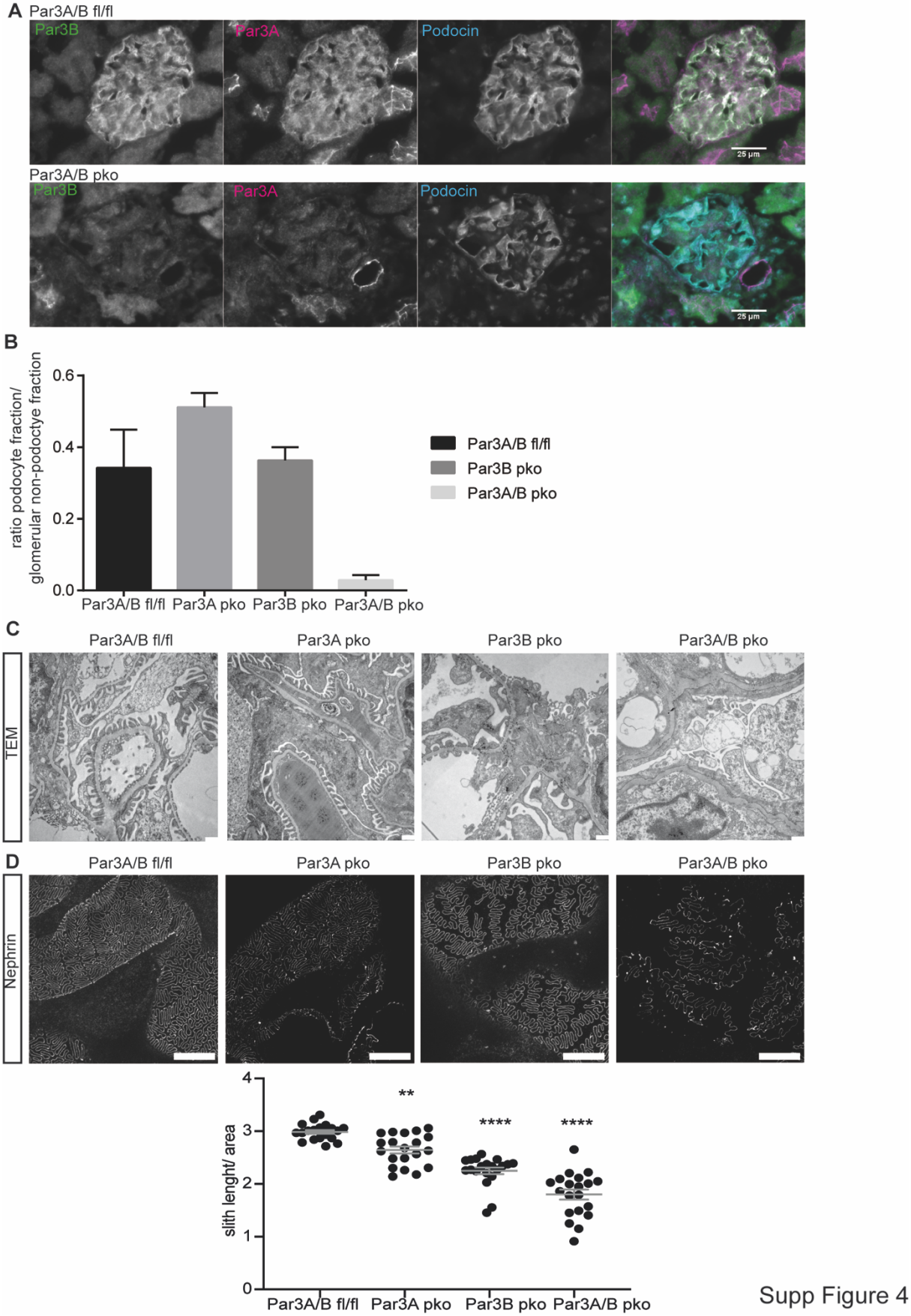

Supp Figure 4

Supplementary Figure 5: Par3A/B double knockout mice present with a progressive disease phenotype.

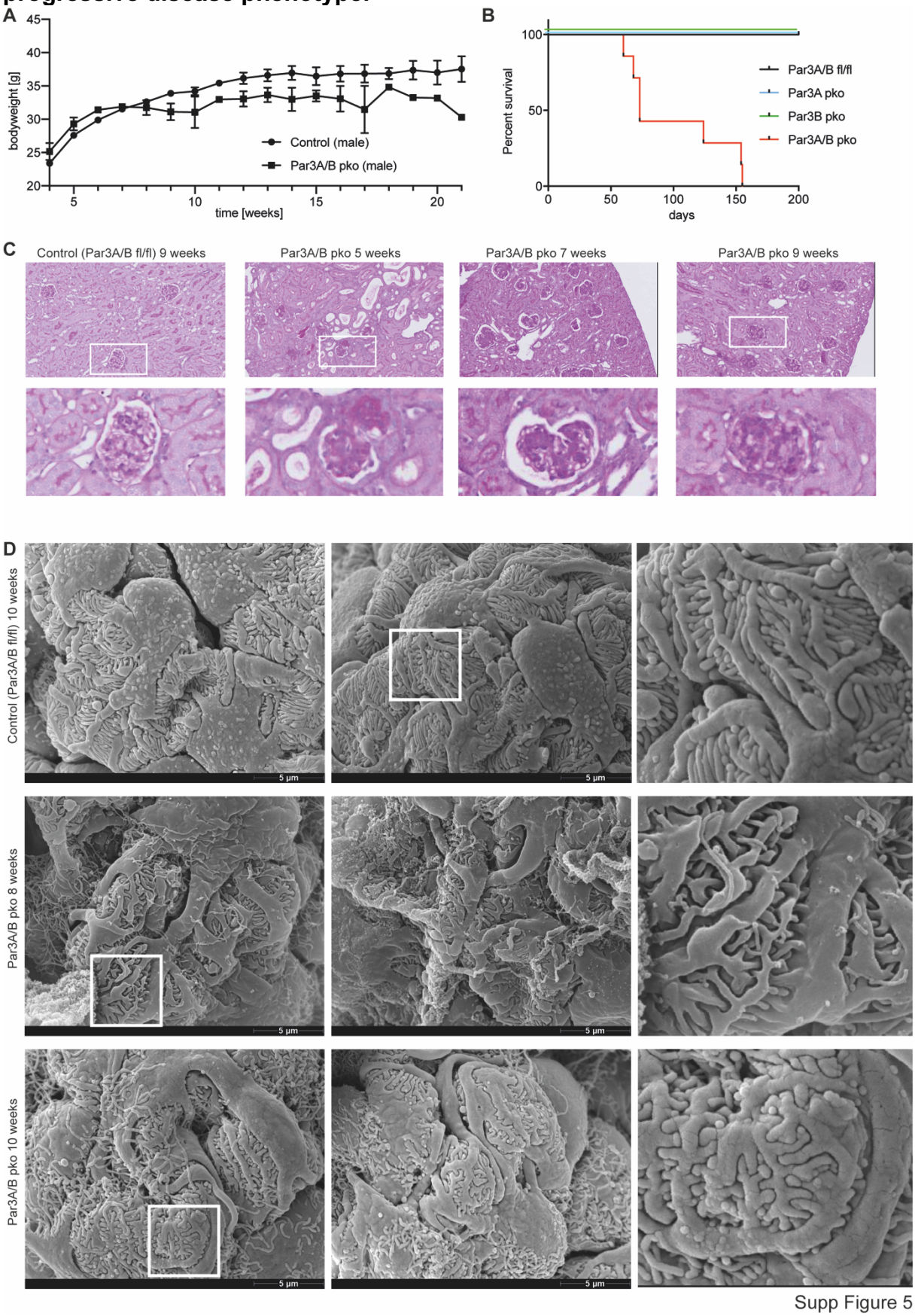

Supp Figure 5

Supplementary Figure 6: Bazooka expression in nephrocytes.

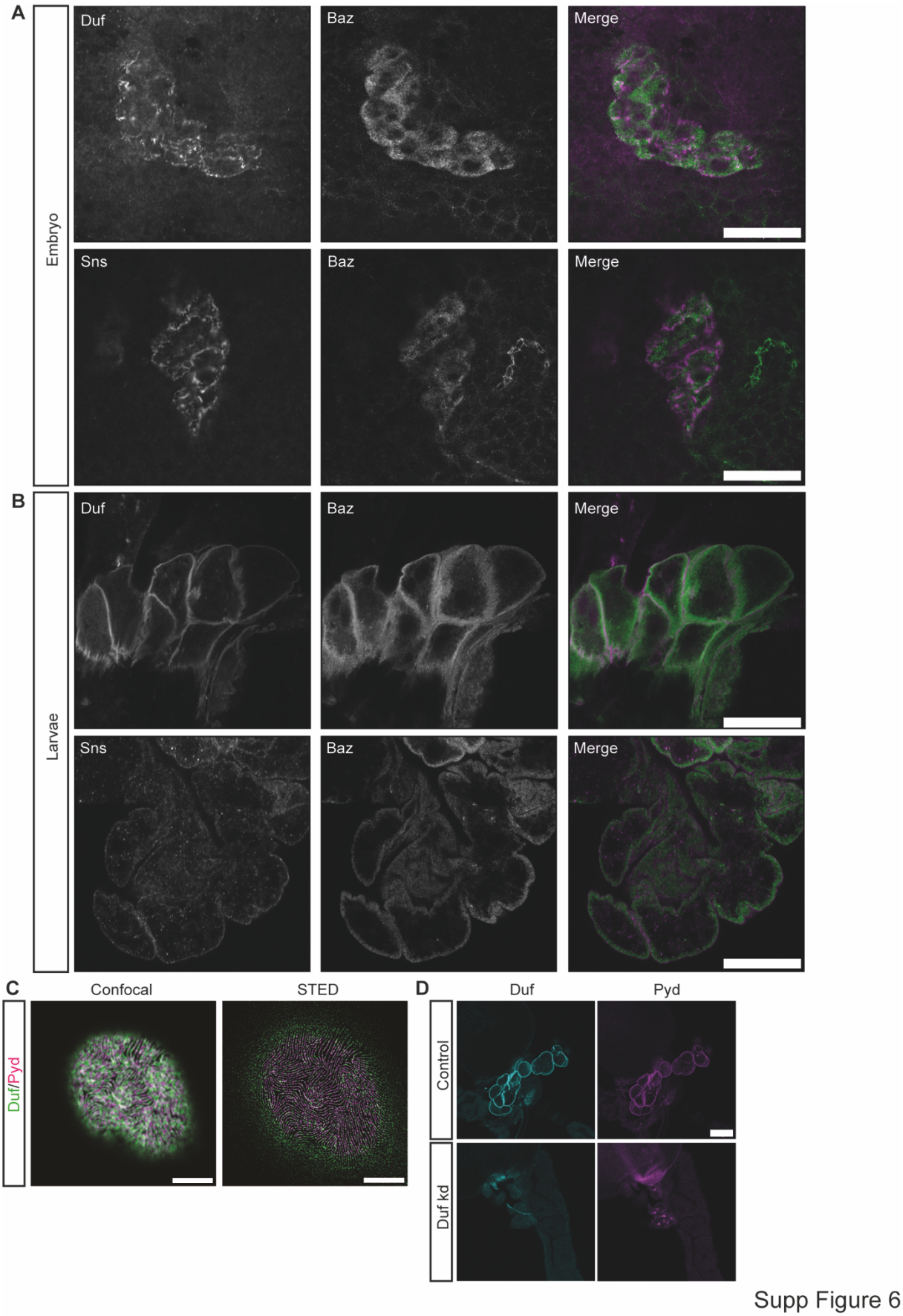

Supp Figure 6

Supplementary Figure 7: Generation of Par3 rescue fly strains.

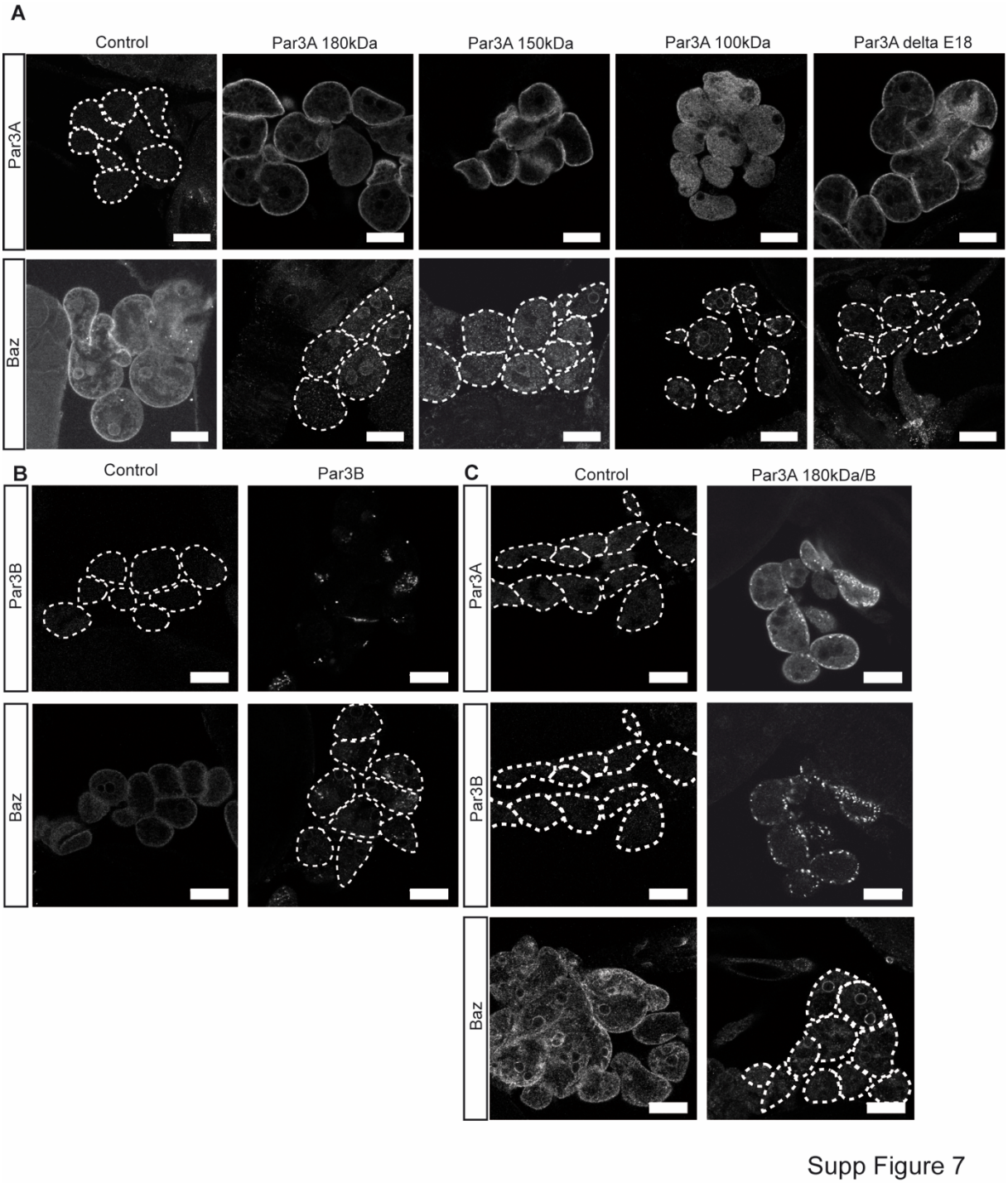

Supplementary Figure 8: Baz exhibits Par6/aPKC-independent functions.

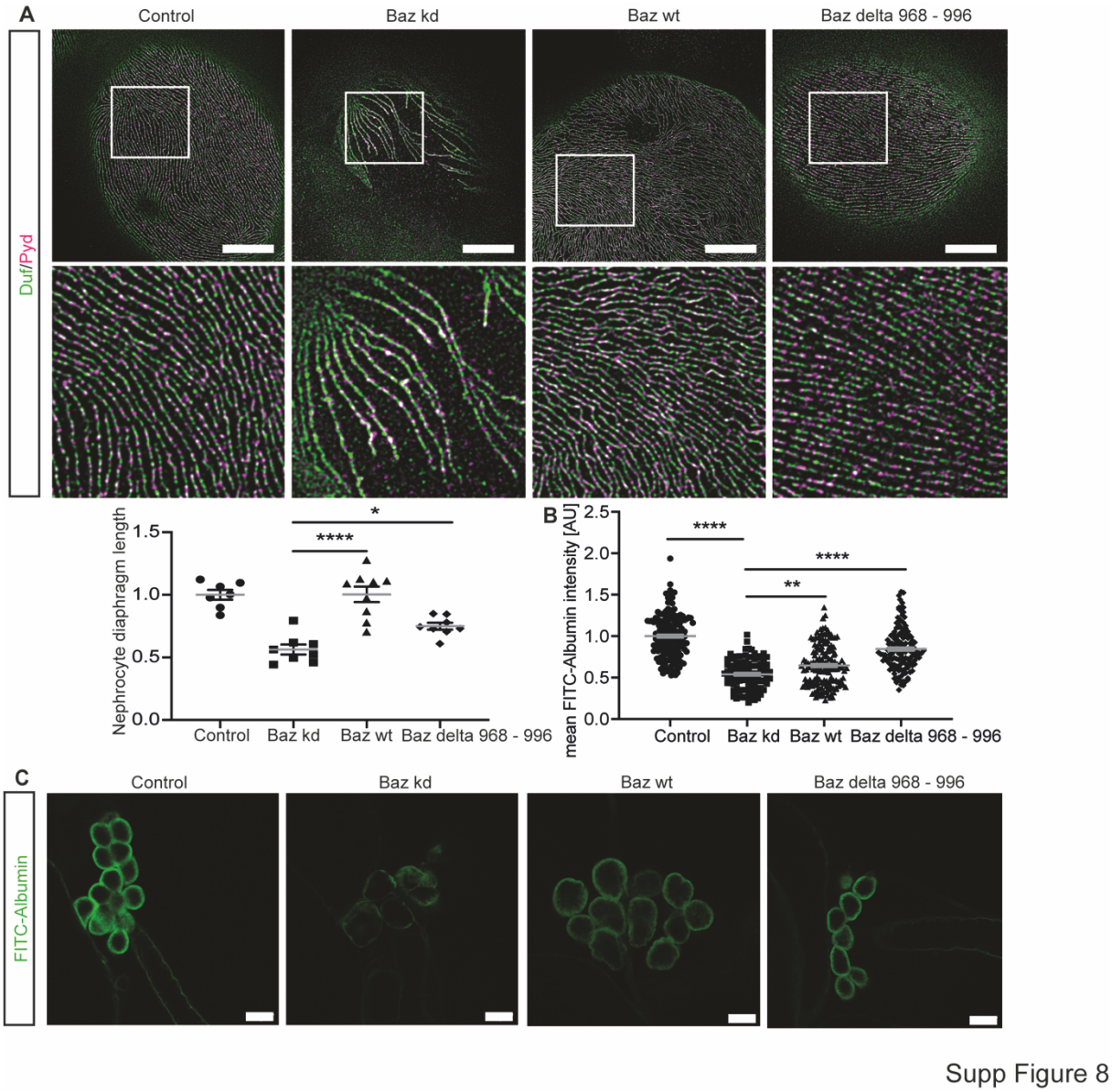

Supp Figure 8

Supplementary Figure 9: Whole proteome analysis of Sns and Mec2 depleted nephrocytes and Par3 interactome studies.

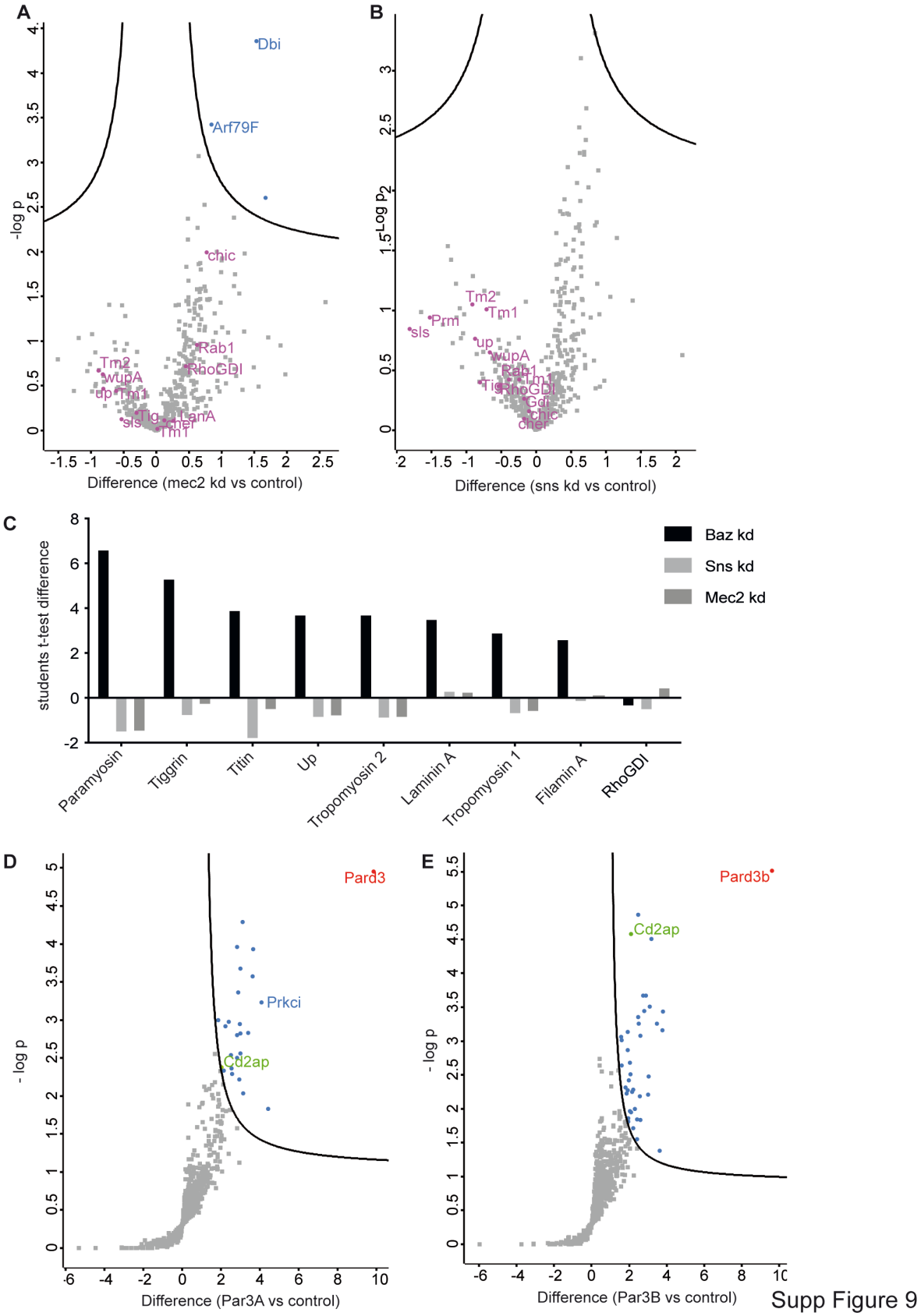

Supp Figure 9

Supplementary Figure 10: Quantification of nephrocyte diaphragm integrity after manipulating Synaptopodin levels and interactome analysis of Par3A and Par3B in IMCDs

A

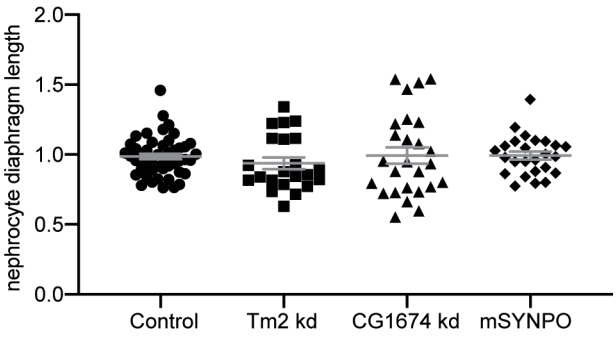

B List of significant Par3A interactors

Protein	Gene
Alpha-centractin	Actr1a
Allograft inflammatory factor 1-like	Aif1l
CD2-associated protein	Cd2ap
DNA damage-binding protein 1	Ddb1
Dihydropyrimidinase-related protein 2	Dpysl2
RNA-binding protein FUS	Fus
	Gcn1l1
Eukaryotic initiation factor 4A-III	Gm8994;Eif4a3
Heterogeneous nuclear ribonucleoprotein L	Hnrnpl
Leucine--tRNA ligase, cytoplasmic	Lars
Lamin-B receptor	Lbr
Afadin	Mllt4
Nucleolar protein 58	Nop58
Partitioning defective 3 homolog	Pard3
Programmed cell death 6-interacting protein	Pdcd6ip
Protein kinase C iota type	Prkci
Ras-related C3 botulinum toxin substrate 1,2,3	Rac1;Rac2;Ra
RNA-binding protein 25	Rbm25
60S ribosomal protein L37a	Rpl37a
Small nuclear ribonucleoprotein Sm D1	Snrpd1
Serine/arginine-rich splicing factor 5	Srsf5
DNA topoisomerase 1	Top1
5-3 exoribonuclease 2	Xrn2

B List of significant Par3B interactors

Protein	Gene
A disintegrin and metalloproteinase with thrombospondin motifs 5	Adamts5
Aly/REF export factor 2; THO complex subunit 4	Alyref2;Alyref
AP complex subunit beta	Ap2b1;Ap1b1
Rho guanine nucleotide exchange factor 2	Arhgef2
Calpain-2 catalytic subunit	Capn2
Caveolin-1;Caveolin	Cav1
CD2-associated protein	Cd2ap
Cell division cycle 5-like protein	Cdc5l
Centrosomal protein of 55 kDa	Cep55
Citron Rho-interacting kinase	Cit
Dihydropyrimidinase-related protein 2	Dpysl2
Desmoglein-2	Dsg2
Interferon-induced, double-stranded RNA activated protein kinase	Eif2ak2
Eukaryotic translation initiation factor 5	Eif5
RNA-binding protein FUS	Fus
Eukaryotic initiation factor 4A-III	Gm8994;Eif4a3
Heterogeneous nuclear ribonucleoprotein	Hnrnpc
Heterogeneous nuclear ribonucleoprotein	Hnrnpl
Isoleucine--tRNA ligase, cytoplasmic	Iars
Junction plakoglobin	Jup
Leucine--tRNA ligase, cytoplasmic	Lars
Lamin-B receptor	Lbr
Protein mago nashi homolog 2	Magohb;Mago

Protein	Gene
Metastasis-associated protein MTA2	Mta2
Bifunctional methylenetetrahydrofolate dehydrogenase/cyclohydrolase	Mthfd2
Nephronectin	Npnt
Platelet-activating factor acetylhydrolase subunit alpha	Pafah1b1
Partitioning defective 3 homolog B	Pard3b
Programmed cell death 6-interacting protein	Pdcd6ip
Pleckstrin homology-like domain family B 2	Phldb2
Serine/threonine-protein phosphatase 2A regulatory subunit B alpha isoform	Ppp2r2a;Ppp2
Splicing factor 1	Sf1
	Sf3b2
Protein SREK1IP1	Srek1ip1
Serine/arginine-rich splicing factor 3	Srsf3
Tight junction protein ZO-1	Tjp1
DNA topoisomerase 1	Top1
DNA topoisomerase 2-alpha	Top2a
Uridine 5-monophosphate synthase;Orota phosphoribosyltransferase;Orotidine 5-ph decarboxylase	Umps

Supp Figure 10

Supplementary Figure 11: Synaptopodin levels in human patient material

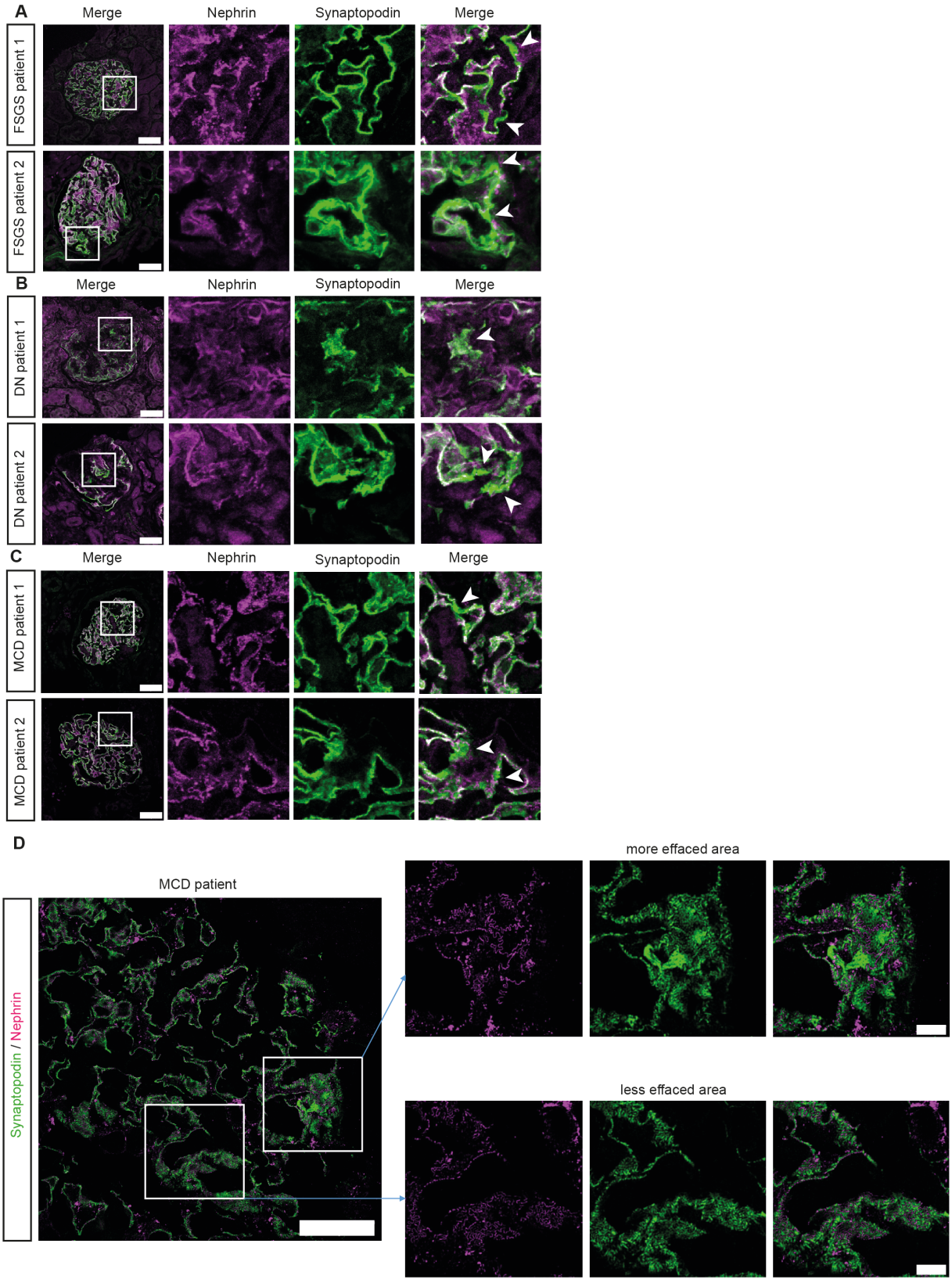

Supp Figure 11

Supplementary Figure 12: Validation of GTPase sensor flies in nephrocytes.

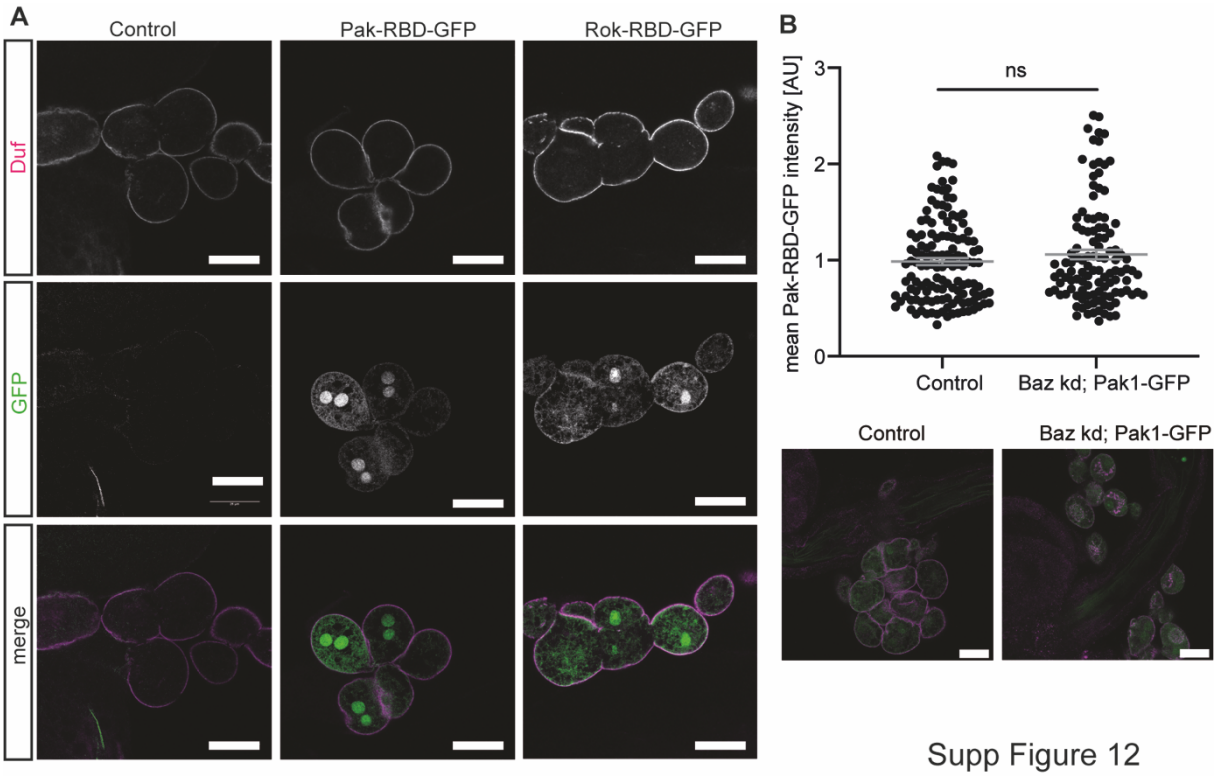

Supplementary Figure legends

Supplementary Figure 1: Single cell sequencing data from murine glomeruli. A Single cell sequencing of murine glomeruli revealed five subclusters of different cell types. **B** Pard3a was found ubiquitously, while **C** Pard3b was highly enriched in the podocyte subcluster.

Supplementary Figure 2: Generation of a novel podocyte-specific Par3B knockout mouse model. A Mating scheme to achieve podocyte-specific knockout mice of Par3A, Par3B and Par3A/B double knockouts. **B** Scheme to present the generation and knockout strategy. Exon 3 was flanked by loxP sites, which results in a premature STOP after Cre-mediated excision. Embryonic stem cells were obtained from EUCOMM and used for *in vitro* fertilization. **C** Deletion PCR with glomerular DNA lysates revealed an additional band after Cre-mediated excision, which represents the truncated gene. As we used glomerular lysates other cell types such as mesangial or endothelial cells still carry the wildtype gene, wherefore a wildtype band can be seen. **D** The remaining mRNA levels were investigated by quantitative PCR and showed a significant reduction of Par3B levels in primary mouse podocytes. For normalization ActinB primers were used. Students t-test: ***: p< 0.001. **E** Immunofluorescence stainings confirmed the loss of Par3B in podocytes. To visualize the slit diaphragm a Podocin antibody was used. Scale bar = 100μm.

Supplementary Figure 3: Loss of Par3B does not result in a glomerular disease phenotype. A Histological analysis such as periodic acid schiff and methylene blue

staining as well as electron microscopy did not reveal any differences between Par3B knockout mice and the control animals. Upper panel: scale bar =100μm, middle panel: scale bar = 30μm, lower panel: 1μm. **B** Urinary albumin levels did not show any significant differences between podocyte-specific Par3B knockout and control animals for up to one year. 1way ANOVA with Sidak's multiple comparison test.

Supplementary Figure 4: Generation of Par3A and Par3B double knockout mice. **A** Immunofluorescence staining revealed complete loss of Par3A and Par3B expression at the slit diaphragm, visualized by Podocin staining, in podocyte-specific Par3A/B double knockout mice. Scale bar = 25μm. **B** FACS analysis of isolated primary podocytes revealed a severely decreased ratio of podocyte to non-podocyte fraction in Par3A/B double knockout cells. **C** Transmission electron microscopy revealed foot process effacement in Par3A/B double knockout mice, while depletion of Par3A and Par3B alone did not result in morphological abnormalities. Scale bar = 500nm. **D** High-resolution microscopy visualizing Nephrin showed a decreased slit diaphragm coverage in all three knockout models, while loss of both Par3 proteins caused the most severe phenotype. Scale bar = 5μm. 3 animals per genotype. 1way ANOVA with Tukey's multiple comparison test: **: $p < 0,01$; ****: $p < 0,0001$.

Supplementary Figure 5: Par3A/B double knockout mice present with a progressive disease phenotype. A Bodyweight analysis of male Par3A/B double knockout and control littermates revealed a similar development until the age of 8 weeks. **B** Survival curve depicting premature death of Par3A/B double knockout mice beginning at 8 weeks, while control littermates and Par3A and Par3B single knockout mice did not present with premature death. **C** Histology (periodic acid schiff staining) revealed early signs of morphological changes in Par3A/B double knockout mice, already evident at an age of 5 weeks. These changes include sclerotic lesion and protein casts in the tubular system. **D** Scanning electron microscopy showed that loss of Par3A/B does not cause severe morphological changes at 8 weeks of age, but shortening of foot processes became visible at 10 weeks of age. Scale bar 5μm.

Supplementary Figure 6: Bazooka expression in nephrocytes. A,B Immunofluorescence staining confirmed expression of Baz in wildtype nephrocytes (w1118), which are visualized by using a Duf (dNeph) and a Sns (dNephrin) antibodies. Baz expression was assessed in garland nephrocytes of **A** late stage embryos and **B** L3 larvae. Scale bar = 25μm. **C** Comparison of confocal and high-resolution microscopy (STED). Scale bar = 5μm. **D** Immunofluorescence staining of control and Duf depleted nephrocytes confirming the Duf antibody specificity. Scale bar = 25μm.

Supplementary Figure 7: Generation of Par3 rescue fly strains. A Four different Par3A variants are expressed in a Baz knockdown background. Expression of the different mammalian variants as well as the Baz knockdown was confirmed by immunofluorescence staining. Scale bar = 25μm. Control (*sns*-GAL4/+), Par3A 180kDa (w;*sns*-GAL4/UAS-*baz*-RNAi;UAS-*Par3A180kDa*/UAS-*dicer2*), Par3A 150kDa (w;*sns*-GAL4/UAS-*baz*-RNAi;UAS-*Par3A150kDa*/UAS-*dicer2*), Par3A 100kDa (w;*sns*-GAL4/UAS-*baz*-RNAi;UAS-*Par3A100kDa*/UAS-*dicer2*), Par3A delta E18 (w;*sns*-GAL4/UAS-*baz*-RNAi;UAS-*Par3A delta Exon 18*/UAS-*dicer2*) **B** Expression of Par3B and simultaneous depletion of Baz was confirmed by immunofluorescence staining. Scale bar = 25μm. Control (*sns*-GAL4/+), Par3B (w;*sns*-GAL4/UAS-*baz*-RNAi;UAS-*Par3B*/UAS-*dicer2*) **C** Par3A and Par3B expression as well as loss of Baz was confirmed by immunofluorescence staining. Scale bar = 25μm.

Control (*sns*-GAL4/+), Par3A 180kDa/B (UAS-*Par3B*;*sns*-GAL4/UAS-*baz*-RNAi;UAS-*Par3A180kDa*/UAS-*dicer2*).

Supplementary Figure 8: Baz exhibits Par6/aPKC-independent functions. A High-resolution microscopy using a Duf and a Pyd antibodies revealed a very efficient rescue, when either wildtype Baz or a Baz mutant lacking the aPKC-binding domain, were expressed in a Baz knockdown background. Scale bar = 5μm. Control (w1118), Baz kd (*Baz-GFP-trap*; *sns*-GAL4/+;UAS-*GFP*-RNAi/+), Baz wt (*Baz-GFP-trap*; *sns*-GAL4/+;UAS-*GFP*-RNAi/UAS-*baz*-wt), Baz delta 968 – 996 (*Baz-GFP-trap*; *sns*-GAL4/+;UAS-*GFP*-RNAi/UAS-*baz-delta968-996*). Quantification of the nephrocyte diaphragm length showed a rescue of the *baz* knockdown phenotype when expressing both, Baz wt and Baz delta 968-996 mutant. 1way ANOVA: *: $p<0.05$; ****: $p<0.0001$. **B,C** FITC-Albumin filtration assays resulted in a partial, but significant rescue of both Baz expressing fly strains when compared to Baz depleted nephrocytes. The expression of the Baz delta 968-996 mutant caused an even better rescue in comparison to the wildtype Baz. 1way ANOVA: **: $p < 0.01$; ****: $p < 0.0001$. Scale bar = 25μm.

Supplementary Figure 9: Whole proteome analysis of Sns and Mec2 depleted nephrocytes and Par3 interactome studies. A Volcano plot depicting differentially regulated proteins in Mec2 (dPodocin) depleted nephrocytes compared to controls (*sns*-GAL4/+). Blue: significant proteins. Purple: proteins, which are significantly up-regulated in Baz knockdown nephrocytes. FDR = 0.05, s0 = 0.1. **B** Volcano plot depicting differentially regulated proteins in Sns (dNephrin) depleted nephrocytes compared to controls (*sns*-GAL4/+). Purple: proteins, which are significantly up-regulated in Baz knockdown nephrocytes. FDR = 0.05, s0 = 0.1. **C** Bar graph comparing the students t-test difference of interesting candidates between Baz, Sns and Mec2 knockdown nephrocytes. **D,E** Interactome analysis of **D** Par3A and **E** Par3B in inner medullary collecting duct cells. As control we used flag expressing cells. aPKC was only identified in the Par3A interactome, further confirming that there is no interaction between Par3B and aPKC. CD2AP (green) was identified as common interactor and potential link between Synaptopodin and Par3A and Par3B. Red: Par3A or Par3B, Blue: significant interactors, FDR = 0.05, s0 = 0.8.

Supplementary Figure 10: Quantification of nephrocyte diaphragm integrity after manipulating Synaptopodin levels and interactome analysis of Par3A and Par3B in IMCDs A Quantification of the nephrocyte diaphragm length did not reveal any differences after depleting Tm2 and CG1674 or expressing mSYNPO. **B** List of significant Par3A interactors. Blue: shared interactors with Par3B, Red: Par3A. **C** List of significant Par3B interactors. Blue: shared interactors with Par3A, Red: Par3B.

Supplementary Figure 11: Synaptopodin levels in human patient material. A,B,C Immunofluorescence staining revealed an increase of Synaptopodin levels in areas of effacement (identified as loss of Nephrin expression, arrowheads) in human material derived from patients suffering from FSGS (**A**), diabetic nephropathy (DN) (**B**) and minimal change disease (MCD) (**C**). Scale bar = 50μm. **D** Confocal microscopy again visualized an Synaptopodin accumulation in effaced areas, as marked by less Nephrin expression (arrowheads). Scale bar = 5 μm and 25μm.

Supplementary Figure 12: Validation of GTPase sensor flies in nephrocytes. A Expression of Rok-RBD-GFP and Pak-RBD-GFP was verified by confocal microscopy.

Garland nephrocytes of L3 larvae were visualized using a Duf antibody and showed a clear GFP signal in both sensor fly strains. Scale bar = 25μm. Control (w;*sns*-GAL4/+:UAS-*dicer2*/+), Pak-RBD-GFP (w; *sns*-GAL4/+;UAS-*Pak-RBD-GFP*/UAS-*dicer2*), Rok-RBD-GFP (w; *sns*-GAL4/+;UAS-*Rok-RBD-GFP*/UAS-*dicer2*). **B** Utilizing a Rac sensor fly strain (Pak-RBD-GFP) revealed no differences in active Rac/Cdc42 levels upon loss of Baz, when compared to control cells. (Control: w; *sns*-GAL4/+;UAS-*Pak-RBD-GFP*/UAS-*dicer2*, Baz kd; Pak1-GFP: w; *sns*-GAL4/UAS-*baz*-RNAi;UAS-*Pak-RBD-GFP*/UAS-*dicer2*).

3 Discussion

Despite recent advances in studying glomerular diseases and ongoing progress in understanding the fundamental mechanisms that underlie podocyte injury and the development of nephrotic syndrome, therapeutic options to treat individuals suffering from nephrotic syndrome remain merely symptomatic. Ultimate options for when the disease progresses to kidney failure still are dialysis and kidney transplantation. It is therefore highly important to gain further evidence on critical unifying pathways that lead to foot process effacement and potential, ideally druggable targets to counteract its progression.

This thesis assessed dysregulated actin dynamics and the loss of podocyte polarization as key principles of FPE and glomerular disease. To investigate the function of polarity and actin-regulating proteins, cell culture, mouse as well as fruit fly models were employed. Hereby, a strong focus was put on utilizing *Drosophila melanogaster* nephrocytes as genetic model for podocyte injury. Complementing the individual discussion of the chapters within the results part, a summary of the main findings and conclusions of this thesis will be given in the following sections.

3.1 *Drosophila* as convenient model to assess podocyte biology and monogenic nephrotic syndrome

To date, *Drosophila melanogaster* has been the most studied model organism in biological research (Rubin & Lewis, 2000; Stephenson & Metcalfe, 2013). Due to the various options of genetic manipulation and transgene expression as well as high genomic conservation, *Drosophila* is nowadays also emerging as a convenient model to address biomedical questions (Jennings, 2011). 50 % of the human genome is conserved in the fly and about 75 % of disease-associated genes have a *Drosophila* homolog (Kornberg & Krasnow, 2000; Reiter et al., 2001). Many disease-models, such as models for diabetes or neurodegenerative diseases have evolved over the years (Cauchi & van den Heuvel, 2006; Wangler et al., 2015). They demonstrate that fly and human proteins are partially interchangeable and that transgenic expression of disease-variants of such proteins recapitulates major hallmarks of the disease, such as aggregate formation, synaptic degeneration, neuronal loss and locomotion defects in

fly models for Alzheimer's disease (Fernandez-Funez et al., 2015; Tsuda & Lim, 2018; Y. Wang et al., 2022).

Chapter 2.1 aimed at introducing the fruit fly and in particular nephrocytes as model for glomerular diseases. Since nephrocytes were introduced as podocyte-equivalent cells in the fly (Weavers et al., 2009; Zhuang et al., 2009), establishing foot process like cell protrusions that flank a filtration slit bridged by SD-homologous proteins, *Drosophila* has gained attention in basic glomerular research and in modelling monogenic glomerular diseases. Meanwhile, it has been shown by several independent research groups that nephrocyte specific depletion of genes associated with nephrotic syndrome results in perturbed morphology of the nephrocyte diaphragm, responsible for filtration of macromolecules from the haemolymph, and consequently reduced filtration function (Fu et al., 2017; Hermle et al., 2017). Hence, manipulating nephrotic syndrome-associated genes in nephrocytes recapitulates the main hallmarks of the human disease. Very recently, also other *Drosophila* models of podocyte injury have been developed such as diet induced models of diabetic nephropathy or renal lipotoxicity (K. Kim et al., 2021; Lubojemska et al., 2021). Within the publication in chapter 2.1, we discuss advantages of the fly model over other model systems such as rodents or cell culture systems with a focus on genetic manipulation. We moreover give examples for read-outs to assess nephrocyte morphology and function by immunofluorescent stainings and tracer uptake assays, respectively (Chapter 2.1, Fig. 4+5), which have been established as experimental standard within the laboratory. It is hereby worth mentioning that we extended our methodical repertoire since the publication in 2019, by performing super resolution microscopy to study the nephrocytes surface in more detail. Visualizing the nephrocyte diaphragm pattern in high resolution enables us to also observe minor morphological changes, which can be quantified using a published Fiji macro (Butt et al., 2020) and plotted as nephrocyte diaphragm length per area.

A significant portion of this thesis was devoted to utilizing *Drosophila* as an *in vivo* tool to characterize novel mutations identified through genetic analysis in patients with nephrotic syndrome (Chapter 2.2). Here, we identified a novel ACTN4 mutation in a paediatric patient suffering from steroid resistant nephrotic syndrome. As an actin-binding and -crosslinking protein, ACTN4 is directly involved in the regulation of actin dynamics and especially during actin-rearrangement upon FPE (Djinović-Carugo et al., 1999; Feng et al., 2015; Kaplan et al.,

2000; Smoyer et al., 1997). Within this chapter, the *Drosophila* model was used to complement *in silico* and *in vitro* analyses (Chapter 2.2, Fig. 2+3). Transgenic expression of several variants of the *ACTN4* gene in nephrocytes enabled us to establish the newly identified variant ACTN4-pM240T as a pathogenic variant of the protein (Chapter 2.2, Fig. 5). Since expression of human ACTN4-pM240T, unlike wildtype human ACTN4, was not able to rescue the morphological and functional phenotypes associated with knockdown of endogenous *actinin* levels, but rescue capacity was rather comparable to that of other, previously published pathogenic ACTN4 variants, we could conclude, that the novel variant is indeed pathogenic and therefore underlying disease development in our patient. Deciphering the pathogenic potential of novel gene variants is of high importance for a) the therapeutic proceeding in the individual patient and b) the evaluation of a possible disease-recurrence after kidney transplantation. Computational modelling and cell culture experiments of course comprise a valuable first hint towards a possible pathogenicity of the genetic variant, but they must be accompanied by further *in vivo* analyses. Mouse models in this regard would of course be most desirable and most convincing, but they come with several disadvantages: In addition to costly and elaborate husbandry as well as longer generation times, the application and acceptance of the animal model, genetic manipulation, and establishment of the mouse line, followed by the experimental workup, would take well over a year, under the best of circumstances. Regarding this time issue, *Drosophila* is clearly advantageous here: As discussed in chapter 2.1, the short generation times and simple husbandry and maintenance are extremely favourable as well as the genetic toolbox provided by large, publicly accessible fly stock repositories. These include mutant libraries, several collections of fly lines for controlled expression of hairpin ribonucleic acids (RNAs) to perform RNA-interference (RNAi) mediated knockdown experiments as well as diverse driver-lines for tissue- and cell-specific expression of target genes. These parameters make *Drosophila* an ideal model organism to express and characterize human transgenes in a simple way and reasonable time frame.

In summary, we hope to have shown that *Drosophila* is a convenient model to assess podocyte biology and in the context of chapter 2.2, to elucidate the potential pathogenicity of newly-identified disease variants, which was implemented as additional diagnostic tool as part of the national FOrMe registry of patients with glomerular diseases in order to help clinicians shape the individual therapy of a patient.

3.2 The Par complex signals to the actin cytoskeleton and is crucial for podocyte integrity

Over the past decades, many proteins have been found to be essential for podocyte integrity in health and disease. Hereby, a recurrent hypothesis is, that perturbed actin dynamics and the re-organization of the actin cytoskeleton is a common final pathway that underlies FPE (Blaine & Dylewski, 2020; Kriz et al., 2013; Shankland, 2006; Shirato et al., 1996). In this context, podocyte polarity and especially the Par complex came into focus, when it was shown that podocyte specific loss of Cdc42, an important actin regulator, leads to glomerular disease and was accompanied by reduced expression levels of aPKCiota and Par3A (Scott et al., 2012). Indeed, knockout of *aPKCiota* in podocytes results in a severe glomerular phenotype, upon which the mice die prematurely within four to five weeks of age (Huber et al., 2009). These data and the fact that upon FPE podocytes experience a de-differentiation from their sophisticated three-dimensional structure back to more columnar shaped epithelial cells (May et al., 2014) raises the following hypothesis: “Would stabilizing the podocyte’s polarization be beneficial in counteracting the progress of FPE and are polarity proteins potential druggable targets in this context?” Seminal subsequent studies have investigated the significance of the three major epithelial polarity complexes in podocytes. Since podocytes are characterized by a sophisticated three-dimensional structure and are missing classical cell-cell contacts like tight or adherens junctions (Kreidberg, 2003; Pavenstädt et al., 2003), the crosstalk of those complexes might be significantly different to what we know from classical epithelial cells. Indeed, knockout of *Scrib* in murine podocytes did not result in glomerular disease (Hartleben et al., 2012), further indicating that the strict concept of how these complexes achieve apico-basal polarity must be reconsidered for podocytes. Within this thesis, we were now able to provide further insight on how polarity signalling functions in podocytes.

Podocyte-specific loss of members of the Par complex was analysed in mouse and *Drosophila* models to study Par polarity signalling and a possible link to cytoskeletal reorganization. Previous work in our group already revealed, that loss of Par3A in podocytes does not lead to an apparent glomerular phenotype and that the predominant Par3 isoform in podocytes is Par3B, which is expressed at higher levels upon *Par3A* knockout (Koehler et al., 2016). We now showed, that also single knockout of *Par3B* in podocytes does not result in glomerular disease and that mice only develop a phenotype, when both Par3 isoforms are lost in

podocytes (Chapter 2.3, Fig. 1). Hence, Par3A and Par3B seem to share redundant functions. This finding is remarkable, since Par3B does not interact with aPKC (Gao et al., 2002; Kohjima et al., 2002) – a protein interaction which is indispensable in the classical concept of epithelial polarity. Yet, Par3B is apparently still able to compensate for Par3A loss in podocytes. To exclude possible indirect binding of aPKC via the third complex member Par6, we went into the fly model and performed further rescue analyses in nephrocytes depleted for both, Bazooka (Baz, the *Drosophila* Par3 homologue) and dPar6 (*Drosophila* Par6). Whereas Par3A was not able to rescue the double knockdown-associated nephrocyte phenotypes, transgenic expression of Par3B in the knockdown background led to partial rescue of nephrocyte diaphragm length and full rescue of filtration capacity (Chapter 2.3, Fig. 5). These data show, that Par3A ultimately functions in a complex with aPKC/Par6 and that Par3B strikingly acts independent of aPKC and Par6. Thus, Par3B might exhibit completely novel functions, which might be worth studying in detail, as will be discussed in the next section.

To understand loss of Par3 and its impact on podocyte biology in more detail, we investigated podocyte-expressed isoforms of Par3A and Par3B and their functions and potential downstream signalling pathways in nephrocytes. Nephrocyte-specific depletion of Baz results in reduced nephrocyte diaphragm length and decreased filtration function, resembling the murine Par3A/B phenotype. This phenotype could be partially rescued when either expressing murine Par3A or Par3B in the knockdown background. However, rescue potential of nephrocyte filtration capacity was best, when expressing both proteins simultaneously, indicating that besides a functional redundancy, the proteins do exhibit independent characteristics that are both needed to maintain podocyte integrity. This hypothesis is strengthened by observations in super resolution microscopy on tissue derived from *Par3A* and *Par3B* single knockout mice: The single knockouts do develop a minor phenotype shown by slight reduction of SD length (Chapter 2.3, Supp. Fig. 4). However, this reduction does not result in proteinuria or sclerotic lesions in the animals. As Butt et al. recently showed, decreasing SD length needs to overcome a certain threshold until it manifests as glomerular disease (Butt et al., 2020). This potentially is what we can observe in our *Par3A* and *Par3B* single knockout mice. Redundant functions of the two proteins are sufficient to compensate for loss of the respective other protein and to not overcome this particular threshold.

However, they do comprise distinct individual functions that lead to a slight reduction in SD length.

We then performed proteomic analyses in *baz* knockdown nephrocytes. These revealed increased expression of various actin-binding and -regulating proteins such as Vinculin, Alpha-actinin and Tropomyosin 2 (Tm2), the functional orthologue of synaptopodin (Chapter 2.3, Fig. 6). Elevated expression levels of these actin-associated proteins could be reversed by transgenic expression of murine Par3A or Par3B, showing that both proteins are signalling to the actin cytoskeleton. Furthermore, an increase in Rho1, the *Drosophila* homologue of mammalian RhoA, which is downstream of Tm2 or synaptopodin, respectively, could be observed in Baz depleted nephrocytes (Chapter 2.3, Fig. 8a). Interestingly, Rho1 activation could be reversed, when either knocking down *tm2* or by expression of Par3A. Expressing Par3B in the *baz* knockdown background on the other hand failed to ameliorate Rho1 activity. From this, we concluded, that there is a possible link from Par3A to actin-regulation via synaptopodin and the small GTPase RhoA. Whether Par3A is directly interacting with synaptopodin leading to RhoA activity or whether there are other intermediary effectors needs to be investigated further.

We were intrigued by the fact, that Tm2 levels are increased in *baz* knockdown nephrocytes. Prior research demonstrated that synaptopodin is dispensable for podocytes under normal conditions, but has a protective effect in the event of podocyte injury (Ning et al., 2020). To examine the synaptopodin effect in the mammalian system, we went back to the mouse model and performed immunofluorescent stainings of synaptopodin in *Par3A/B* double knockout mice and could observe an increase in synaptopodin intensity (Chapter 2.3, Fig. 7, c+d). This could then also be observed in renal specimen derived from patients suffering from glomerular diseases (Chapter 2.3, Supp. Fig. 11). Here, increased expression of synaptopodin could be seen in areas where FPE was advanced. Whether increased levels or ‘aggregation’ of synaptopodin in effaced areas has a protective effect, as postulated before, remains however elusive. To this end, we overexpressed murine synaptopodin in nephrocytes, which resulted in impaired filtration function (Chapter 2.3, Fig. 7b), indicating a rather negative impact of elevated synaptopodin levels on nephrocyte integrity. Aggregation of the protein in podocytes has also been described in other studies. Mutations in *ACTN4* for example lead to the formation of ACTN4 positive aggregates into which the synaptopodin protein is

sequestered, leading to perturbed synaptopodin localization (Weins et al., 2005, 2007). Concerning this issue, it is worth mentioning, that the ACTN4 patient reported in chapter 2.2, initially responded to Cyclosporin A therapy over a course of two years, which is known to have a stabilizing effect on the synaptopodin protein. Hence, stabilization of synaptopodin at its native location seems to counteract the progression of FPE to some extent. This further hints towards a negative impact of synaptopodin mislocalization and aggregation in podocyte injury and lets us speculate whether the enrichment of synaptopodin to effaced areas of the podocytes in mice and human tissues is potentially driving FPE progression.

In conclusion, our data provide further evidence on a link between the Par polarity complex and the regulation of actin dynamics. Therefore, the Par complex constitutes an important target to maintain proper actin cytoskeleton regulation in health and disease. Moreover, our data describe redundant functions of Par3A and Par3B but also novel functions of the two proteins. We could show that Par3A exerts its functions in a complex with aPKC and Par6, as known from classical epithelial cells. Par3B on the other hand acts independent of the complex. To what extent these novel functions are important for podocyte biology and upon podocyte injury now need to be analysed in more detail.

3.3 Outlook – Redefining podocyte polarity

In addition to studying the Par3 proteins and their role in podocytes, ongoing work in the laboratory has been focussing on investigating the role of aPKCiota and its kinase function for podocyte integrity. The following section therefore serves as short discussion of so far unpublished data and an experimental outlook into future experimental plans.

In columnar epithelial cells, aPKC functions as a molecular switch, by either phosphorylating Par3A or Lgl1 and -2 (Nagai-Tamai et al., 2002; Plant et al., 2003; Yamanaka et al., 2003). Par3 phosphorylation leads to localization of Par3 to tight junctions, whereas phosphorylated Lgl will dissociate from aPKC and translocate to basal regions where it then interacts with SCRIB. Hence, kinase activity of aPKC is indispensable in classical epithelial cells to assure proper segregation into apical and basal properties. In podocytes, knockout of *aPKCiota* leads to severe glomerular disease (Huber et al., 2009), highlighting that the protein is essential for podocyte biology. Due to the growing evidence, that polarity in podocytes might be quite different most notably because Par3B can compensate for loss of Par3A despite the lacking aPKC interaction, we were intrigued and asked, whether aPKCiota has other functions besides being a kinase. Kinase-independent functions of aPKC have already been reported in several *Drosophila* tissues (S. Kim et al., 2009), underlining the importance of other aPKC domains. As part of our publication in chapter 2.3, we could also observe kinase-independent functions of aPKC in nephrocytes (Chapter 2.3, Fig. 4). Overexpression of a membrane targeted aPKC variant, aPKC-CAAX, in the *baz* knockdown background was able to ameliorate the morphological phenotype of Baz depleted nephrocytes. Surprisingly, this was also observed when overexpressing a kinase dead, dominant negative (DN) variant of the same construct, aPKC-CAAX-DN. A significant rescue for both, aPKC-CAAX and aPKC-CAAX-DN could also be observed in filtration capacity, however, this functional rescue did not reach the levels achieved with Par3A and -B transgene expression. These data hint towards aPKC being more important for establishing and maintaining nephrocyte morphology and Par3 being most relevant for exerting filtration function, possibly uncoupling aPKC and Par3 functions. Ongoing work in our group therefore focusses on investigating aPKC and its role for nephrocyte/podocyte biology. We first characterized the nephrocyte specific knockdown of endogenous *aPKC* (Appendix, Fig. 6). For this, three independent RNAi-lines were used (aPKC-RNAi1, -RNAi2 and RNAi3) to exclude off-target effects. Performing immunofluorescent

stainings it was observed that depletion of aPKC leads to mislocalization of Polychaetoid (Pyd), the ZO-1 homologue and component of the nephrocyte diaphragm, as well as a significant reduction in nephrocyte diaphragm length with all three experimental lines (Fig. 6, A-C). Electron micrographs could validate this finding: The characteristic architecture of the nephrocyte, as seen in controls, where nephrocyte diaphragms are bridging the filtration slit which leads into the lacunar system, is almost completely lost upon knockdown of *aPKC* (Fig. 6D). These data are in line with observations upon assessing the nephrocyte's function. By performing tracer uptake assays, it was revealed that depletion of aPKC results in diminished filtration capacity of the nephrocytes (Fig. 6, E+F). To ensure, that the observed phenotype is due to decreased aPKC levels and not a secondary result of nephrocytes being apoptotic, the apoptosis inhibitor p35 was overexpressed in the *aPKC* knockdown background, which did not result in ameliorated tracer uptake capacity (Fig. 6G). Thus, the *aPKC* knockdown-associated morphological and functional phenotypes are indeed attributed to reduced aPKC protein levels. To investigate to what extent the aPKC kinase domain is important for nephrocyte function, subsequent studies comprised the transgenic expression of murine aPKCiota-wildtype (aPKCiota-WT) as well as aPKCiota-K273E, a previously described kinase dead variant of aPKCiota (Hartleben et al., 2008). Upon morphological analyses, a significant but partial rescue of nephrocyte diaphragm length could be observed when transgenically expressing aPKCiota-WT in the *aPKC* knockdown background (Fig. 7, A+B). The same holds true for transgenic expression of aPKCiota-K273E. Upon assessing nephrocyte function, it was furthermore revealed that both, aPKCiota-WT and aPKCiota-K273E, are restoring filtration function to control levels (Fig. 7, C+D). From these observations, we can draw two important conclusions: 1) There are indeed kinase-independent functions of aPKCiota that are important for nephrocyte/podocyte function and 2) the kinase domain seems to be completely neglectable for filtration function and rather for nephrocyte/podocyte morphology, complementing the findings within chapter 2.3 and described above. Further experiments will now be done to understand aPKCiota function in more detail. These include the analysis of an aPKCiota PB1-domain truncation variant in nephrocytes, analogous to the above-described approach. Furthermore, it is of interest, to establish an aPKCiota interactome in murine podocytes as well as renal tubulus cells. By comparing podocytes to tubulus cells, which are considered conventional epithelial cells, we hope to identify podocyte-specific, potentially

unknown aPKCiota interacting proteins and to hereby contribute further to re-defining the concept of polarity in podocytes.

One of the most interesting findings within this thesis is clearly Par3B independence of Par complex members aPKC/Par6, which attributes completely new functions to Par3B and opens up a new chapter of polarity definition in podocytes. In general, Par3B and its function is poorly understood. Initial studies on Par3B revealed that the protein is co-localizing with the tight junction marker ZO-1 but can also be found in the cytoplasm of cells (Burford et al., 2014; Gao et al., 2002). In podocytes, Par3B is primarily located at the SD (Koehler et al., 2016). Whether the protein interacts with any of the SD-associated proteins as well as general podocyte specific interactors of Par3B remains elusive. Interestingly, Par3B downregulation, on mRNA as well as protein level, is a recurrent finding in omics data sets of different murine glomerular disease models (personal communication with Martin Kann, University Hospital Cologne). Downregulation of Par3A on the other hand cannot be observed, making Par3B a novel slit diaphragm protein that appears to be highly significant for glomerular diseases. Whether Par3B downregulation is driving the disease or a potential compensatory mechanism upon podocyte injury, needs to now be investigated. Future work in our group will therefore focus on the detailed functional analysis of Par3B in podocytes. How is Par3B expression regulated in podocytes? What are podocyte specific interactors of Par3B? Does overexpression of Par3B in different disease background ameliorate or worsen disease progression? We will tackle all these open questions with additional mouse and *Drosophila* models and hope to thereby contribute to the concept of polarity in podocytes and to understanding of how podocyte polarity maintains and ensures proper actin-regulation and podocyte integrity in health and disease.

Appendix

Supplementary data

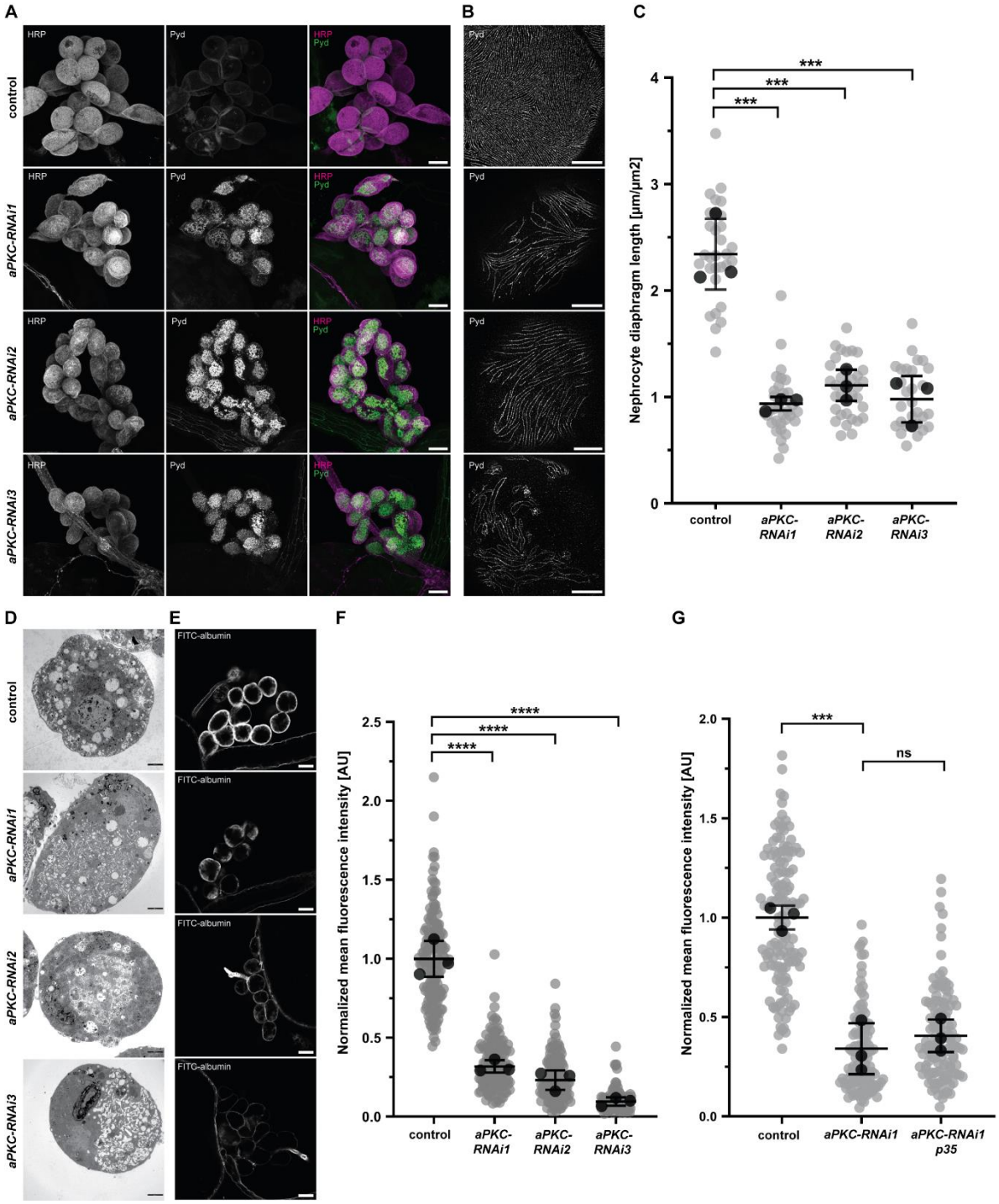

Figure 6: Nephrocyte specific depletion of aPKC leads to severe morphological and functional phenotypes. (A) Fluorescent micrographs of nephrocytes stained with antibodies against horse radish peroxidase (HRP, a marker for nephrocytes in *Drosophila*) and Polychaetoid (Pyd, the ZO-1 homologue, associated with the nephrocyte diaphragm, ND). Knockdown of *aPKC* in nephrocytes was achieved by combining a nephrocyte specific GAL4-

driver line (Sns-GAL4;UAS-dcr2, (Odenthal & Brinkkoetter, 2019)) and three independent UAS-aPKC-RNAi lines (VDRC #105624; BDSC #25946 and #34332), hereafter referred to as aPKC-RNAi1, -2 and -3, respectively. Control nephrocytes were expressing UAS-GFP-RNAi (BDSC #41553). In contrast to controls, where Pyd was located at the outer aspect of the cell closely associated with the membrane, knockdown of *aPKC* led to severe mislocalization of Pyd towards the centre of the cell. **(B+C)** Representative fluorescent micrographs of nephrocytes depicting the cell surface in super resolution and stained with anti-Pyd (B) and quantification of the ND length (C). The ND can be seen as characteristic fingerprint like pattern in controls. Upon knockdown of *aPKC*, a perturbed, loosened ND pattern can be observed in all three RNAi-lines. Quantification of the micrographs was done using a previously published Fiji macro (Butt et al., 2020) and revealed that the ND length in aPKC depleted nephrocytes is significantly reduced when compared to control nephrocytes (grey dots show individual nephrocytes that were measured, black dots indicate means of n=3 independent experiments performed in three experimental crossings, error bars represent STDV, ***p<0.001, One-way ANOVA with Tukey's *post-hoc* test). **(D)** Electron micrographs of control and *aPKC* knockdown nephrocytes. In the control nephrocyte, on can appreciate the presence of numerous NDs that bridge the entrance of many lacunae, into which molecules are filtered through the ND and finally endocytosed. Knockdown of *aPKC* leads to complete disruption of NDs and the lacuna system. Instead, an unidentified black mass constitutes the rim of the nephrocyte. **(E+F)** Representative fluorescent micrographs of nephrocytes subjected to FITC-albumin tracer (E) and quantification of fluorescence intensity as measure of uptake capacity (F). Control and *aPKC* knockdown nephrocytes were incubated in 0.2 mg/ml FITC-albumin solution for 30 seconds and fluorescence intensity was quantified using Fiji (Odenthal & Brinkkoetter, 2019). The data are presented as normalized to control levels. Compared to control nephrocytes, the uptake capacity of *aPKC* knockdown nephrocytes is significantly diminished, indicating severe functional defects (grey dots show individual nephrocytes that were measured, black dots indicate means of n=3 independent experiments performed in three experimental crossings, error bars represent STDV, ****p<0.0001, One-way ANOVA with Tukey's *post-hoc* test). **(G)** Quantification of fluorescence intensity in micrographs of nephrocytes subjected to FITC-albumin tracer. The uptake assay and quantification were done as described above. The apoptosis inhibitor p35 (UAS-p35, kind gift of A. Wodarz, Cologne) was expressed in the background of aPKC-RNAi1. Expression of p35 does not ameliorate the *aPKC* knockdown-associated phenotype (grey dots show individual nephrocytes that were measured, black dots indicate means of n=3 independent experiments performed in three experimental crossings, error bars represent STDV, ***p<0.001, ns, not significant, One-way ANOVA with Tukey's *post-hoc* test). Scale bars indicate 25 µm in A and E, 5 µm in B and 2,5 µm in D. aPKC, atypical protein kinase C; RNAi, ribonucleic acid interference; FITC, Fluorescein isothiocyanate; AU, Arbitrary units; Sns, Sticks and stones; UAS, Upstream activating sequence; dcr2, dicer2; VDRC, Vienna Drosophila Resource Centre; BDSC, Bloomington Drosophila Stock Center; GFP, Green Fluorescent Protein; STDV, standard deviation; ANOVA, Analysis of variance.

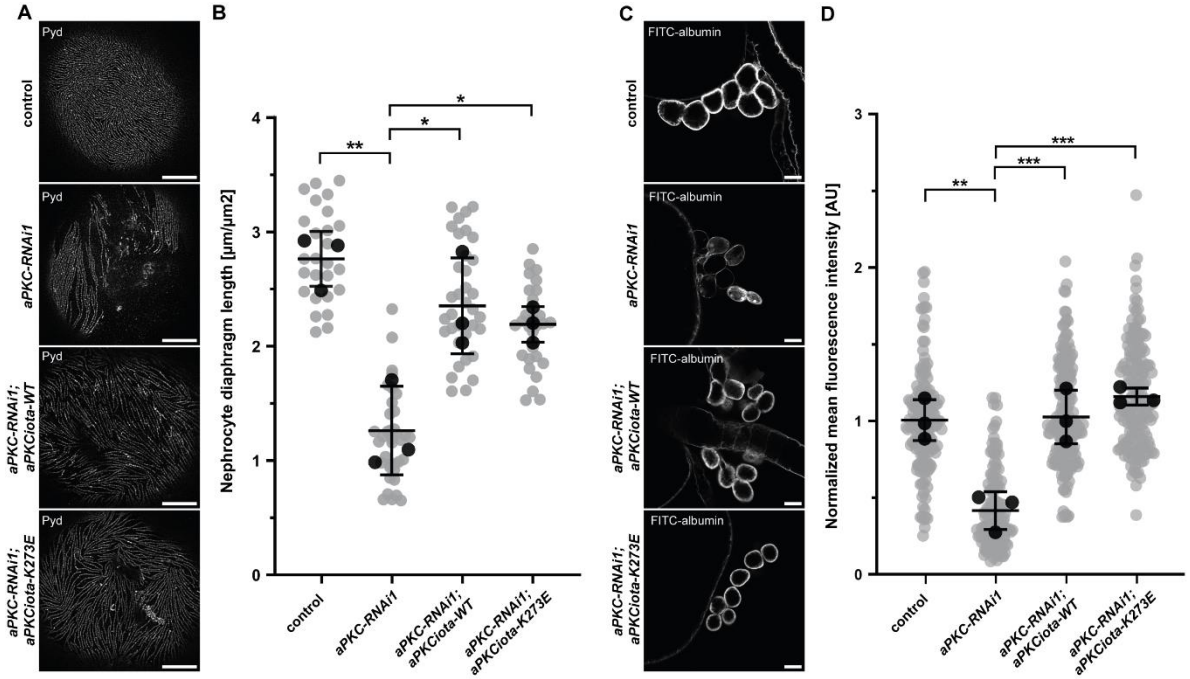

Figure 7: A kinase dead aPKCiota variant is able to rescue aPKC knockdown-associated nephrocyte phenotypes. (A+B) Representative fluorescent micrographs of nephrocytes stained with anti-Polychaetoid (Pyd) (A) and quantification of the nephrocyte diaphragm (ND) length (B). Nephrocytes derived from either control larvae, larvae with nephrocyte-specific knockdown of *aPKC* (aPKC-RNAi1) or nephrocytes that express a wildtype as well as kinase dead variant of murine aPKCiota in the *aPKC* knockdown background (aPKC-RNAi1;aPKCiota-WT and aPKC-RNAi1;aPKCiota-K273E, respectively). Control larvae were expressing UAS-GFP-RNAi (BDSC #41553), knockdown larvae were expressing UAS-aPKC-RNAi1 (VDRC #105624). UAS-aPKCiota-WT and UAS-aPKCiota-K273E are self-made (transgenesis by GenetiVision). As nephrocyte specific GAL4-driver line served Sns-GAL4;UASdcr2 (Odenthal & Brinkkoetter, 2019). Imaging and subsequent quantification revealed that both, aPKCiota-WT and aPKCiota-K273E are able to partially rescue the *aPKC* knockdown-associated reduction in ND length (grey dots show individual nephrocytes that were measured, black dots indicate means of n=3 independent experiments performed in three experimental crossings, error bars represent STDV, **p<0.01, *p<0.05, One-way ANOVA with Tukey's *post-hoc* test). **(C+D)** Representative fluorescent micrographs subjected to FITC-albumin tracer (C) and quantification of fluorescence intensity as measure of uptake capacity (D). Nephrocytes of the above-mentioned fly lines were incubated in 0.2 mg/ml FITC-albumin solution for 30 seconds and fluorescence intensity was quantified using Fiji. The data are presented as normalized to control levels. Transgenic expression of both, murine aPKCiota-WT and aPKCiota-K273E, in the *aPKC* knockdown background results in full rescue of the knockdown-associated functional phenotype (grey dots show individual nephrocytes that were measured, black dots indicate means of n=3 independent experiments performed in three experimental crossings, error bars represent STDV, ***p<0.001, **p<0.01, One-way ANOVA with Tukey's *post-hoc* test). Scale bars indicate 5 µm in A and 25 µm in C. aPKC, atypical kinase C; RNAi, ribonucleic acid interference; FITC, Fluorescein isothiocyanate; AU, Arbitrary units, GFP, Green Fluorescent Protein, UAS, Upstream Activating Sequence; VDRC, Vienna Drosophila Resource Centre; BDSC, Bloomington Drosophila Stock Center, Sns, Sticks and stones; dcr2, dicer2; STDV, standard deviation; ANOVA, Analysis of variance.

Acknowledgement

After a long and interesting journey, it is time to express my appreciation and gratitude to all the people who have contributed to this work and to my time at the University Hospital Cologne.

I would first like to thank my advisor Prof. Thomas Benzing for giving me the opportunity to conduct my studies in his department and to always taking the time for discussion and finding advisory and cheerful words. Your wisdom and dedication concerning research of all topics are inspiring and will serve as great example to me in the future.

Moreover, I would like to thank Prof. Siegfried Roth for being the second reviewer of this thesis and for taking time for discussion over the past years. Furthermore, many thanks to Prof. Ines Neundorf for being the chair of the reviewing committee.

I am deeply grateful to Andreas Wodarz, who advised me a lot on the set up of *Drosophila* experiments and who, as part of my thesis advisory committee, was a great mentor over the past years. I hope to continue the exchange on our research in the future.

Many thanks to Christian Jüngst and Ferdi Grawe, who helped a lot with confocal and electron microscopy and for all the cheerful microscopy sessions we had together!

I would like to thank all people in the Nephrolab and especially the Brinkkötter-CMMC-devision for being there whenever I needed help. A special thanks to Serena Greco-Torres, Angelika Köser, Steffi Keller and Claudia Dafinger, for always helping out with experimental support, mouse issues or simply lessons in 'how to run a lab'. A big thank you also to David Unnersjö-Jess, who managed to always cheer me up and giving me the best time in Stockholm learning all things STED! My sincerest gratitude however goes to Martin Höhne, my *Drosophila* peer, who was always there for me and helped with analyses, fruitful discussion and not least, who took a vast amount of time over the past years to carefully advise and comment on the manuscripts building the basis of this thesis and who accompanied me also during my finishing straight. Thank you!!

My biggest appreciation goes to Paul Brinkkötter, who gave me the opportunity to start in his laboratory and to convey my love for *Drosophila* onto the new grounds of glomerular diseases. Thank you for always supporting me, also in tougher times, sending me around the world and for pushing my scientific career and well…also pushing me to my limits from which I learned what I am capable of. Let's see what the future holds.

Lastly, I would like to thank my family and friends. Thank you to my parents, who were always there for me and supported me throughout my whole course of education. Thank you to my "family" here in Cologne – Marc, Julie, Mahsa, Cem, Liam and Emil – you made the past years unforgettable. And to my best friends Vivi, Sita and my person – Lisa – you were always there for me, in good times and the worst. Whitout you I could not have done it!

Danksagung

Nach einer langen und interessanten Reise ist es nun an der Zeit ein paar Worte des Dankes auszusprechen an all die Leute, die zu dieser Arbeit und zu meiner Zeit an der Uniklinik Köln beigesteuert haben.

Zunächst möchte ich mich bedanken bei meinem Doktorvater Prof. Thomas Benzing für die Möglichkeit in der Abteilung zu promovieren und dafür, dass immer Zeit für Diskussion und helfende und aufmunternde Worte war! Dein Wissen und deine Hingabe hinsichtlich der verschiedensten Forschungsthemen ist inspirierend und werden mir zukünftig ein großes Beispiel sein.

Desweiteren möchte ich mich gerne bei Prof. Siegfried Roth für die Zweitbegutachtung meiner Arbeit bedanken und für die Zeit für Diskussion in den letzten Jahren. Ebenfalls bedanke ich mich bei Prof. Ines Neundorf für den Vorsitz meines Prüfungskommittees.

Mein besonderer Dank gilt Andreas Wodarz, der mich oft mit dem Planen von *Drosophila* Experimenten unterstützt hat und, als Teil meines Thesis Advisory Committees, ein toller Mentor über die letzten Jahre war. Ich hoffe sehr, dass wir uns auch weitherhin über unsere Forschung austauschen werden. Vielen Dank an Christian Jüngst und Ferdi Grawe, die eine große Unterstützung waren mit Konfokal- sowie Elektronen-Mikroskopie und für all die lustigen Mikroskopie-Sessions. Ich möchte mich bei allen Leuten des Nephrolabors und speziell der AG Brinkkötter bedanken und dass ihr bei Fragen immer ein offenes Ohr hattet. Speziell bedanken möchte ich mich bei Serena Greco-Torres, Angelika Köser, Steffi Keller und Claudia Dafinger, für experimentelle Hilfe, Hilfe bei Mausproblemen oder einfach Rat bei „Wie leite ich ein Labor“. Ein großes Dankeschön auch an David Unnersjö-Jess, der mich immer aufgemuntert hat und mir die beste Zeit in Stockholm und beim STED-Lernen bereitet hat. Mein größter Dank gilt jedoch Martin Höhne, meinem *Drosophila*-Gleichgesinnten, der immer für mich da war und mit Analysen und Diskussionen geholfen hat und der sich nicht zuletzt viel Zeit über die letzten Jahre genommen hat die Manuskripte dieser Arbeit gewissenhaft zu kommentieren und auch in meiner Zielgerade wieder eine große Hilfe war. Danke!!

Meine größte Dankbarkeit geht an Paul Brinkkötter, der mir die Möglichkeit gegeben hat in seinem Labor zu starten und meine Liebe für *Drosophila* auf das mir unbekannte Feld der glomerulären Erkrankungen zu übertragen. Danke, für die immerwährende Unterstützung, für die vielen Reisen, für das Fördern meiner Karriere und…das Herausfordern meiner Grenzen, durch das ich gelernt habe was ich bewerkstelligen kann. Ich bin gespannt, was die Zukunft mit sich bringt.

Zuletzt möchte ich mich bei meiner Familie und meinen Freunden bedanken. Danke an meine Eltern, die immer für mich da sind und mich während meines gesamten Bildungswegs fortwährend unterstütz haben. Danke an meine Kölner Familie – Marc, Julie, Mahsa, Cem, Liam und Emil – ihr habt die letzten Jahre unvergesslich gemacht. Tausend Dank an meine Besten Vivi, Sita und meiner Lisa – ihr wart immer für mich da, in den guten und den schlechtesten Zeiten. Ohne euch hätte ich es nicht geschafft!

References

Asanuma, K., Kim, K., Oh, J., Giardino, L., Chabanis, S., Faul, C., Reiser, J., & Mundel, P. (2005). Synaptopodin regulates the actin-bundling activity of alpha-actinin in an isoform-specific manner. *The Journal of Clinical Investigation*, *115*(5), 1188–1198.

Assémat, E., Bazellières, E., Pallesi-Pocachard, E., le Bivic, A., & Massey-Harroche, D. (2008). Polarity complex proteins. *Biochimica et Biophysica Acta*, *1778*(3), 614–630.

Badal, S. S., & Danesh, F. R. (2014). New insights into molecular mechanisms of diabetic kidney disease. *American Journal of Kidney Diseases*, *63*(2 SUPPL.2), 63-83.

Batzoglou, S., Pachter, L., Mesirov, J., Berger, B., & Lander, E. S. (2000). Human and mouse gene structure: comparative analysis and application to exon prediction. *Genome Research, 10(7), 950-958*.

Benzing, T. (2004). Signaling at the slit diaphragm. *Journal of the American Society of Nephrology, 15,* 1382-1391.

Bilder, D., Li, M., & Perrimon, N. (2000). Cooperative regulation of cell polarity and growth by Drosophila tumor suppressors. *Science (New York, N.Y.)*, *289*(5476), 113–116.

Blaine, J., & Dylewski, J. (2020). Regulation of the Actin Cytoskeleton in Podocytes. *Cells*, *9*(7).

Blattner, S. M., Hodgin, J. B., Nishio, M., Wylie, S. A., Saha, J., Soofi, A. A., Vining, C., Randolph, A., Herbach, N., Wanke, R., Atkins, K. B., Gyung Kang, H., Henger, A., Brakebusch, C., Holzman, L. B., & Kretzler, M. (2013). Divergent functions of the Rho GTPases Rac1 and Cdc42 in podocyte injury. *Kidney International*, *84*(5), 920–930.

Bose, R., & Wrana, J. L. (2006). Regulation of Par6 by extracellular signals. *Current Opinion in Cell Biology*, *18*(2), 206–212.

Brand, A. H., & Perrimon, N. (1993). Targeted gene expression as a means of altering cell fates and generating dominant phenotypes. *Development (Cambridge, England)*, *118*(2), 401–415.

Brenner, B. M., Hostetter, T. H., & Humes, H. D. (1978a). Molecular Basis of Proteinuria of Glomerular Origin. *New England Journal of Medicine*, *298*(15), 826–833.

Brenner, B. M., Hostetter, T. H., & Humes, H. D. (1978b). Glomerular permselectivity: barrier function based on discrimination of molecular size and charge. *American Journal of Physiology-Renal Physiology*, *234*(6), F455–F460.

Brinkkoetter, P. T., Ising, C., & Benzing, T. (2013). The role of the podocyte in albumin filtration. *Nature Reviews Nephrology*, *9*(6), 328–336.

Burford, J. L., Villanueva, K., Lam, L., Riquier-Brison, A., Hackl, M. J., Pippin, J., Shankland, S. J., & Peti-Peterdi, J. (2014). Intravital imaging of podocyte calcium in glomerular injury and disease. *The Journal of Clinical Investigation*, *124*(5), 2050–2058.

Butt, L., Unnersjö-Jess, D., Höhne, M., Edwards, A., Binz-Lotter, J., Reilly, D., Hahnfeldt, R., Ziegler, V., Fremter, K., Rinschen, M. M., Helmstädter, M., Ebert, L. K., Castrop, H., Hackl, M. J., Walz, G., Brinkkoetter, P. T., Liebau, M. C., Tory, K., Hoyer, P. F., … Benzing, T. (2020). A molecular mechanism explaining albuminuria in kidney disease. *Nature Metabolism*, *2*(5), 461–474.

Butt, L., Unnersjö-Jess, D., Höhne, M., Schermer, B., Edwards, A., & Benzing, T. (2021). A mathematical estimation of the physical forces driving podocyte detachment. *Kidney International*, *100*(5), 1054–1062.

Cagan, R. L. (2011). The Drosophila nephrocyte. *Current Opinion in Nephrology and Hypertension*, *20*(4), 409–415.

Cauchi, R. J., & van den Heuvel, M. (2006). The fly as a model for neurodegenerative diseases: is it worth the jump? *Neuro-Degenerative Diseases*, *3*(6), 338–356.

Chang, J. W., Pardo, V., Sageshima, J., Chen, L., Tsai, H. L., Reiser, J., Wei, C., Ciancio, G., Burke, G. W., & Fornoni, A. (2012). Podocyte Foot Process Effacement in Post-reperfusion Allograft Biopsies Correlates with Early Recurrence of Proteinuria in Focal Segmental Glomerulosclerosis. *Transplantation*, *93*(12), 1238–1244.

Chen, J., & Zhang, M. (2013). The Par3/Par6/aPKC complex and epithelial cell polarity. *Experimental Cell Research*, *319*(10), 1357–1364.

Chen, X., & Macara, I. G. (2005). Par-3 controls tight junction assembly through the Rac exchange factor Tiam1. *Nature Cell Biology*, *7*(3), 262–269.

D'Agati, V. (2003). Pathologic classification of focal segmental glomerulosclerosis. *Seminars in Nephrology*, *23*(2), 117–134.

Dandapani, S. v., Sugimoto, H., Matthews, B. D., Kolb, R. J., Sinha, S., Gerszten, R. E., Zhou, J., Ingber, D. E., Kalluri, R., & Pollak, M. R. (2007). α-actinin-4 is required for normal podocyte adhesion. *Journal of Biological Chemistry*, *282*(1), 467–477.

Davin, J. C. (2016). The glomerular permeability factors in idiopathic nephrotic syndrome. *Pediatric Nephrology (Berlin, Germany)*, *31*(2), 207–215.

Deegens, J. K. J., Dijkman, H. B. P. M., Borm, G. F., Steenbergen, E. J., van den Berg, J. G., Weening, J. J., & Wetzels, J. F. M. (2008). Podocyte foot process effacement as a diagnostic tool in focal segmental glomerulosclerosis. *Kidney International*, *74*(12), 1568–1576.

Denholm, B., & Skaer, H. (2009). Bringing together components of the fly renal system. *Current Opinion in Genetics & Development*, *19*(5), 526–532.

Djinović-Carugo, K., Young, P., Gautel, M., & Saraste, M. (1999). Molecular Basis for Cross-Linking of Actin Filaments: Structure of the α-Actinin Rod. *Cell*, *98*(4), 537–546.

Donoviel, D. B., Freed, D. D., Vogel, H., Potter, D. G., Hawkins, E., Barrish, J. P., Mathur, B. N., Turner, C. A., Geske, R., Montgomery, C. A., Starbuck, M., Brandt, M., Gupta, A., Ramirez-Solis, R., Zambrowicz, B. P., & Powell, D. R. (2001). Proteinuria and perinatal lethality in mice lacking NEPH1, a novel protein with homology to NEPHRIN. *Molecular and Cellular Biology*, *21*(14), 4829–4836.

Dow, L. E., Kauffman, J. S., Caddy, J., Peterson, A. S., Jane, S. M., Russell, S. M., & Humbert, P. O. (2007). The tumour-suppressor Scribble dictates cell polarity during directed epithelial migration: regulation of Rho GTPase recruitment to the leading edge. *Oncogene*, *26*(16), 2272–2282.

Ebnet, K., Suzuki, A., Horikoshi, Y., Hirose, T., Meyer Zu Brickwedde, M. K., Ohno, S., & Vestweber, D. (2001). The cell polarity protein ASIP/PAR-3 directly associates with junctional adhesion molecule (JAM). *The EMBO Journal*, *20*(14), 3738–3748.

Feng, D., DuMontier, C., & Pollak, M. R. (2015). The role of alpha-actinin-4 in human kidney disease. *Cell & Bioscience*, *5*(1), 44.

Ferguson, S. M., & de Camilli, P. (2012). Dynamin, a membrane-remodelling GTPase. *Nature Reviews. Molecular Cell Biology*, *13*(2), 75–88.

Fernandez-Funez, P., de Mena, L., & Rincon-Limas, D. E. (2015). Modeling the complex pathology of Alzheimer's disease in Drosophila. *Experimental Neurology*, *274*(0 0), 58.

Fu, Y., Zhu, J.-Y., Richman, A., Zhao, Z., Zhang, F., Ray, P. E., & Han, Z. (2017). A Drosophila model system to assess the function of human monogenic podocyte mutations that cause nephrotic syndrome. *Human Molecular Genetics*, *26*(4), 768–780.

Fujii, H., Goto, S., & Fukagawa, M. (2018). Role of Uremic Toxins for Kidney, Cardiovascular, and Bone Dysfunction. *Toxins 2018, 10*(5), 202.

Fukasawa, H., Bornheimer, S., Kudlicka, K., & Farquhar, M. G. (2009). Slit diaphragms contain tight junction proteins. *Journal of the American Society of Nephrology*, *20*(7), 1491–1503.

Gao, L., Macara, I. G., & Joberty, G. (2002). Multiple splice variants of Par3 and of a novel related gene, Par3L, produce proteins with different binding properties. *Gene*, *294*(1–2), 99–107.

Garg, P., Verma, R., Nihalani, D., Johnstone, D. B., & Holzman, L. B. (2007). Neph1 cooperates with nephrin to transduce a signal that induces actin polymerization. *Molecular and Cellular Biology*, *27*(24), 8698–8712.

Garrard, S. M., Capaldo, C. T., Gao, L., Rosen, M. K., Macara, I. G., & Tomchick, D. R. (2003). Structure of Cdc42 in a complex with the GTPase-binding domain of the cell polarity protein, Par6. *The EMBO Journal*, *22*(5), 1125–1133.

Glorieux, G., Mullen, W., Duranton, F., Filip, S., Gayrard, N., Husi, H., Schepers, E., Neirynck, N., Schanstra, J. P., Jankowski, J., Mischak, H., Argilés, À., Vanholder, R., Vlahou, A., & Klein, J. (2015). New insights in molecular mechanisms involved in chronic kidney disease using high-resolution plasma proteome analysis. *Nephrology, Dialysis, Transplantation : Official Publication of the European Dialysis and Transplant Association - European Renal Association*, *30*(11), 1842–1852.

Greka, A., & Mundel, P. (2012). Cell Biology and Pathology of Podocytes. *Annual Review of Physiology*, *74*, 299–323.

Gu, C., Yaddanapudi, S., Weins, A., Osborn, T., Reiser, J., Pollak, M., Hartwig, J., & Sever, S. (2010). Direct dynamin-actin interactions regulate the actin cytoskeleton. *The EMBO Journal*, *29*(21), 3593–3606.

Hales, K. G., Korey, C. A., Larracuente, A. M., & Roberts, D. M. (2015). Genetics on the Fly: A Primer on the Drosophila Model System. *Genetics*, *201*(3), 815–842.

Haraldsson, B., Nyström, J., & Deen, W. M. (2008). Properties of the glomerular barrier and mechanisms of proteinuria. *Physiological Reviews*, *88*(2), 451–487.

Hartleben, B., Schweizer, H., Lübben, P., Bartram, M. P., Möller, C. C., Herr, R., Wei, C., Neumann-Haefelin, E., Schermer, B., Zentgraf, H., Kerjaschki, D., Reiser, J., Walz, G., Benzing, T., & Huber, T. B. (2008). Neph-nephrin proteins bind the Par3-Par6-atypical protein kinase C (aPKC) complex to regulate podocyte cell polarity. *Journal of Biological Chemistry*, *283*(34), 23033–23038.

Hartleben, B., Widmeier, E., Suhm, M., Worthmann, K., Schell, C., Helmstädter, M., Wiech, T., Walz, G., Leitges, M., Schiffer, M., & Huber, T. B. (2013). aPKCγ/ι and aPKCζ contribute to podocyte differentiation and glomerular maturation. *Journal of the American Society of Nephrology*, *24*(2), 253–267.

Hartleben, B., Widmeier, E., Wanner, N., Schmidts, M., Kim, S. T., Schneider, L., Mayer, B., Kerjaschki, D., Miner, J. H., Walz, G., & Huber, T. B. (2012). Role of the Polarity Protein Scribble for Podocyte Differentiation and Maintenance. *PLoS ONE*, *7*(5), e36705.

Heigwer, F., Port, F., & Boutros, M. (2018). RNA Interference (RNAi) Screening in Drosophila. *Genetics*, *208*(3), 853–874.

Helmstädter, M., Huber, T. B., & Hermle, T. (2017). Using the Drosophila Nephrocyte to Model Podocyte Function and Disease. *Frontiers in Pediatrics*, *5*, 262.

Hermle, T., Braun, D. A., Helmstädter, M., Huber, T. B., & Hildebrandt, F. (2017). Modeling Monogenic Human Nephrotic Syndrome in the Drosophila Garland Cell Nephrocyte. *Journal of the American Society of Nephrology*, *28*(5), 1521–1533.

Hirose, T., Satoh, D., Kurihara, H., Kusaka, C., Hirose, H., Akimoto, K., Matsusaka, T., Ichikawa, I., Noda, T., & Ohno, S. (2009). An essential role of the universal polarity protein, aPKCλ, on the maintenance of podocyte slit diaphragms. *PLoS ONE*, *4*(1), e4194.

Huber, T. B., & Benzing, T. (2005). The slit diaphragm: a signaling platform to regulate podocyte function. *Current Opinion in Nephrology and Hypertension*, *14*(3), 211–216.

Huber, T. B., Hartleben, B., Winkelmann, K., Schneider, L., Becker, J. U., Leitges, M., Walz, G., Haller, H., & Schiffer, M. (2009). Loss of podocyte aPKClambda/iota causes polarity defects and nephrotic syndrome. *Journal of the American Society of Nephrology*, *20*(4), 798–806.

Humbert, P. O., Dow, L. E., & Russell, S. M. (2006) The Scribble and Par complexes in polarity and migration: friends or foes? *TRENDS in Cell Biology, 16*(12), 622–630.

Hurd, T. W., Gao, L., Roh, M. H., Macara, I. G., & Margolis, B. (2003). Direct interaction of two polarity complexes implicated in epthelial tight junction assembly. *Nature Cell Biology*, *5*(2), 137–142.

Ichimura, K., Kurihara, H., & Sakai, T. (2007). Actin filament organization of foot processes in vertebrate glomerular podocytes. *Cell and Tissue Research*, *329*(3), 541–557.

Itoh, M., Sasaki, H., Furuse, M., Ozaki, H., Kita, T., & Tsukita, S. (2001). Junctional adhesion molecule (JAM) binds to PAR-3: a possible mechanism for the recruitment of PAR-3 to tight junctions. *The Journal of Cell Biology*, *154*(3), 491–497.

Jennings, B. H. (2011). Drosophila – a versatile model in biology & medicine. *Materials Today*, *14*(5), 190–195.

Jiang, L., Ding, J., Tsai, H., Li, L., Feng, Q., Miao, J., & Fan, Q. (2011). Over-expressing transient receptor potential cation channel 6 in podocytes induces cytoskeleton rearrangement through increases of intracellular Ca2+ and RhoA activation. *Experimental Biology and Medicine (Maywood, N.J.)*, *236*(2), 184–193.

Joberty, G., Petersen, C., Gao, L., & Macara, I. G. (2000). The cell-polarity protein Par6 links Par3 and atypical protein kinase C to Cdc42. *Nature Cell Biology*, *2*(8), 531–539.

Jones, N., Blasutig, I. M., Eremina, V., Ruston, J. M., Bladt, F., Li, H., Huang, M., Larose, L., Li, S. S. C., Takano, T., Quaggin, S. E., & Pawson, T. (2006). Nck adaptor proteins link nephrin to the actin cytoskeleton of kidney podocytes. *Nature*, *440*(7085), 818–823.

Kaplan, J. M., Kim, S. H., North, K. N., Rennke, H., Correia, L. A., Tong, H. Q., Mathis, B. J., Rodríguez-Pérez, J. C., Allen, P. G., Beggs, A. H., & Pollak, M. R. (2000). Mutations in ACTN4, encoding α-actinin-4, cause familial focal segmental glomerulosclerosis. *Nature Genetics*, *24*(3), 251–256.

Kerjaschki, D. (2001). Caught flat-footed: podocyte damage and the molecular bases of focal glomerulosclerosis. *Journal of Clinical Investigation*, *108*(11), 1583–1587.

Kestilä, M., Lenkkeri, U., Männikkö, M., Lamerdin, J., McCready, P., Putaala, H., Ruotsalainen, V., Morita, T., Nissinen, M., Herva, R., Kashtan, C. E., Peltonen, L., Holmberg, C., Olsen, A., & Tryggvason, K. (1998). Positionally cloned gene for a novel glomerular protein--nephrin--is mutated in congenital nephrotic syndrome. *Molecular Cell*, *1*(4), 575–582.

Kim, K., Cha, S. J., Choi, H. J., Kang, J. S., & Lee, E. Y. (2021). Dysfunction of Mitochondrial Dynamics in Drosophila Model of Diabetic Nephropathy. *Life*, *11*(1), 1–8.

Kim, S., Gailite, I., Moussian, B., Luschnig, S., Goette, M., Fricke, K., Honemann-Capito, M., Grubmüller, H., & Wodarz, A. (2009). Kinase-activity-independent functions of atypical protein kinase C in Drosophila. *Journal of Cell Science*, *122*(Pt 20), 3759–3771.

Koehler, S., Tellkamp, F., Niessen, C. M., Bloch, W., Kerjaschki, D., Schermer, B., Benzing, T., & Brinkkoetter, P. T. (2016). Par3A is dispensable for the function of the glomerular filtration barrier of the kidney. *American Journal of Physiology. Renal Physiology*, *311*(1), F112–F119.

Kohjima, M., Noda, Y., Takeya, R., Saito, N., Takeuchi, K., & Sumimoto, H. (2002). PAR3β, a novel homologue of the cell polarity protein PAR3, localizes to tight junctions. *Biochemical and Biophysical Research Communications*, *299*(4), 641–646.

Kopp, J. B., Anders, H. J., Susztak, K., Podestà, M. A., Remuzzi, G., Hildebrandt, F., & Romagnani, P. (2020). Podocytopathies. *Nature Reviews. Disease Primers*, *6*(1).

Kornberg, T. B., & Krasnow, M. A. (2000). The Drosophila Genome Sequence: Implications for Biology and Medicine. *Science*, *287*(5461), 2218–2220.

Kos, C. H., Le, T. C., Sinha, S., Henderson, J. M., Kim, S. H., Sugimoto, H., Kalluri, R., Gerszten, R. E., & Pollak, M. R. (2003). Mice deficient in α-actinin-4 have severe glomerular disease. *Journal of Clinical Investigation*, *111*(11), 1683–1690.

Kovalevsky, A. (1886). Zur Verhalten des Rückengefässes und des guirlandenförmigen Zellenstrangs der Musciden während der Metamorphose. *Biologisches Zentralblatt*, *6*, 74–79.

Kovalevsky, A. (1889). Ein Beitrag zur Kenntnis der Exkretionsorgane. *Biologisches Zentralblatt*, *9*, 74–79.

Kreidberg, J. A. (2003). Podocyte differentiation and glomerulogenesis. *Journal of the American Society of Nephrology* , *14*(3), 806–814.

Kriz, W. (2020). The Inability of Podocytes to Proliferate: Cause, Consequences, and Origin. *The Anatomical Record*, *303*(10), 2588–2596.

Kriz, W., Shirato, I., Nagata, M., LeHir, M., & Lemley, K. v. (2013). The podocyte's response to stress: The enigma of foot process effacement. *American Journal of Physiology. Renal Physiology*, *304*(4), 333–347.

Lehtonen, S., Ryan, J. J., Kudlicka, K., Iino, N., Zhou, H., & Farquhar, M. G. (2005). Cell junction-associated proteins IQGAP1, MAGI-2, CASK, spectrins, and alpha-actinin are components of the nephrin multiprotein complex. *Proceedings of the National Academy of Sciences of the United States of America*, *102*(28), 9814–9819.

Lehtonen, S., Zhao, F., & Lehtonen, E. (2002). CD2-associated protein directly interacts with the actin cytoskeleton. *American Journal of Physiology. Renal Physiology*, *283*(4), F734–F743.

Lemmers, C., Michel, D., Lane-Guermonprez, L., Delgrossi, M. H., Médina, E., Arsanto, J. P., & le Bivic, A. (2004). CRB3 Binds Directly to Par6 and Regulates the Morphogenesis of the Tight Junctions in Mammalian Epithelial Cells. *Molecular Biology of the Cell*, *15*(3), 1324–1333.

Levy, J. (2007). Secondary glomerular disease. *Medicine*, *35*(9), 497–499.

Liebeskind, D. S. (2014). Nephrotic syndrome. *Handbook of Clinical Neurology*, *119*, 405–415.

Lin, D., Edwards, A. S., Fawcett, J. P., Mbamalu, G., Scott, J. D., & Pawson, T. (2000). A mammalian PAR-3-PAR-6 complex implicated in Cdc42/Rac1 and aPKC signalling and cell polarity. *Nature Cell Biology*, *2*(8), 540–547.

Liu, J., & Wang, W. (2017). Genetic basis of adult-onset nephrotic syndrome and focal segmental glomerulosclerosis. *Frontiers of Medicine*, *11*(3), 333–339.

Lubojemska, A., Irina Stefana, M., Sorge, S., Bailey, A. P., Lampe, L., Yoshimura, A., Burrell, A., Collinson, L., & GouldID, A. P. (2021). Adipose triglyceride lipase protects renal cell endocytosis in a Drosophila dietary model of chronic kidney disease. *PLoS Biology*, *19*(5).

Margolis, B., & Borg, J. P. (2005). Apicobasal polarity complexes. *Journal of Cell Science*, *118*(Pt 22), 5157–5159.

Matsusaka, T., Sandgren, E., Shintani, A., Kon, V., Pastan, I., Fogo, A. B., & Ichikawa, I. (2011). Podocyte Injury Damages Other Podocytes. *Journal of the American Society of Nephrology*, *22*(7), 1275–1285.

May, C. J., Saleem, M., & Welsh, G. I. (2014). Podocyte dedifferentiation: A specialized process for a specialized cell. *Frontiers in Endocrinology*, *5*, 148.

McCarthy, E. T., Sharma, M., & Savin, V. J. (2010). Circulating permeability factors in idiopathic nephrotic syndrome and focal segmental glomerulosclerosis. *Clinical Journal of the American Society of Nephrology*, *5*(11), 2115–2121.

Mertens, A. E. E., Pegtel, D. M., & Collard, J. G. (2006). Tiam1 takes PARt in cell polarity. *Trends in Cell Biology*, *16*(6), 308–316.

Mertens, A. E. E., Rygiel, T. P., Olivo, C., van der Kammen, R., & Collard, J. G. (2005). The Rac activator Tiam1 controls tight junction biogenesis in keratinocytes through binding to and activation of the Par polarity complex. *Journal of Cell Biology*, *170*(7), 1029–1037.

Mizuno, K., Suzuki, A., Hirose, T., Kitamura, K., Kutsuzawa, K., Futaki, M., Amano, Y., & Ohno, S. (2003). Self-association of PAR-3-mediated by the conserved N-terminal domain contributes to the development of epithelial tight junctions. *The Journal of Biological Chemistry*, *278*(33), 31240–31250.

Mullins, R. D. (2000). How WASP-family proteins and the Arp2/3 complex convert intracellular signals into cytoskeletal structures. *Current Opinion in Cell Biology*, *12*(1), 91–96.

Mundel, P., Gilbert, P., & Kriz, W. (1991). Podocytes in glomerulus of rat kidney express a characteristic 44 KD protein. *The Journal of Histochemistry and Cytochemistry : Official Journal of the Histochemistry Society*, *39*(8), 1047–1056.

Mundel, P., & Shankland, S. J. (2002). Podocyte biology and response to injury. *Journal of the American Society of Nephrology*, *13*(12), 3005–3015.

Murdoch, J. N., Henderson, D. J., Doudney, K., Gaston-Massuet, C., Phillips, H. M., Paternotte, C., Arkell, R., Stanier, P., & Copp, A. J. (2003). Disruption of scribble (Scrb1) causes severe neural tube defects in the circletail mouse. *Human Molecular Genetics*, *12*(2), 87–98.

Nadeau, J. H., & Taylor, B. A. (1984). Lengths of chromosomal segments conserved since divergence of man and mouse. *Proceedings of the National Academy of Sciences of the United States of America*, *81*(3), 814–818.

Nagai-Tamai, Y., Mizuno, K., Hirose, T., Suzuki, A., & Ohno, S. (2002). Regulated protein-protein interaction between aPKC and PAR-3 plays an essential role in the polarization of epithelial cells. *Genes to Cells : Devoted to Molecular & Cellular Mechanisms*, *7*(11), 1161–1171.

Nelson, W. J. (2003). Adaptation of core mechanisms to generate cell polarity. *Nature 2003 422:6933*, *422*(6933), 766–774.

New, L. A., Chahi, A. K., & Jones, N. (2013). Direct regulation of nephrin tyrosine phosphorylation by Nck adaptor proteins. *The Journal of Biological Chemistry*, *288*(3), 1500–1510.

Ning, L., Suleiman, H. Y., & Miner, J. H. (2020). Synaptopodin is dispensable for normal podocyte homeostasis but is protective in the context of acute podocyte injury. *Journal of the American Society of Nephrology*, *31*(12), 2815–2832.

Nishimura, T., Yamaguchi, T., Kato, K., Yoshizawa, M., Nabeshima, Y. I., Ohno, S., Hoshino, M., & Kaibuchi, K. (2005). PAR-6-PAR-3 mediates Cdc42-induced Rac activation through the Rac GEFs STEF/Tiam1. *Nature Cell Biology*, *7*(3), 270–277.

Odenthal, J., & Brinkkoetter, P. T. (2019). Drosophila melanogaster and its nephrocytes: A versatile model for glomerular research. *Methods in Cell Biology*, *154*(B), 217–240.

Pavenstädt, H., Kriz, W., & Kretzler, M. (2003). Cell biology of the glomerular podocyte. *Physiological Reviews*, *83*(1), 253–307.

Pearson, H. B., Perez-Mancera, P. A., Dow, L. E., Ryan, A., Tennstedt, P., Bogani, D., Elsum, I., Greenfield, A., Tuveson, D. A., Simon, R., & Humbert, P. O. (2011). SCRIB expression is deregulated in human prostate cancer, and its deficiency in mice promotes prostate neoplasia. *The Journal of Clinical Investigation*, *121*(11), 4257–4267.

Perico, L., Conti, S., Benigni, A., & Remuzzi, G. (2016). Podocyte-actin dynamics in health and disease. *Nature Reviews. Nephrology*, *12*(11), 692–710.

Pieczynski, J., & Margolis, B. (2011). Protein complexes that control renal epithelial polarity. *Am J Physiol Renal Physiol*, *300*, 589–601.

Plant, P. J., Fawcett, J. P., Lin, D. C. C., Holdorf, A. D., Binns, K., Kulkarni, S., & Pawson, T. (2003). A polarity complex of mPar-6 and atypical PKC binds, phosphorylates and regulates mammalian Lgl. *Nature Cell Biology 2003 5:4*, *5*(4), 301–308.

Politano, S. A., Colbert, G. B., & Hamiduzzaman, N. (2020). Nephrotic Syndrome. *Primary Care: Clinics in Office Practice*, *47*(4), 597–613.

Pozdzik, A., Brochériou, I., David, C., Touzani, F., Goujon, J. M., & Wissing, K. M. (2018). Membranous Nephropathy and Anti-Podocytes Antibodies: Implications for the Diagnostic Workup and Disease Management. *BioMed Research International*, *2018*, 6281054.

Raman, R., Pinto, C. S., & Sonawane, M. (2018). Polarized Organization of the Cytoskeleton: Regulation by Cell Polarity Proteins. *Journal of Molecular Biology*, *430*(19), 3565–3584.

Reiser, J., Kriz, W., Kretzler, M., & Mundel, P. (2000). The Glomerular Slit Diaphragm Is a Modified Adherens Junction. *Journal of the American Society of Nephrology*, *11*(1), 1–8.

Reiter, L. T., Potocki, L., Chien, S., Gribskov, M., & Bier, E. (2001). A systematic analysis of human disease-associated gene sequences in Drosophila melanogaster. *Genome Research*, *11*(6), 1114–1125.

Rennke, H. G., & Venkatachalam, M. A. (1979). Glomerular permeability of macromolecules. Effect of molecular configuration on the fractional clearance of uncharged dextran and neutral horseradish peroxidase in the rat. *Journal of Clinical Investigation*, *63*(4), 713–717.

Rico-Fontalvo, J., Aroca, G., Cabrales, J., Daza-Arnedo, R., Yánez-Rodríguez, T., Martínez-Ávila, M. C., Uparella-Gulfo, I., & Raad-Sarabia, M. (2022). Molecular Mechanisms of Diabetic Kidney Disease. *International Journal of Molecular Sciences*, *23*(15), 8668.

Rodewald, R., & Karnovsky, M. J. (1974). Porous substructure of the glomerular slit diaphragm in the rat and mouse. *The Journal of Cell Biology*, *60*(2), 423–433.

Roh, M. H., Makarova, O., Liu, C. J., Shin, K., Lee, S., Laurinec, S., Goyal, M., Wiggins, R., & Margolis, B. (2002). The Maguk protein, Pals1, functions as an adapter, linking mammalian homologues of Crumbs and Discs Lost. *The Journal of Cell Biology*, *157*(1), 161–172.

Roignot, J., Peng, X., & Mostov, K. (2013). Polarity in Mammalian Epithelial Morphogenesis. *Cold Spring Harbor Perspectives in Biology*, *5*(2), a013789.

Rubin, G. M., & Lewis, E. B. (2000). A brief history of Drosophila's contributions to genome research. *Science (New York, N.Y.)*, *287*(5461), 2216–2218.

Sachs, N., & Sonnenberg, A. (2013). Cell-matrix adhesion of podocytes in physiology and disease. *Nature Reviews. Nephrology*, *9*(4), 200–210.

Sadowski, C. E., Lovric, S., Ashraf, S., Pabst, W. L., Gee, H. Y., Kohl, S., Engelmann, S., Vega-Warner, V., Fang, H., Halbritter, J., Somers, M. J., Tan, W., Shril, S., Fessi, I., Lifton, R. P., Bockenhauer, D., El-Desoky, S., Kari, J. A., Zenker, M., … Zolotnistskaya, A. (2015). A single-gene cause in 29.5% of cases of steroid-resistant nephrotic syndrome. *Journal of the American Society of Nephrology*, *26*(6), 1279–1289.

Saran, R., Robinson, B., Abbott, K. C., Agodoa, L. Y. C., Bhave, N., Bragg-Gresham, J., Balkrishnan, R., Dietrich, X., Eckard, A., Eggers, P. W., Gaipov, A., Gillen, D., Gipson, D., Hailpern, S. M., Hall, Y. N., Han, Y., He, K., Herman, W., Heung, M., … Shahinian, V. (2018). US Renal Data System 2017 Annual Data Report: Epidemiology of Kidney Disease in the United States. *American Journal of Kidney Diseases : The Official Journal of the National Kidney Foundation*, *71*(3S1), A7.

Schell, C., Wanner, N., & Huber, T. B. (2014). Glomerular development--shaping the multi-cellular filtration unit. *Seminars in Cell & Developmental Biology*, *36*, 39–49.

Schnabel, E., Anderson, J. M., & Farquhar, M. G. (1990). The tight junction protein ZO-1 is concentrated along slit diaphragms of the glomerular epithelium. *The Journal of Cell Biology*, *111*(3), 1255–1263.

Scott, R. P., Hawley, S. P., Ruston, J., Du, J., Brakebusch, C., Jones, N., & Pawson, T. (2012). Podocyte-specific loss of Cdc42 leads to congenital nephropathy. *Journal of the American Society of Nephrology*, *23*(7), 1149–1154.

Seiler, M. W., Rennke, H. G., Venkatachalam, M. A., & Cotran, R. S. (1977). Pathogenesis of polycation induced alterations ('fusion') of glomerular epithelium. *Laboratory Investigation*, *36*(1), 48–61.

Sever, S., & Schiffer, M. (2018). Actin dynamics at focal adhesions: a common endpoint and putative therapeutic target for proteinuric kidney diseases. *Kidney International*, *93*(6), 1298–1307.

Shankland, S. J. (2006). The podocyte's response to injury: Role in proteinuria and glomerulosclerosis. *Kidney International*, *69*(12), 2131–2147.

Shih, N. Y., Li, J., Karpitskii, V., Nguyen, A., Dustin, M. L., Kanagawa, O., Miner, J. H., & Shaw, A. S. (1999). Congenital nephrotic syndrome in mice lacking CD2-associated protein. *Science (New York, N.Y.)*, *286*(5438), 312–315.

Shirato, I. (2002). Podocyte process effacement in vivo. *Microscopy Research and Technique*, *57*(4), 241–246.

Shirato, I., Sakai, T., Kimura, K., Tomino, Y., & Kriz, W. (1996). Cytoskeletal changes in podocytes associated with foot process effacement in Masugi nephritis. *The American Journal of Pathology*, *148*(4), 1283–1296.

Smoyer, W. E., Mundel, P., Gupta, A., & Welsh, M. J. (1997). Podocyte alpha-actinin induction precedes foot process effacement in experimental nephrotic syndrome. *The American Journal of Physiology*, *273*(1 Pt 2).

Stephenson, R., & Metcalfe, N. H. (2013). Drosophila melanogaster: a fly through its history and current use. *The Journal of the Royal College of Physicians of Edinburgh*, *43*(1), 70–75.

Suzuki, A., & Ohno, S. (2006). The PAR-aPKC system: lessons in polarity. *Undefined*, *119*(6), 979–987.

Suzuki, A., Yamanaka, T., Hirose, T., Manabe, N., Mizuno, K., Shimizu, M., Akimoto, K., Izumi, Y., Ohnishi, T., & Ohno, S. (2001). Atypical Protein Kinase C Is Involved in the Evolutionarily Conserved Par Protein Complex and Plays a Critical Role in Establishing Epithelia-Specific Junctional Structures. *Journal of Cell Biology*, *152*(6), 1183–1196.

Tang, J., Taylor, D. W., & Taylor, K. A. (2001). The three-dimensional structure of α-actinin obtained by cryoelectron microscopy suggests a model for Ca2+-dependent actin binding. *Journal of Molecular Biology*, *310*(4), 845–858.

Tossidou, I., Teng, B., Worthmann, K., Müller-Deile, J., Jobst-Schwan, T., Kardinal, C., Schroder, P., Bolanos-Palmieri, P., Haller, H., Willerding, J., Drost, D. M., de Jonge, L., Reubold, T., Eschenburg, S., Johnson, R. I., & Schiffer, M. (2019). Tyrosine Phosphorylation of CD2AP Affects Stability of the Slit Diaphragm Complex. *Journal of the American Society of Nephrology*, *30*(7), 1220–1237.

Tryggvason, K., & Wartiovaara, J. (2001). Molecular basis of glomerular permselectivity. *Current Opinion in Nephrology and Hypertension*, *10*(4), 543–549.

Tsuda, L., & Lim, Y. M. (2018). Alzheimer's Disease Model System Using Drosophila. *Advances in Experimental Medicine and Biology*, *1076*, 25–40.

Venken, K. J. T., Sarrion-Perdigones, A., Vandeventer, P. J., Abel, N. S., Christiansen, A. E., & Hoffman, K. L. (2016). Genome Engineering: Drosophila melanogaster and beyond. *Wiley Interdisciplinary Reviews. Developmental Biology*, *5*(2), 233–267.

Verma, R., Kovari, I., Soofi, A., Nihalani, D., Patrie, K., & Holzman, L. B. (2006). Nephrin ectodomain engagement results in Src kinase activation, nephrin phosphorylation, Nck recruitment, and actin polymerization. *The Journal of Clinical Investigation*, *116*(5), 1346–1359.

Verma, R., Wharram, B., Kovari, I., Kunkel, R., Nihalani, D., Wary, K. K., Wiggins, R. C., Killen, P., & Holzman, L. B. (2003). Fyn binds to and phosphorylates the kidney slit diaphragm component Nephrin. *The Journal of Biological Chemistry*, *278*(23), 20716–20723.

Vivante, A., & Hildebrandt, F. (2016). Exploring the genetic basis of early-onset chronic kidney disease. *Nature Reviews Nephrology*, *12*(3), 133–146.

Völker, L. A., Ehren, R., Grundmann, F., Benzing, T., Weber, L. T., & Brinkkötter, P. T. (2019). A newly established clinical registry of minimal change disease and focal and segmental glomerulosclerosis in Germany. *Nephrology, Dialysis, Transplantation : Official Publication of the European Dialysis and Transplant Association - European Renal Association*, *34*(12), 1983–1986.

Wang, C. shi, & Greenbaum, L. A. (2019). Nephrotic Syndrome. *Pediatric Clinics of North America*, *66*(1), 73–85.

Wang, L., Ellis, M. J., Gomez, J. A., Eisner, W., Fennell, W., Howell, D. N., Ruiz, P., Fields, T. A., & Spurney, R. F. (2012). Mechanisms of the proteinuria induced by Rho GTPases. *Kidney International*, *81*(11), 1075–1085.

Wang, Y., Huang, C., & Zhao, W. (2022). Recent advances of the biological and biomedical applications of CRISPR/Cas systems. *Molecular Biology Reports*, *49*(7), 7087.

Wangler, M. F., Yamamoto, S., & Bellen, H. J. (2015). Fruit Flies in Biomedical Research. *Genetics*, *199*(3), 639–653.

Wanner, N., Hartleben, B., Herbach, N., Goedel, M., Stickel, N., Zeiser, R., Walz, G., Moeller, M. J., Grahammer, F., & Huber, T. B. (2014). Unraveling the Role of Podocyte Turnover in Glomerular Aging and Injury. *Journal of the American Society of Nephrology*, *25*(4), 707–716.

Waterston, R. H., Lindblad-Toh, K., Birney, E., Rogers, J., Abril, J. F., Agarwal, P., Agarwala, R., Ainscough, R., Alexandersson, M., An, P., Antonarakis, S. E., Attwood, J., Baertsch, R., Bailey, J., Barlow, K., Beck, S., Berry, E., Birren, B., Bloom, T., … Lander, E. S. (2002). Initial sequencing and comparative analysis of the mouse genome. *Nature*, *420*(6915), 520–562.

Weavers, H., Prieto-Sánchez, S., Grawe, F., Garcia-López, A., Artero, R., Wilsch-Bräuninger, M., Ruiz-Gómez, M., Skaer, H., & Denholm, B. (2009). The insect nephrocyte is a podocyte-like cell with a filtration slit diaphragm. *Nature*, *457*(7227), 322–326.

Weins, A., Kenlan, P., Herbert, S., Le, T. C., Villegas, I., Kaplan, B. S., Appel, G. B., & Pollak, M. R. (2005). Mutational and Biological Analysis of alpha-actinin-4 in focal segmental glomerulosclerosis. *Journal of the American Society of Nephrology*, *16*(12), 3694–3701.

Weins, A., Schlondorff, J. S., Nakamura, F., Denker, B. M., Hartwig, J. H., Stossel, T. P., & Pollak, M. R. (2007). Disease-associated mutant α-actinin-4 reveals a mechanism for regulating its F-actin-binding affinity. *Proceedings of the National Academy of Sciences of the United States of America*, *104*(41), 16080–16085.

Welsch, T., Endlich, N., Kriz, W., & Endlich, K. (2001). CD2AP and p130Cas localize to different F-actin structures in podocytes. *American Journal of Physiology. Renal Physiology*, *281*(4), F769–F777.

Wiggins, J. E., Goyal, M., Sanden, S. K., Wharram, B. L., Shedden, K. A., Misek, D. E., Kuick, R. D., & Wiggins, R. C. (2005). Podocyte hypertrophy, "adaptation," and "decompensation" associated with glomerular enlargement and glomerulosclerosis in the aging rat: prevention by calorie restriction. *Journal of the American Society of Nephrology*, *16*(10), 2953–2966.

Wilson, P. D. (1997). Epithelial cell polarity and disease. *American Journal of Physiology. Renal Physiology, 272*(4), F434–F442.

Wilson, P. D. (2011). Apico-basal polarity in polycystic kidney disease epithelia. *Biochimica et Biophysica Acta*, *1812*(10), 1239–1248.

Wilson, P. D., Sherwood, A. C., Palla, K., Du, J., Watson, R., & Norman, J. T. (1991). Reversed polarity of Na(+) -K(+) -ATPase: mislocation to apical plasma membranes in polycystic kidney disease epithelia. *Amreican Journal of Physiology. Renal Physiology, 260*(3), F420–F430.

Wodarz, A., Ramrath, A., Grimm, A., & Knust, E. (2000). Drosophila Atypical Protein Kinase C Associates with Bazooka and Controls Polarity of Epithelia and Neuroblasts. *The Journal of Cell Biology*, *150*(6), 1361–1374.

Yamanaka, T., Horikoshi, Y., Sugiyama, Y., Ishiyama, C., Suzuki, A., Hirose, T., Iwamatsu, A., Shinohara, A., & Ohno, S. (2003). Mammalian Lgl Forms a Protein Complex with PAR-6 and aPKC Independently of PAR-3 to Regulate Epithelial Cell Polarity. *Current Biology*, *13*(9), 734–743.

Ye, Q., Lan, B., Liu, H., Persson, P. B., Lai, E. Y., & Mao, J. (2022). A critical role of the podocyte cytoskeleton in the pathogenesis of glomerular proteinuria and autoimmune podocytopathies. *Acta Physiologica (Oxford, England)*, *235*(4), e13850.

Zhan, L., Rosenberg, A., Bergami, K. C., Yu, M., Xuan, Z., Jaffe, A. B., Allred, C., & Muthuswamy, S. K. (2008). Deregulation of scribble promotes mammary tumorigenesis and reveals a role for cell polarity in carcinoma. *Cell*, *135*(5), 865–878.

Zhu, L., Jiang, R., Aoudjit, L., Jones, N., & Takano, T. (2011). Activation of RhoA in podocytes induces focal segmental glomerulosclerosis. *Journal of the American Society of Nephrology*, *22*(9), 1621–1630.

Zhuang, S., Shao, H., Guo, F., Trimble, R., Pearce, E., & Abmayr, S. M. (2009). Sns and Kirre, the Drosophila orthologs of Nephrin and Neph1, direct adhesion, fusion and formation of a slit diaphragm-like structure in insect nephrocytes. *Development*, *136*(14), 2335–2344.

Erklärung

Hiermit versichere ich an Eides statt, dass ich die vorliegende Dissertation selbstständig und ohne die Benutzung anderer als der angegebenen Hilfsmittel und Literatur angefertigt habe. Alle Stellen, die wörtlich oder sinngemäß aus veröffentlichten und nicht veröffentlichten Werken dem Wortlaut oder dem Sinn nach entnommen wurden, sind als solche kenntlich gemacht. Ich versichere an Eides statt, dass diese Dissertation noch keiner anderen Fakultät oder Universität zur Prüfung vorgelegen hat; dass sie - abgesehen von unten angegebenen Teilpublikationen und eingebundenen Artikeln und Manuskripten - noch nicht veröffentlicht worden ist sowie, dass ich eine Veröffentlichung der Dissertation vor Abschluss der Promotion nicht ohne Genehmigung des Promotionsausschusses vornehmen werde. Die Bestimmungen dieser Ordnung sind mir bekannt. Darüber hinaus erkläre ich hiermit, dass ich die Ordnung zur Sicherung guter wissenschaftlicher Praxis und zum Umgang mit wissenschaftlichem Fehlverhalten der Universität zu Köln gelesen und sie bei der Durchführung der Dissertation zugrundeliegenden Arbeiten und der schriftlich verfassten Dissertation beachtet habe und verpflichte mich hiermit, die dort genannten Vorgaben bei allen wissenschaftlichen Tätigkeiten zu beachten und umzusetzen. Ich versichere, dass die eingereichte elektronische Fassung der eingereichten Druckfassung vollständig entspricht.

Teilpublikationen:

Odenthal J and Brinkkoetter PT. *Drosophila melanogaster and its nephrocytes: A versatile model for glomerular research.* Methods in Cell Biology Volume 154 – Methods in Kidney Cell Biology – Part B (2019)

Koehler S*, **Odenthal J***, Ludwig V, Unnersjö Jess D, Höhne M, Jüngst C, Grawe F, Helmstädter M, Janku JL, Bergmann C, Hoyer PF, Hagmann HH, Walz G, Bloch W, Niessen C, Schermer B, Wodarz A, Denholm B, Benzing T, Iden S, Brinkkoetter PT. *Scaffold polarity proteins Par3A and Par3B share redundant functions while Par3B acts independent of atypical protein kinase C/Par6 in podocytes to maintain the kidney filtration barrier.* Kidney International (2021)

Odenthal J, Dittrich S, Ludwig V, Merz T, Reitmeier K, Reusch B, Höhne M, Cosgun ZC, Hohenadel M, Putnik J, Göbel, H, Rinschen MM, Altmüller J, Koehler S, Schermer B, Benzing T, Beck BB, Brinkkötter PT, Habbig S, Bartram MP. *Modeling of ACTN4-based podocytopathy using Drosophila nephrocytes.* Kidney International Reports (2023)

Johanna Odenthal

Köln, Juni 2023